THESE

Présentée en vue de l'obtention du grade de

DOCTEUR DE L'UNIVERSITE DE LA MEDITERRANEE, AIX-MARSEILLE II

SPECIALITE : OCEANOGRAPHIE

par

Julien PARA

Etude de la Matière Organique Dissoute Chromophorique et du rayonnement solaire (UV-visible) dans les eaux de surface côtières Méditerranéennes et Arctiques

Le 17 juin 2011

Devant le jury composé de :

Rapporteurs :

Olivier Donard	Directeur de Recherche CNRS, IPREM, Univ. Pau
Fabien Joux	Maître de Conférences, LOMIC, Univ. Pierre et Marie Curie

Examinateurs :

Paula Coble	Associate Professor, College of Marine Science, Univ. of South Florida
Vincent Vantrepotte	Ingénieur de Recherche CNRS, LOG, Univ. Littoral Côte d'Opale
Jean-Christophe Poggiale	Professeur, LMGEM-COM, Univ. Aix-Marseille II

Directeurs de thèse :

Richard Sempéré	Directeur de Recherche CNRS, LMGEM-COM, Univ. Aix-Marseille II
Bruno Charrière	Ingénieur de Recherche CNRS, LMGEM-COM, Univ. Aix-Marseille II

Avant-propos

Cette thèse a été co-encadrée par Richard Sempéré et Bruno Charrière (LMGEM-COM) et financée par la région PACA, en partenariat avec l'association AtmoPACA.

Je tiens tout d'abord à remercier Olivier Donard et Fabien Joux d'avoir accepté d'être les rapporteurs de ce travail. Je remercie également Paula Coble, Vincent Vantrepotte et Jean-Christophe Poggiale d'avoir accepté de faire partie de ce jury de thèse.

Je tiens à exprimer mes sincères remerciements à Richard Sempéré qui m'a fait confiance et donné l'opportunité de travailler sur ce sujet si passionnant.

Je remercie profondement et chaleureusement Bruno Charrière et Marc Tedetti pour toute l'aide qu'ils m'ont apporté. Leurs commentaires et critiques se sont revelés très précieux tout au long de ce travail.

Un grand merci à Patrick Raimbault et Michel Fornier du service d'observation du COM pour leur aide et bonne humeur.

Merci à toutes les personnes du 1er étage (et anciennement 7ème) pour leur soutien, leurs encouragements et leur sympathie.

Un grand merci à tous mes amis Marseillais, Haut-Alpins et Bretons pour leur écoute, leurs conseils et encouragements.

Enfin, mes pensées affectueuses se tournent vers ma Famille et Morgane qui ont toujours été là et qui m'ont permis d'arriver jusqu'ici, merci pour tout !

TABLE DES MATIERES

CHAPITRE I

INTRODUCTION GENERALE ET OBJECTIFS DE THESE

1. Préambule

Les océans renferment l'un des plus grands réservoirs de carbone bio-réactif à la surface de la Terre sous forme de matière organique (MO, Hedges, 1992). La MO océanique se trouve essentiellement (90%) sous forme dissoute (DOM), définie comme étant la fraction inférieure à 0,2 ou 0,45 µm, alors que la fraction particulaire (POM) est minoritaire (10%). Dans la zone euphotique de l'océan ouvert, la DOM provient principalement de l'activité biologique au travers des processus d'exsudation du phytoplancton et des bactéries, d'excrétion par le zooplancton et de dissolution des pelotes fécales (Mague et al., 1980 ; Jumars et al., 1989 ; Nagata, 2000 ; Myklestad, 2000 ; Sempéré et al., 2000). La DOM fraichement produite, en grande partie labile (LDOM), est rapidement consommée par les bactéries hétérotrophes (50 % de la production primaire mondiale). Cette assimilation de DOM aboutit soit à (i) sa minéralisation en CO_2 et en sels nutritifs, (ii) son incorporation en biomasse (POM) devenant ainsi disponible pour les échelons trophiques supérieurs (Azam *et al*., 1983 ; Cho et Azam, 1990), ou (iii) la production de DOM réfractaire (RDOM) à la base de la pompe microbienne du carbone (MCP ; Figure I-1 ; Jiao et al., 2010; Eichinger et al., 2011).

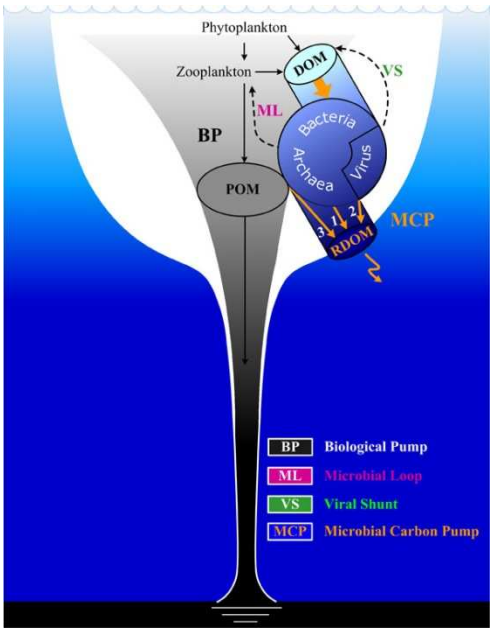

Figure I-1. *Représentation des processus biologiques majeurs intervenant dans le cycle du carbone océanique : concept de pompe biologique et de pompe microbienne (Jiao et al., 2010).*

En milieu côtier les apports fluviaux de MO d'origine terrestre peuvent contribuer de manière significative au stock de DOM (Opsahl et Benner, 1997) ; cependant à l'échelle de l'océan global, ces apports allochtones ne représentent que 1% de la DOM issue de la production primaire (Hedges, 1992). Le représentant majeur de la DOM est le carbone organique dissous (DOC) qui présente un stock de 662 Gt C (Jiao et al., 2010), équivalent à ceux se trouvant dans les végétaux terrestres (570 Gt C) et dans l'atmosphère (750 Gt C; Hedges, 1992, 2002). La valeur de ce réservoir carboné, associée à sa forte bio-réactivité souligne, l'importance de l'étude de la DOM océanique dans le cycle global du carbone (Figure I-2). Cependant, la bio-réactivité de la DOM océanique évolue en fonction de sa nature et de sa structuration chimique. En effet, dans l'océan, trois principaux types de DOM se distinguent par rapport à leur temps de résidence qui souligne un degré de disponibilité spécifique de cette matière vis-à-vis des bactéries hétérotrophes : (i) le stock de DOM labile (LDOM), avec un temps de résidence de l'ordre de l'heure à la journée, est constitué de monomères (monosaccharides, acides aminés, acides organiques) rapidement assimilables et est donc le stock le moins abondant ; (ii) le stock de DOM semi-labile (SLDOM), avec un temps de résidence de l'ordre de la saison, est composé de polymères de poids moléculaire > 10 kDa (polysaccharides, protéines et lipides) assimilables après hydrolyse enzymatique ; et (iii) le stock de DOM réfractaire (RDOM), avec un temps de résidence supérieur à l'année, est constitué de substances bio-réfractaires et est donc le stock le plus abondant (accumulation de substances humiques). Une fraction de ces composés organiques de nature très hétérogène présente une capacité spécifique d'absorber la lumière solaire UV et visible. Cette fraction optiquement active de la DOM est appelée DOM colorée ou chromophorique (CDOM).

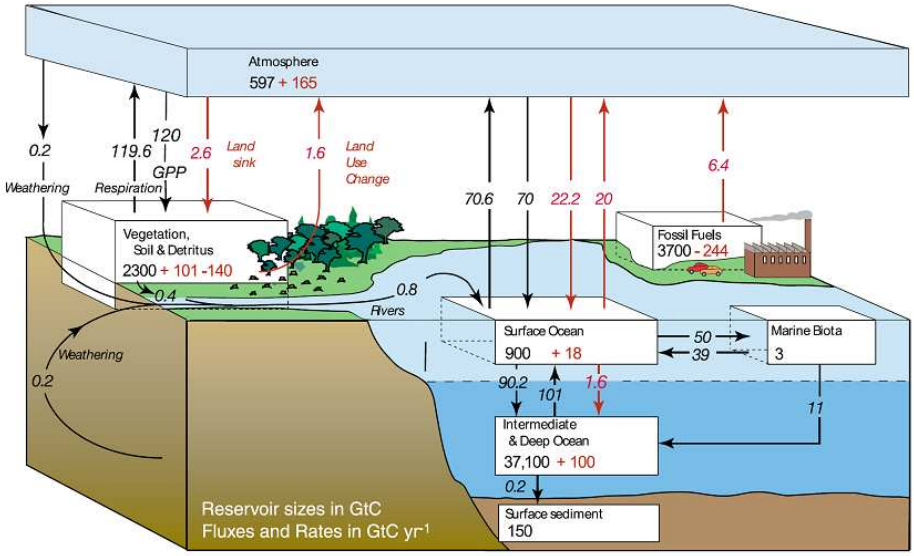

Figure I-2. *Cycle global du carbone : réservoirs (Gt C) et flux (Gt C an^{-1}) naturels (flèches noires) et anthropogéniques (flèches rouges) (IPCC, 2007).*

2. Définition et intérêts d'étude de la CDOM

Historiquement connue sous les termes « gelbstoff», « gilvin » (Kalle, 1937, 1949) et substances jaunes (Shifrin, 1988) à cause de sa haute teneur en substances humiques, la matière organique dissoute colorée ou chromophorique (CDOM) est la fraction dissoute de la matière organique océanique optiquement active et mesurable dans les eaux naturelles. Elle représente entre 20 (océan ouvert) et 70% (océan côtier) du DOC (Coble, 2007). La CDOM est le principal atténuateur des radiations UV dans l'eau et dans une moindre mesure, des radiations visibles du spectre solaire atteignant la surface terrestre (Smith et Baker, 1979 ; Kirk, 1994a ; Diaz et al., 2000). Elle joue donc un rôle clé sur la disponibilité et la qualité de l'éclairement pénétrant dans l'océan (Siegel et al., 1995 ; Siegel et Michaels, 1996 ; Vodacek et al., 1997 ; Nelson et al., 1998 ; Blough et Del Vecchio, 2002).

Dans un cadre de réchauffement climatique, les recherches océanographiques se sont logiquement focalisées durant ces trois dernières décennies sur le rôle de l'océan dans les différents cycles des éléments biogènes, notamment celui du carbone. Dans un tel contexte, l'étude de la composante chromophorique de la DOM est devenue un enjeu de l'océanographie contemporaine car elle est apparue comme une alternative pertinente pour étudier la dynamique du DOC. En effet, l'analyse de la DOM est soumise à des difficultés techniques et des limitations analytiques (Benner et al., 1992 ; Rich et al., 1996), alors que la caractérisation de la CDOM peut se faire via des techniques optiques (absorbance et

fluorescence) faciles à mettre en œuvre, peu coûteuses, et permettant de traiter un grand nombre d'échantillons.

Le développement de capteurs « couleur de l'océan » équipant les satellites océanographiques est à la base de l'intérêt pour la CDOM. En effet, ces capteurs ont pour objectif premier d'estimer la distribution spatio-temporelle de la chlorophylle *a* (Chl*a*) et donc de la production primaire. Or, dans certaines zones océaniques relativement riches en CDOM telles que les zones côtières et estuariennes, il s'est avéré que l'absorbance de la CDOM pouvait interférer avec celle de la Chl*a* (Siegel et al., 2005) et ainsi induire des biais de mesure. De nombreuses études se sont donc focalisées sur la distribution et la dynamique de la CDOM à l'échelle locale afin d'affiner les estimations de Chl*a* dans le but ultime d'en fournir une meilleure quantification globale (Carder et al., 1991, 1999 ; Hoge et al., 1999 ; Garver et Siegel, 1997 ; O'Reilly et al., 1998 ; Kahru et Mitchell, 2001).

D'autre part, l'intérêt d'étudier le rôle de la CDOM dans les écosystèmes aquatiques et terrestres a été relancé suite au constat de la destruction de la couche d'ozone stratosphérique impliquant l'augmentation de l'éclairement UV de surface (Blough et Zepp, 1990 ; Williamson et al., 1996 ; Häder et al., 1998 ; Zepp et al., 1998 ; de Mora et al., 2000 ; Neale et Kieber, 2000, WMO, 2003). En effet, dans les eaux de surface, la CDOM agit comme un écran anti-UV et donc protège les organismes aquatiques de ces radiations délétères (Whitehead et al., 2000 ; Vasseur et al., 2003). Cependant, au niveau des zones côtières riches en CDOM, l'absorbance de la lumière induite par cette dernière peut s'étendre jusque dans le domaine visible, réduisant ainsi l'énergie lumineuse disponible pour le développement phytoplanctonique et entraînant une diminution de la production primaire de l'écosystème (Arrigo et Brown, 1996 ; Vodacek et al., 1995, 1997 ; DeGrandpre et al., 1996 ; Williamson et al., 1996 ; Morris et Hargreaves, 1997 ; Khun et al., 1999 ; Conde et al., 2000 ; de Mora et al., 2000 ; Kuwahara et al., 2000 ; Häder et al., 2003).

La CDOM joue également un rôle central dans la photochimie des eaux de surface océaniques. En effet, les processus photochimiques océaniques sont initiés par l'absorption du rayonnement solaire par la CDOM (Zepp, 1988) et aboutissent, de manière directe et sensibilisée (*via* l'intervention d'espèces radicalaires), à la formation de photo-produits stables et d'intérêts dans le cycle du carbone.

Enfin, le caractère conservatif de la CDOM fournit un outil très utile pour étudier les phénomènes de dilution et de mélange des masses d'eau dans la plupart des zones côtières et au delà de la zone euphotique océanique (Niewiadomska et al., 2008). La CDOM est utilisée comme traceur des apports fluviatiles d'origine naturelle (Huguet et al., 2009) et anthropique

tels que les hydrocarbures aromatiques polycycliques, les composés issus des eaux usées et de l'agriculture (Clark et al., 2007, Hudson et al., 2007). La CDOM permet également d'identifier des caractéristiques physiques de la circulation océanique tels que des tourbillons (Hoge et al., 2005).

3. Caractérisation de la CDOM

3. 1. Propriétés optiques de la CDOM

L'étude de la CDOM se fait *via* ses propriétés optiques d'absorbance et de fluorescence. Ces dernières fournissent des informations d'ordre quantitatif (coefficient d'absorption et intensité de fluorescence) et qualitatif (identification de fluorophores, pente spectrale d'absorbance) permettant d'identifier l'origine allochtone/autochtone et les processus biotiques/abiotiques affectant la CDOM. Ces méthodes d'études, dites spectrométriques permettent également d'appréhender des phénomènes de transformation (production et dégradation) de la CDOM induits par les forçages physiques, biologiques et chimiques du milieu. De plus, la spectrométrie présente de nombreux avantages : les analyses sont rapides, non destructrices, sensibles et nécessitent un faible volume d'échantillon.

3. 1 .1. Principes généraux de l'absorbance et de la fluorescence de la DOM

L'absorbance de la DOM provient de la présence de groupements fonctionnels, appelés chromophores, pourvus d'orbitales électroniques liantes de type π (double, triple liaisons, noyaux aromatiques), et non liantes de type n (hétéroatomes). Ces chromophores possèdent des états d'énergie propre (énergies électroniques rotationnelles et vibrationnelles) et donc une absorptivité spécifique. Aux longueurs d'ondes UV et visibles, l'énergie des photons est suffisante (c'est-à-dire qu'elle correspond à une énergie équivalente à celle qui existe entre deux niveaux d'énergie de la molécule) pour être absorbée. L'absorption de ce rayonnement électromagnétique induit les transitions électroniques de π à π^* et de n à π^* illustrant le passage de l'état fondamental à un état excité de la molécule (Figure I-3).

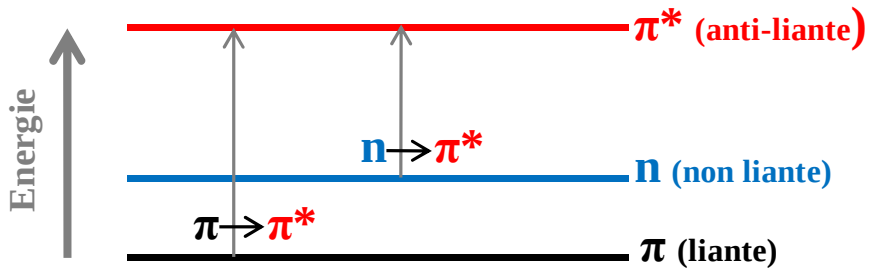

Figure I-3. *Transitions électroniques entre orbitales moléculaires induites par l'absorption du rayonnement solaire UV-visible d'un chromophore*

Une fois la molécule portée dans un état excité, plusieurs voies de désexcitation sont possibles dont le processus radiatif de fluorescence (Figure I-4). L'excès d'énergie vibrationnelle de la molécule excitée (S_2) est transféré vers d'autres niveaux d'énergie par conversion interne (processus non-radiatif). Lorsque la molécule atteint le niveau vibrationnel d'un état électronique plus bas (S_1), elle émet alors une radiation, appelée spectre de fluorescence, afin de retourner à son état fondamental (S_0). Du fait de la dissipation d'énergie, le spectre de fluorescence émis est moins énergétique que celui de l'absorption.

L'absorbance et l'intensité de fluorescence de la DOM sont quantifiées selon les limites de la loi de Beer-Lambert à l'aide d'un spectrophotomètre et d'un spectrofluorimètre, dont les principes de mesure sont présentés dans les annexes 1 et 2, respectivement.

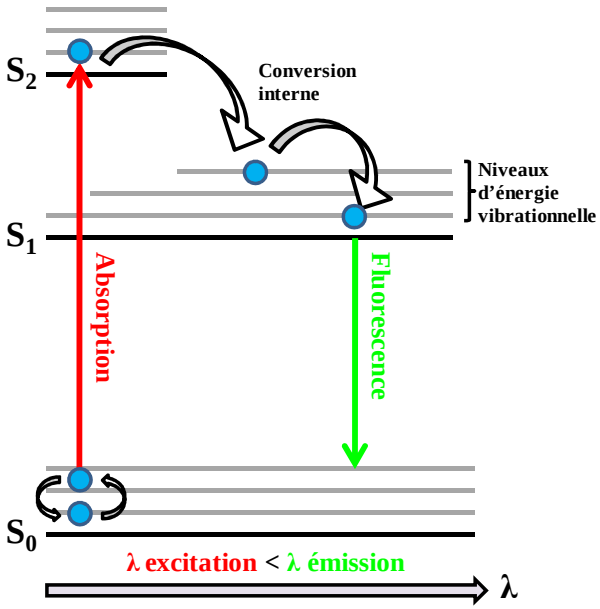

Figure I-4. *Diagramme simplifié de Jablonski illustrant le processus radiatif de fluorescence.*

3. 1. 2. Absorption de la CDOM

Le spectre d'absorption de la CDOM est continu, sans pic distinct du fait que la CDOM est un mélange complexe de nombreux chromophores, et il décroit de façon exponentielle avec l'augmentation de la longueur d'onde (Figure I-5 ; Bricaud et al., 1981) :

$$a_{CDOM}(\lambda) = a_{CDOM}(\lambda_0) \exp^{-S(\lambda - \lambda 0)} \qquad (1)$$

Où $a_{CDOM}(\lambda)$ est le coefficient d'absorption (m^{-1}) à la longueur d'onde λ, $a_{CDOM}(\lambda_0)$ est le coefficient d'absorption (m^{-1}) à la longueur d'onde de référence, et S est la pente spectrale (nm^{-1}). $a_{CDOM}(\lambda)$ est obtenu en utilisant la formule suivante :

$$a_{CDOM}(\lambda) = 2{,}303\ A(\lambda)/l \qquad (2)$$

Où $A(\lambda)$ est l'absorbance à la longueur d'onde λ ($A = \log I_0/I$, sans dimension), l est la longueur du chemin optique (m ou cm), et où le facteur 2,303 permet le passage du logarithme népérien en logarithme décimal.

La tendance linéaire de la transformation logarithmique du coefficient d'absorption de la CDOM le long d'une gamme de longueurs d'ondes a longtemps été utilisé pour calculer S (Jerlov, 1968 ; Bricaud et al., 1981). Cependant, des régressions non-linéaires fournissent de meilleures estimations de S en donnant plus de poids aux régions spectrales d'importance, c'est-à-dire dans le domaine UV où l'absorption de la CDOM est la plus élevée (Stedmon et al., 2000). De plus, la valeur de S dépend également de la gamme de longueur d'ondes utilisée pour la régression (Blough et Del Vecchio, 2002). Etant donné l'absence de méthode standard pour calculer S, il est important de spécifier à la fois la technique et la gamme de longueur d'ondes utilisée afin de permettre une inter-comparaison des résultats.

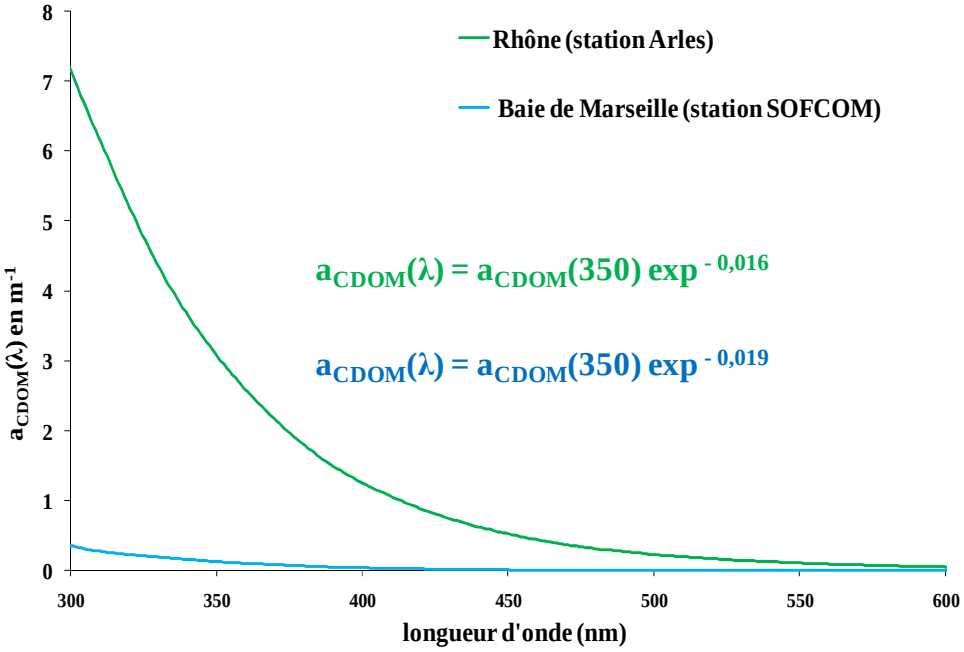

Figure I-5. *Spectres caractéristiques du coefficient d'absorption de la CDOM mesurés entre 300 et 600 nm dans un milieu relativement riche (Rhône ; vert) et pauvre en CDOM (Baie de Marseille ; bleu).*

La valeur du $a_{CDOM}(\lambda)$ fournit une information quantitative du contenu en CDOM de l'échantillon. Cette valeur est généralement donnée à une longueur d'onde se trouvant dans la gamme des 340-360 nm car cette gamme correspond aux plus courtes radiations reçues sur Terre et fournit donc un signal d'absorbance relativement élevé. Cependant, il est important de considérer que l'étude du $a_{CDOM}(\lambda)$ à d'autres longueurs d'ondes permet d'apporter des informations complémentaires (communication personnelle C. Stedmon). La gamme de variation du $a_{CDOM}(350)$ décrite dans la littérature pour divers environnements aquatiques est très grande. En effet, elle s'étend de 0,02 m^{-1} au niveau des eaux les plus claires du monde (Gyre du Pacifique Sud ; Tedetti et al., 2007; Bricaud et al., 2010) à plus de 30 m^{-1} dans les eaux noires de certaines rivières (Green et Blough, 1994 ; Moran et al., 2000).

La valeur de la pente spectrale (S) est un indicateur de l'origine de la CDOM. En effet, S présente généralement des valeurs élevées ($S > 0.018$ nm^{-1}) pour les systèmes océaniques où l'origine de la MO est autochtone et/ou photoblanchie, alors que ces valeurs sont plus faibles ($S < 0.018$ nm^{-1}) pour les zones côtières influencées par des apports en MO d'origine terrestre (Blough et Del Vecchio, 2002). Au niveau de ces zones côtières, la CDOM d'origine terrestre est très réactive (Figure I-6) car riche en DOM de haut poids moléculaire (HMWDOM) et en composés aromatiques comme la lignine (Opsahl et Benner, 1997).

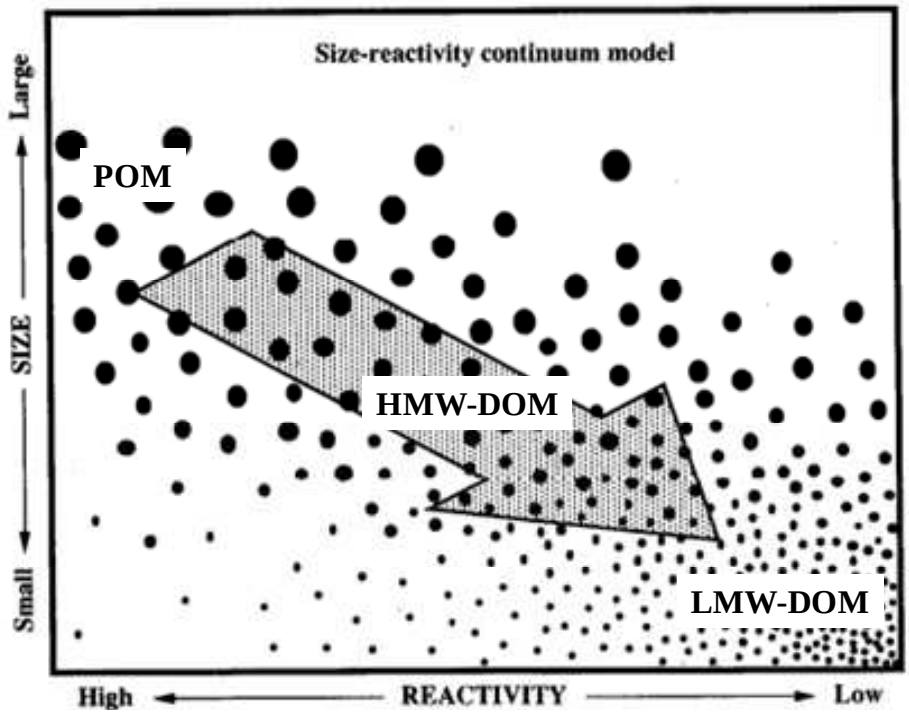

Figure I-6. *Diagramme schématique du modèle continu de la réactivité selon la taille pour la décomposition de la MO dans les environnements aquatiques. La taille des points est représentative de la taille de la MO et la flèche indique le sens de la réactivité (Amon et Benner, 1996).*

Lors de sa dégradation, la DOM est rapidement incorporée dans le pool biologique marin et participe à la formation de la CDOM autochtone récente, enrichie en DOM de bas poids moléculaire (LMWDOM) de type protéique et humique marin absorbant la lumière à de plus courtes longueurs d'ondes que la CDOM terrestre (Parlanti et al., 2000 ; Huguet et al., 2009). Les structures théoriques de ces divers composés organiques sont représentées dans la Figure I-7. Le processus de dégradation de la CDOM terrestre se traduit donc généralement par une augmentation de la pente spectrale S (Vodacek et al., 1997) qui illustre un transfert de matière depuis la HMWDOM vers la LMWDOM (Figure 6). Cette propriété permet d'expliquer qu'au niveau des zones côtières influencées par des apports d'eau douce, les processus de mélange et de dégradation de la CDOM terrestre avec de la CDOM marine se traduisent par une augmentation de S au delà d'une certaine salinité (Figure I-8 ; Blough et Del Vecchio, 2002 ; Coble, 2007).

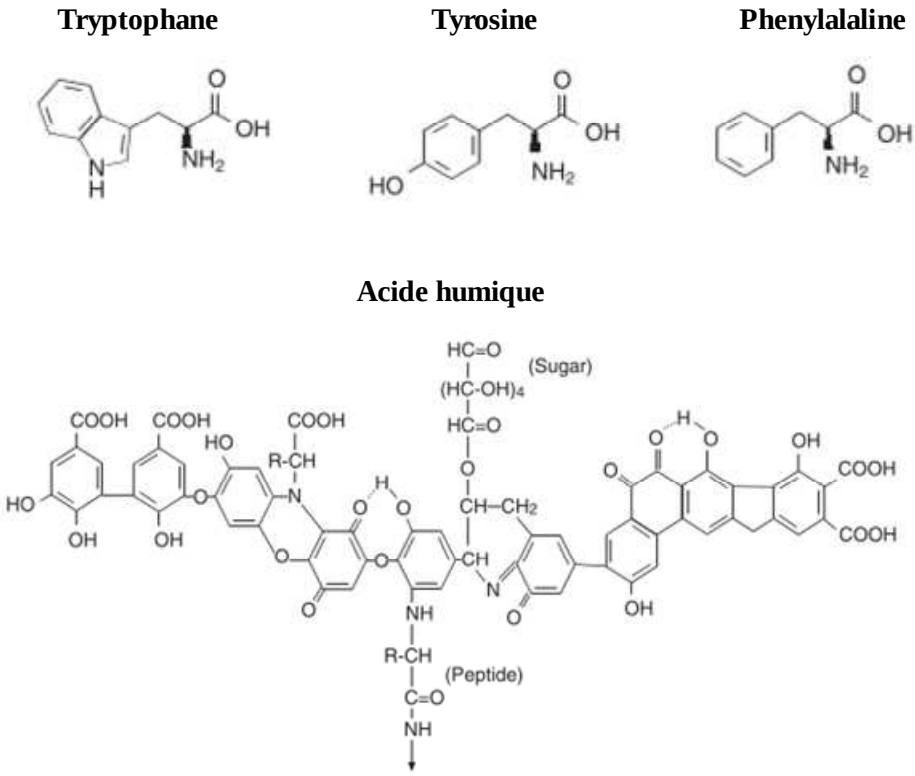

***Figure** I-7. Structures théoriques des composés de type protéique et humique marin (Hudson et al., 2007).*

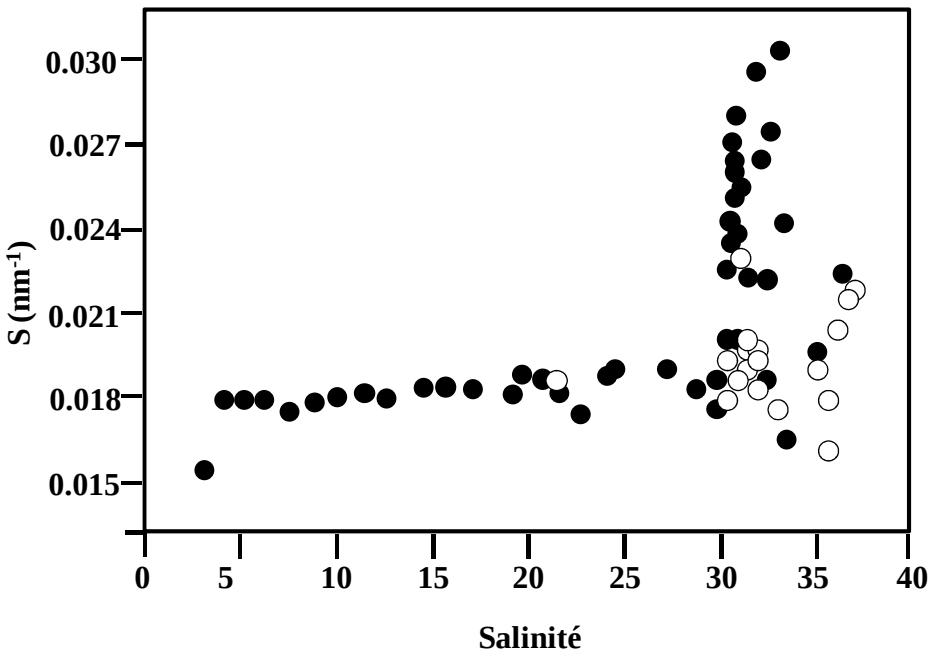

***Figure I-8.** Dépendance de la pente spectrale de la CDOM (S) avec la salinité observée dans (ronds noirs) et en dessous (ronds blancs) de la couche de surface d'une région côtière et tempérée de l'Océan Atlantique (d'après Blough et Del Vecchio, 2002)*

3. 1. 3. Fluorescence de la CDOM

Une fraction inconnue de la DOM est fluorescente et donc à fortiori absorbante ; cependant toutes les molécules absorbantes (chromophores) ne fluorescent pas. Cette propriété s'illustre en examinant les spectres d'absorbance et de fluorescence d'un échantillon naturel de DOM qui ne présentent respectivement aucun pic distinct (spectre continu, Figure I-5) et plusieurs pics distincts (spectre discontinu, Figure I-9). Chaque molécule organique fluorescente (fluorophore) présente des spécificités propres se caractérisant par (i) un couple de longueurs d'ondes d'excitation/émission (Ex/Em) où l'intensité de fluorescence est maximale, (ii) une durée de vie de fluorescence et (iii) un rendement quantique de fluorescence. La spectrofluorimétrie et l'ensemble des techniques de fluorescence sont par ailleurs beaucoup plus sensibles que la spectrophotométrie et donc fournissent des informations plus fines et pertinentes notamment lors d'études menées dans des milieux oligotrophes. En effet, l'analyse des spectres d'excitation et d'émission renseignent sur la nature des fluorophores contenus dans l'échantillon de DOM et permettent également d'appréhender les processus biotiques et abiotiques qui les affectent.

Actuellement la collection de matrices d'excitation-emission (EEMs) est la technique de fluorescence hyper-spectrale la plus performante et accessible pour étudier la CDOM (Hudson et al., 2007). Les EEMs sont obtenues par concaténation des spectres d'émission acquis le long d'une gamme d'excitation et fournissent au final une représentation en 3D des « pics » ou composés fluorescents (groupes de fluorophores) dominants dans l'échantillon (Figure I-9). Actuellement, 8 types principaux de composés fluorescents ont été identifiés dans les systèmes aquatiques (Tableau 1).

Tableau 1. *Principaux composés fluorescents identifiés dans les systèmes aquatiques (Coble et al., 1998 ; 2007)*

component	peak name	Ex/Em
tyrosine-like, protein-like	B	275/305
tryptophan-like, protein-like	T	275/340
unknown	N	280/370
UVC humic-like	A	260/400−460
UVA marine humic-like	M	290−310/370−410
UVA humic-like	C	320−360/420−460
pigment-like	P	398/660
UVA humic-like		250 (385)/504

EEM d'un échantillon naturel de CDOM

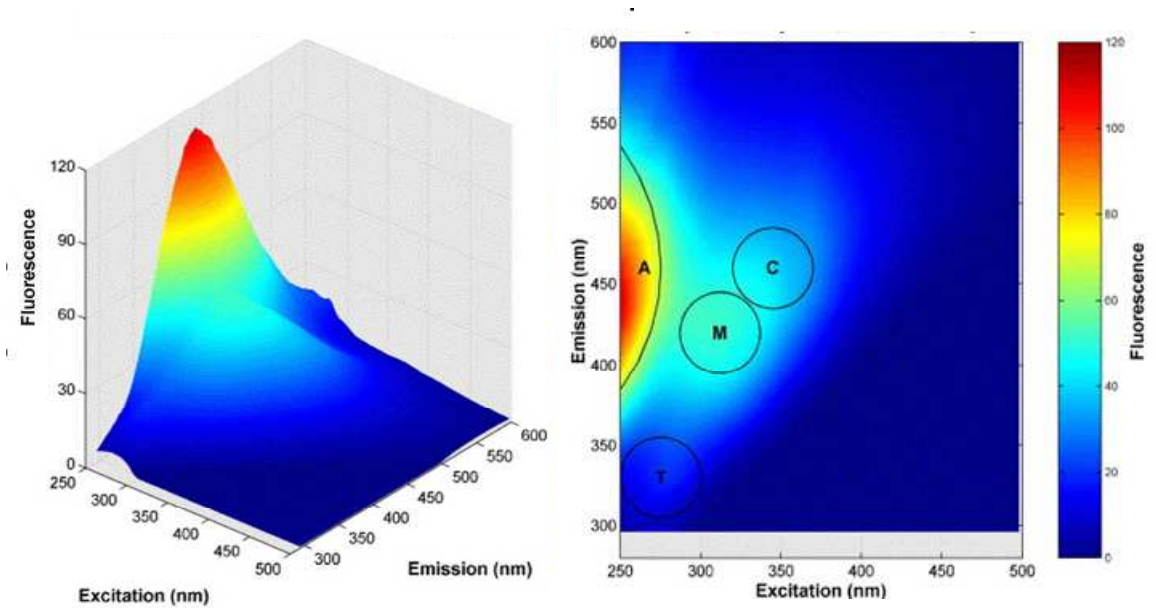

Figure I-9. *Représentations d'une matrice d'excitation-émission (EEM) d'un échantillon de CDOM collecté à proximité de l'estuaire de la Rivière Swina (faible salinité). Les lettres A, C, M et T représentent les pics fluorescents identifiés dans l'échantillon et les cercles délimitent les gammes d'excitation/émission correspondant à l'intensité maximale de fluorescence de ces pics (voir Tableau 1). Ces deux graphiques illustrent également que les spectres d'excitation et d'émission de la CDOM se composent de plusieurs pics distincts (Kowalczuk et al., 2005).*

Le pic UVA humic-like (pic C), d'origine essentiellement terrestre (Komada et al., 2002), présente, à proximité de sa source (zone de faible salinité), une intensité maximale de fluorescence pour le couple d'Ex/Em = 320-360/420-460 nm. En revanche, dans les eaux marines, ce pic présente une intensité maximale de fluorescence à un couple d'Ex/Em décalé vers le bleu (290-310/370-410 nm), qui correspond à celui de son homologue marin, le pic M, aussi appelé UVA marine humic-like (Figure I-10). Ce déplacement hypsochrome qui illustre une diminution du degré aromatique et du haut poids moléculaire caractéristiques de la CDOM terrestre est attribué à la synergie de processus tels que le mélange avec le matériel humique marin (moins aromatique) et les processus de dégradation/production dont notamment la photo-transformation (Del Castillo et al., 1999 ; Coble, 1996 ; Coble et al., 1998). Les pics protein-like (T et B), chlorophyll-like (P) et marine humic-like (M) résultent de l'activité biologique, notamment lors des efflorescences algales (Coble et al., 1998 ; Myklestad, 2000 ; Stedmon et Markager, 2005 ; Nieto-Cid et al., 2006 ; Romera-Castillo et al., 2010).

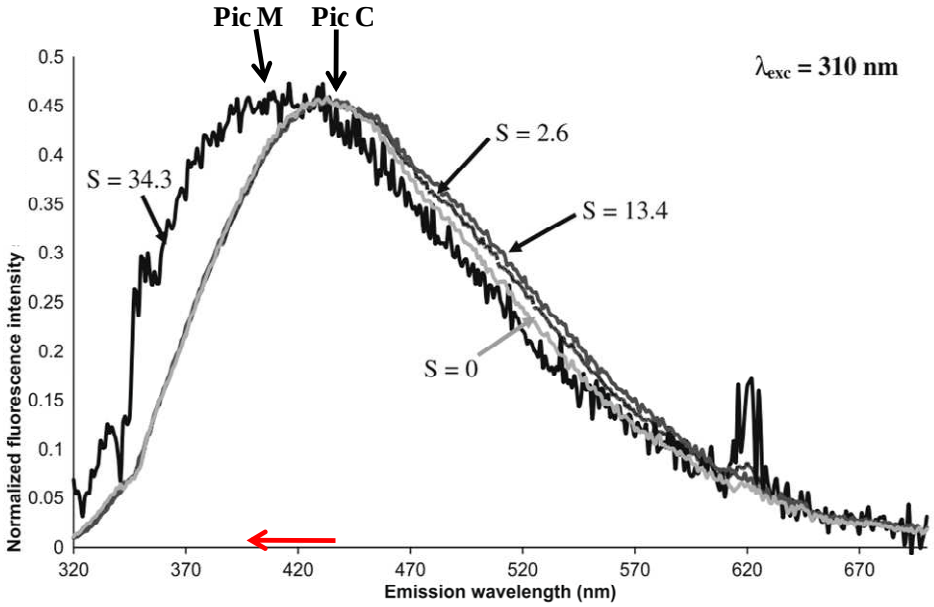

Figure I-10. *Spectres d'émission normalisés issus d'échantillons de CDOM collectés au niveau de l'estuaire de la Gironde selon une gamme de salinité variable (S = 0-34,3). La flèche rouge indique le déplacement hypsochrome de l'émission maximale du pic C (origine terrestre) vers celui de son homologue marin (pic M) (Huguet et al., 2009)*

L'analyse des données issues des EEMs s'est d'abord faite par simple observation de la présence des pics : technique du «peak picking ». Cette technique est souvent utilisée pour des jeux de données réduits (< 25 EEMs). Pour des jeux de données plus importants cette technique devient rapidement fastidieuse et difficile à interpréter. C'est pourquoi de nouvelles techniques d'analyses des données basées sur la statistique ont rapidement émergé comme l'analyse en composante principale (ACP) et l'analyse factorielle parallèle (PARAFAC ; annexe 3) qui sont désormais couramment utilisées et permettent d'appréhender de manière originale et rapide l'étude qualitative et quantitative de la fraction fluorescente de la CDOM (Stedmon et al., 2003 ; Boehme et al., 2004).

3. 2. Distribution de la CDOM dans l'océan

3. 2. 1. Sources de CDOM

Au niveau des zones côtières influencées par des apports fluviaux, la source principale de CDOM est d'origine terrestre. Cette dernière provient essentiellement de la décomposition des tissus constituant les végétaux terrestres supérieurs et présente donc une forte teneur en substances humiques (acides humiques et fulviques) caractérisées par un haut degré d'aromaticité (polyphénols) et un haut poids moléculaire. Ces caractéristiques intrinsèques confèrent à la CDOM terrigène une grande réactivité (Figure I-6) qui se traduit par une forte capacité à absorber la lumière. Ainsi, de nombreuses études menées dans les environnements côtiers rapportent une relation inverse entre le coefficient d'absorption de la CDOM et la salinité, illustrant le caractère conservatif de la CDOM allochtone (Figure I-11, courbe a).

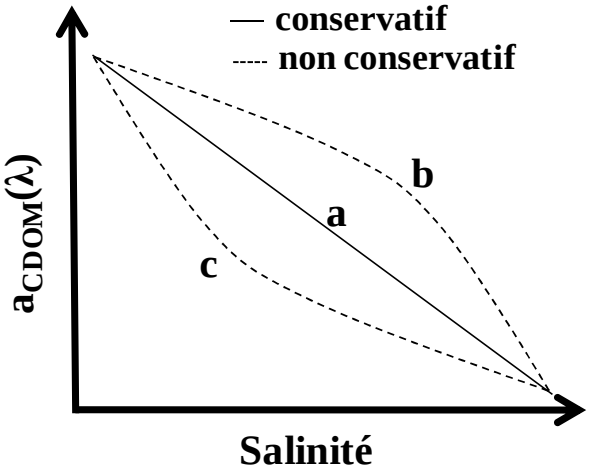

Figure I-11. *Courbes de mélange d'une eau riche en CDOM terrestre (faible salinité) avec de l'eau marine (forte salinité).*

Dans certains cas, cependant, l'allure des courbes de mélange suggère un caractère non conservatif de la CDOM terrigène (Figure I-11, courbes b et c) et renseigne sur l'existence de sources (Figure I-11, courbe b) ou de puits autochtones (Figure I-11, courbe c) de CDOM. Les sédiments et les upwellings côtiers sont également des sources ponctuelles importantes de CDOM d'origine autochtone plus ou moins récente, essentiellement de types protéique et humique marin (Mayer, 1999 ; Yamashita et Tanoue, 2003, 2004 ; Komada et al., 2002 ; Romera-Castillo et al., 2010). Il faut préciser aussi que ces zones exutoires reçoivent parfois

de la CDOM d'origine anthropique (eaux usées, activités agricoles, polluants ; Clark et al., 2007, Hudson et al., 2007).

Dans les régions côtières non influencées par des apports allochtones, l'origine de la CDOM est essentiellement biologique (autochtone). En effet, de nombreuses études ont montré l'implication de plusieurs échelons trophiques dans la production de CDOM (Nelson et al., 1998 ; Bricaud et al., 1981 ; Tranvik, 1993 ; Nagata, 2000 ; Kahru et Mitchell, 2001 ; Rochelle-Newall et Fisher, 2002, Steinberg et al., 2004, Romera-Castillo et al., 2010) dont les mécanismes de formation/dégradation restent encore à préciser du fait de la réponse singulière de chaque type de chromophores à ces mécanismes. Une autre source allochtone de CDOM potentiellement importante pour les zones oligotrophes proviendrait des dépôts atmosphériques contenus dans les pluies (Kieber et al., 2006).

3. 2. 2. Puits de CDOM

En l'absence de processus de dégradation de la CDOM se trouvant dans l'océan, la 'planète bleue' serait certainement appelée la 'planète jaune' en raison de l'accumulation des substances humiques. La photo-oxydation est le processus dominant de dégradation de la CDOM terrestre (Mopper et Kieber, 2000), alors que la CDOM autochtone est plus sensible à la biodégradation (Obernosterer et Benner, 2004). Cependant, ces deux processus sont étroitement liés et agissent de concert dans la dégradation de la CDOM. En effet, la dégradation bactérienne de la CDOM terrestre (bio-réfractaire) est favorisée après photo-oxydation du fait de la photo-production de substrats labiles plus aisément assimilables par le bactérioplancton (Kieber et al., 1990 ; Wetzel et al., 1995 ; Miller et Moran, 1997 ; Moran et al, 2000) alors que la dégradation bactérienne de la CDOM autochtone produit de la CDOM humique qui peut-être rapidement photo-dégradée (Stedmon et Markager, 2005). A cette synergie de processus de dégradation de la CDOM déjà complexe, s'ajoute le processus de photo-blanchiment de la CDOM. Ce processus provient de l'exposition de la CDOM aux rayonnements solaires UV dans les eaux de surface et se traduit par la perte de la propriété d'absorbance de la CDOM. Cette perte d'absorbance peut résulter d'une part, de la conversion de DOC en CO_2 (Miller and Zepp 1995) mais également d'une modification de la structure chimique de la MOD (Reche et al., 2000).

4. Le rayonnement solaire

4. 1. Au niveau de la surface terrestre

Le flux total de photons émis par le soleil et atteignant la surface terrestre est composé de différentes radiations présentant une énergie inversement proportionnelle à leur longueur d'onde. Il se compose de 1 à 5 % de radiations ultraviolettes (UVR : 280-400 nm), de 46 à 52 % de radiations actives pour la photosynthèse (PAR : 400-700 nm), et de 43 à 53 % de radiations infrarouges (IR : 700-1000 nm ; Whitehead et al., 2000). Les radiations les plus énergétiques, les UVR, sont reconnues pour avoir des effets délétères sur les systèmes et processus biologiques (Heisler et al., 2003 ; Häder et al., 2003 ; Diffey, 2004). Elles se décomposent en trois sous domaines spectraux : les UVR-C (200-280 nm), qui n'atteignent pas la surface terrestre car elles sont totalement absorbées par les molécules d'oxygène et d'ozone stratosphérique, les UVR-B (280-315 nm) et les UVR-A (315-400 nm), qui atteignent toutes deux la surface terrestre de manière atténuée. Cette atténuation, due à leurs transits à travers les différents compartiments atmosphériques, est particulièrement prononcée pour les UVR-B. Ceux-ci ne représentent en effet que 1 à 5% des UVR atteignant la surface terrestre, les UVR-A représentant les 95 à 99% restants.

Les principaux facteurs influençant l'intensité et la qualité des radiations solaires reçues au sol sont l'angle solaire (solar zenith angle : SZA), qui est fonction de la latitude et de facteurs astronomiques telles que les variations saisonnières et nycthémérales, et la couverture nuageuse. Ces deux facteurs impactent le rapport diffus/direct du rayonnement solaire atteignant la surface terrestre : plus le SZA ou l'épaisseur nuageuse augmente, plus le risque de rencontrer des molécules (vapeur d'eau, oxygène…) augmente, plus la fraction diffusive du rayonnement sera grande et plus la fraction directe du rayonnement sera petite (Figure I-12).

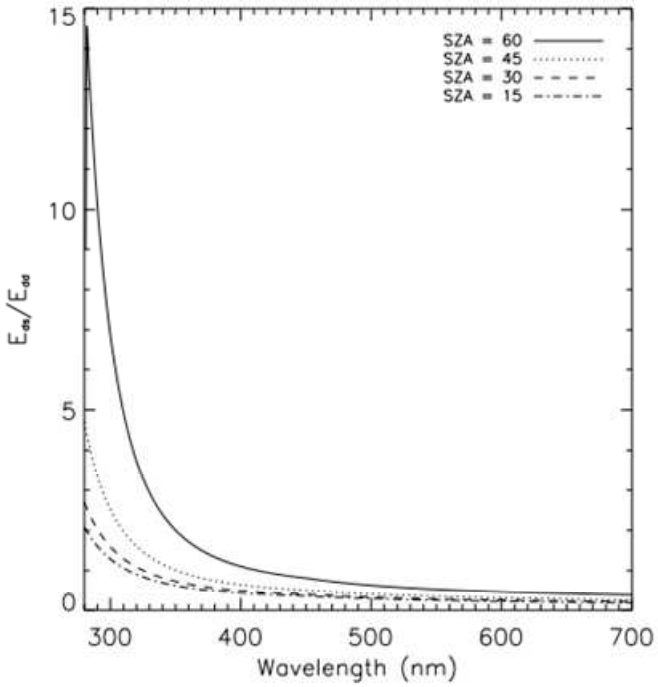

Figure I-12. *Dépendance spectrale du rapport: E_d diffus / E_d direct selon différents SZA (Vantrepotte et Mélin, 2006).*

Ensuite, d'autres facteurs tels que l'épaisseur de la couche d'ozone stratosphérique, l'albedo de surface, les aérosols atmosphériques et la pollution urbaine influencent le budget radiatif terrestre. Par exemple, la diminution de la couche d'ozone stratosphérique observée aux pôles mais également au niveau des latitudes moyennes (Hofman et Deshler, 1991 ; Smith et al., 1992 ; Kerr et McElroy, 1993 ; McKenzie et al., 1999) a initié de nombreuses études portant sur l'impact dans les écosystèmes du rayonnement UVR-B qui a augmenté depuis les années 1980 (WMO, 2003). La destruction de la couche d'ozone stratosphérique est liée à l'accumulation de gaz anthropogéniques tels que les chlorofluorocarbones (CFCs) (Molina et Rowland, 1974). Bien que les CFCs soient des composés désormais interdits depuis 1987 (Protocole de Montréal), ils persistent et agissent toujours dans l'atmosphère du fait de leur caractère rémanent (durée de vie des CFC dans l'atmosphère : 60-110 ans). D'autre part, dans un contexte de réchauffement global, s'ajoutent d'autres facteurs tels que la modification de la nébulosité et le refroidissement de la stratosphère qui pourraient avoir un impact sur les UVR atteignant le sol, mais dans des proportions non quantifiées à ce jour (McKenzie et al., 2003 ; Kerr et al., 2003 ; WMO, 2006). Ainsi, la proportion des UVR atteignant la surface terrestre pourrait être modifiée en fonction de l'intensité du changement global dans des modifications plus importantes que celles envisagées ne considérant que l'évolution des CFCs.

4. 2. Dans la colonne d'eau

La pénétration de la lumière ou inversement, l'atténuation de la lumière dans l'océan est appréhendée *via* la détermination du coefficient d'atténuation diffusive ($K_d(\lambda)$ en m^{-1}) de l'éclairement descendant ($E_d(\lambda)$ en W m^{-2} nm^{-1}). Ce dernier est un paramètre écologique et biogéochimique primordial dans l'océan. En effet, sa détermination dans le domaine spectral UV permet d'établir la profondeur limite où l'ensemble des processus photochimiques se déroulent et il intervient dans le calcul de flux de photo-produits, alors que dans le domaine spectral visible il permet d'établir la profondeur de la couche euphotique dans laquelle la production primaire se développe. K_d est déterminé à partir de la formule traduisant la décroissance exponentielle de E_d avec la profondeur (loi de Beer-Lambert ; Smith et Baker, 1978) :

$$E_d(Z,\lambda) = E_d(0^-,\lambda) \exp(-K_d(\lambda)\, Z) \qquad (3)$$

Où $E_d(Z,\lambda)$ et $E_d(0^-,\lambda)$ sont respectivement les éclairements descendant à la profondeur Z et juste au dessous de la surface de l'eau. $E_d(0^-,\lambda)$ est directement calculé à partir de l'éclairement de surface : $E_d(0^+,\lambda)$, en appliquant le facteur de perte d'éclairement par réflexion (albedo de Fresnel au midi solaire : $\alpha = 0{,}043$) à l'interface air-eau (loi de Fresnel) :

$$E_d(0^-,\lambda) = E_d(0^+,\lambda)/\ 1 + \alpha \qquad (4)$$

Dans certaines conditions (faible nébulosité, vent modéré), E_d présente dans les premiers mètres de la colonne d'eau d'intenses et rapides fluctuations (Figure I-13) produites par la focalisation des rayons à travers les vagues (Schenck, 1957). Ces fluctuations peuvent excéder d'un facteur cinq la valeur moyenne de l'éclairement descendant dans les premiers mètres (Dera and Stramski, 1986; Dera and Olszewski, 1978) et tendent à disparaitre quand l'éclairement devient diffus, c'est-à-dire au delà d'une certaine profondeur (profondeur focale) ou par ciel couvert (Stramska et Dickey, 1998). Généralement, les fluctuations de sub-surface de E_d sont assimilées à du bruit et ne sont donc pas considérées dans le calcul du K_d (Mueller and Austin, 1995). Cependant, il s'agit de l'éclairement réel observé sous la surface auquel toute la matière (organique et inorganique) est soumise et donc à partir duquel la détermination du K_d devrait se faire.

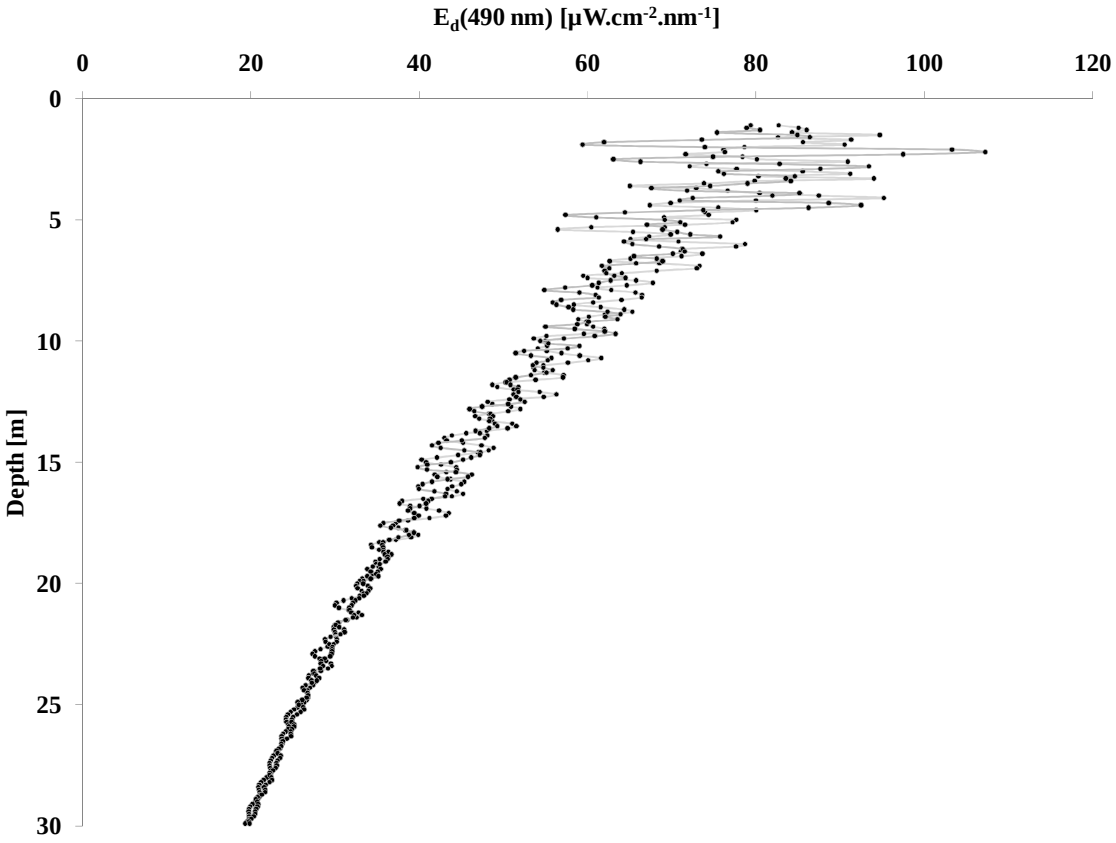

Figure I-13. *Profil de l'éclairement descendant à 490 nm mesuré en Baie de Marseille par temps calme et ensoleillé (éclairement direct) avec un profiler SATLANTIC.*

Pour déterminer et comparer la valeur de pénétration du rayonnement solaire UV et visible dans différentes provinces océaniques, on utilise respectivement la profondeur du 10% et du 1% d'éclairement descendant ($Z_{10\%}$ et $Z_{1\%}$ ou Z_{eu} en m) qui correspond à la profondeur où l'éclairement descendant vaut respectivement 10% et 1% de sa valeur de surface. En regard de la formule (3), cette profondeur de pénétration est donc inversement proportionnelle à la valeur du K_d :

$$Z_{10\%}(UV) = \ln(10)/K_d(UV) = 2{,}3 / K_d(UV) \qquad (5)$$

$$Z_{1\%}(PAR) \text{ ou } Z_{euph} = \ln(100)/K_d(PAR) = 4{,}6 / K_d(PAR) \qquad (6)$$

La distribution spectrale du rayonnement solaire dans la colonne d'eau est fonction de l'atténuation (absorption + diffusion) induite par l'ensemble des composés optiquement actifs présents dans le milieu, c'est-à-dire des propriétés optiques inhérentes (IOPs) au milieu. Dans

les océans, l'absorption totale (a_{tot}) résulte de l'absorption de quatre composés alors que la diffusion totale (b_{tot}) résulte de la diffusion de deux composés :

$$a_{tot}(\lambda) = a_W(\lambda) + a_{ph}(\lambda) + a_{CDOM}(\lambda) + a_{NAP}(\lambda) \quad (7)$$

$$b_{tot}(\lambda) = b_w(\lambda) + b_p(\lambda) \quad (8)$$

Où les indices w, ph, CDOM, NAP et p font référence respectivement à l'eau de mer pure, au phytoplancton, à la matière organique dissoute chromophorique, aux particules non algales et aux particules.

4. 3. Effets du rayonnement solaire sous marin :

4. 3. 1. Sur la CDOM

Les processus photo-chimiques sont initiés par l'absorption du rayonnement solaire par la CDOM (Zepp, 1988) et aboutissent, de manière directe et sensibilisée, c'est-à-dire *via* l'intervention d'espèces radicalaires, à la formation de photo-produits stables (Figure I-14). La photo-transformation de la CDOM se déroule majoritairement à la surface de l'océan (zone d'action des UVR) et se fait selon deux processus : un processus abiotique impliquant la production directe de CO et CO_2 (3-12 Gt C an^{-1} ; Mopper et Kieber, 2000 ; Johanessen et al., 2000) et un processus séquentiel abiotique/biotique impliquant la photo-production préalable de substrats plus ou moins labiles et leurs assimilations par le bactérioplancton formant ainsi de la biomasse et du CO_2 (Mopper et Kieber, 2002). La bio-disponibilité des substrats photo-produits dépend de l'origine de la CDOM irradiée (Obernosterer et al, 2001b ; Moran et Covert, 2003 ; Tedetti et al., 2009). En effet, l'irradiation de la CDOM présentant un important degré d'humification (la CDOM d'origine terrestre ou provenant des eaux profondes) aboutit à la production de substrats labiles stimulant la respiration et la production bactérienne (30-500 % ; Obernosterer et al., 1999a ; Mopper et Kieber, 2002 ; McCallister et al., 2005). A l'inverse, l'irradiation de la CDOM d'origine biologique récente (type protéique) produit des substrats bio-réfractaires diminuant la respiration et la production bactérienne (10-100 % ; Obernosterer et al., 2001b ; Tranvik et Bertilsson, 2001 ; Mopper et Kieber, 2002).

Les principaux effets et produits issus des processus photochimiques sont : l'oxydation et le blanchiment de la CDOM (Zepp, 1988 ; Kieber et al., 1990), la consommation d'oxygène

(Amon et Benner, 1996), la fragmentation moléculaire des substances humiques (Lindell et al., 1995), la production de gaz climatiquement actifs potentiellement transférables dans l'atmosphère tels que le monoxyde de carbone (CO, Johannessen et al., 2000), le dioxyde de carbone (CO_2, Mopper et al., 1991 ; Miller et Zepp, 1995) et le sulfure de carbonyle (SCO, Uher et Andreae, 1997). A cela se rajoutent la réduction des métaux traces (Faust, 1994), la production d'eau oxygénée (H_2O_2, Yocis et al., 2000), de phosphate (PO_4^{3-}, Francko et Heath, 1982) et d'ammonium (NH_4^+, Bushaw et al., 1996), et la production de composés organiques labiles de faible poids moléculaire (composés carbonylés et des acides mono-carboxyliques ; Mopper et Stahovec, 1986 ; Kieber et al., 1990 ; Mopper et al., 1991). Enfin, les processus photochimiques induisent la dégradation sensibilisée du dimethylsulfure (DMS ; Kieber et al., 1996 ; Bouillon et Miller, 2005) ainsi que la perte de substrats labiles par minéralisation (Bertilsson et Tranvik, 1998) ou par transformation en composés réfractaires suite à une succession de processus de condensation, polymérisation (Kieber et al., 1997 ; Kovac et al., 1998).

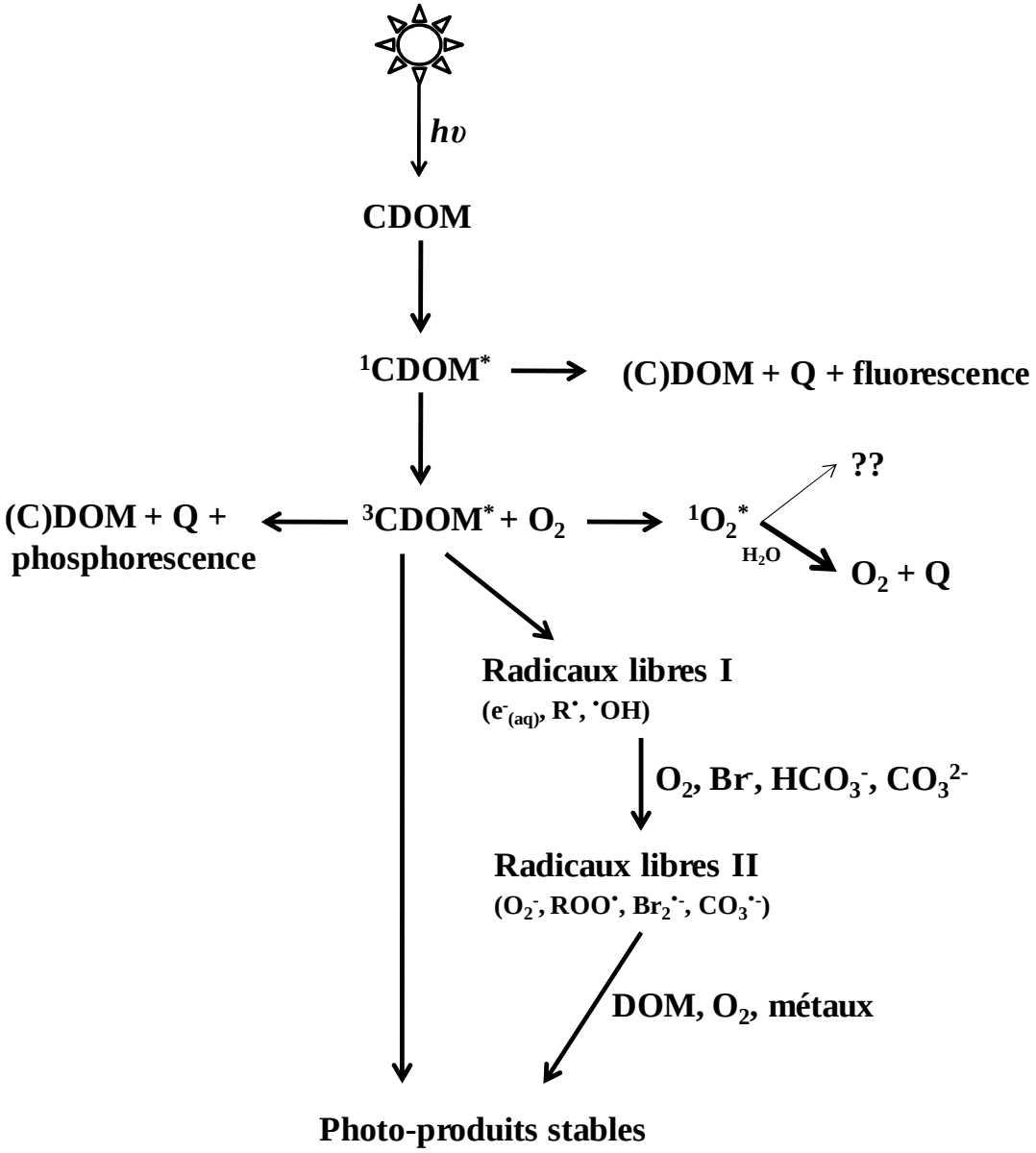

Figure I-14. *Photo-transformation de la CDOM : L'absorption du rayonnement solaire (hυ) par la CDOM produit des espèces à l'état excité singulet (^{1}CDOM*) puis triplet (^{3}CDOM*) qui vont revenir à leur état stable en dissipant l'énergie absorbée par émission de chaleur (Q) et de lumière (fluorescente et phosphorescente). Une partie de l'énergie est transférée à l'oxygène dissous (accepteur d'électrons) formant l'oxygène excité singulet ($^1O_2$*) qui se désactivera au contact des molécules d'eau. Le réarrangement ou la fragmentation moléculaire à partir de la ^{3}CDOM* aboutissent à la formation de photo-produits stables de manière directe ou via l'intervention de radicaux libres. Les radicaux libres I (très réactifs) vont interagir avec l'oxygène, l'ion bromure et le système des carbonates pour former des radicaux libres II qui aux contacts de l'oxygène, des métaux et de la DOM vont former des produits stables. Adapté de Mopper et Kieber (2000).*

4. 3. 2. Sur les organismes

Le rayonnement solaire joue un rôle vital pour la vie sur Terre en fournissant l'énergie nécessaire au développement des premiers maillons de chaque réseau trophique. Cependant, le rayonnement solaire et particulièrement les UVR induisent divers effets délétères sur l'ensemble des organismes vivants et impacte donc la structuration de l'écosystème dans sa globalité (Vincent and Roy, 1993). Ces effets néfastes ciblent préférentiellement et directement les organismes les 'moins évolués' caractérisés généralement par de petites tailles (bactéries) et dans une moindre mesure, les organismes « plus évolués » (plancton, poissons) ; ces derniers subissant majoritairement les effets délétères de manière indirecte du fait qu'ils se trouvent à des échelons trophiques supérieurs.

Parmi les différents dommages causés par le rayonnement solaire, ceux causés à l'ADN sont les plus importants. Les bactéries sont de petites tailles et pourvues d'un simple génome haploïde et donc ne peuvent pas se protéger efficacement contre les UVR en synthétisant des pigments photo-protecteurs tels que les acides aminés de type mycosporine (MAAs), qui sont présents chez de nombreuses cellules phytoplanctoniques (Garcia-Pichel, 1994). L'absorption directe de photons UVR-B par l'ADN entraîne la formation de liaisons entre des bases pyrimidines (Sinha et Häder, 2002). Les UVR-A entraînent quant à eux des dommages indirects qui résultent de l'absorption de photons par différents chromophores (NADH, NADPH, flavines, protéines). Ces molécules peuvent alors transférer leur énergie à l'ADN et l'endommager ou conduire à la formation d'espèces oxygénées réactives, qui vont à leur tour provoquer des dommages à l'ADN. Ces altérations mènent à l'inhibition de fonction biologique telles que la production de biomasse, la respiration et l'activité exo-enzymatique (Jeffrey et al., 2000).

5. Cadre et objectifs de la thèse

5. 1. Problématique

Les zones côtières, influencées par les apports nutritifs continentaux, concentrent 15 à 30% de la production primaire mondiale (Wollast, 1998 ; Muller-Karger et al., 2005) . Elles sont donc d'un intérêt majeur en océanographie, notamment concernant l'étude de leurs rôles dans les cycles biogéochimiques globaux. Ces environnements côtiers présentent des spécificités physiques, chimiques et biologiques particulièrement sensibles aux changements climatique et anthropique. Par exemple, le réchauffement et la stratification des eaux ainsi que l'augmentation des UVR pourraient stimuler la production et/ou la minéralisation de la MO. La multiplication et l'intensification des événements intenses (tempêtes et crues) devraient accentuer le transit de MO de la côte vers les océans. Afin de comprendre, caractériser et prédire la sensibilité de l'océan au changement climatique global, il est donc nécessaire d'appréhender au mieux la dynamique de la MO au niveau des interfaces terre/océan, même si la complexité des phénomènes mis en jeu (sources et puits de MO étroitement liés) et les variations temporelles des apports en MO rendent les bilans du devenir de la MO côtière très difficiles à établir.

5. 2. Objectifs de la thèse

Dans ce contexte, l'objectif général de cette thèse est d'améliorer les connaissances sur la nature et la dynamique de la (C)DOM des eaux de surface côtières de zones d'intérêts, et de déterminer l'impact de cette (C)DOM sur l'atténuation de l'éclairement UV-visible sous marin.

Les objectifs spécifiques sont donc (i) d'étudier la distribution des propriétés optiques d'absorbance et de fluorescence de la CDOM dans des eaux de surface côtières et (ii) de déterminer et d'expliquer la variabilité de l'atténuation du rayonnement solaire (UV-visible) dans ces eaux en fonction des facteurs bio-optiquement actifs, dont spécialement la CDOM.

5. 3. Zones d'étude

Les deux principaux sites où ces questions scientifiques sont abordées sont la Baie de Marseille (Mer Méditerranée Nord-Occidentale) et le plateau Canadien de la Mer de Beaufort (Océan Arctique). La Mer Méditerranée et l'Océan Arctique sont qualifiés de « hotspot » pour l'étude des changements climatiques (Arctic Climate Impact Assessement, ACIA, 2005 ; The Mermex group, 2011). De plus, ces deux systèmes océaniques côtiers présentent de forts contrastes en termes d'anthropisation, d'apports allochtones, et d'éclairement solaire. La zone côtière en Méditerranée Nord-Occidentale peut être considérée comme un modèle des aires côtières des latitudes moyennes (5°17'30''E, 43°14'30''N) à fort ensoleillement et situées à proximité de sources allochtones naturelles et anthropiques (respectivement le fleuve Rhône et la zone urbaine de la ville de Marseille), alors que la zone côtière de la Mer de Beaufort en Océan Arctique peut être considérée comme un cas d'étude typique de système côtier des hautes latitudes (125°-140°W, 68°-72°N) soumis à un éclairement lumineux continu et à des apports fluviaux importants lors du dégel (printemps-été).

La Mer Méditerranée est une mer oligotrophe semi-fermée, constituée de deux bassins, et présentant un gradient Ouest-Est d'oligotrophie (Figure I-15). Les eaux méditerranéennes présentent un court temps de résidence (70 ans) et une circulation thermohaline propre (The Mermex group, 2011 et références internes). Du fait de sa faible couverture nuageuse, la Méditerranée présente un fort taux d'ensoleillement comparé à d'autres zones océaniques tempérées (Bishop et Rossow, 1991). Cela a un impact important sur la photochimie et la biologie des eaux Méditerranéennes oligotrophes, soumises à une forte pénétration du rayonnement solaire (Tedetti et Sempéré, 2006). Ces caractéristiques font de la Mer Méditerranée un site unique pour étudier les changements climatiques, notamment au regard de son haut potentiel photochimique. Les apports hydriques majeurs en Méditerranée proviennent de l'Atlantique *via* le détroit de Gibraltar, de la Mer Noire *via* le détroit du Bosphore, et des fleuves. Depuis la mise en service du barrage d'Assouan en 1974, le Rhône est devenu le principal fleuve de Méditerranée, contribuant à 50% des apports d'eau douce et de matière, favorisant ainsi la production biologique du bassin Occidental et accentuant le gradient Ouest-Est d'oligotrophie (Margat, 1992).

La première partie de ces travaux de thèse s'est déroulée en Baie de Marseille, au niveau de la station de référence SOFCOM (5°17'30''E, 43°14'30'' N). Cette station d'observation est localisée à 5 km des côtes de l'agglomération marseillaise (900 000

habitants, 3300 hab/km^2) et est étudiée depuis 1994 (http://somlit.epoc.u-bordeaux1.fr/fr/). Elle est située dans une zone oligotrophe soumise à un éclairement solaire de surface relativement important et ne présentant pas d'apports significatifs de matières allochtones. Cependant, des dessalures (salinité < 38) pouvant illustrer l'extension du panache du Rhône jusqu'au large des côtes de Marseille (Gatti et al., 2006). ont été observées de manière récurrente en début de période estivale dans les eaux de surface et intermédiaires (20-30m).

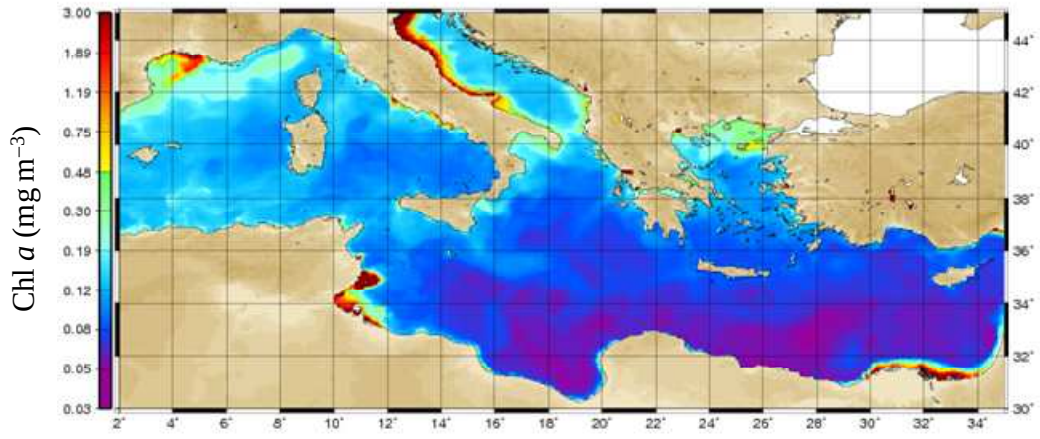

Figure I-15. *Image satellite représentant la concentration moyenne en chlorophylle-a en Juin 2008 en Mer Méditerranée (source : E. Bosc)*

L'Océan Arctique est un acteur primordial de la machine climatique terrestre. Il permet notamment de réguler les transferts d'énergie (chaleur) de la planète au travers de la formation d'eau dense (froide et salée) qui alimentent ensuite la circulation océanique globale (circulation thermohaline). Bien que l'Océan Arctique ne représente que 1% du volume de l'Océan Global, il reçoit annuellement 11% des apports fluviaux mondiaux (Opsahl et al., 1999 ; Rachold et al., 2004). Ces eaux douces s'étalent en surface pour former la couche polaire de mélange (PML) riche en MOD terrestre (Opsahl et al., 1999; Amon and Meon, 2004). L'Arctique suscite depuis quelques années une attention particulière à mesure que les symptômes des changements climatiques globaux s'y accumulent et s'y amplifient. Actuellement les régions Arctiques sont sujettes à plusieurs changements. D'une part, la fonte du permafrost, qui séquestre 50% du stock de carbone organique mondial (Tarnocai et al., 2009), couplée à une augmentation du débit des fleuves (+ 7% ; Peterson et al., 2002), entraîne une hausse de l'export du carbone organique terrestre en mer. L'Arctique subit par ailleurs une augmentation du rayonnement UV (WMO, 2003 ; ACIA, 2005), ainsi qu'une réduction du couvert estival de glace, qui a pour conséquence d'exposer la surface de l'océan au rayonnement solaire et aux forçages physiques (Barber and Hanesiak, 2004). Ces

phénomènes sont favorables à une hausse de la minéralisation biotique/abiotique de la matière organique et donc à une augmentation du CO_2 atmosphérique.

La deuxième partie des travaux de thèse s'est déroulée au niveau du Plateau Canadien (125°-140°W, 68°-72°N) de la Mer de Beaufort (Océan Arctique Ouest, Figure I-16), en été (2009). Ce vaste plateau continental de 80 m de profondeur en moyenne se trouve dans les territoires canadiens du Nord Ouest et est très peu peuplé (0,03 hab./km^2). Durant la période libre de glace (Juin-Septembre), il est fortement influencé par des apports allochtones issus de la crue printanière du Mackenzie. Le Mackenzie est le fleuve d'Arctique exportant le plus de matière organique particulaire, et le troisième plus important fleuve au monde concernant l'export de carbone organique total d'origine terrigène (Rachold et al., 2004). L'éclairement quasi perpétuel durant cette période favoriserait la minéralisation de la MO allochtone ainsi que la photo-production de substrats labiles (Osburn et al., 2009). Cependant la faible pénétration du rayonnement solaire induite par le panache du Mackenzie, ainsi que le couvert de glace résiduel et la faible élévation du soleil rendent les effets photo-dégradatifs très variables dans cette zone (Johannessen et Miller, 2001; Osburn et al., 2009).

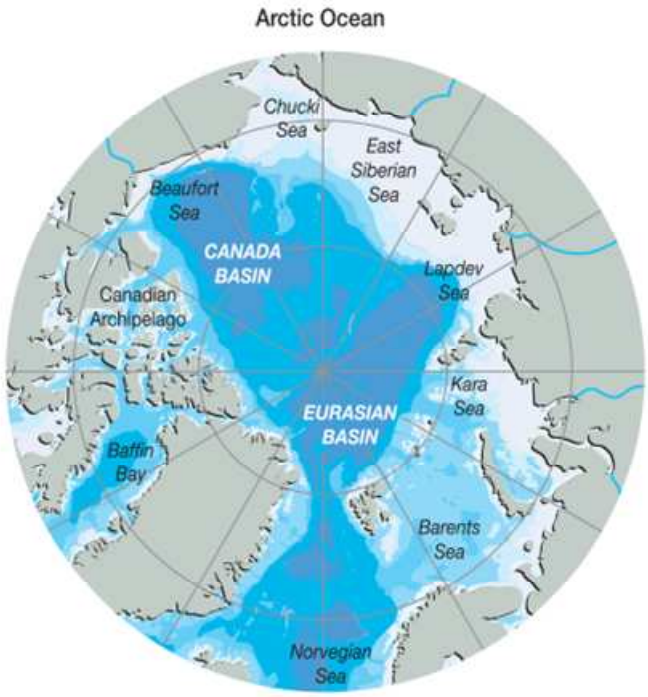

Figure I-16. *Carte de l'Océan Arctique (source : http://maps.grida.no/go/graphic/arctic-ocean)*

5. 4. Déroulement de la thèse – stratégie

Cette étude multidisciplinaire a nécessité le développement au laboratoire de nouvelles techniques d'analyses basées sur la spectrométrie, dont la spectrophotométrie et la

spectrofluorimétrie. Ces techniques d'analyses permettent d'acquérir des spectres permettant de quantifier et qualifier les chromophores et fluorophores contenus dans des échantillons de DOM naturels. Le traitement et l'interprétation des données issues de ces spectres a nécessité une importante exploration bibliographique afin d'identifier et de déterminer les paramètres et les méthodes d'analyses les plus pertinents, telles que l'identification et la quantification des fluorophores via la méthode d'analyse statistique PARAFAC (Annexe 3). Un autre aspect de ce travail a consisté à effectuer des mesures radiométriques du rayonnement solaire UV-visible atmosphérique et sous marin avec un profileur sous-marin (SATLANTIC OCR-504), en association avec des prélèvements hydrologiques discrets, afin de déterminer les concentrations en CDOM, en DOC et en composés labiles comme les sucres et les acides dicarboxyliques. Ces mesures radiométriques et prélèvements hydrologiques ont été effectués mensuellement en Baie de Marseille à la station SOFCOM (étude temporelle) entre Novembre 2007 et Décembre 2008, ainsi qu'au niveau du Rhône à la station d'Arles, sur la même période et dans le cadre du programme d'observation du COM (PI: P. Raimbault) et du programme de l'ANR CHACCRA (PI: C. Rabouille). En Mer de Beaufort, des mesures radiométriques et prélèvements hydrologiques similaires ont été effectués durant l'été 2009 dans le cadre du programme de l'ANR MALINA (Mackenzie Light and Carbon, PI. M. Babin). Ce travail a également été complété par des expériences d'irradiation de DOM issue du Rhône afin de mieux appréhender le processus de photoblanchiment de la CDOM d'origine terrestre. Cette étude s'inscrit dans les objectifs définis par le programme international SOLAS (http://www.solas-int.org/) de l'IGBP (http://www.igbp.kva.se/).

5. 5. Organisation du manuscrit

Ce manuscrit est organisé sous forme d'articles publiés ou en préparation (Chapitre 2, 3 et 4) rédigés en anglais et précédés d'un résumé en français, ainsi que d'un chapitre de conclusions et perspectives. L'étude des propriétés de fluorescence et d'absorbance de la CDOM dans les eaux de surface de la Baie de Marseille est abordée dans le Chapitre 2 de ce manuscrit. L'étude de l'atténuation du rayonnement UV et PAR en relation avec les paramètres biogéochimiques dans les eaux côtières de la Baie de Marseille est décrite dans le chapitre 3. Les propriétés optiques de la CDOM et l'atténuation du rayonnement solaire dans les eaux de surface de la mer de Beaufort sont étudiées dans le chapitre 4. Enfin le chapitre 5 de conclusion et perspectives synthétise les faits marquants de ce travail et donne quelques pistes pour des recherches futures.

CHAPITRE II

PROPRIETES OPTIQUES DE LA CDOM DANS LES EAUX DE SURFACE DE LA BAIE DE MARSEILLE

Dans le cadre de l'ANR CHACCRA (P.I. C. Rabouille, LSCE), des échantillons d'eau de mer ont été collecté chaque mois dans les eaux de surface (à 2 et 5 m de profondeur) en Baie de Marseille (Méditerranée Nord-Occidentale; 5°17'30"E, 43°14'30"N) pendant un an, de Novembre 2007 à Décembre 2008. L'étude a porté sur la compréhension des propriétés optiques (absorption et de fluorescence) de la CDOM. La valeur annuelle moyenne de l'absorption à 350 nm de la CDOM dans les eaux de surface [$a_{CDOM}(350)$] était très faible ($0,10 \pm 0,02$ m^{-1}) par rapport aux valeurs habituellement trouvées dans les eaux côtières, et aucune tendance saisonnière significative du $a_{CDOM}(350)$ n'a pu être mise en évidence. En revanche, la pente spectrale d'absorption de la CDOM (S_{CDOM}) était significativement plus élevée ($0,023 \pm 0,003$ nm^{-1}) en été qu'en automne et en hiver ($0,017 \pm 0,002$ nm^{-1}), reflétant soit un photoblanchiment de la CDOM soit une production de CDOM fraîche dans les eaux de surface stratifiées en été. La fluorescence de la CDOM, évaluée par des matrices d'excitation-émission (EEM), reflétait majoritairement la présence de composés biologiques de type protéique (pic T; 1.30-21.94 QSU) et humique marin (pic M; de 0.55 à 5.82 QSU), et la fluorescence issue de composés d'origine terrestre (pic C; 0,34 à 2,99 QSU) restait très faible tout au long de l'année. À la fin de l'été, la fluorescence de la CDOM en surface était très faible et fortement décalée vers le bleu, ce qui renforce l'hypothèse de photoblanchiment de la CDOM. Par ailleurs, des images satellite suggèrent que des intrusions épisodiques du panache du Rhône peuvent atteindre la Baie de Marseille en 2-3 jours et induire une augmentation de la production primaire, identifiable par les pics M et T, sans qu'aucune signature terrestre significative ne soit pourtant mesurée. Il est aussi apparut que les événements de mélange de la colonne d'eau sont une source importante de CDOM dans les eaux de surface de la Baie de Marseille, car ils se traduisent notamment par des transferts de CDOM relativement âgée (pics C et M) du fond vers les eaux de surface. Ainsi, la détermination des propriétés optiques de la

CDOM dans un contexte hydrobiologique à permis la mise en évidence de plusieurs facteurs biotiques (production biologique *in situ* et issue de la plume du Rhône) et abiotiques (photoblanchiment, mélange de la colonne d'eau) contrôlant la production et la dynamique de la CDOM en zone côtière de la mer Méditerranée Nord-Occidentale.

FLUORESCENCE AND ABSORPTION PROPERTIES OF CDOM IN COASTAL SURFACE WATERS OF THE NORTHWESTERN MEDITERRANEAN SEA, INFLUENCE OF THE RHONE RIVER

Julien Para[1, 2], Paula Coble[3], Bruno Charrière[1, 2], Marc Tedetti[1, 2], Clément Fontana[4, 5] and Richard Sempéré[1, 2]

[1] *Université de la Méditerranée, LMGEM, Centre d'Océanologie de Marseille, Case 901, 13288 Marseille Cedex 9, France*

[2] *CNRS/INSU, UMR 6117, LMGEM, Case 901, 13288 Marseille Cedex 9, France*

[3] *College of Marine Science, University of South Florida, 140 7th Avenue, St. Petersburg, Florida 33701*

[4] *Université de la Méditerranée, LOPB, Centre d'Océanologie de Marseille, UMR 6535, Station Marine d'Endoume, Chemin Batterie des Lions, F13007 Marseille, France*

[5] *CNRS/INSU, UMR 6535, LOPB, Centre d'Océanologie de Marseille, Station Marine d'Endoume, Chemin Batterie des Lions, F13007 Marseille, France*

Biogeosciences (2010): 7, 4083-4103

1. Abstract

Seawater samples were collected monthly in surface waters (2 and 5 m depths) of the Bay of Marseilles (northwestern Mediterranean Sea; 5°17'30''E, 43°14'30''N) during one year from November 2007 to December 2008 and studied for total organic carbon (TOC) as well as chromophoric dissolved organic matter (CDOM) optical properties (absorbance and fluorescence). The annual mean value of surface CDOM absorption coefficient at 350 nm [$a_{CDOM}(350)$] was very low (0.10 ± 0.02 m^{-1}) in comparison to values usually found in coastal waters, and no significant seasonal trend in $a_{CDOM}(350)$ could be determined. By contrast, the spectral slope of CDOM absorption (S_{CDOM}) was significantly higher (0.023 ± 0.003 nm^{-1}) in summer than in fall and winter periods (0.017 ± 0.002 nm^{-1}), reflecting either CDOM photobleaching or production in surface waters during stratified sunny periods. The CDOM fluorescence, assessed through excitation emission matrices (EEMs), was dominated by protein-like component (peak T; 1.30-21.94 QSU) and marine humic-like component (peak M; 0.55-5.82 QSU), while terrestrial humic-like fluorescence (peak C; 0.34-2.99 QSU) remained very low. This reflected a dominance of relatively fresh material from biological origin within the CDOM fluorescent pool. At the end of summer, surface CDOM fluorescence was very low and strongly blue shifted, reinforcing the hypothesis of CDOM photobleaching. Our results suggested that unusual Rhône River plume eastward intrusion events might reach Marseilles Bay within 2-3 days and induce local phytoplankton blooms and subsequent fluorescent CDOM production (peaks M and T) without adding terrestrial fluorescence signatures (peaks C and A). Besides Rhône River plumes, mixing events of the entire water column injected relative aged (peaks C and M) CDOM from the bottom into the surface and thus appeared also as an important source of CDOM in surface waters of the Marseilles Bay. Therefore, the assessment of CDOM optical properties, within the hydrological context, pointed out several biotic (*in situ* biological production, biological production within Rhône River plumes) and abiotic (photobleaching, mixing) factors controlling CDOM transport, production and removal in this highly urbanized coastal area.

2. Introduction

Dissolved organic matter (DOM) represents one of the largest bioreactive organic reservoirs at earth's surface (Hedges, 1992; 2002) and constitutes the main substrate for heterotrophic bacteria growth (Azam et al., 1983). The dominant source of DOM in the ocean is phytoplankton through release of organic compounds during bacterial and viral lysis, exudation, excretion and grazing (Mague et al., 1980; Jumars et al., 1989; Nagata, 2000; Myklestad, 2000). Though the inputs of terrestrial DOM represent only 0.7-2.4% of the total oceanic DOM pool, river inputs may be important in coastal oceanic areas (Opsahl and Benner, 1997) by fueling alternative labile carbon source to sustain local carbon demand in addition to autochthonous carbon source derived from phytoplankton and heterotrophic microbial food web (Sempéré et al., 2000) and increasing light attenuation (Blough and Del Vecchio, 2002; Nelson and Siegel, 2002).

Chromophoric (or colored) dissolved organic matter (CDOM), which is the fraction of DOM that absorbs light over a broad range of ultraviolet (UV) and visible wavelengths, is essentially controlled by *in situ* biological production, terrestrial inputs (sources), photochemical degradation, microbial consumption (sinks), as well as deep ocean circulation (Siegel et al., 2002; Nelson et al., 2007; Coble, 2007) and upwelling and/or vertical mixing (Coble, 1996; Parlanti et al., 2000). CDOM is the major factor controlling the attenuation of UV radiation in the ocean (Kirk, 1994) and is highly photoreactive and efficiently destroyed upon exposure to solar radiation (Mopper and Kieber, 2000; 2002).

In the past 20 years, CDOM fluorescence properties have been widely studied owing to excitation-emission matrices (EEMs). Coble et al. (1990) highlighted that the fluorescence properties of the Black Sea CDOM came from two types of fluorescent peaks (humic-like and protein-like). Protein-like fluorescence, considered as a proxy for labile DOM (Yamashita and Tanoue, 2003), has been frequently reported (Mopper and Schultz, 1993; De Souza-Sierra et al., 1994; Determann et al., 1994, 1996; Coble 1996; Mayer et al., 1999). The identification/quantification of humic-like and protein-like peaks from EEMs has thus allowed determining the dynamics of DOM in relation to its biological reactivity. In addition, fluorescence indices have also been used to assess the origin and dynamics of fluorescent CDOM, especially in the coastal areas subjected to freshwater inputs. The humification index (HIX, Zsolnay et al., 1999) and the biological index (BIX, Huguet et al., 2009) have been

employed to determine the relative degree of humification and autotrophic productivity of fluorescent CDOM, respectively.

Freshwater inputs play a major role in the biogeochemistry of the coastal areas with a world annual fresh water discharge of 40,000 km^3, more than 25 billions tons of particulate and dissolved matter (Milliman et al., 1995) and transporting on average 1±0.2Gt of carbon per year in particulate and dissolved forms (Amiotte-Suchet et al., 2003). In the Mediterranean Sea, freshwater inputs enhance significantly primary productivity (Cruzado and Velasquez, 1990; Joux et al., 2009). The annual fluvial loading of TOC to the Mediterranean Sea comprises 0.08-0.3% of the standing stock of TOC in the whole Mediterranean Basin (Sempéré et al., 2000), which is much higher than the average value reported for the World Ocean (0.024%, Smith and Hollibaugh, 1993). Since the damming of the Nile, the Rhône River became the major source of fresh water and terrigenous particles to the Mediterranean basin (Margat, 1992). Its mean freshwater discharge is around 1700 $m^3 s^{-1}$, which represents 90% of the total freshwater input in the Gulf of Lion's continental shelf (Durrieu de Madron et al., 2003) and ~ 3-14% and 10-12% of the overall total organic and inorganic carbon (TOC and TIC) river inputs to the Mediterranean Sea (Sempéré et al., 2000). Remote sensing observations (Forget et al., 1990; Devenon et al., 1992; Broche et al., 1998) and modeling studies (Estournel et al., 2001; Arnoux-Chiavassa et al., 2003; Reffray et al., 2004) shown the predominant westward direction of the Rhône River plume with an extent and a thickness depending on its discharge, the meteorological conditions and the surrounding circulation, particularly the Northern Current. A less common orientation of the Rhône River plume, towards the east as far as 40 km from the Rhône River mouth and offshore of Marseilles Bay, has been recently documented by using the acoustic Doppler current profiler (ADCP) measurements (Gatti et al., 2006).

Despite its relative significant role in the Mediterranean carbon cycle, there are only a few studies showing CDOM originating either directly from the Rhône River or from by-products of primary production in coastal areas or more generally in the northwestern Mediterranean Sea (Ferrari et al., 2000; Babin et al., 2003; Vignudelli et al., 2004). Moreover, with an annual average of total solar radiation of 162 W m^{-2} (Ruiz et al., 2008), the western Mediterranean basin is characterized by relatively high solar radiation levels due to its weak cloud cover (Vasilkov et al., 2001; Seckmeyer et al., 2008; Cristofanelli and Bonasoni, 2009; the Mermex group, submitted). High surface irradiances coupled to a strong penetration of UV and visible radiation (Tedetti and Sempéré, 2006 and references therein; Joux et al., 2009)

could impact the CDOM content as well as primary productivity in the surface waters of the Mediterranean Sea.

Here we report CDOM absorbance and fluorescence data from a one-year time series in the Bay of Marseilles. This study aims to better understand coastal surface CDOM distribution and dynamics of the Mediterranean Sea. Origins as well as seasonal variation of CDOM are discussed considering the potential influence of Rhône River plume.

3. Material and method

3. 1. Study site and sample collection

From November 2007 to December 2008, surface seawater samples (2 and 5 m depths) were collected monthly close to solar noon on board the R/V Antedon II at the observation station of the Oceanology Center of Marseilles: SOFCOM. This coastal station is located 5 km off Marseilles in the northwestern Mediterranean Sea (Fig. II-1) and is one of the French Service d'Observation en Milieu LITtoral (SOMLIT, http://www.domino.u-bordeaux.fr/somlit national/) coastal stations, which have been regularly sampled (twice a month) for 13 years. Samples were collected using Niskin bottles equipped with Teflon-O-ring and silicon tubes. Surface irradiance ($E_s(\lambda)$ in µW. cm^{-2}) measurements in the UV (305, 325, 340, 380 nm) spectral domain were also performed using OCR-504 downward irradiance sensors on the ship's deck. During this study period, water samples were also collected at 2 m depth in the Rhône River at Arles station, and from 2 and 5 m depths at two stations in the Rhône River Estuary during the CHACCRA-plume cruise (May 2008) (Fig. II-1).

For TOC determination, samples were directly transferred from the Niskin bottle into precombusted (6 h at 450 °C) ampoules, immediately acidified with 85% of H_3PO_4 (final pH ~2) and flame sealed without filtration. For the determination of CDOM optical properties (absorbance and fluorescence), samples were transferred from Niskin bottles into 10% HCl washed and precombusted (6 h at 450 °C) glass bottles and stored in the dark. Samples were brought back to the laboratory, filtered in dim light through precombusted 0.7 µm GF/F filters, which had been pre-rinsed with Milli-Q water and sample, and then through 0.2 µm Nuclepore polycarbonate filters, presoaked in 10% HCl solution and rinsed with Milli-Q water and with sample according to the SeaWiFS protocols (Mueller and Austin, 1995).

Filtered samples were kept in the dark at room temperature (24 h maximum) until absorbance and fluorescence analyses. During the study period, *in situ* hydrological context was determined at least twice a month by the Service d'Observation of the Oceanology Center of Marseilles by using a SeaBird Electronics 19*plus* conductivity temperature depth (CTD) profiler. In addition, from February 2008 onwards, the hydrological data set was completed with a SeaBird Electronics 19*plus* CTD equipped with chlorophyll *a* (Chl*a*) fluorometer (WET Labs Inc.) deployed during our sampling.

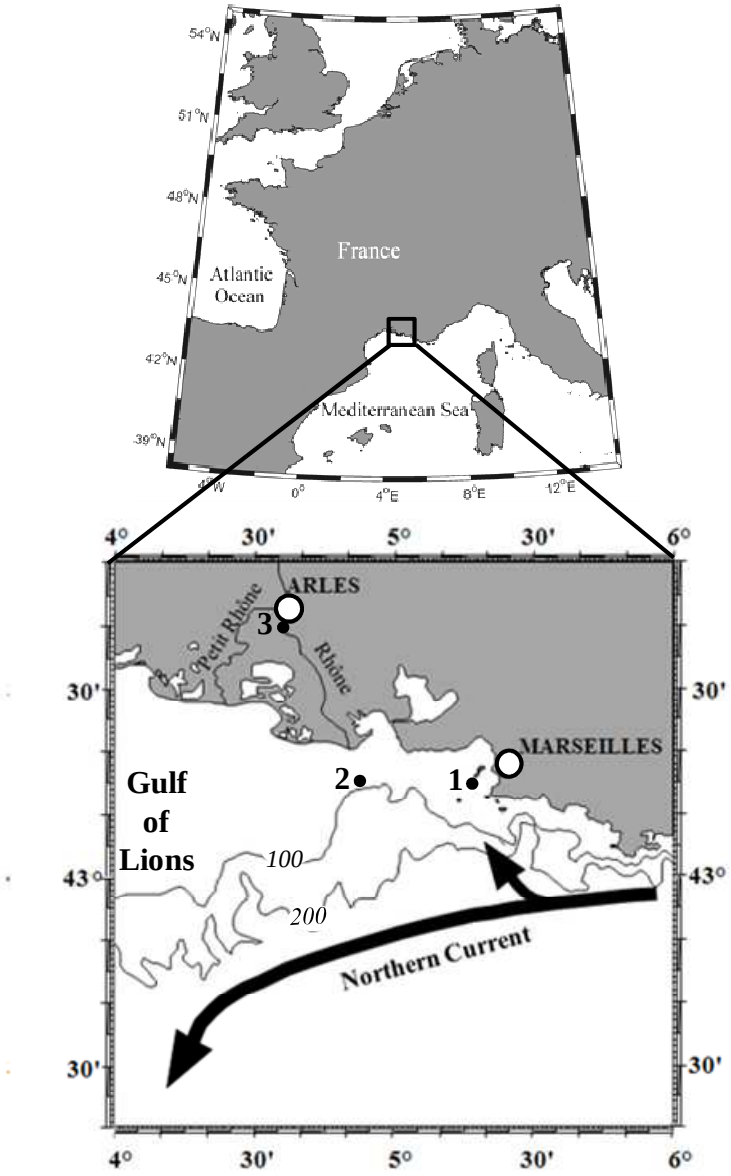

Figure II-1. *Map of the Bay of Marseilles marking the location of SOFCOM station (black dot 1) in the Bay of Marseilles, the two Rhône Estuary stations (black dot 2) and Arles station (black dot 3). Distance separating SOFCOM station from Rhône River Estuary is around 40 Km.*

3. 2. CDOM optical properties

3. 2. 1. Absorbance measurements

Absorbance of CDOM was measured throughout the UV and visible spectral domains (280-700 nm) using the multiple pathlength, liquid core waveguide system Ultrapath (MPLCW, WPI Inc.). Absorbance spectra of marine and freshwater samples were measured through 2 m and 50 cm long pathlengths respectively. Marseilles'Bay (SOFCOM station) and Rhône plume (marine) samples were analysed with reference to a filtered salt solution prepared with Milli-Q water and precombusted NaCl (Sigma) reproducing the refractive index of samples to minimize baseline offsets in absorption spectra induced by the effect of salinity changes between sample and the corresponding reference (D'Sa et al., 1999). Rhône River (freshwater) samples were analyzed with reference to filtered Milli-Q water. Reference salt solution and samples were brought to room temperature before analysis. Between each sample, the sample cell was flushed with successively diluted detergent (Cleaning solution concentrate, WPI Inc.), high reagent grade MeOH, 2 M HCl and Milli-Q water. Cleanliness of the sample cell was checked by comparing with a reference value for the transmittance of the reference salt solution. Trapped microbubbles were minimized by using a peristaltic pump to draw the sample into the sample cell. The spectral absorption coefficients, $a_{CDOM}(\lambda)$ (m^{-1}) were obtained using the following relationship, $a_{CDOM}(\lambda) = 2.303A(\lambda)/L$, where $A(\lambda)$ is the absorbance at wavelength λ (dimensionless) and L is the pathlength in meters. All samples that had an absorbance value above 0.2 at 300 nm for a 10 cm cell were corrected for the inner filter effect according to the formula proposed by Ohno (2002). Value of spectral slope of CDOM absorption (S_{CDOM}) has most often been determined using an exponential regression (Jerlov, 1968; Bricaud et al., 1981) but non-linear regression fitting provides a better estimate of S_{CDOM}, by weighting regions of higher CDOM absorption (Stedmon et al., 2000). Here, S_{CDOM} was determined after applying a non-linear exponential regression to original $a_{CDOM}(\lambda)$ data measured on the range 350-500 nm. All the determination coefficients (R^2) calculated from these exponential fits were always > 0.99. S_{CDOM} provides information concerning CDOM origin (terrestrial *versus* marine), with generally lower slopes in fresh and coastal waters than in the open ocean due to the presence of marine humics and new biological CDOM (Ferrari et al., 2000; Blough and Del Vecchio, 2002). Additionally, higher S_{CDOM} have been reported for photobleached CDOM (Vodacek et al., 1997).

3. 2. 2. Fluorescence measurements

For fluorescence measurements, performed monthly, from June 2008 to December 2008, samples were transferred into a 1 cm pathlength far UV silica quartz cuvette (170-2600 nm; LEADER LAB), thermostated at 20°C, and analyzed with a Hitachi (Japan) Model F-7000 spectrofluorometer. Instrument settings, measurement procedures and spectral correction procedures are fully described in Tedetti et al. (2010). Briefly, the correction of spectra for instrumental response was conducted according to the procedure recommended by Hitachi (Hitachi F-7000 Instruction Manual). First, the Ex instrumental response was obtained by using Rhodamine B as standard and a single-side frosted red filter in Ex scan mode. Then, the Em side calibration was done with a diffuser in synchronous scan mode. The Ex and Em spectra obtained over the range 200-600 nm were applied internally by the instrument to correct subsequent spectra. EEMs were generated over Ex wavelengths between 200 and 550 nm in 5 nm intervals and Em wavelengths between 280 and 600 nm in 2 nm intervals, with 5 nm bandwidths (FWHMs) on both Ex and Em sides and a scan speed of 2400 nm min^{-1}. Milli-Q water as well as solutions of quinine sulphate (Fluka) in 0.05 M H_2SO_4 (1-10 ppb) were run with each set of samples. Before being processed, all the data (blanks, standards, samples) were normalized to the intensity of the Raman scatter peak at Ex/Em: 275/303 nm (5 nm bandwidths) of pure water (Coble et al., 1993; Coble, 1996; Belzile et al., 2006), which varied by less than 4% over the study period. Samples were then corrected for the corresponding blanks and converted into quinine sulphate units (QSU). EEM data processing and contour plots were conducted with MATLAB 7.1.

Besides the identification of common fluorescent peaks by the traditional “peak picking” technique (examination of Ex and Em spectra), we determined two indices: the humification index (HIX) and the biological index (BIX). HIX was introduced on the basis of the position of the emission spectra in order to estimate the degree of maturation of DOM in soil (Zsolnay et al., 1999). It is the ratio (H/L) of two areas of emission spectrum from excitation at 254 nm (here 255 nm). These two areas are calculated between 300 and 345 nm (here, between 300-346 nm) for L and between 435 and 480 nm (here, between 434-480 nm) for H. In natural aquatic ecosystem (Gironde and Seine estuaries and Mediterranean Sea), high values of HIX (10-16) illustrated the presence of strongly humic organic material (terrestrial origin), whereas low values (< 4) represent authochtonous organic material (Huguet et al., 2009). BIX allows the determination of the presence of the marine humic-like peak (peak M), which reflects autochthonous biological activity (Huguet et al., 2009). It is

calculated at Ex=310 nm, by dividing the fluorescence intensity at Em=380 nm (maximum of M peak) by the fluorescence intensity at Em=430 nm, which corresponds to the maximum of peak C. High values of BIX (> 1) correspond to a biological origin and lowest values (< 1) illustrate low abundance of organic matter of biological origin (Huguet et al., 2009). Analytical errors of these indices were within 5%.

3. 2. 3. TOC analysis

The Shimadzu instrument used in this study is the commercially available model TOC-5000 Total Carbon Analyzer with a quartz combustion column filled with 1.2% Pt on silica pillows. Several aspects of our modified unit have been previously described (Sohrin and Sempéré, 2005). The accuracy and the system blank of our instrument were determined by the analysis of the reference material (D. Hansell, Rosenstiel School of Marine and Atmospheric Science, Miami, USA) including Deep Atlantic Water (DAW) and low carbon water (LCW) reference standards. The average DOC concentrations in the DAW and in the LCW reference standards were 45 ± 2 µM C, n = 24 and 1 ± 0.3 µM C, n = 24, respectively. Carbon levels in the LCW ampoules were similar to and often higher than the Milli-Q water produced in our laboratory. The nominal analytical precision of the analysis procedure was within 2%.

3. 2. 4. Remotely sensed data

Remotely sensed images of SST and Chl*a* concentration (Fig. II-2) were obtained by applying respectively the long-wave SST algorithm and the OC5 coastal-oriented optical algorithm (Gohin et al., 2002; 2005) to water leaving irradiances derived from the Moderate Resolution Imaging Spectroradiometer (MODIS) sensor. Accuracy of the OC5 algorithm applied to the Rhône River plume region has been estimated to be 40% absolute percentage of difference by comparing 332 *in situ* and co-localized remotely sensed values of Chla concentrations using the Sea-viewing Wide Field of View Sensor (SeaWiFS) (Fontana et al., 2009).

3. 2. 5. Irradiation experiment on Rhône River water

A kinetic irradiation experiment was carried out on a Rhône River sample collected at Arles station on 7 February 2009 (2 m depth). The 0.2 µm filtered solution was distributed in 50 ml precombusted (450° C, 6 hours) quartz tubes and placed in thermostated bath at 13°C. Samples were exposed to a simulated sunlight using a Suntest CPS + solar simulator (Atlas, GmbH) in Full Sun (FS) light condition (i.e., FS = PAR + UVB + UVA) giving an optical output of 700 W m^{-2}. Exposure for 2.8 hours at this intensity corresponds to a natural daily (12 hours) dose received in the Western Mediterranean Basin by taking an annual average of total solar radiation of 162 W m^{-2} (Ruiz et al., 2008). Samples were irradiated in duplicate during 8 (T1) and 20 h (T2) which corresponds to 3 and 7 days of natural solar irradiation, respectively. Simultaneous dark control (quartz tube wrapped in black bag) was performed under the same conditions.

4. Results

4. 1. Hydrological context and trophic status

During winter and fall periods, the action of winds mixed entirely the water column of Marseilles Bay (60 m depth). The general trend observed from the surface to the bottom during this stormy period was a salinity around 38.1-38.2 and a temperature decreasing from 18 to 15 °C in fall and from 15 to 13 °C in winter (Fig. II-2). These are the typical values recorded for the northwestern Mediterranean Sea (Brasseur et al., 1996). At the beginning of spring, the entire water column was still well mixed and exhibited a temperature and a salinity corresponding to those observed during winter (Fig. II-2). During May, water began warming (16-17 °C) causing the formation of a thermocline around 40 m depth. Early in May, an intrusion of a less salty water mass (37-37.8) was observed in the upper 10 m. The low salinity surface water mass, perhaps coupled with physical forcing, seems to have also impacted the salinity signature of the deepest water because the salinity of the latter was < 38 down to 45 m, whereas the salinity value of deeper Mediterranean water masses are usually close to 38.3 (Brasseur et al., 1996). At the end of June, another important surface intrusion of low salinity water occurred with a salinity ranging from 37.3 to 37.8 and a temperature ranging from 21.5 to 18 ° C between 1 and 30 m depth, respectively. As for the previous low

salinity intrusion, this one also appeared to influence the salinity signature of deeper water masses.

These two surface intrusions of low salinity water were also identified by remotely sensed pictures of SST and Chla concentration on 7 May 2008 (nearest date available corresponding to the sampling date 6 May 2008) on 23 June 2008 (sampling date) and were shown on Fig. II-2 (insets b and c). These remotely sensed pictures plus those available encompassing sampling dates (not shown) illustrate clearly that surface inputs of freshwater observed on 6 May 2008 and on 23 June 2008 in Bay of Marseilles came from the eastward extent of the Rhône River plume. In order to have an estimate of the spreading time of the Rhône River plume, successive satellite pictures were used to track the plume. Using the ones encompassing the Rhône River plume intrusion observed on 6 May 2008, we estimated the spreading time to be on the order of 2-3 days, which is in good agreement with the time scale determined by Fontana et al. (2010).

In July, 3 consecutive days of wind from north (Mistral wind) mixed the water column, removing all signs of the Rhône River plume and resulting in a cooling (14-15 °C) coupled to an increase of salinity (38.1) of surface waters (Fig. II-2). Sea surface temperature dropped to 16.5 °C at 1 m depth, which is a specific feature of the Bay of Marseilles during stratification period under Mistral wind influence. The last part of summer (August) was more common with the re-establishment of the thermocline around 15-20 m depths separating warm (18-23 °C) and salty (38.2) surface waters from cold deep waters (14-18 °C) of slightly lower salinity (38). At the end of summer (23 September 2008), a warm (21-22 °C) high salinity (> 38.4) water mass was observed from a depth of 20 m to the surface which was replaced on 14 October 2008 by a shallower low salinity water mass (37.6) in the upper 3 m due to intense rains. Other slightly less saline water masses in surface were observed at the end of November 2007 and early in December 2008 but during these windy periods, surface low salinity water masses were attenuated and disappeared rapidly due to the mixing (Fig.II2).

In early May and at the end of June 2008, the influence of the eastward extent of the Rhône River could have increased nitrate concentrations within the plume along a gradient of salinity (10-36) from 90 to 15 µM (Pujo-Pay et al., 2006) as well as others nutrients to lesser extent. Phytoplankton biomass in the Bay of Marseilles was enhanced with a value of Chla concentration >1 µg l^{-1}, while without the influence of the Rhône River plume Chla concentration remained <1 µg l^{-1} (Table II-1, Fig. II-2 insets). In May 2008, surface (2m depth) DOC values decrease from 113 ± 12 µM C in the Rhône River to 74-78 µM C in the

Rhône Estuary. These latest values are lower than those previously reported in the Rhône Estuary by Ferrari et al., 2000 (140 µM C).

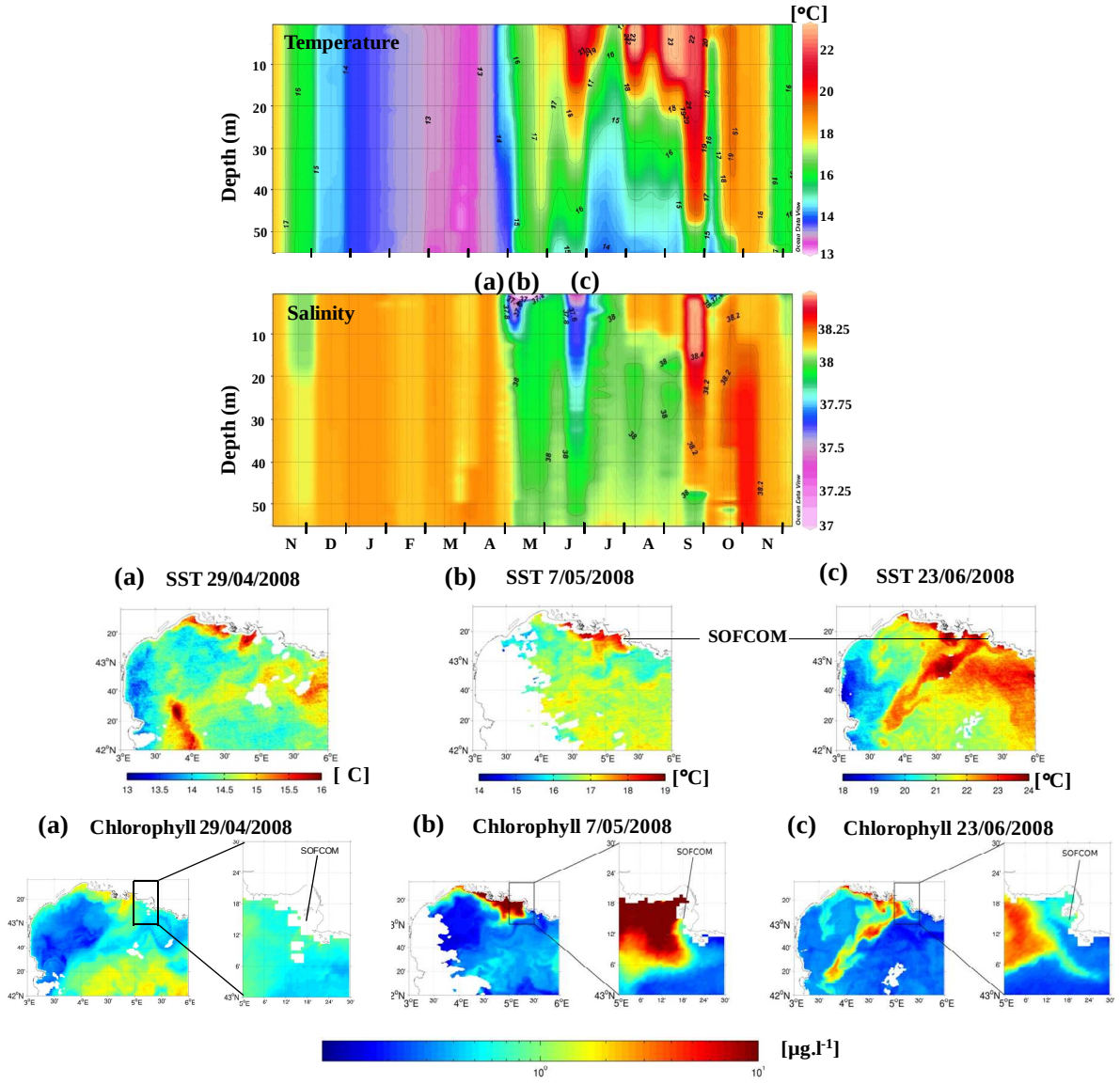

Figure II-2. *Top panels: Temporal evolution of temperature and salinity at SOFCOM station from November 2007 to December 2008 from surface to bottom. Data come from CTD profiles carried out twice a month by the SOMLIT network (n = 30) and completed since February 2008 by CTD data acquired on sampling dates (n = 11). Bottom panels: remotely sea surface temperature (SST) and chlorophyll concentrations are from the points in the time series labeled (a), (b) and (c) corresponding respectively to the sampling date 29 April (non-intrusion of Rhône plume), 7 May and 23 June 2008 (intrusion of Rhône plume). Remotely SST and Chlorophyll concentrations from satellite images were obtained respectively by applying the long-wave SST algorithm and the OC5 coastal-oriented optical algorithm (Gohin et al., 2002; 2005) to water leaving irradiances derived from the Moderate Resolution Imaging Spectroradiometer (MODIS).*

At SOFCOM station (Table II-1), TOC concentrations at both depths studied were similar and were also comparable to DOC concentrations previously reported in open waters of Mediterranean Sea (Doval et al., 1999; Dafner et al., 2001; Santinelli et al., 2002; Sempéré et al., 2002; Seritti et al., 2003), with a stable annual mean of 67 ± 7 µM C at 2 m and 63 ± 6 µM C at 5 m. Thus, despite some episodic influence of the Rhône River plume, this coastal area exhibited features including Chla concentration <1 µg l^{-1} and TOC concentration ~ DOC concentration, which is usually encountered offshore. It is important to notice that during the period study, this coastal oligotrophic area is subjected to a strong UV surface irradiance particularly in spring and summer periods for UVB (305 nm) radiation with surface irradiance (Es) values as high as 4.64 µW cm^{-2} nm^{-1} for UVB (305 nm) in summer time (Table II-1) around solar noon. With the exception of sampling dates that were cloudy, we observed around 10 fold more UVB (305nm) and 2-3 fold more UVA (325, 340 and 380 nm) radiation in summer and spring compared to fall and winter periods.

Table II-1. *Absorption coefficient of CDOM at 350 nm [$a_{CDOM}(350)$], spectral slope of CDOM (S_{CDOM}), total organic carbon (TOC) concentration, chlorophyll a concentration (Chla) and mean surface irradiance (E_s) in the UVB (305 nm) and UVA (325, 340, 380 nm) spectral domains measured during one hour close to solar noon, determined at SOFCOM and Rhône Estuary stations at 2 and 5 m depths and Arles station (Rhône and Rhône irradiation experiment: Rhône Irrad. Exp.) at 2 m depth.*

		$a_{CDOM}(350)$ [m^{-1}]		S_{CDOM} [nm^{-1}]		TOC [µMC]		Chla [µg l^{-1}]		E_s(UV) [µW cm^{-2} nm^{-1}]				T [°C]		Salinity	
End-member	Date	2m	5m	2m	5m	2m	5m	2m	5m	305 nm	325 nm	340 nm	380 nm	2m	5m	2m	5m
SOFCOM [(a)]	07/11/07	0.11	0.1	0.018	0.019	68	62	_	_	0.51 ± 0.03	12.78 ± 0.39	20.74 ± 0.59	29.17 ± 0.73	17.8	17.8	38.1	38.1
SOFCOM	19/12/07	0.1	0.1	0.017	0.018	60	54	_	_	0.14 ± 0.01	9.94 ± 0.06	17.13 ± 0.11	26.46 ± 0.11	14.4	14.4	38.2	38.2
SOFCOM	05/02/08	0.11	0.11	0.016	0.015	_	55	0.90	0.92	0.48 ± 0.01	15.72 ± 0.09	25.56 ± 0.17	36.19 ± 0.38	13.2	13.2	38.1	38.1
SOFCOM	14/02/08	0.09	0.09	0.018	0.018	78	61	0.20	1.03	0.42 ± 0.01	16.86 ± 0.08	27.90 ± 0.19	38.81 ± 0.23	13.2	13.3	38.1	38.1
SOFCOM [(a)]	26/03/08	_	0.1	_	0.016	56	59	0.21	0.24	1.39 ± 0.03	25.85 ± 0.34	39.09 ± 0.61	52.86 ± 0.98	12.8	12.8	38.1	38.1
SOFCOM	29/04/08	0.11	0.11	0.018	0.020	70	63	0.85	0.89	3.09 ± 0.09	36.62 ± 1.25	54.67 ± 2.29	74.18 ± 3.17	14.5	14.4	38.1	38.1
SOFCOM [(a)]	06/05/08	0.13	0.13	0.018	0.018	65	_	1.55	1.69	0.93 ± 0.05	12.83 ± 0.72	18.81 ± 1.08	24.47 ± 1.48	16.1	16.0	37.1	37.3
SOFCOM [(a)]	09/06/08	0.11	0.1	0.022	0.023	70	61	0.77	0.86	2.26 ± 0.09	27.87 ± 1.07	40.55 ± 1.65	53.69 ± 2.57	17.2	17.0	37.9	38.0
SOFCOM	23/06/08	0.12	0.11	0.026	0.026	79	76	1.42	1.33	4.64 ± 0.06	39.14 ± 0.25	56.51 ± 0.43	77.51 ± 0.81	21.4	20.8	37.5	37.5
SOFCOM [(b)]	10/07/08	0.09	0.09	0.023	0.023	67	68	0.19	0.20	4.06 ± 0.09	40.14 ± 0.92	58.88 ± 1.35	79.62 ± 1.69	18.6	17.7	37.9	37.9
SOFCOM [(a)]	23/09/08	0.07	0.06	0.021	0.023	72	67	0.40	0.45	1.13 ± 0.12	15.92 ± 1.64	23.38 ± 2.62	30.98 ± 4.06	22.2	22.1	38.4	38.4
SOFCOM [(b)]	14/10/08	0.09	0.09	0.018	0.018	70	67	0.33	0.35	1.17 ± 0.01	19.58 ± 0.08	30.08 ± 0.27	43.75 ± 0.51	19.4	19.4	38.2	38.2
SOFCOM	25/11/08	0.13	0.13	0.014	0.014	55	56	0.58	0.56	0.32 ± 0.01	13.73 ± 0.01	22.88 ± 0.01	33.78 ± 0.01	15.3	15.3	38.2	38.2
SOFCOM [(a)]	04/12/08	0.11	0.1	0.017	0.019	63	65	0.76	0.96	0.18 ± 0.01	7.34 ± 0.30	11.65 ± 0.48	15.28 ± 0.62	16.1	16.1	38.1	38.1
Rhône estuary [(c)]	22/05/08	0.25	0.09	0.019	0.021	74	71	_	_	_	_	_	_	16.8	17.4	33.5	37.9
Rhône estuary [(c)]	23/05/08	0.33	0.09	0.017	0.024	78	67	_	_	_	_	_	_	16.7	17.6	29.9	37.7
Rhône (Arles) (n=14) [(c)]	17/01/08-18/11/08	2.42 ± 1.05	_	0.017 ± 0.001	_	136 ± 38	_	_	_	_	_	_	_	_	_	_	_
Rhône Irrad. Exp. [(c)]	T0	3.11	_	0.018	_	163	_	_	_	_	_	_	_	_	_	_	_
Rhône Irrad. Exp. [(c)]	Dark control	3.12	_	0.018	_	157	_	_	_	_	_	_	_	_	_	_	_
Rhône Irrad. Exp. [(c)]	T1 duplicate	2.23 ± 0.09	_	0.018 ± 0.001	_	158 ± 2	_	_	_	_	_	_	_	_	_	_	_
Rhône Irrad. Exp. [(c)]	T2 duplicate	1.17 ± 0.05	_	0.018 ± 0.000	_	150 ± 0	_	_	_	_	_	_	_	_	_	_	_

[(a)] Cloudy day

[(b)] Sea mist

[(c)] For Rhône Estuary, Rhône and Rhône Irrad. Exp. end-members, DOC concentration was measured in place of TOC concentration.

4. 2. CDOM absorbance

The a_{CDOM} at 350 nm was chosen for describing changes in CDOM quantity, and S_{CDOM} to differentiate CDOM quality (Table II-1). In the Bay of Marseilles (SOFCOM station), the annual mean values of $a_{CDOM}(350)$ at 2 and 5 m depths were comparable and very low (0.10 ± 0.02 m^{-1}) with regard to the entire range of the $a_{CDOM}(350)$ found in the literature for diverse aquatic environments (i.e. 0.046 – 29.9 m^{-1}) (Kowalczuck et al., 2003) and thus were more similar to those found offshore. The $a_{CDOM}(350)$ maximum value of 0.13 m^{-1} at 2 and 5 m was observed under Rhône River plume influence (6 May 2008) and during the fall mixing period (25 November 2008), right after 12 consecutive days of Mistral wind that initiated a strong mixing of the entire water column. By contrast, $a_{CDOM}(350)$ minimum value at 2 m (0.07 m^{-1}) and 5 m (0.06 m^{-1}) occurred at the end of summer time (23 September 2008) (Table II-1), when the highest salinity (>38.4) and high temperature (22 °C) water was observed (Fig. II-2). Since no significant seasonal trend of $a_{CDOM}(350)$ appeared during this period, our results suggest that external influences such as Rhône River plume intrusion and mixing events control CDOM surface content and variability in Marseilles coastal area. At Arles station, Rhône River's $a_{CDOM}(350)$ annual mean (2.42 ± 1.05 m^{-1}) was likely higher than the marine one (Table II-1). In the Rhône River plume, $a_{CDOM}(350)$ was 3-4 fold more important at 2 m compared at 5 m depth. Irradiation experiment on the Rhône River CDOM induced 30 and 60% losses of $a_{CDOM}(350)$ in T1 and T2 samples compared to T0 and dark control, respectively (Table II-1).

In the Bay of Marseilles, the annual mean of S_{CDOM} determined during this study was 0.019 ± 0.003 nm^{-1} at both depths which is consistent to that previously reported for October 1997 at the surface in vicinity of Rhône River mouth (0.018 ± 0.003 nm^{-1}) and for surface blue waters of the Gulf of Lions (0.017 ± 0.003 nm^{-1}) by Ferrari (2000). S_{CDOM} extreme values (2 and 5 m) ranged from 0.014 nm^{-1} on 25 November 2008 to 0.026 nm^{-1} on 23 June 2008 (Table II-1). Seasonal means of S_{CDOM} were the lowest and comparable during fall and winter periods (S_{CDOM} at 2 and 5 m = 0.017 ± 0.002 nm^{-1}) while during summer time S_{CDOM} were significantly higher (U-Test, $p < 5\%$, n = 3-4) with seasonal mean value reaching 0.023 ± 0.003 nm^{-1} and 0.024 ± 0.002 nm^{-1} at 2 and 5 m depths, respectively. Spring means of S_{CDOM} were in the middle of the range with 0.020 ± 0.002 nm^{-1} and 0.019 ± 0.003 nm^{-1} at 2 and 5 m depths, respectively.

The S_{CDOM} annual mean of Rhône River samples (Arles Station) was lower (0.017 ± 0.001 nm^{-1}) than the marine one, whereas no apparent change in S_{CDOM} value presented with a

precision in the thousandth was observed after full sun exposure in T1 and T2 samples compared to T0 and dark control samples (S_{CDOM} = 0.018 nm^{-1}, Table II-1). However, it tended to increase during the irradiation experiment (from 0.0175 to 0.0180 nm^{-1}). In addition, this tendency was comforted by the slope ratio (S_R) values defined by Helms et al. (2008). S_R consistently increased during irradiation in relation to the shifts in molecular weight. Indeed, between T0 (initial time) and T2 (final time), S_R increased respectively from a terrestrial value (0.8) to a more typical coastal value (1.36 ± 0.05). Interestingly, in the Rhône River plume S_{CDOM} values at 2 m depth (0.017-0.019 nm^{-1}) were strongly lower than at 5 m depth (0.021-0.024 nm^{-1}; Table II-1).

The significant inverse relationship between salinity and $a_{CDOM}(350)$ for the shallowest depth studied (2 m) indicates a theoretical conservative behavior for surface CDOM absorbance (Fig. II-3). The CDOM absorption mixing line established using all SOFCOM data at 2 m depth plus two data points acquired close to the Rhône Estuary in the Rhône River plume at 2 m depth in May 2008 has an intercept of 1.20 ± 0.06 m^{-1}, which is in the range of that calculated for the Rhône River end member at Arles station (2.42 ± 1.05 m^{-1}) (Table II-1). Moreover, when data from the Rhône River plume are excluded and all the SOFCOM data at both 2 and 5 m depths were used except the extreme values (23 September 2008 and 25 November 2008), another significant inverse relation was observed ($p < 1\%$, n = 11 at 2 m and n = 12 at 5 m), with $a_{CDOM}(350)$ = -0.032 ± 0.007 salinity + 1.33 ± 0.25), which is comparable to the previous calculation. However several data deviate significantly from the regression line. Points above the mixing line in Fig. II-3 represent a net production of CDOM. The most important net production of CDOM was associated with low TOC concentration values (55-56 µM C) and with the lowest S_{CDOM} (0.014 nm^{-1}) values and occurred at both depths during a strong mixing event (25 November 2008). By contrast, the two points that fall far below the mixing line also present the highest salinities (38.4), high temperature (22 °C), high S_{CDOM} values (0.021-0.023 nm^{-1}), as well as moderately high surface irradiance [E_s = 1.13 µW cm^{-2} $nm^{-1}$for UVB (305 nm)] and were collected at the end of summer time (23 September 2008).

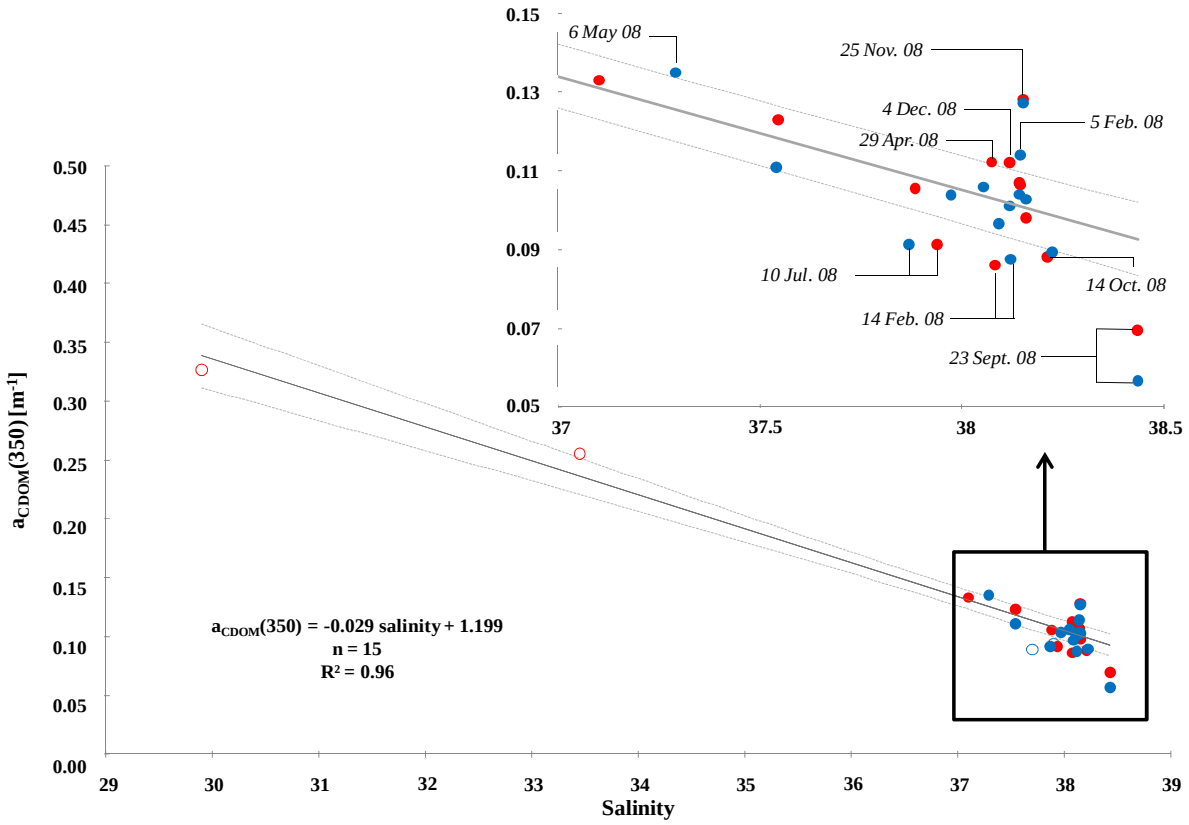

Figure II-3. *Relationship between salinity and CDOM absorption at 350 nm (in m^{-1}) determined at SOFCOM station at 2 m (red circle, n = 13) and 5 m (blue circle, n = 14) depths. Data from Rhône Estuary stations collected in May 2008 during CHACCRA cruise at 2 m (red open circle, n = 2) and 5 m (blue open circle, n = 2) were also plotted. The mixing line (black line) with its confidence interval at 95% (dashed line) was established using all SOFCOM station data at 2 m depth (n=13) plus Rhône Estuary stations (CHACCRA cruise data) at 2 m depth as well (n = 2).*

4. 3. CDOM fluorescence

All the fluorescence peaks observed in this study in the Bay of Marseilles (SOFCOM Station) can be summarized from 3 samples showing contrasting hydrological conditions and collected on 23 June 2008 (Rhône plume intrusion), 23 September 2008 (photobleached water) and 25 November 2008 (well mixed water). On the other side, the fluorescence peaks determined from Rhône River samples (Arles Station) can be observed from the sample collected on 7 February 2009 and used for the irradiation experiment. EEMs for these samples are presented in Figs. II-4 and II-5 for SOFCOM and Arles samples respectively, while peaks intensities for all samples are reported in Table II-2. During the fluorescence study period (i.e. June 2008- December 2008), in Marseilles' Bay, peak T (tryptophan-like, Ex/Em = 225/340 nm and 275/340 nm) was the major fluorescent peak present (6.45 ± 8.25 QSU at 2 m depth

and 1.94 ± 0.93 QSU at 5 m depth), followed by peak M (UVA marine humic-like, Ex/Em = 290-310/370-410 nm) with a mean value of 2.38 ± 2.15 QSU at 2 m depth and 1.74 ± 1.65 QSU at 5 m depth, and peak C (UVA humic-like Ex/Em= 320-360/420-460 nm) which was the least intense (1.10 ± 0.99 QSU at 2 m depth and 0.93 ± 0.95 QSU at 5 m depth). Peak B (tyrosine-like, Ex/Em = 225/305 nm and 275/305 nm) was found only on 23 June 2008. The most striking feature about all EEMs is the lack of peak A (UVC humic-like, Ex/Em = 260/400-460 nm) for marine samples which was not the case for Rhône River samples. The Rhône River fluorescent CDOM had a strong terrestrial signature (humic-like components, peaks A and C). Indeed, the peak A was the major fluorescent peak with an annual mean value of 43.09 ± 18.93 QSU, followed by peaks C (16.91 ± 7.98 QSU), and B (7.96 ± 0.82 QSU). However this fluorescent terrestrial signature decreased strongly after irradiation exposure as suggest the irradiation experiment results (Fig. II-5 and Table II-2). Indeed at T1 and T2, the intensity of peaks A and C was divided by 3 and 4.5 respectively compared to the ones determined at T0 and dark control, while the intensity of peak B remained constant.

For Marseilles' Bay samples, maximum fluorescence intensities of peaks C, M and T (Table II-2) at both depths occurred on 25 November 2008, during a strong mixing event enhanced by 12 consecutive days of Mistral wind and during a Rhône River plume extent event observed on 23 June 2008. For all other samples, all peak intensities were stable and low, especially in summer as observed on 10 July 2008 (despite the minor mixing event due to 3 consecutive days of Mistral wind) and 23 September 2008 (Table II-2). The sample from 23 September 2008 showed a strong fluorescence signal in short Ex/Em wavelengths at both depths and possibly a slight signal of peak T as well (Fig. II-4). This kind of signal at short wavelengths has been previously observed in strongly photobleached samples (P. Coble, unpublished data).

In contrast to the significant apparent relationship between surface $a_{CDOM}(350)$ and salinity, there was only a weak inverse relationship ($p < 5\%$, $n = 6$, $R^2 = 0.69$ and 0.67 for peaks C and M respectively, data not shown) between fluorescence of peaks C and M (Table II-2) and salinity at 5 m depth when excluding the maximum values (25 November 2008). This result indicates that fluorescent CDOM character in the surface water is mainly driven by other processes than water mixing and thus highlights the dissimilar trends in CDOM absorption and fluorescence properties.

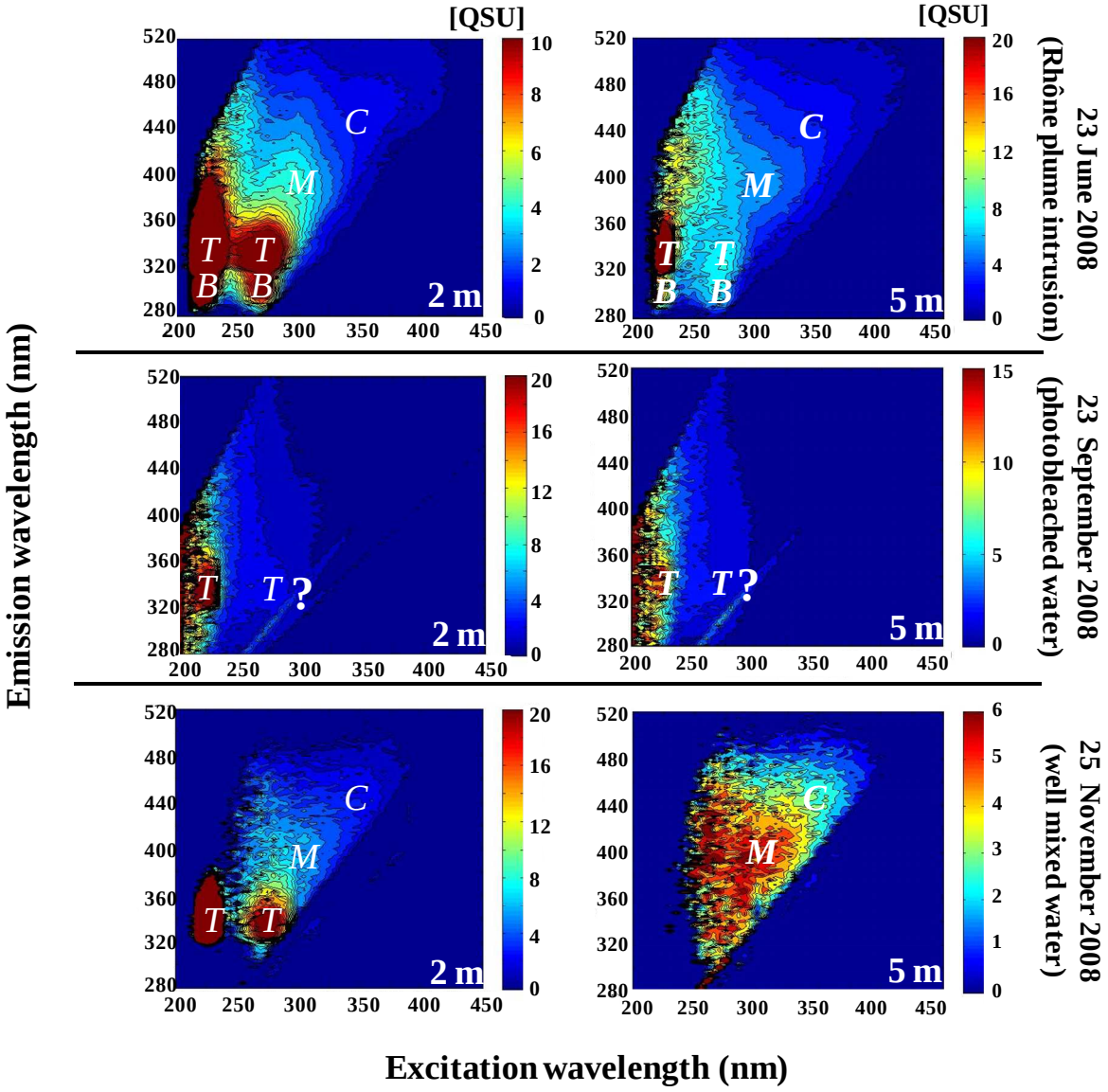

Figure II-4. *2-D EEM contour plots of CDOM (in QSU) collected in the Bay of Marseilles (SOFCOM station) at 2 (left panels) and 5 m depths (right panels) on 23 June (upper panels), 23 September (middle panels) and 25 November 2008 (bottom panels). These spectra illustrated fluorescent peaks positions observed during this study. Corresponding peaks fluorescence intensities are reported on Table II-2. On middle panels, question marks indicate a possible slight signature of the peak T.*

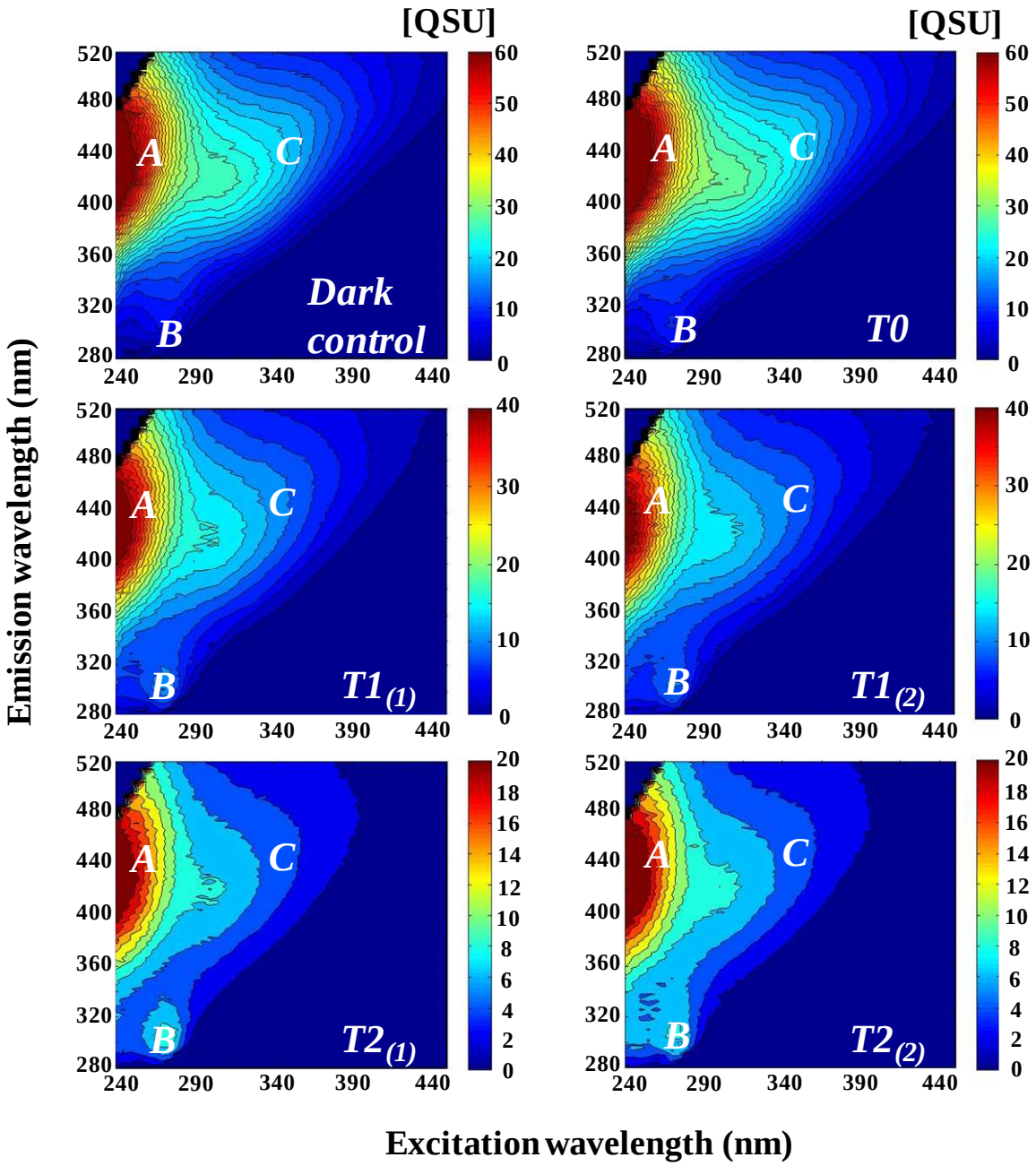

Figure II-5. *2-D EEM contour plots of CDOM (in QSU) collected from Rhône River sample, before (T0: upper panel right), and after a full sun exposure of 8 (T1: middle panels) and 20h (T2: bottom panels) using solar simulator. Color-bars' scales are different. Dark control is indicated in upper panel (left). Corresponding peaks fluorescence intensities are reported on Table II-2.*

HIX and BIX values determined for marine (SOFCOM) and freshwater (Arles) samples are presented on Table II-3. During the study period, for SOFCOM samples at both depths, HIX values were low and variable with 0.84 ± 0.38 and 0.90 ± 0.35 at 2 m and 5 m depths, respectively, while BIX values were high and stable: 1.10 ± 0.17 and 1.09 ± 0.05, respectively. These results suggest a predominantly autochthonous origin of DOM in surface marine waters. BIX maximum values were observed at 2 m depth on 23 June 2008 and 25 November 2008 while the lowest one was observed on 7 July 2008 at 2 m depth. This date corresponded also at the maximum values observed at both depths for HIX. At Arles station, Rhône River CDOM likely contains compounds of higher molecular weight compared to marine CDOM. Indeed, high HIX values (4.85 ± 1.55) and low BIX values (0.74 ± 0.05) suggest a predominantly allochthonous origin of DOM. The high variability of HIX (CV = 32%), which is the ratio of H/L, for these freshwater samples came from the variability concerning the presence of complex high molecular weight components (i.e., H, C.V. = 41%), while low molecular weight components part remained more steady (i.e., L, C.V. = 13%). The Rhône River irradiation experiment shows a strong decrease in HIX at T1 and T2 triggered by H value decreased (H = 1433, 1326, 810 ± 44 and 426 ± 15 QSU at T0, Dark control, T1 and T2 respectively) while corresponding BIX remained constant (Table II-3), due to an alteration in similar proportion of humic-like components, compared to T0 and dark control. Such results, strong decrease of HIX (~ 50%) coupled to a constant BIX between T0 (initial time) and T2 (final time) underline the higher photosensitivity feature of high molecular weight DOM (i.e. humic-like components) compared to low molecular weight DOM (i.e. protein-like components) (Table II-2).

Table II-2. *Fluorescence intensity (in QSU) and peak positions of tyrosine-like (B), tryptophan-like (T), UVA humic-like (C), marine humic-like (M) and UVC humic-like (A) determined at SOFCOM (2 and 5 m depths) and Arles station (Rhône and Rhône irradiation experiment: Rhône Irrad. Exp.) at 2 m depth. Emission ranges represent the band from which a mean of fluorescence intensity was calculated. (nd = not determined).*

	Peak fluorescence intensity (QSU)									
	B		C		M		T		A	
	Ex/Em (nm) = 275/300-310		Ex/Em (nm) = 350/430-450		Ex/Em (nm) = 300/380-400		Ex/Em (nm) = 275/330-350		Ex/Em (nm) = 260/430-440	
End-member	2m	5m	2m	5m	2m	5m	2m	5m	2m	5m
SOFCOM 09/06/2008	nd	nd	0.56 ± 0.04	0.57 ± 0.04	1.02 ± 0.06	1.24 ± 0.08	1.70 ± 0.18	1.74 ± 0.13	nd	nd
SOFCOM 23/06/2008	11.06 ± 0.81	3.51 ± 0.67	1.40 ± 0.06	1.54 ± 0.08	4.34 ± 0.13	2.73 ± 0.12	14.13 ± 1.57	3.78 ± 0.20	nd	nd
SOFCOM 10/07/2008	nd	nd	0.49 ± 0.03	0.51 ± 0.04	0.85 ± 0.06	0.96 ± 0.06	1.25 ± 0.13	1.46 ± 0.09	nd	nd
SOFCOM 23/09/2008	nd	nd	0.57 ± 0.04	0.42 ± 0.03	1.26 ± 0.07	0.90 ± 0.09	2.77 ± 0.20	1.87 ± 0.09	nd	nd
SOFCOM 14/10/2008	nd	nd	nd	0.27 ± 0.03	nd	0.55 ± 0.08	1.30 ± 0.18	1.58 ± 0.17	nd	nd
SOFCOM 25/11/2008	nd	nd	2.99 ± 0.18	2.85 ± 0.22	5.82 ± 0.49	5.11 ± 0.52	21.94 ± 2.66	nd	nd	nd
SOFCOM 04/12/2008	nd	nd	0.59 ± 0.04	0.34 ± 0.03	0.98 ± 0.05	0.71 ± 0.07	2.08 ± 0.18	nd	nd	nd
Mean	_	_	**1.10**	**0.93**	**2.38**	**1.74**	**6.45**	**1.94**	_	_
SD	_	_	*0.99*	*0.95*	*2.15*	*1.65*	*8.25*	*0.93*	_	_
Rhône (Arles) (Jun-Dec. 2008, n = 6)	7.96 ± 0.82	_	16.91 ± 7.98	_	nd	_	nd	_	43.09 ± 18.93	_
Rhône Irrad. Exp. T0	8.99 ± 0.76	_	21.35 ± 0.33	_	nd	_	nd	_	56.30 ± 0.72	_
Rhône Irrad. Exp. Dark control	7.12 ± 0.50	_	19.71 ± 0.21	_	nd	_	nd	_	53.60 ± 1.56	_
Rhône Irrad. Exp. T1 duplicate	10.24 ± 0.65	_	9.67 ± 0.52	_	nd	_	nd	_	31.36 ± 1.59	_
Rhône Irrad. Exp. T2 duplicate	8.34 ± 0.58	_	4.57 ± 0.21	_	nd	_	nd	_	16.77 ± 0.22	_

Shape of normalized emission spectra to the corresponding maximum emission intensity can provide information on the nature as well as on biogeochemical processes affecting DOM. Normalized emission spectra of peaks C and M were both determined (Fig. II-6) for the 3 marine samples influenced by contrasted hydrological conditions (23 June 2008, 23 September 2008 and 25 November 2008) (Fig. II-6). Additional normalized emission spectra of the peak C corresponding to T0 (initial time), dark control and T2 (final time) of the Rhône River sample irradiation experiment were also plotted on Fig. II-6. At SOFCOM station, both humic-like peaks (C and M) presented the same pattern at both depths, with the broadest emission spectra observed on photobleached water samples (23 September 2008) followed by the Rhône River intrusion one (23 June 2008) while the narrowest spectra were determined during the mixing event (25 November 2008). For the Rhône River, emission spectra of peak C were likely broader than the SOFCOM ones. Interestingly, after irradiation (i.e. T2 sample) corresponding emission spectra were widening towards the longer Em wavelengths compared to T0 and Dark control.

Table II-3. *Values of Humification (HIX; Zsolnay et al., 1999), Biological (BIX; Huguet et al., 2009) indices and the ratio of marine humic-like (Ex/Em = 300/380-400 nm) to humic like (Ex/Em = 350/430-450 nm) (M/C) fluorescence determined at SOFCOM (2 and 5 m depths) and Arles station (Rhône and Rhône irradiation experiment: Rhône Irrad. Exp.) at 2 m depth. (nd = not determined).*

	HIX		BIX		M/C	
End-member	2m	5m	2m	5m	2m	5m
SOFCOM 09/06/2008	0.93	0.96	1.04	1.00	1.81	2.17
SOFCOM 23/06/2008	0.42	1.22	1.34	1.10	3.11	1.77
SOFCOM 10/07/2008	1.32	1.35	0.86	1.09	1.74	1.89
SOFCOM 23/09/2008	1.04	0.96	1.02	1.06	2.22	2.12
SOFCOM 14/10/2008	nd	0.27	nd	1.12	nd	2.08
SOFCOM 25/11/2008	1.01	0.77	1.26	1.15	1.95	1.79
SOFCOM 04/12/2008	0.35	0.76	1.05	1.11	1.68	2.08
Mean	**0.84**	**0.90**	**1.10**	**1.09**	**2.09**	**1.99**
SD	*0.38*	*0.35*	*0.17*	*0.05*	*0.54*	*0.17*
Rhône (Arles) (Jun-Dec. 2008, n = 6)	4.85 ± 1.55	_	0.74 ± 0.05	_	nd	_
Rhône Irrad. Exp. T0	6.19	_	0.66	_	nd	_
Rhône Irrad. Exp. Dark control	6.41	_	0.69	_	nd	_
Rhône Irrad. Exp. T1 duplicate	4.10 ± 0.15	_	0.67 ± 0.01	_	nd	_
Rhône Irrad. Exp. T2 duplicate	3.21 ± 0.10	_	0.67 ± 0.02	_	nd	_

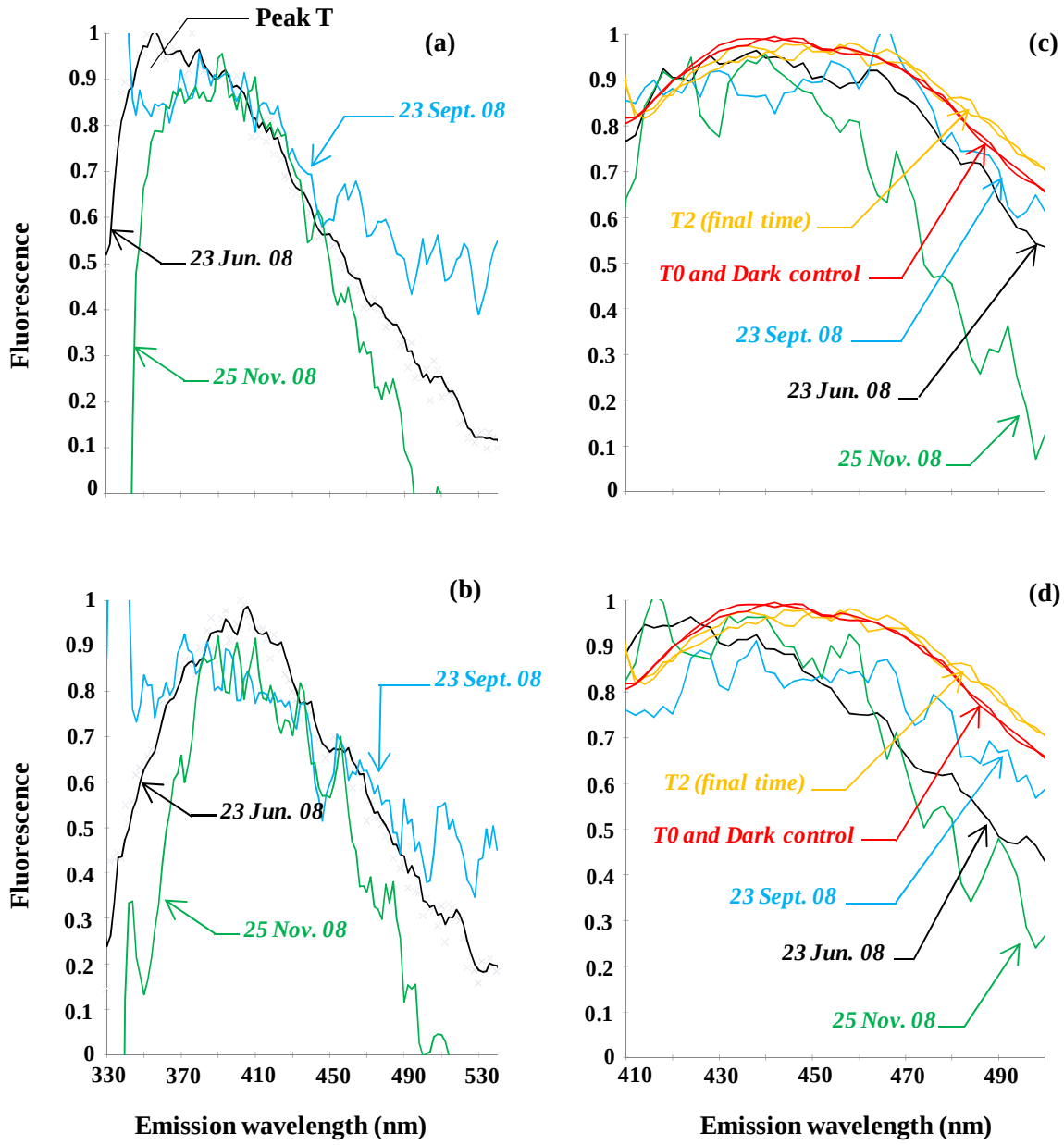

Figure II-6. *Normalized emission spectra of peak M at Ex = 300 nm (a and b) and peak C at Ex = 350 nm (c and d) acquired at SOFCOM station on 23 June (Rhône plume intrusion sample, black solid line), 23 September (photobleached sample, blue solid line) and 25 November 2008 (well mixed sample, green solid line) at 2 (upper panel) and 5 m (bottom panel) depths. Normalized emission spectra of peak C determined at T0, dark control (red solid line) and T2 (duplicate, orange solid line) of the irradiation experiment performed on Rhône River sample collected on 7 February 2009 at 2 m depth were also plotted on both panels c and d. These emission spectra were normalized to the maximum emission intensity in the range 380-400 nm for the peak M and 430-450 nm for the peak C. These spectra were smoothed by a moving average order 3 which imposes a red shifted of 5 nm.*

5. Discussion

5. 1. Evidence for a biological origin of CDOM at SOFCOM station

Despite the low and quite stable values of $a_{CDOM}(350)$ determined in surface waters of the Bay of Marseilles, the significant inverse linear relationship observed at both depths between $a_{CDOM}(350)$ and salinity illustrated a theoretical conservative behavior of surface CDOM in this area. This represents the first report of the potential biogeochemical influence of the Rhône River plume in this oligotrophic coastal area. Such a strong significant inverse relationship between salinity and fluorescent/absorbant CDOM is typically observed in coastal areas subjected to high river inputs (Blough et al., 1993; Green and Blough, 1994; Nelson and Guarda, 1995; Højerslev et al., 1996; Nieke et al., 1997; Vodacek et al., 1997; Seritti et al., 1998; Del Castillo et al., 2000; Ferrari, 2000; Stedmon et al., 2000).

By contrast, the lack of correlation between salinity and fluorescence intensities of peaks C and M at 2 m depth (excluding the maximum values, 25 November 2008) and the only weakly significant correlation observed for 5 m depth samples suggest that the Rhône River plume is not a dominant source of fluorescent CDOM in the Bay of Marseilles. Fluorescent CDOM content in surface waters is likely driven by others processes such as *in situ* production or photo-oxidation rather than water mixing as already hypothesized by Vignudelli et al. (2004) for coastal waters of the northern Tyrrhenian Sea (Italy). The first of these processes is photobleaching, which has more impact on fluorescence than on absorbance properties (Moran et al., 2000; Nieto-Cid et al., 2006). This phenomenon is likely observed during water stratification, especially during spring and summer periods when UV irradiance is high (Table 1). Therefore, it is very likely that samples collected at the end of summer period (23 September 2008), were strongly photobleached explaining the lack (loss) of peaks M and C (Fig. II-4). This assumption would be consistent with high S_{CDOM} coupled to low $a_{CDOM}(350)$ values (Table II-1) that fell beneath the mixing line in Fig. II-3, and suggest a net loss of CDOM at this time (i.e. on 10 July 2008 and 23 September 2008). In addition, the lowest specific absorption coefficient ($a_{CDOM}(350)$/TOC = 0.0010 and 0.0009 at 2 and 5 m depths respectively) was determined at this date too. *In situ* production is another process that may modify CDOM fluorescence character. Indeed, phytoplankton production (Romera-Castillo et al., 2010), zooplankton grazing (Coble et al., 1998) and bacterial activity (Stedmon and Markager, 2005) may induce production of fluorescent CDOM through by-

products, especially peaks B, T, and M. Primary production and bacterial activity promoted by the Rhône River plume intrusion event rich in nutrients (Chla concentration > 1 µg l^{-1}; on 6 May 2008 and 23 June 2008) may have produced fluorescent CDOM. Finally, the strong mixing observed on 25 November 2008 sample could have injected relatively aged CDOM from the bottom to the surface as well as nutrients and thus explain an increase of surface CDOM concentrations (Coble et al., 1998; Nelson et al., 2004, Nieto-Cid et al., 2006). Moreover, this humic CDOM showed the highest specific absorption coefficient ($a_{CDOM}(350)$/TOC = 0.0024 and 0.0023 at 2 and 5 m depths, respectively) at both depths and that could explain the highest $a_{CDOM}(350)$ determined at this date.

Surface CDOM content in the Bay of Marseilles results, therefore, from the combination of several processes which differentially affect its fluorescence and absorbance properties. In any case, our results put forward that CDOM properties in this area is much more affected by autochthonous production induced by the Rhône River plume intrusion than by the original Rhône River DOM (i.e. system truly non-conservative).

In Marseilles Bay, during the one year survey, surface CDOM exhibited very low and stable $a_{CDOM}(\lambda)$ and high variability of S_{CDOM}, highest values being observed during summer time. Generally such signals as well as low surface TOC concentration and Chla concentration are observed offshore (Blough and Del Vecchio, 2002) or in an oligotrophic coastal area not influenced by river inputs. High S_{CDOM} could reflect either CDOM photobleaching if $a_{CDOM}(\lambda)$ is low as observed during summer (10 July 2008 and 23 September 2008) or fresh biological CDOM production in surface waters if $a_{CDOM}(\lambda)$ is high as observed on 23 June 2008. By contrast, low S_{CDOM} with high $a_{CDOM}(\lambda)$ as observed on 25 November 2008 suggest the presence of aged CDOM in surface that could be the consequence of the strong mixing of deep water that was reported at this period.

Concerning CDOM fluorescence properties, our study showed the dominance of recent autochthonous compounds (peak T, BIX >1) and extremely low values of humic substances (peaks C and M, HIX ≈ 1) within marine surface CDOM pool. Fluorescence intensity of peak T observed on all dates (except on 23 June 2008 and 25 November 2008) at 2 and 5 m depths (Table II-2) was in accordance to that reported in surface Ise Bay in the Pacific coastal area (Yamashita and Tanoue, 2003). Interestingly, during Rhône River plume intrusion and mixing events in Marseilles Bay, fluorescence intensity of peak T was one order of magnitude higher at 2 m depth (Table II-2). The origins of peaks T and M have been attributed to planktonic activity (Determann et al., 1998; Myklestad, 2000; Nieto-Cid et al., 2006; Romera-Castillo et al., 2010) while the origin of peak C is known to be terrestrial and

thus coming from freshwater inputs (Sierra et al., 1997; 2005; Komada et al., 2002). However, peak C which is relatively abundant in deep waters could also originate from the humification of marine DOM and thus may reach surface waters during upward mixing events (Coble et al., 1998; Parlanti et al., 2000). Mayer et al. (1999) in two Maine estuaries (Atlantic Ocean) observed that seawater samples tended to show higher tyrosine (peak B) while upstream samples were richer in tryptophan (peak T). These observations are in accordance with our results: presence of peak T and absence of peak B in coastal waters (except on 23 June 2008). According to Lakowicz (2006) and Mayer et al. (1999) tyrosine fluorescence is quenched by tryptophan in folded proteins. This implies that the tryptophan observed at SOFCOM station is probably bounded in proteins rather than in free dissolved form.

To reinforce the hypothesis of the biological source of surface fluorescent CDOM in the Bay of Marseilles, 3 fluorescence indices were also calculated including HIX, BIX and M/C peaks ratio (Table II-3). Our results showed low and variable values of HIX and high constant values of BIX, suggesting a predominantly autochthonous origin of DOM and the presence of organic matter freshly released in marine surface waters. The lack of terrestrial signature of CDOM is surprising particularly during Rhône River plume intrusion, easily detected on 23 June 2008 from remote sensing observations. At this date, the lowest HIX value was observed at 2m depth (0.42) while it was around 3 fold more important at 5 m depth (1.22). The efficiency of photo-oxidation process in surface layer could explain such different HIX values between 2 and 5 m depths. Indeed, a significant proportion, as high as 96%, of CDOM from freshwater (i.e. humic material) might be destroyed during long term exposure to solar radiation (Vähätalo and Wetzel, 2004). Grzybowski (2000) estimated riverine CDOM to be 10 fold more sensitive than coastal CDOM to photobleaching, with the effects of this process being detectable after only 6 hours of exposure under natural sunlight. During the eastward spreading of the buoyant Rhône River plume on surface marine waters, an important part of the terrestrial CDOM pool could be removed, as well as a part of the autochthonous CDOM freshly produced, if any, due to photobleaching (Fig. II-5; Vodacek et al., 1997; Del Castillo et al., 1999). Thus, photobleaching could explain the lack of terrestrial fluorescence signature in this coastal area during Rhône River plume intrusion.

High and constant BIX values at both depths illustrated the omnipresence of the peak M, characterizing an autochthonous biological activity which was slightly more important at 2 m than 5 m depth (except on 10 July 2008 during a mixing event), particularly under Rhône River plume influence (23 June 2008) (Table II-3). The competing process of photobleaching

probably hid a part of this biological activity especially in the surface waters. The highest BIX values at 2 m depth determined on 23 June 2008 and 25 November 2008 corresponded respectively to an important Rhône River plume intrusion containing freshly produced CDOM and to a strong water column mixing that may injected humic CDOM in surface waters. The M/C ratio reflects the relative amount of new (marine) to old (terrestrial) CDOM. On 23 June 2008, higher values found at 2 m relative to 5 m depth (Table II-3) reinforces the hypothesis that biological activity and/or photobleaching are more important in the surface layer.

The discrimination between marine phytoplankton and bacteria as the predominant biological source of peak T can be assessed through spectral analyses of this peak according to the criteria of Determann et al. (1998). Normalized emission spectra at Ex = 230 nm at both depths (Fig. II-7, panels b and d) exhibited peaks position in the 325-345 nm range while the one of free dissolved L-tryptophan used as standard was around 360 nm, in agreement with the findings of Determann et al. (1998). A weak second band at 300 nm, specific to phytoplankton species, was only observed for samples from 23 June 2008 (black solid line) and 23 September 2008 (blue solid line) and was more pronounced at 5 m than at 2 m. In normalized excitation spectra at Em = 340 nm (Fig. II-7, panels a and c), the main absorption band in the 220-230 nm range was clearly red shifted around the range 230-235 nm on 9 June 2008 (orange solid line) at both depths and on 10 July 2008 (red solid line) at 5 m depth, as observed by Determann et al. (1998) with bacteria cultures. Moreover, at these dates and depths another absorption band (specific to bacteria) in the range 275-280 nm was observed while at the other dates a signal more or less constant was observed. Therefore, such results perhaps illustrated a dominant phytoplankton origin for tryptophan at both depths on 23 June 2008 and 23 September 2008 while tryptophan had a dominant bacterial origin on 9 June 2008 at both depths and on 10 July 2008 at 5 m depth.

Assessing the predominant biological origin for the other dates studied regarding emission and excitation spectra of tryptophan results is not straightforward, possibly due to an equal contribution of phytoplankton and bacteria origin to the tryptophan content. It is important to note that these results obtained on spectral analyses of peak T are extrapolated from those obtained from *in vitro* experiments (Determann et al., 1998) and thus should be taken to some extent with caution. Interestingly the results of this discrimination were logical regarding the hydrological context. Indeed, dominant phytoplankton origin of tryptophan took place during bloom periods enhanced by nutrients inputs through an intrusion of the Rhône River plume (23 June 2008) and or through a mixing (23 September 2008), whereas dominant

bacteria origin of tryptophan took place (9 June 2008 and 10 July 2008) after or during bloom events. This ecological succession (phytoplankton / bacteria) was in a good agreement with the work of Lemée et al. (2002), which highlights the net heterotrophic character of bacteria in the upper layer of the northwestern Mediterranean Sea.

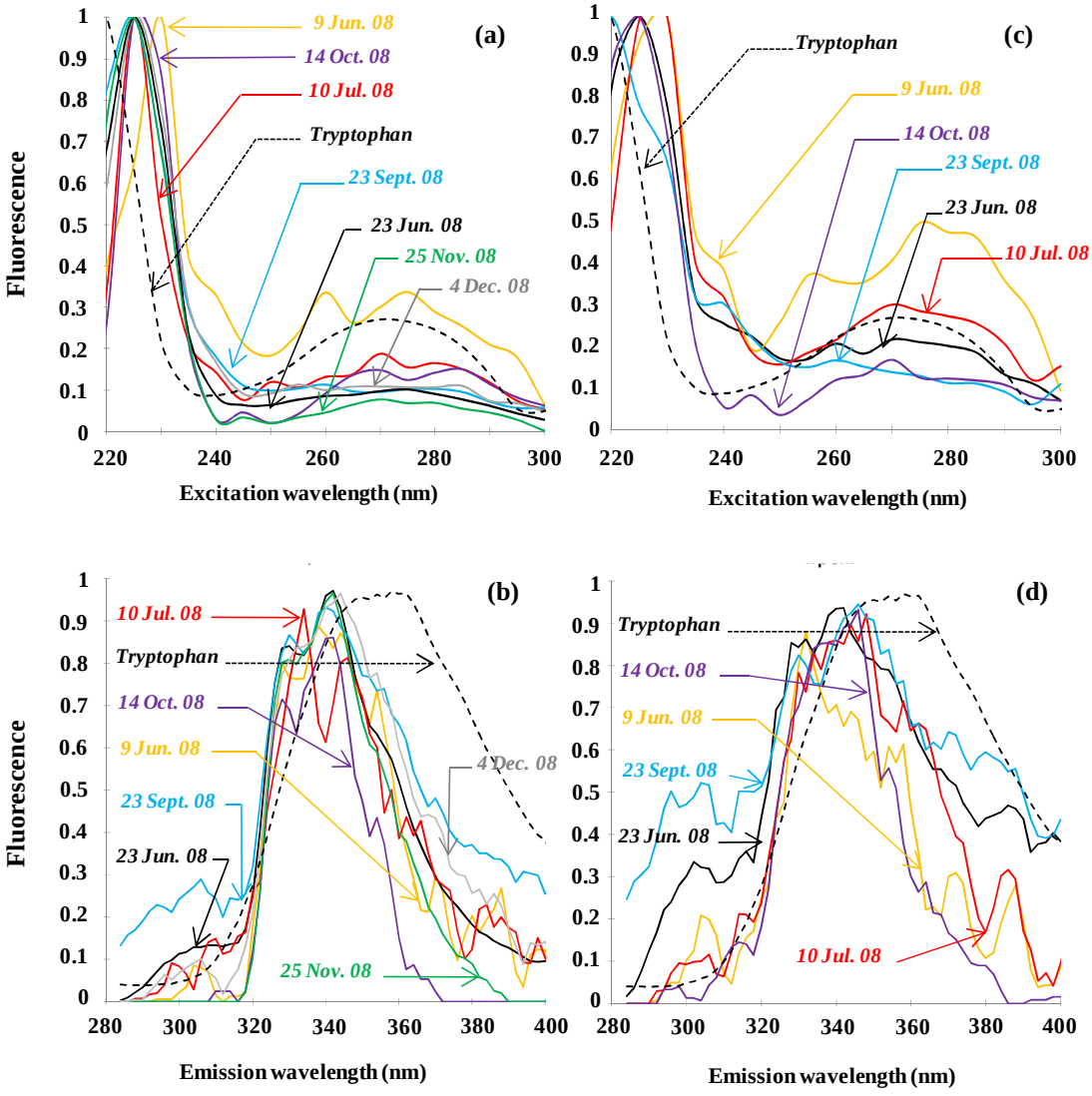

Figure II-7. *Normalized excitation and emission spectra of peak T collected on 9 June (orange solid line), 23 June (black solid line), 10 July (red solid line), 23 September (blue solid line), 14 October (purple solid line), 25 November (green solid line) and 4 December 2008 (grey solid line). All these spectra are compared to a standard solution (75 µg l^{-1} of free dissolved L-tryptophan, > 98%, Sigma-Aldrich, black dashed line). (a) and (c) excitation spectra with Em = 340 nm at 2 and 5 m depth respectively, normalized to the maximum value intensity in the 220-240 nm range. (b) and (d) emission spectra with Ex = 230 nm at 2 and 5 m depth respectively, normalized to the maximum value intensity in the 320-360 nm range. In order to reduce the noise, all these emission-excitation spectra were smoothed by a moving average order 3 which imposes a red shifted of 5 nm.*

5. 2. Seasonal evolution of surface CDOM at SOFCOM station

The results taken as a whole allow seasonal features of the surface CDOM content to be established for the Bay of Marseilles. In spring and summer time, when the water column becomes stratified, freshwater intrusions of the Rhône River plume were easily identifiable by lowered salinities (Fig. II-2). The high nutrient content of this buoyant plume enhanced marine primary production in surroundings surface marine waters (Cruzado and Velasquez, 1990; Pujo-Pay et al., 2006; Joux et al., 2009) (Fig. II-8). This would be consistent with our observations on 6 May 2008 and 23 June 2008. The time scale of its transport to the Bay of Marseilles under solar radiation certainly play a major role in the state of development of primary production associated with bacteria communities and also in the terrestrial CDOM content and properties (Fig. II-8). At the end of spring, on 9 June 2008 (post blooms period), the biological origin of the major fluorescent peak released (peak T, tryptophan-like) was logically dominated by bacteria at 2 and 5 m depths.

At the beginning of summer (23 June 2008) during an important surface extent of the Rhône River plume in the Bay of Marseilles, CDOM content showed a high absorption coefficient along with the highest spectral slope (Table II-1) underlining the biological origin of CDOM. In addition, high fluorescence intensities for all peaks (T, M, C, and B) (Table II-2), as well as fluorescence indices values (HIX, BIX and M/C) (Table II-3) indicated a well developed surface biological activity producing fresh fluorescent CDOM. Moreover, at this period, tryptophan-like material originated from phytoplankton at both depths.

Two weeks after this important bloom, on 10 July 2008, bacteria dominated the biological input of tryptophan at 5 m depth. On this date, the autochthonous production of CDOM was weak while S_{CDOM} was high despite a minor mixing event that probably injected nutrients and humic CDOM into surface waters (Fig. II-8). This could explain the significant values of HIX and BIX. Nevertheless, low $a_{CDOM}(350)$ coupled to a high S_{CDOM} also point out the efficiency of photobleaching effect of CDOM and could explain its net loss observed on 10 July 2008 at both depths.

During the summer time, under any influence of Rhône River plume, photobleaching appeared as a significant sink for CDOM (Fig. II-8). This process was most clearly illustrated at the end of summer time, on 23 September 2008, with respect to the quality and quantity of CDOM content. Indeed, on 23 September 2008 the warm and salty water mass present had persisted at the surface since late July (Fig. II-2) and had thus spent 6-8 weeks exposed to high UV radiation. Values of $a_{CDOM}(350)$ exhibited minima at both depths and spectral slopes

were high especially at 5 m depth where the water was saltiest (Table II-1). Moreover, EEMs illustrated a strong signal of fluorescence in short Ex/Em wavelengths (Fig. II-4), which was attributed to photobleaching. Thus, it was logical that the most important net loss of CDOM due to photobleaching appeared at the end of summer time just before fall mixing.

Finally, during fall, on 25 November 2008, 12 consecutive days of Mistral wind enhanced strong deep mixing that put nutrients back in the surface waters as well humic CDOM, from bottom water (Coble, 1998; Sierra et al., 1997; 2005; Komada et al., 2002) (Fig. II-8). The maximum of value for peak C was observed on this date (Table II-2). Maximum values for autochthonous humic CDOM (peak M) were also observed at this time, probably of bacterial origin (Nieto-Cid et al., 2006). Therefore, the inputs of humic CDOM (peaks C and M) explain the highest $a_{CDOM}(350)$ and the lowest spectral slope of CDOM observed at both depths during this period.

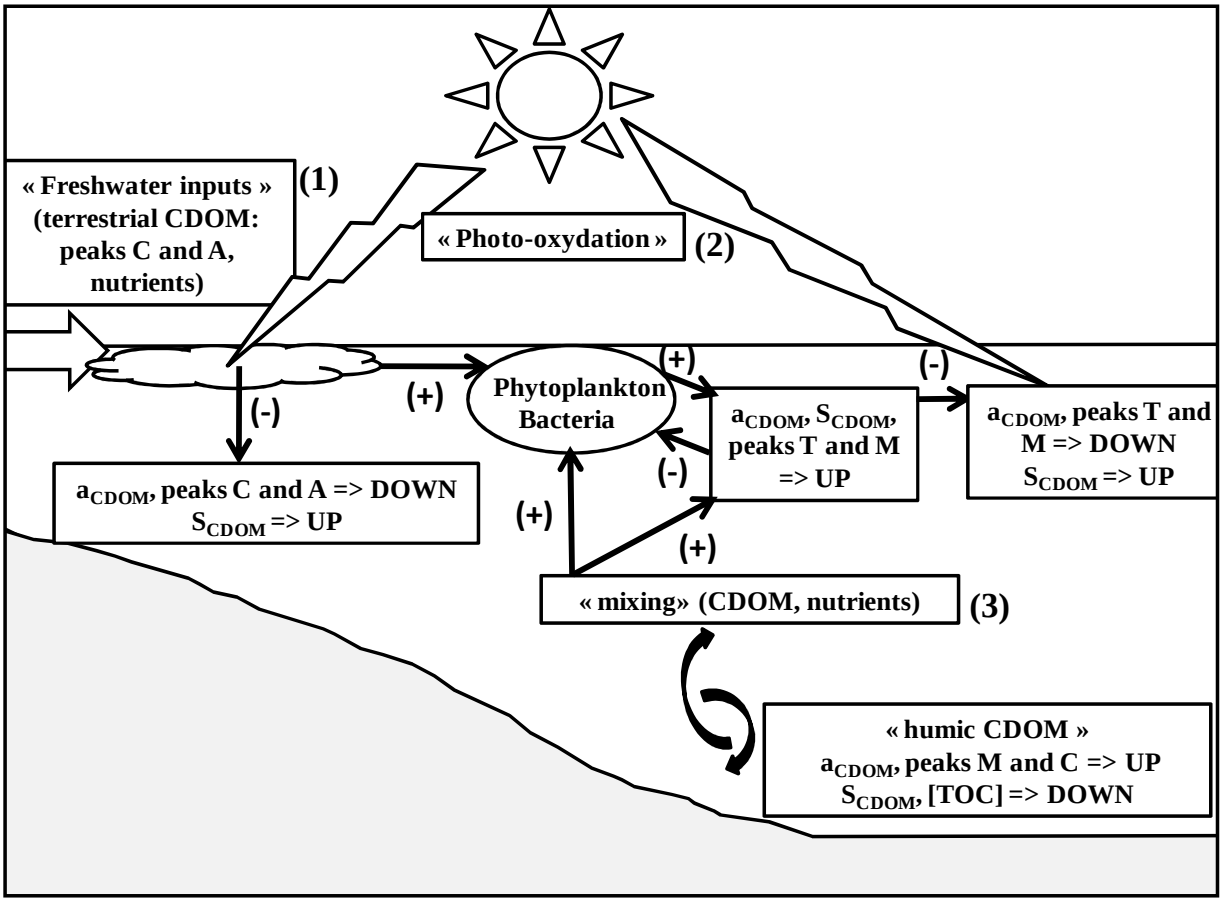

Figure II-8. *Synthesis of processes (Rhône River plume intrusion (1), photo-oxydation of CDOM (2) and water mixing (3)) driving surface CDOM dynamic and content in the Bay of Marseilles and their direct and indirect effects (positive or negative) on CDOM optical properties.*

6. Conclusions and perspectives

This study highlights the low surface CDOM content in the Bay of Marseilles through $a_{CDOM}(350)$ and TOC concentration values. Stable and very low annual mean value of $a_{CDOM}(350)$ prevents the establishment of a seasonal trend, while S_{CDOM} values were significantly higher during the summer time period and thus could reflect either photobleaching or biological production of CDOM in the surface waters. Values of $a_{CDOM}(350)$ in this well-urbanized coastal area were comparable to those usually found in the open ocean. The different fluorescent peaks identified in this study show the predominance of protein-like component, peak T, and marine humic-like component, peak M. The omnipresence of these fluorescent peaks is related to the biological activity occurring mainly in the surface waters of the Bay of Marseilles. The very low content in UVA humic-like peak C demonstrates the quasi absence of terrestrial or aged material within surface fluorescent CDOM composition. Our observations show that the optical properties of water in the Bay of Marseilles are governed mostly by phytoplankton with their accompanying by-products whereas the sporadic terrigeneous influence is negligible. Therefore, this coastal system may be considered as truly non-conservative. In such oligotrophic environment, it appears that fluorescence analyses gather more pertinent information on CDOM composition and dynamics than absorbance analyses.

This study points out for the first time that the surface waters of the Bay of Marseilles are influenced by episodic events of the eastward extent of the Rhône plume. In this coastal oligotrophic area, these events enhance surface primary production and bacterial activity in surroundings waters which in turn increase the surface CDOM production. This source of CDOM appears more efficient at 2 m and during water stratification. On the other side, photobleaching acts as a significant sink of CDOM in summer, whereas the mixing of bottom waters containing humic CDOM may enrich the surface waters.

From the results presented in this work, it appears clearly that the Rhône River plume intrusions as well as mixing of the water column have a significant impact on the biogeochemical cycles in the Bay of Marseilles. Determining photobleaching rates of surface CDOM appears also as an important issue. A higher temporal determination of these processes in this coastal area will enable a better understanding of the biogeochemical/physical processes driving the CDOM distribution, dynamics and fate in the Marseilles Bay and will shed light on some features, not observed in this study, such as

interseasonal trend of CDOM, and relationships between fluorescence, absorbance and DOC concentration, commonly observed in coastal area.

CHAPITRE III

ATTENUATION DU RAYONNEMENT UV ET PAR EN RELATION AVEC LES PARAMETRES BIOGEOCHIMIQUES DANS LES EAUX COTIERES DE LA MEDITERRANEE NORD OCCIDENTALE

Des mesures radiométriques couplées à la collecte d'échantillons discrets d'eau de mer de surface ont été effectuées mensuellement au midi solaire, au niveau de la station SOFCOM en Baie de Marseille (5°17'30"E, 43°14'30"N), entre Novembre 2007 et Décembre 2008. Les éclairements de surface ($E_s(\lambda)$) et les profils d'éclairement sous-marin descendant ($E_d(\lambda)$) ont été mesurés simultanément à 305 nm (UVR-B), 325, 340, 380 nm (UVR-A) et dans le PAR. Durant l'année d'étude, les $E_s(\lambda)$ à 305 nm (UVR-B), 340 nm (UVR-A) et dans le PAR ont varié respectivement de 0,14 à 4,7 µW cm^{-2}, de 11 à 59 µW cm^{-2} et de 0,04 à 0,20 µE cm^{-2} s^{-1}. Les $E_s(\lambda)$ présentaient une variation saisonnière en accord avec celle de l'élévation du soleil, avec un rayonnement solaire 7 à 8 fois plus enrichi en UVR-B en été qu'aux autres saisons. Les moyennes annuelles des valeurs du coefficient d'atténuation diffus ($K_d(\lambda)$) à 305 nm (UVR-B), 340 nm (UVR-A) et dans le PAR étaient faibles et constantes (respectivement 0,403 ± 0,059, 0,229 ± 0,025 et 0,097 ± 0,014 m^{-1}), illustrant une forte transparence des eaux de surface aux UVR et au PAR toute l'année. Cette transparence des eaux de surface, couplée à la qualité du rayonnement solaire enrichi en UVR-B l'été, souligne un fort potentiel de la photochimie dans cette zone. Les relations établies entre K_d(UVR), K_d(PAR) et la CDOM démontrent le rôle prépondérant de la CDOM dans le contrôle de la pénétration des UVR et du PAR dans cette zone oligotrophe. De plus, cette CDOM d'origine essentiellement biologique présente des variations dans son spectre d'absorption en fonction de son état de fraicheur. En effet, la CDOM récente absorbe préférentiellement les courts UVR, alors que la CDOM plus ancienne, qui s'accumule dans les eaux de surface, aura tendance à absorber les UVR ainsi que le PAR.

ATTENUATION OF UVR AND PAR IN RELATION WITH BIOGEOCHEMICAL FACTORS IN SURFACE COASTAL WATERS OF THE NORTHWESTERN MEDITERRANEAN SEA

Julien Para[1, 2], Richard Sempéré[1, 2], Marc Tedetti[1, 2] and Bruno Charrière[1, 2]

[1] *Université de la Méditerranée, Centre d'Océanologie de Marseille, Case 901, 13288 Marseille Cedex 9, France.*

[2] *CNRS/INSU, UMR 6117, LMGEM, Case 901, 13288 Marseille Cedex 9, France*

In preparation

1. Abstract

Radiometric measurements and the collection of discrete surface seawater samples for chromophoric dissolved organic matter (CDOM) and total organic carbon (TOC) were performed monthly at noon in a coastal northwestern Mediterranean Sea station (5° 17' 30" E, 43° 14' 30" N) from November 2007 to December 2008 and completed by CTD cast equipped with turbidity and chlorophyll *a* (Chl*a*) sensors. Sea surface irradiance [($E_s(\lambda)$, µW cm^{-2})] and in-water profiles of downwelling irradiance [$E_d(Z, \lambda)$, µW cm^{-2}] were simultaneously measured in UVB (305 nm); UVA (325, 340 and 380 nm) and PAR spectral domains. The results showed that surface irradiance ($E_s(\lambda)$, µW cm^{-2}) for UVR-B (305 nm), UVR-A (340 nm) and PAR ranging from 0.14 to 4.7, 11 to 59 µW cm^{-2} and from 0.04 to 0.20 µE cm^{-2} s^{-1}, respectively, present clear seasonal variation upon to the season (sun elevation) and underline the important amount of energetic UVR-B, 7-8 folds richer during summer time compared to winter period. Annual mean values of diffuse attenuation coefficient for downwelling UVR and PAR irradiances K_d(UVR) at 305 nm (UVR-B), 340 nm (UVR-A) and K_d(PAR) were relatively constant with 0.403 ± 0.059, 0.229 ± 0.025 and 0.097 ± 0.014 m^{-1}, respectively. Solar radiation quality, coupled at these low constant values of $K_d(\lambda)$ illustrating a high solar transparency of surface waters throughout the year, highlights that UVR is an important physical forcing that may influenced the overall biogeochemistry in this area. Relationships linking CDOM absorption with both K_d(UVR) and K_d(PAR), suggested strongly that CDOM is the preponderant optical active component in the UVR and PAR attenuation in this surface oligotrophic system. In addition, the dominant aged freshest state of the CDOM appeared to act as a persistent background of CDOM which control mostly underwater UVR and PAR fields throughout the year.

2. Introduction

In the ocean, solar radiation influences strongly the biogeochemical cycles and ecosystem functioning (Vincent and Roy, 1993; Häder et al., 1998; 2003). The key role of photosynthetically available radiation (PAR: 400-700 nm) is to provide the energy for photosynthesis and induce primary production, upon which all marine food webs ultimately depend. The penetration of PAR in the water column controls the depth of the euphotic zone (Z_{eu} in m). By contrast, energetic ultraviolet radiation (UVR: 280-400 nm) is well known to have numerous deleterious effects on living organisms through inhibition of photosynthetic activity and the production of DNA damages (Vincent and Neale 2000; Helbling et al., 2001; Häder et al. 2007; Villafane et al. 2008). The penetration depth, intensity and spectral distribution of solar radiation in the water column depend on the amount and quality of optically active constituents of seawater, also called inherent optical properties (IOPs), and on the quality and intensity of surface solar irradiance, which is strongly influenced by solar zenith angle (SZA) and meteorological conditions. Surface waves may also impact the surface underwater light field by focusing and defocusing solar radiation refracted by the sea surface (Schenck, 1957).

Several IOPs contribute to the overall attenuation of PAR and UVR in the water column, the attenuation of light at a specific wavelength [$c(\lambda)$ in m^{-1}] being the resultant of both absorption [$a(\lambda)$ in m^{-1}] and backscattering [$b_b(\lambda)$ in m^{-1}] processes at this wavelength. They include water itself [$a_w(\lambda)$ and $b_{bw}(\lambda)$], phytoplankton [($a_{ph}(\lambda)$ and $b_{bph}(\lambda)$], non-algal particulate [($a_{nap}(\lambda)$ and $b_{bnap}(\lambda)$] and chromophoric dissolved organic matter [$a_{CDOM}(\lambda)$]. The contribution of CDOM to scattering is very small relative to the other terms and is thus usually neglected. The absorption and backscattering coefficients of pure water have been recently re-assessed by Morel et al. (2007). Absorption of pure water is characterized by very low values in the blue, and increase in the red and UV portions of the spectrum. Phytoplankton absorption varies significantly in relation to community composition. Peaks are typically found around 440 and 683 nm and are linked to chlorophyll *a* (Chl*a*) (Kirk, 1994). CDOM and NAP absorption spectra tend to decrease monotonically with increasing wavelength (Bricaud et al., 1981; Nelson et al., 1998). The penetration of solar radiation in the water column is evaluated through the determination of the vertical diffuse attenuation coefficient for downwelling irradiance ($K_d(\lambda)$ in m^{-1}). $K_d(\lambda)$ is defined as the slope of the linear regression of the log-transformed downwelling irradiance ($E_d(\lambda)$ in $\mu W\ cm^{-2}$) *versus*

depth (Kirk, 1994) and referred to as a quasi-IOP because it is influenced by the IOP content. In the ocean, Chl*a* and CDOM are the main contributors to the attenuation of PAR and UVR, respectively (Diaz et al., 2000). Interestingly, the role of CDOM in the attenuation of PAR is still controversial since it has been found minimal (Hargreaves, 2003; Zepp et al., 2008) or, on the contrary, significant (equal to the contribution of Chl*a* at 440 nm; Siegel et al., 2005).

The Mediterranean basin is characterized by relatively high solar radiation levels, compared to similar latitudes in the Atlantic Ocean (Bishop and Rossow, 1991), due to its weak cloud cover (Vasilkov et al., 2001; Seckmeyer et al., 2008; Cristofanelli and Bonasoni, 2009; the Mermex group, 2011). Solar radiation flux reaching the whole Mediterranean exhibited a strong seasonal cycle (Ruiz et al., 2008) and might be locally attenuated by anthropogenic (Horvath et al., 2002; Markowicz et al., 2002; Mallet et al., 2006) or natural aerosols (Saha et al., 2008; Cachorro et al., 2008). The Mediterranean Sea is known as low chlorophyll low nutrients (LNLC) system and contains blue clears waters. However, the Mediterranean waters blueness is not as deep as expected from chlorophyll content due to an excessive level of CDOM (Claustre et al., 2002; Lee and Hu, 2006; Morel et al., 2007a) and/or the presence of coccoliths and aeolian dust (Claustre and Maritorena, 2003). The amount of CDOM in the Mediterranean Sea is around twice the one of the Atlantic Ocean at similar latitudes at same chlorophyll level and the amount of CDOM is not only higher in the western basin than in the eastern basin but also inside the western basin with higher amount in the northern part compared to the southern part (Morel and Gentili, 2009). *In situ* radiometric measurements indicated that overall euphotic layer (Z_{eu}) varies from 40-60 m depth in the western basin (Moran and Estrada, 2001) to 100 m in the eastern basin (Moutin and Raimbault, 2002). However, in some northern coastal areas subjected to high nutrients (Ludwig et al., 2009) and dissolved organic carbon (DOC) inputs from rivers (Sempéré et al., 2000) the usual oligotrophic regime is sporadically modified. Indeed, phytoplankton blooms enhancing by these inputs lead to a red shift of the sea color from blue toward blue-green shades typical of meso to eutrophic status and thus reflecting a decrease of the euphotic layer depth. While the attenuation of PAR has been largely documented, there are currently very punctual few data concerning the attenuation of UVR-B (280-315 nm) and UVR-A (315-400 nm) in the surface waters of the Mediterranean Sea, especially with regard to their temporal variation. Paradoxically, the values measured for the penetration of UVR in the Mediterranean Sea appear at the high end of those reported for other marine systems (Tedetti and Sempéré, 2006; Morel et al., 2007; Tedetti et al., 2007).

The goals of this study are: (i) to document and describe the annual temporal variability of UVR and PAR attenuation in surface coastal waters of the Northwestern Mediterranean Sea (Bay of Marseilles) with a special care dedicated to the $K_d(\lambda)$ determination in the surface waters, and (ii) to investigate the biogeochemical parameters controlling surface $K_d(\lambda)$ in both UV and PAR spectral domains.

3. Materials and methods

3. 1. Study area and field measurements

Field measurements were performed monthly at solar noon under different sky (sunny, overcast) and calm conditions (slightly wind and swell) from November 2007 to December 2008 (Table III-1) on board the R/V Antedon II at the 60 m depth coastal SOFCOM station (5°17'30''E; 43°14'30''N) located at 5 km off Marseilles in the northwestern Mediterranean Sea (Figure III-1). Field measurements included atmospheric and in-water radiometric measurements and collection of discrete samples at 2 m depth using a 4 l Niskin bottle, equipped with silicon ribbons and Viton o-rings, for the determination of total organic carbon (TOC) and chromophoric dissolved organic matter (CDOM). Temperature, salinity, Chlorophyll *a* concentration ([Chl*a*]) and turbidity *in situ* profiles were obtained from a 19*plus* SeaBird Electronics conductivity-temperature-depth (CTD) equipped with a WETStar Chlorophyll *a* fluorometer (WETLabs) and a STM turbidity meter (Seapoint).

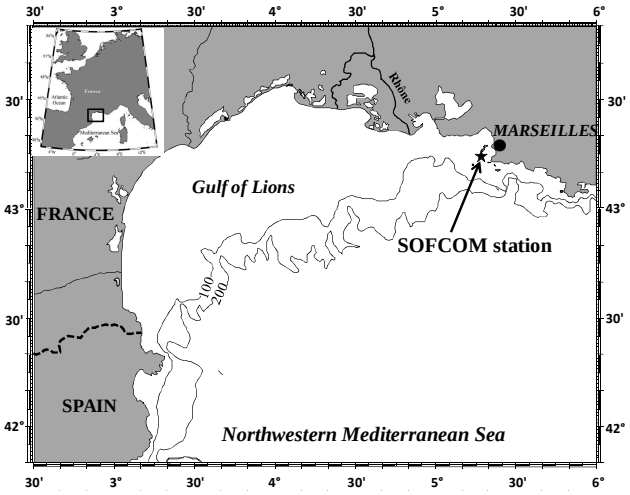

Figure III-1. *Map of the Gulf of Lions located in the northwestern Mediterranean Sea marking the location of SOFCOM station in the Bay of Marseilles.*

3. 2. *In situ* radiometric measurements

Two consecutive downcast radiometric profiles of $E_d(Z, \lambda)$ were performed at solar noon (Table III-1) using a MicroPro free-fall profiler (Satlantic), equipped with pressure, temperature and tilt sensors and OCR-504 downward irradiance sensors in the UVB (305 nm), UVA (325, 340 and 380 nm) and PAR (412, 443, 490 and 565 nm) spectral domains. Profiler was operated with a sampling rate of 7 Hz (sampling resolution of 10 cm) and from the rear of the ship and deployed 30 m away to minimize the shadowing effects and disturbances of the ship. Surface irradiance ($E_s(\lambda)$, $\mu W\ cm^{-2}$) [which is equivalent to the downwelling irradiance just above the sea surface ($E_d(0^+,\lambda)$)], was simultaneously measured at the same channels on the ship deck using other OCR-504 downwelling irradiance sensors (surface reference) to account for the variations of cloud conditions during the cast.

Measurements were logged using Satlantic's Satview 2.6 software that allowed for initial data processing, such as PAR data calculation, the application of radiometric calibration, dark correction, pressure tare and the removal of data with tilt > 5°. The interpolation data option of the software was not used in order to work with the raw radiometric data and to avoid smoothing of the latest. Profiles of $E_d(Z, \lambda)$ in the total PAR range were estimated from the four PAR channels. $E_d(Z,\lambda)$ was first interpolated onto an 1 nm interval from 400 to 700 nm and then integrated using the formula:

$$E_{d,PAR}(Z) = \int_{400\,nm}^{700\,nm} \lambda / hc\ E_d(Z,\lambda)\ d\lambda \quad (1)$$

where $E_{d,PAR}(Z)$ is the downwelling irradiance in the PAR range at depth Z ($\mu E\ cm^{-2}\ s^{-1}$), λ is the wavelength (nm), h is the Planck's constant ($6.63.10^{-34}$ J s), c is the speed of light in the vacuum (3.10^8 m s^{-1}) and $E_d(Z,\lambda)$ is the downwelling irradiance at depth Z ($\mu W\ cm^{-2}$).

3. 3. Determination of diffuse attenuation coefficient for downwelling irradiance

K_d(UVR) and K_d(PAR) were calculated in an homogeneous surface water mass from $E_d(Z,\lambda)$ and $E_{d,PAR}(Z)$ data, by using the method of Zaneveld et al. (2001) or the standard method depending of significant surface irradiance fluctuations observation or not, respectively (Table III-2). In the standard method, $K_d(\lambda)$ was calculated from the slope of the linear regression of the log-transformed downwelling irradiance *versus* depth in accordance with the relationship:

$$E_d(Z,\lambda) = E_d(0^-,\lambda)\ \exp^{(-Kd(\lambda)\ Z)} \quad (2)$$

where $E_d(0^-, \lambda)$, the downwelling irradiance beneath the sea surface, was theoretically computed from deck measurements using the formula (Smith and Baker, 1984):

$$E_d(0^-,\lambda) = E_d(0^+,\lambda) / (1 + \alpha) \quad (3)$$

where α (0.043) is the Fresnel reflection albedo for irradiance from sun and sky. The depth ranges, from which $K_d(\lambda)$ were derived, were reported in Table III-2. In the Zaneveld method, $K_d(\lambda)$ determination is based on the upward integration of $E_d(\lambda)$ starting at the focal depth (Z_0, m), at which the irradiance profile is considered as not affected by the wave focusing, to successively shallower depths according to the following formula (Zaneveld, 2001):

$$I'(z) = \int_{Z0}^{Z} Ed(z)dz \approx I(z) \quad (4)$$

where the slope of ln (dI'(z)/dz) is $K_d(\lambda)$. The usual criterion to determine Z_0 was to see how much the next point (depth) will change the calculation of $K_d(\lambda)$ by using the standard method. If adding the next depth (Z+1) changes $K_d(\lambda, Z)$ by less than 5% thus Z_0 was reached. In our study, Z_0 ranged from 5 to 9.5 m according to the wavelength (Table III-2). The mean variability (CV %) of K_d(UVR) and K_d(PAR) determined between the two profiles done was less than 6 and 7 %, respectively. Since attenuation decreases with increasing wavelength in the UV range, any $K_d(\lambda)$ value that was lower than those at longer wavelengths were deleted. Values of $K_d(\lambda)$ at 305 nm were particularly prone to error.

3. 4. CDOM absorbance measurements

CDOM absorbance was measured throughout the UVR and PAR spectral domains (280-700 nm) using the multiple pathlength, liquid core waveguide system Ultrapath (MPLCW, WPI Inc.). Absorbance spectra of samples were measured through the longest pathlength (2 m long) and with reference to a filtered salt solution prepared with Milli-Q water and precombusted NaCl (Sigma) reproducing the refractive index of samples to minimize baseline offsets in absorption spectra (D'Sa et al., 1999). Reference salt solution and samples were brought to room temperature before analysis. Between each sample, the sample cell was flushed with successively diluted detergent (cleaning solution concentrate, WPI Inc.), high reagent grade MeOH, 2 M HCL and Milli-Q water. Trapped microbubbles were minimized by using a peristaltic pump to draw the sample into the sample cell. The spectral absorption coefficients, $a_{CDOM}(\lambda)$ (m^{-1}) were obtained using the following relationship:

$$a_{CDOM}(\lambda) = 2.303A(\lambda)/L \quad (5)$$

where $A(\lambda)$ is the absorbance at wavelength λ (dimensionless) and L is the pathlength in meters. Here, S_{CDOM} was determined after applying a non-linear exponential regression to original $a_{CDOM}(\lambda)$ data measured on the range 350-500 nm. All the determination coefficients (R^2) calculated from these exponential fits were always larger than 0.99.

3. 5. TOC analysis

For TOC determination, samples were analyzed by using the commercially available model TOC-5000 Total Carbon Analyzer. The accuracy and the system blank of our instrument were determined by the analysis of the reference material (D. Hansell, Rosenstiel School of Marine and Atmospheric Science, Miami, USA) including Deep Atlantic Water (DAW) and low carbon water (LCW) reference standards (Sohrin and Sempéré, 2005). The average DOC concentrations in the DAW and in the LCW reference standards were 45 ± 2 µM C, n = 24 and 1 ± 0.3 µM C, n = 24, respectively. The nominal analytical precision of the analysis procedure was within 2%.

4. Results and discussion

4. 1. Biogeochemical and hydrological contexts

During the study period, dynamics of CDOM, [TOC] and [Chl*a*] in surface waters as well as water column conditions (temperature and salinity) in the Bay of Marseilles (SOFCOM station) were largely described in Para et al. (2010). Briefly, this study showed low annual averaged [TOC] (67 ± 7 µM C) as well as very low CDOM absorption coefficient at 350 nm ($a_{CDOM}(350)$ = 0.10 ± 0.02 m^{-1}) and [Chl*a*] (0.64 ± 0.45 µg l^{-1}) (Table III-1). However, CDOM dynamics and content in this coastal oligotrophic system were evidenced to be controlled by biogeochemical/physical processes. Indeed, episodic events of the eastward extent of the buoyant Rhône plume in surface waters of Marseilles' Bay, observed on 6 May and 23 June 2008, enhanced surface primary production ([Chla]> 1µg l^{-1}; Table III-1) which in turn increase fresh CDOM production characterized by relatively low molecular weight components (Para et al., 2010). On the other side, photobleaching acts as a significant sink of CDOM in summer (photobleached sample on 23 September 2008 presented high S_{CDOM} and low $a_{CDOM}(350)$ values; Table III-1), whereas in fall and winter periods the mixing of bottom waters containing aged/humic CDOM may enrich the surface waters (mixed sample on 25 November 2008 shown low S_{CDOM} and high $a_{CDOM}(350)$ values; Table III-1).

Table III-1. *Sampling dates with corresponding sky conditions and biogeochemical factors available for the coastal waters of the Northwestern Mediterranean Sea (SOFCOM station; Figure* III-*1). Solar zenith angle (SZA) was determined by using the look up table and solar position calculator of the National Oceanic and Atmospheric Administration (NOAA).*

			$a_{CDOM}(350)$ [m^{-1}]	S_{CDOM} [nm^{-1}]	TOC [µMC]	Chl*a* [µg l^{-1}]	Turbidity [NFU]
Date	Sky condition	SZA (deg.)	2m	2m	2m	2m	2m
7 Nov. 2007	sunny	61	0.11	0.018	68	0.25	_
19 Dec. 2007	sunny	67	0.10	0.017	60	0.57	_
5 Feb. 2008	sunny	63	0.11	0.016	55	0.90	_
14 Feb. 2008	sunny	59	0.09	0.018	78	0.20	_
26 Mar. 2008	sunny	41	0.10	0.016	56	0.21	0.67
29 Apr. 2008	sunny	30	0.11	0.018	70	0.85	4.83
6 May 2008	overcast	36	0.13	0.018	65	1.55	5.31
9 Jun. 2008	overcast	32	0.11	0.022	70	0.77	22.04
23 Jun. 2008	sunny	26	0.12	0.026	79	1.42	7.70
10 Jul. 2008	sunny	22	0.09	0.023	67	0.19	0.64
23 Sep. 2008	overcast	45	0.07	0.021	72	0.40	3.94
14 Oct. 2008	sunny	52	0.09	0.018	70	0.33	0.10
25 Nov. 2008	sunny	64	0.13	0.014	55	0.58	4.82
4 Dec. 2008	overcast	66	0.11	0.017	63	0.76	5.46

4. 2. Seasonal evolution of surface irradiances

Averaged annual UVR-B (305 nm), UVR-A (340 nm) and PAR $E_s(\lambda)$ values at solar noon were 1.49 ± 1.48, 32.15 ± 15.46 µW cm^{-2} nm^{-1} and 0.12 ± 0.05 µE cm^{-2} s^{-1}, respectively (Figure III-2 A). The maximum $E_s(\lambda)$ values measured were 4.64, 40.14, 58.88, 79.62 µW cm^{-2} nm^{-1} and 0.2 µE cm^{-2} at 305, 325, 340 380 nm and PAR, respectively. At the same wavelengths, maximum $E_s(\lambda)$ values of this study are twice lower at 305 nm but in the same range for the other wavelengths than those reported in the South East Pacific (9.26, 46.34, 61.29, 87.15 µW cm^{-2} nm^{-1} and 0.22 µE cm^{-2} s^{-1}) (BIOSOPE cruise, Tedetti, unpublished data) and are representative of the Mediterranean Basin (Obernosterer et al., 1999a). Excluding cloudy days' measurements (6 May, 9 June, 23 September and 4 December 2008) during which UVR and PAR surface irradiances declined strongly, $E_s(\lambda)$ at all wavelengths studied were inversely correlated with SZA ($R^2 > 0.92$, n = 10, $p < 0.1\%$, not shown). This came from the spectral dependence of diffuse/direct $E_s(\lambda)$ ratio for various SZA upon the season (Vantrepotte and Mélin, 2006). Therefore, $E_s(\lambda)$ values increased from December 2007 (highest SZA) to July 2008 (lowest SZA), and then decreased until December 2008 (second highest SZA) (Figure III-2 A).

Examination of UVR-B/PAR, UVR-A/PAR and UVR-B/UVR-A surface irradiance ratios (Figure III-2 B and C) indicated similar seasonal evolution of UVR-A and PAR while the UVR-B increased 7-8 folds more than its UVR-A and PAR counterparts during summer time. Such UVR-B strong seasonal variability could be explained by its stronger spectral dependence of diffuse/direct $E_s(\lambda)$ ratio compared to UVR-A and PAR. The significant inverse relations observed (not shown) between UVR-B/PAR ($R^2 = 0.93$, $p < 0.1\%$, n = 14) and UVR-B/UVR-A ($R^2 = 0.91$, $p < 0.1\%$, n = 14) ratio and SZA reinforced this explanation. These results are consistent with previous report indicating strongly photobleached CDOM at the end of summer time (Para et al., 2010) and suggest that during summer, stratified surface waters and higher relative abundance of UVR-B favor photochemical reactions on chemical and biological species.

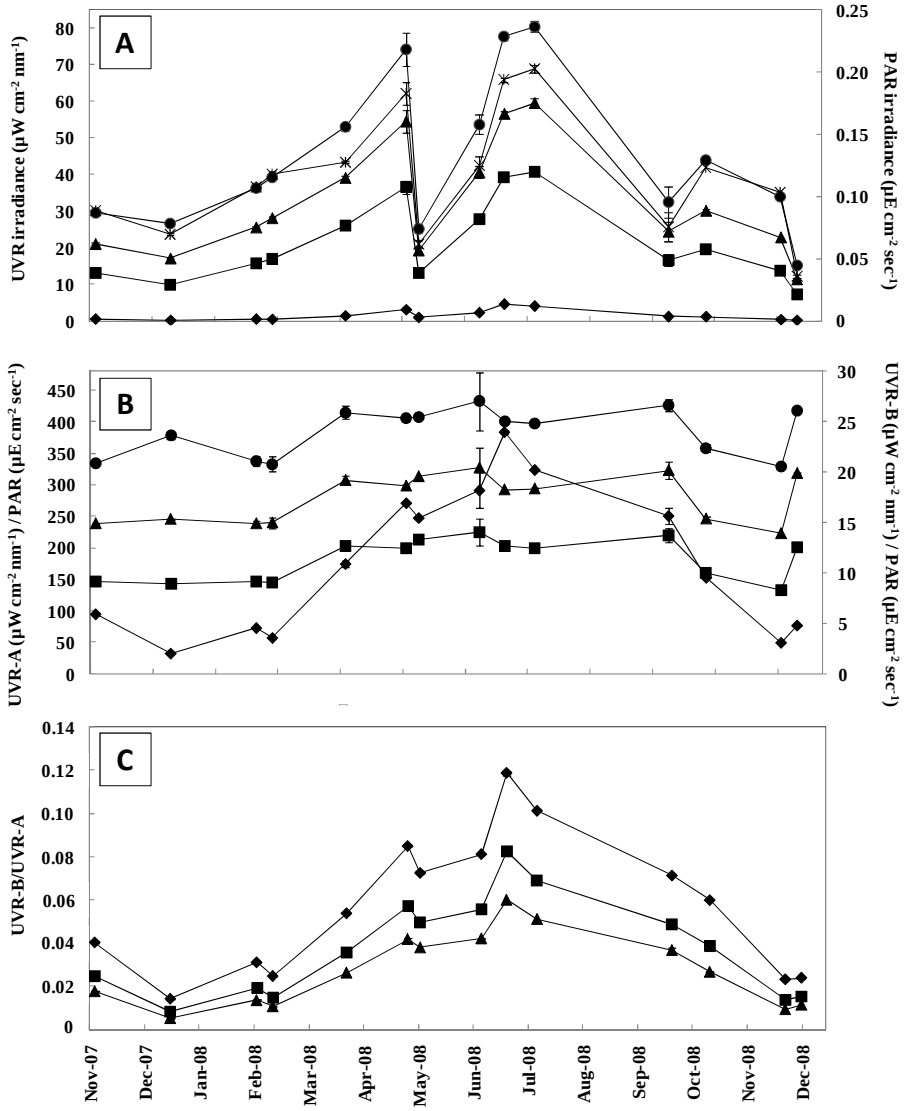

Figure III-2. *Temporal evolution of UVR at 305 (rhombus), 325 (squares), 340 (triangles), 380 nm (circles) and PAR (crosses) surface irradiances (A), UVR-A/PAR and UVR-B/PAR ratios (B) and UVR-B/UVR-A ratios (C) ($E_s(305)/E_s(PAR)$, $E_s(340)/E_s(PAR)$ and $E_s(305)/E_s(340)$). $E_s(\lambda)$ were recorded by irradiance sensors on the ship deck during the vertical profiling of underwater UVR and PAR at SOFCOM station from November 2007 to December 2008. Standard deviations illustrate $E_s(\lambda)$ variability observed during the two profiles done. Full-Width Half-Maximum (FWHM) of the channels was 2 nm for 305, 325 and 340 nm, and 10 nm for UVR and PAR in-water sensors, 2 nm for 305, 325 and 340 nm and 10 nm for PAR for in-air sensors. For the UV channels, the accuracy of the cosine response for irradiance within 0-60° for in-water and in air sensors was 8 and 4%, respectively. For the PAR channels, the accuracy of the cosine response for irradiance within 0-60° was 3%. The typical noise equivalent irradiance (NEI) was $1.5.10^{-3}$ (UVR-B), $4.5.10^{-3}$ (UVR-A) and $2.5.10^{-3}$ (PAR) $\mu W\ cm^{-2}$.*

4. 3. Seasonal evolution of diffuse attenuation coefficient in surface waters

The percentage of surface irradiances fluctuation observations and the distribution of $Z_0(\lambda)$ varied according to the wavelength studied. Indeed, $Z_0(\lambda)$ deepened monotonically from UVR to PAR and the percentage of surface irradiances' fluctuations observations increased also from UVR-B (13%) to PAR (85%; Table III-2). This is connected to higher fraction of diffusive irradiance at shorter wavelengths than at longer wavelengths (especially in oligotrophic oceanic system) in relation with the wavelength dependence of molecular scattering following a power law with the exponent of - 4.32 (Stramska and Dickey, 1998). This process may very likely explain that significant surface fluctuation of UVR and PAR were not observed during most of overcast days (6 May, 9 June, 23 September and 4 December 2008) and beyond Z_0 (λ (diffuseness of solar radiation; Table III-2). Averaged of downwelling irradiance profiles at 305 nm (UVR-B), 340 nm (UVR-A) and PAR are illustrated in Figure III-3.

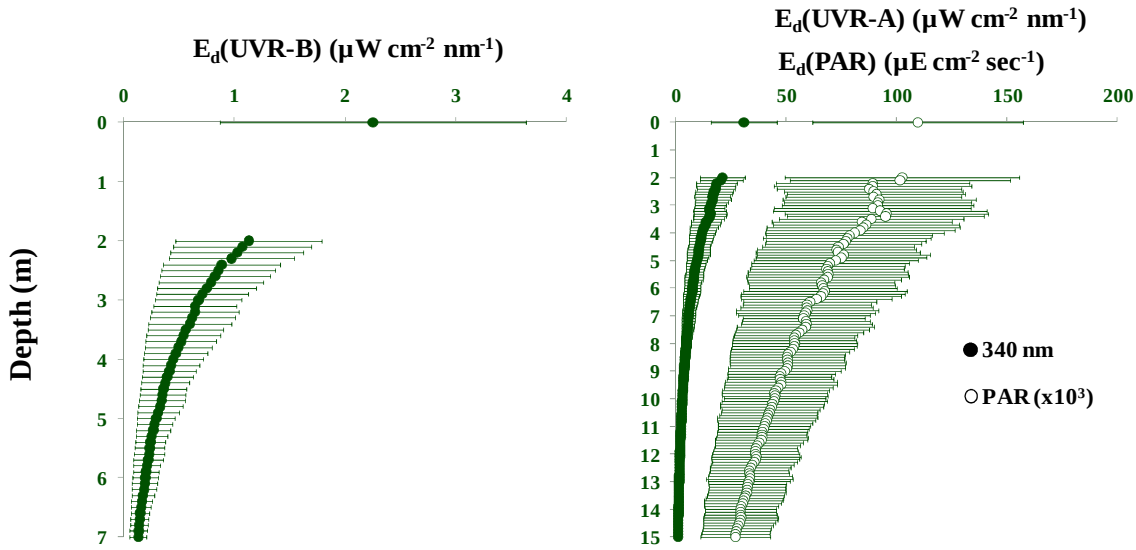

Figure III-3. *Averaged of downwelling irradiance (E_d) profiles and irradiances just beneath the sea surface in UVB (305 nm, n=8), UVA (340 nm, n=14) and PAR (x10^3, n=14) spectral domains recorded in the Bay of Marseilles from November 2007 to December 2008.*

The highest K_d(UVR) and K_d(PAR) values observed on 9 June 2008 can be directly explained by the unusual turbidity value (22.04 NFU, Table III-1) due to the release of rocks for artificial reefs establishment in the Marseilles' Bay and is not further considered in the discussion. Higher K_d(UVR) values were determined during the two Rhône River plume intrusion events (6 May and 23 June 2008; Table III-2) that induced marine phytoplankton

blooms ([Chla] > 1 µg l^{-1}; Table III-1) and subsequent fresh CDOM production. By contrast, K_d(PAR) maximum value (0.125 m^{-1}, 25 November 2008; Table III-2) was observed after a strong mixing of the entire water column enhanced by 12 consecutive days of Mistrals' wind that injected nutrients (enhancing biological activity) and aged CDOM such as humic-like compounds in surface waters. Both K_d(UVR) and K_d (PAR) minimum values (Table III-2) were observed at the end of summer time (on 23 September 2008 sample) when surface CDOM content was strongly photobleached. Maximum and minimum values of K_d(PAR) determined in surface waters of Marseilles' s Bay were in good agreement to those reported for the western basin (Alboran Sea; Moran and Estrada, 2001) and higher to those determined in the eastern basin (Moutin and Raimbault, 2002). By contrats, K_d(UVR) values were lower than that found in North Aegean (Obernosterer et al., 1999b), Adriatic Sea (Sommaruga et al., 1997; Herndl et al., 1998; Brugger et al., 1998) and in coastal waters of the southern Spain (Cabo de Gata; Figueroa et al., 2002) and were higher than corresponding values determined in South Aegean Sea (Obernosterer et al., 1999b) and Algerian Basin (Llabrés et al., 2010). Whereas, it is important to note that our K_d(UVR) values as well as those already determined punctually in Mediterranean Sea appear in the low range of those reported for other marine systems (Tedetti and Sempéré, 2006; Morel et al., 2007; Tedetti et al., 2007). Therefore, our study highlights particularly high solar radiation transparency of the surface coastal waters of the Marseilles' Bay.

Table III-2. *Diffusive attenuation coefficients (K_d in m^{-1}) of UVR and PAR determined in the surface waters (corresponding depth ranges or focal depths from which $K_d(\lambda)$ values were derived were shown in brackets) at SOFCOM station from the two radiometric profiles done by using the most appropriate method: standard (bold characters) and Zaneveld (normal characters) methods. Corresponding annual mean, standard deviation (SD), coefficient of variation (CV %) and the percentage of surface irradiances fluctuations observations (% of fluctuate obs.) are shown as well as corresponding attenuation coefficient values of water molecules ($K_w(\lambda)$) determined by Baker and Smith (1982). K_w(PAR) was determined by averaging the same fourth visible wavelengths (i.e. 412, 443, 490 and 565 nm) used to calculated PAR. Mean and SD values were determined without taking into account the observation performed on 9 June 2008 due to an anthropogenic forcing for the establishment of artificial reefs in the Bay. The 10% irradiance depth ($Z_{10\%}(\lambda)$) could be estimated from $K_d(\lambda)$ ($Z_{10\%}(\lambda) = 2.3/ K_d(\lambda)$)*

	Attenuation coefficient Kd (λ) (m-1)									
	K_d(305)		K_d(325)		K_d(340)		K_d(380)		K_d(PAR)	
7 Nov. 2007	nd.		**0.293**	**(0-20)**	0.236	(5.5)	0.141	(5.5)	0.105	(7.0)
19 Dec. 2007	nd.		**0.265**	**(0-20)**	**0.210**	**(0-30)**	**0.133**	**(0-30)**	0.085	(7.0)
5 Feb. 2008	nd.		**0.252**	**(0-20)**	0.206	(5.5)	0.118	(6.5)	0.110	(9.0)
14 Feb. 2008	nd.		**0.250**	**(0-20)**	**0.199**	**(0-30)**	0.109	(6.0)	0.104	(8.0)
26 Mar. 2008	**0.387**	**(0-7.5)**	**0.342**	**(0-20)**	0.245	(5.5)	0.163	(6.0)	0.109	(6.0)
29 Apr. 2008	0.386	(5.5)	0.281	(6.0)	0.255	(7.0)	0.152	(6.5)	0.098	(9.0)
6 May 2008	**0.463**	**(0-5)**	**0.345**	**(0-8)**	**0.270**	**(0-8)**	**0.150**	**(0-8)**	0.105	(5.0)
9 Jun. 2008	**0.593**	**(0-4)**	**0.492**	**(0-12)**	**0.398**	**(0-12)**	**0.277**	**(0-13.5)**	**0.169**	**(0-13.5)**
23 Jun. 2008	**0.484**	**(0-6)**	**0.332**	**(0-18)**	**0.264**	**(0-15)**	0.170	(6.0)	0.091	(8.0)
10 Jul. 2008	**0.422**	**(0-8)**	**0.315**	**(0-13)**	0.220	(6.0)	0.112	(6.0)	0.086	(8.0)
23 Sep. 2008	**0.308**	**(0-12)**	**0.215**	**(0-11.8)**	**0.158**	**(0-12)**	**0.081**	**(0-12)**	**0.072**	**(0-30)**
14 Oct. 2008	**0.370**	**(0-6)**	**0.271**	**(0-20)**	0.190	(5.0)	0.093	(6.0)	0.084	(6.5)
25 Nov. 2008	nd.		0.317	(5.0)	0.254	(5.0)	0.155	(6.0)	0.125	(9.5)
4 Dec. 2008	nd.		**0.282**	**(0-17)**	**0.226**	**(0-17)**	**0.136**	**(0-17)**	**0.089**	**(0-17)**
Mean	0.403		0.289		0.229		0.132		0.097	
SD (±)	0.059		0.039		0.025		0.027		0.014	
CV (%)	15		14		15		21		15	
% of fluctuate obs.	13		15		54		69		85	
$K_w(\lambda)$	0.135		0.086		0.064		0.027		0.033 ± 0.029	

Basically, surface K_d(UVR) and K_d(PAR) varied seasonally with the development of phytoplankton ([Chl*a*]) excepted during winter time (Figure III-4). Indeed, [Chl*a*] and $K_d(\lambda)$ values increased strongly at the beginning of the stratification period (April-June) triggered by the Rhône River plume extents influence in the bay of Marseilles and neighboring surface waters (Joux et al., 2009). Then, during summer time [Chl*a*] and $K_d(\lambda)$ values decreased following primary production collapse due to nutrients depletion. Finally, in fall period $K_d(\lambda)$ values increased with the development of phytoplankton (Figure III-4) enhanced by favorable environmental conditions characterized by the alternation of mixing periods that put nutrients

upward, with clear skies and stable weather periods (St. Martin's summer). This observation is consistent with previous long term [Chl*a*] observations performed in northwestern Mediterranean Sea coastal waters (≥ 3 years) of the Blanes' Bay (Duarte et al., 1999). Relationships linking $K_d(\lambda)$ with [Chl*a*] are well known and have been studied empirically (Baker and Smith, 1982; Austin and Petzold, 1981) for the development of [Chl*a*]-dependent bio-optical models for case 1 waters (Gordon and Morel, 1983; Gordon et al., 1988; Morel, 1988). Therefore, the concomitant seasonal trend observed between $K_d(\lambda)$ and the primary production underlines probably the existence of relationship linking them and/or linking $K_d(\lambda)$ with subsequent primary production by-products such as fresh CDOM in surface coastal waters of the Bay of Marseilles.

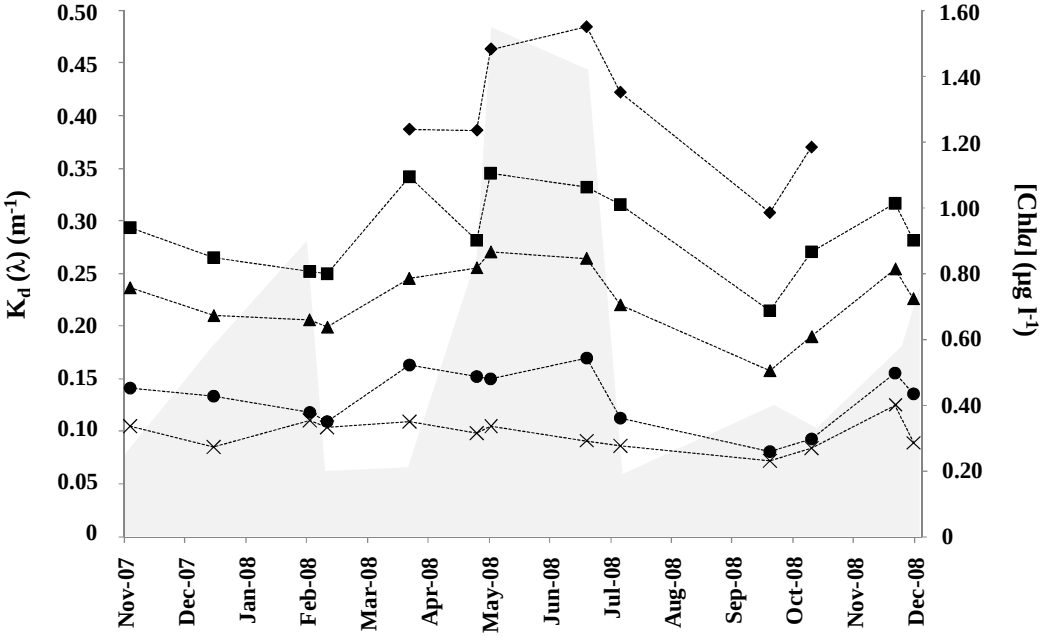

Figure III-4. *Seasonal evolution, from November 2007 to December 2008 of surface K_d(UVR) at 305 (rhombus), 325 (squares), 340 (triangles), 380 nm (circles) and K_d(PAR) (crosses) values. Chlorophyll a concentration values ([Chla]) are illustrated by the grey area. The observation performed on the 9 June 2008 (anthropogenic forcing) was not reported in this figure.*

4. 4. Biogeochemical factors controlling surface K_d(UVR) and K_d(PAR)

Interestingly, K_d(UVR) and K_d(PAR) were significantly correlated to $a_{CDOM}(350)$ (Figure III-5 A) while $K_d(\lambda)$ versus [Chl*a*] significant relationships were solely observed for [Chl*a*] greater than 0.4 µg l^{-1} and for the shortest UVR (305, 325 and 340 nm; Figure III-5 B). When we compare the residual attenuation values (y-intercepts values; Figure III-5 A and B), we see that CDOM induces stronger UVR attenuation than Chl*a*. The sudden increase of $K_d(\lambda)$ when [Chl*a*] $\leq$ 0.4 µg l^{-1} (Figure III-5 B) may shed light on notable changes of the autochthonous CDOM composition according to the degree of primary production. Indeed, biotic processes (*in situ* biological production, biological production within Rhône River plume) produced fresh autochthonous CDOM characterized mostly by relatively low molecular weight DOM (Coble et al., 1998; Stedmon and Markager, 2005; Romera-Castillo et al., 2010) such as protein-like compounds that have the specificity to absorb light in the short UVR (Coble, 1996). By contrast, when abiotic processes (mixing, photo-bleaching) prevailed, their impacts on the autochthonous CDOM content were to produce complex and bio-refractory CDOM (Obernosterer et al., 2001b; Tranvik and Bertilsson, 2001; Mopper and Kieber, 2002) characterized by relatively higher molecular weight DOM such as humic-like compounds that absorb light at longer wavelengths than recent biological CDOM (Coble, 1996; Coble et al., 1998; Parlanti et al., 2000).

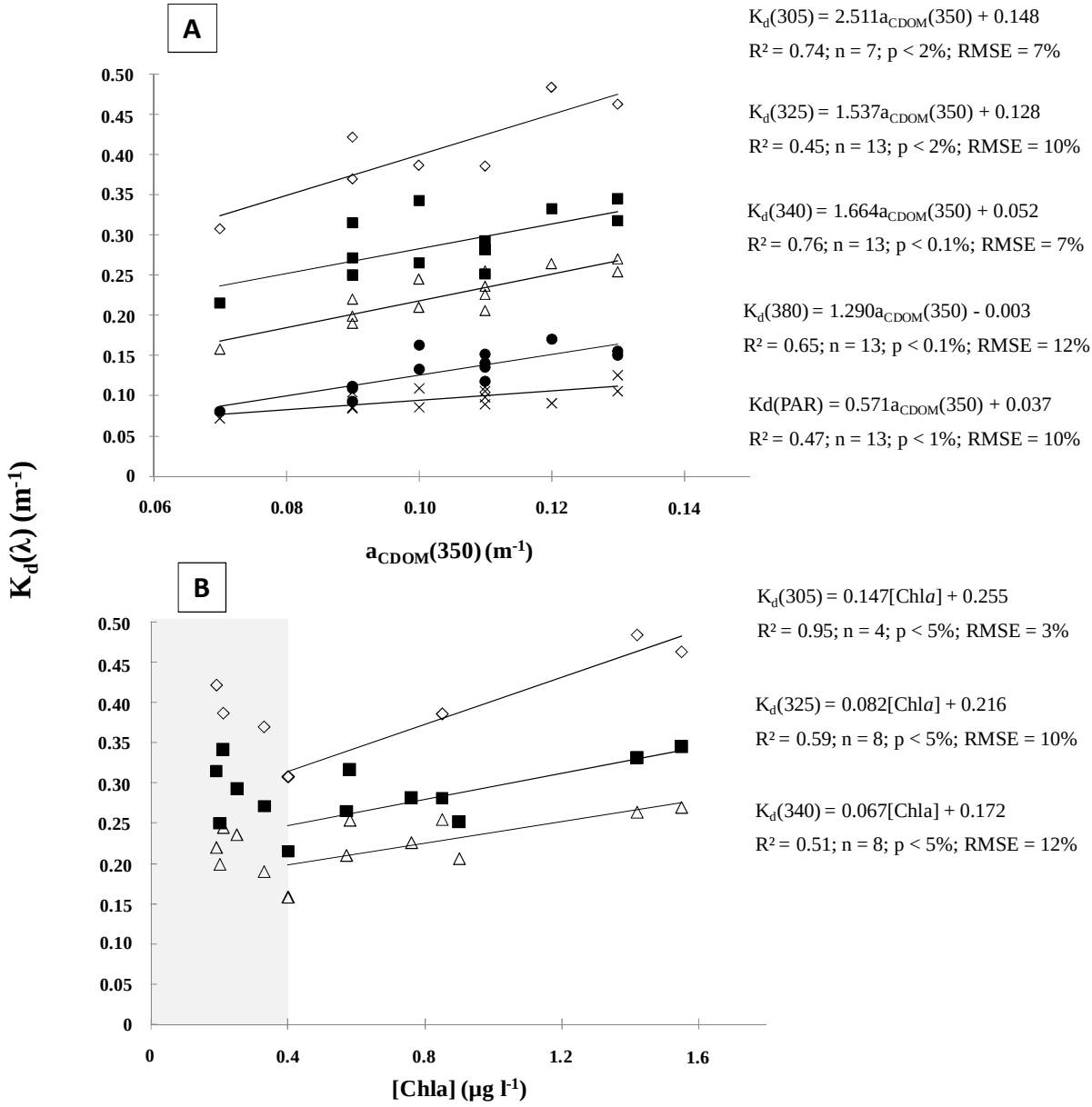

Figure III-5. *Significant relationships observed between surface attenuation coefficient of irradiance ($K_d(\lambda)$) at 305 (rhombus), 325 (squares), 340 (triangles), 380 nm (circles) and PAR (crosses) with surface $a_{CDOM}(350)$ (A) and surface [Chla] values (B) at SOFCOM station from November 2007 to December 2008 (without the observation performed on the 9 June 2008, anthropogenic forcing). The linear regression equations obtained from these relationships are also shown as well as their significance and robustness.*

The significant linear correlation obtained between $a_{CDOM}(350)$ and [Chl*a*] (Figure III-6) became scattered when [Chl*a*] $\leq$ 0.4 µg l^{-1} and thus reinforces the degree of primary production below/above which complex/recent autochthonous CDOM was suspected to influence UVR attenuation, respectively. In addition, the relatively high $a_{CDOM}(350)$ residual value of this relationship (y-intercept = 0.09 m^{-1}) compared to the averaged annual $a_{CDOM}(350)$ value (0.10 ± 0.02 m^{-1}) illustrates the superimposition of recent CDOM pulses on a important amount of complex CDOM. When we remove photobleached and well mixed samples (extremes samples; Figure III-6) and [Chl*a*] < 0.4 µg l^{-1}, the significance and robustness of $a_{CDOM}(350)$ *versus* [Chl*a*] relationship revaluation were both greatly improved (n = 6; p < 1 %; RMSE = 2%) while the linear regression equation obtained, y-intercept value included, remained unchanged (not shown). This reinforced the presence of a constant high background level of CDOM in surface waters of the Bay of Marseilles throughout the year which appears to be independent of the phytoplankton development.

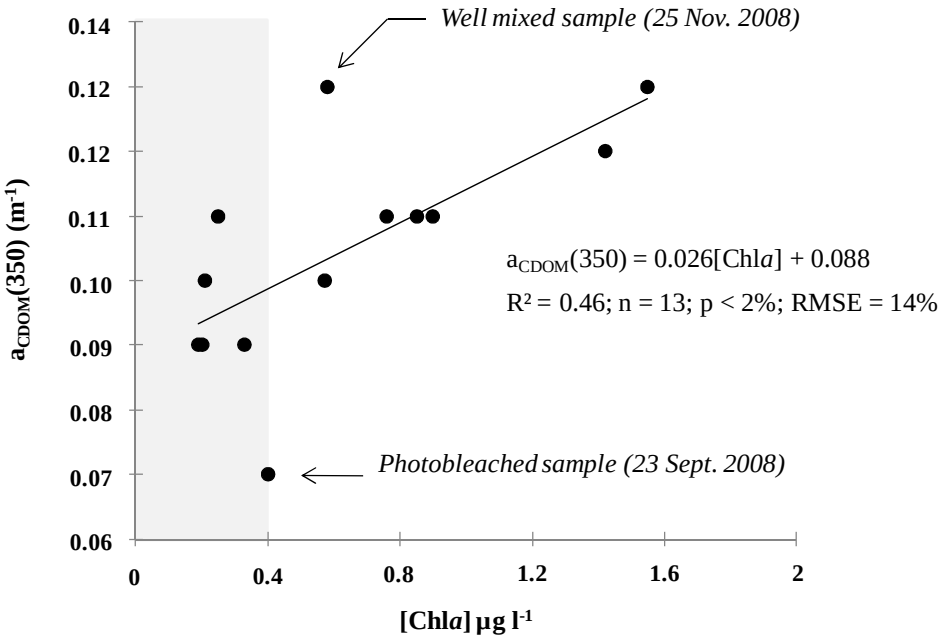

Figure III-6. *Significant relationships observed between surface $a_{CDOM}(350)$ and surface [Chla] at SOFCOM station from November 2007 to December 2008 (without the observation performed on the 9 June 2008, anthropogenic forcing). The linear regression equation obtained from this relationship is reported as well as its significance and robustness. The grey shadow illustrated the theoretical surface background of persistent CDOM evolving in surface waters of the Bay of Marseilles.*

Interestingly, when primary production was relatively high ([Chl*a*] > 0.4 µg l^{-1}) significant relationships linking $K_d(\lambda)$ and $a_{CDOM}(350)$ were established for the shortest UVR-A (325 and 340 nm) (Figure III-7 A) while, when primary production was relatively low ([Chl*a*] ≤ 0.4 µg l^{-1}; Figure III-7 B), they were determined for the longest UVR-A (340 and 380 nm) and PAR. Besides reinforcing the spectral dependence towards short UVR of the recent CDOM as it was expected, these relationships highlight a strong impact of the complex CDOM (background) on the longest UVR attenuation but above all on PAR attenuation in these surface waters. Given that residual attenuation values (y-intercepts values, Figure III-7 A and B) at all wavelengths (excepted at 380 nm) could be explained only by the corresponding attenuation coefficient values of water molecules ($K_w(\lambda)$) (Baker and Smith, 1982; Table III-2), CDOM appeared as a preponderant optical factor controlling UVR and PAR underwater fields in this area. All of these results point to the necessity of taking into account the persistent background of CDOM for the retrieval of optical components from ocean colour data in this area as previously shown for chlorophyll by Morel and Gentili (2009) for the Mediterranean Sea.

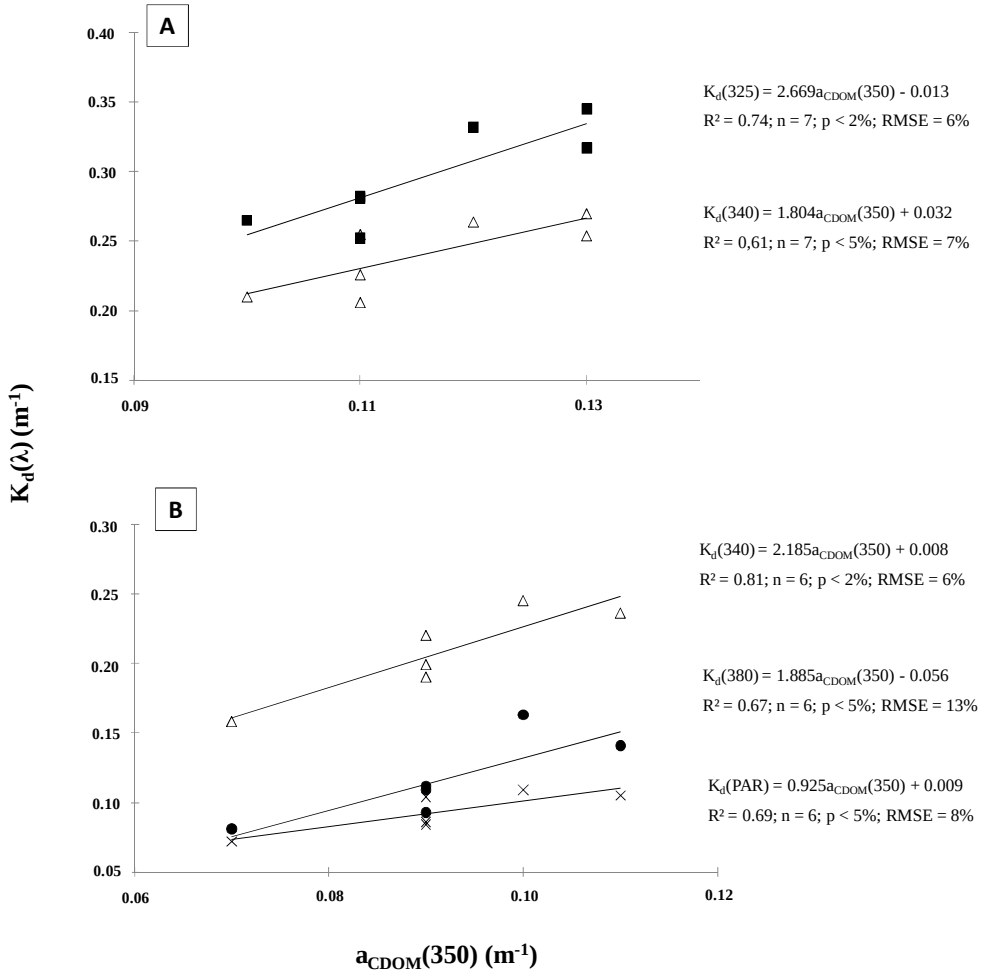

Figure III-7. *Significant relationships observed between attenuation coefficient of irradiance ($K_d(\lambda)$) at 325 (squares), 340 nm (triangles), 380 nm (circles) and PAR (crosses) with surface $a_{CDOM}(350)$ by considering solely the observations where [Chla] > 0.4 µg l^{-1} (A) and where [Chla] ≤ 0.4 µg l^{-1} (B) at SOFCOM station from November 2007 to December 2008 (without the observation performed on the 9 June 2008, anthropogenic forcing). The linear regression equations obtained from these relationships are also shown as well as their significance and robustness.*

5. Conclusion

This study shows no significant temporal variability of solar radiation quality reaching the sea surface, excepting concerning the amount of UVR-B 7-8 fold richer during water stratification period (summer) than during winter time. This in addition, of the relatively low and constant K_d(UVR) and K_d(PAR) values observed throughout which illustrate an important solar radiation transparency of these coastal surface waters underline that UVR is an important physical forcing that may affect the biological surface CDOM content and influence the overall biogeochemistry in this area.

UVR and PAR attenuation were closely linked to surface CDOM absorption and content. CDOM appeared as a preponderant optical factor controlling UVR and PAR underwater fields in this area. Moreover, the freshest state of the CDOM, dependent of the primary production level, controls its absorption spectral dependence. Recent CDOM absorbs preferentially the short UVR while aged CDOM absorbs long UVR-A and PAR. The important amount of aged CDOM appeared constant through the year due to its bio-refractory nature leading at its accumulation. By contrast, the level of recent CDOM was controlled by punctual pulses of phytoplankton and subsequent by-products.

CHAPITRE IV

PROPRIETES OPTIQUES DE LA CDOM ET ATTENUATION DU RAYONNEMENT SOLAIRE DANS LES EAUX COTIERES DE LA MER DE BEAUFORT

Dans le cadre de l'ANR MALINA (P.I. M. Babin, LOV), des prélèvements hydrologiques sur l'ensemble du plateau Canadien de la mer de Beaufort en Océan Arctique ont été effectués afin de caractériser les propriétés optiques d'absorbance et de fluorescence de la CDOM. Durant cette campagne, les éclairements de surface ($E_s(\lambda)$) quotidiens et plusieurs profils d'éclairement sous-marin ($E_d(\lambda)$) ont été mesurés à 305 nm (UVR-B), 325, 340 et 380 nm (UVR-A) ainsi que dans le PAR. Les doses moyennes journalières reçues en surface à 305 nm (UVR-B), 340 nm (UVR-A) et pour le PAR étaient respectivement de 0,12 ± 0,03 ; 8,46 ± 1,64 et 18,09 ± 4,20 kJ m^{-2}. Dans les eaux influencées par le panache du Mackenzie (15 < salinité < 25), la lumière est rapidement absorbée, et tout particulièrement les UVR (K_d(UVR-A) à 340 nm = 0.924 ± 0.430 m^{-1}), alors que dans les eaux marines (salinité > 25), la pénétration des UVR et du PAR est respectivement 2,5 et 1,5 fois plus importante. La faible intensité des UVR de surface associée à des valeurs de K_d(UVR) relativement élevées mettent en avant une limitation des processus de photo-dégradation de la CDOM durant la période étudiée. Le coefficient d'absorption de la CDOM ($a_{CDOM}(\lambda)$) à 350 nm présente une large gamme de variation allant de 0.12 m^{-1} à 6.36 m^{-1} pour des salinités comprises entre 30 et 0. Sur l'ensemble du plateau Canadien, la CDOM présente des pentes spectrales (S_{CDOM}) élevées, même au niveau du delta du Mackenzie (moyenne S_{CDOM} = 0,019 ± 0,001 nm^{-1}). Les matrices d'excitation-émission (EEM) ont permis d'identifier 3 composés fluorescents : les composés C1, C2 et C3 correspondant respectivement au pic M « marine humic-like », au pic C « humic-like » et au pic T-B « protein-like », selon la classification de Coble (1996) et Coble et al. (1998). La décroissance de l'intensité de fluorescence du composé C1, selon le gradient de salinité 0-25 et son augmentation au delà (salinité > 25) suggèrent respectivement une origine allochtone et autochtone de ce dernier. Au niveau du

delta du Mackenzie, la forte signature de ce composé pourrait provenir du drainage des nombreux lacs de faible profondeur constituant le delta et dans lesquels se développe une intense activité biologique de macrophytes. Cette source de CDOM biologique couplée aux processus de photoblanchiment et d'absorption sur les particules de la CDOM terrestre pourrait expliquer les valeurs étonnamment élevées de S_{CDOM} du Mackenzie en été. De plus, ce fort apport de matière organique biologique par le Mackenzie peut être une piste d'étude pour expliquer en partie la récente observation de Stedmon et al. (2011) concernant la plus grande proportion de CDOM autochtone au niveau du Bassin Canadien comparé à celle du Bassin Eurasien.

SPATIAL DISTRIBUTION OF FLUORESCENCE AND ABSORPTION PROPERTIES OF DOM IN SURFACE COASTAL WATERS OF THE CANADIAN SHELF OF THE BEAUFORT SEA DURING SUMMER 2009

Julien Para[1, 2], Bruno Charrière[1, 2], Atsushi Matsuoka[3], William Miller[4] and Richard Sempéré[1, 2]

[1] *Université de la Méditerranée, LMGEM, Centre d'Océanologie de Marseille, Case 901, 13288 Marseille Cedex 9, France*

[2] *CNRS/INSU, UMR 6117, LMGEM, Case 901, 13288 Marseille Cedex 9, France*

[3] *Laboratoire d'Océanographie de Villefranche, Université Pierre et Marie Curie, Centre National de la Recherche Scientifique, Villefranche-sur-Mer, France*

[4] UGAMI / UGA Marine Science, Athens, GA 30602 USA.

In preparation

1. Introduction

Increasing air temperature (+3 to 4°C; IPCC, 2007) enhances numerous biogeochemical changes, particularly by affecting the integrity of the permafrost (Guo et al., 2007; Walvoord and Striegl, 2007). Approximately 50% of the global terrestrial organic carbon pool is trapped in the Arctic and sub-Arctic permafrost regions (Tarnocai et al., 2009) which are warming (Foley, 2005). Therefore, the flux of terrestrial Dissolved Organic Matter (DOM) coupled with the subsequent increase of freshwater discharge is expected to change (Lawrence and Slater, 2005). This could lead to an increase in the amount of terrestrial DOM that is delivered to the Arctic Ocean and modified water circulation and sea ice coverage (Barber and Hanesiak, 2004). Currently, the Arctic Ocean receives 11% of global river runoff (Opsahl et al., 1999) despite being the smallest of the world's five oceans. Therefore, the already important amount of terrestrial DOM contained in Arctic waters (Opsahl et al., 1999; Amon and Meon, 2004) is also expected to increase.

The DOM content in Western Arctic region of the Beaufort Sea is strongly impacted by freshwater inputs from the Mackenzie River which has the fourth highest discharge rate of all Arctic rivers (Gordeev, 2006) and is the dominant source of terrestrial DOM. The corresponding transport of terrestrial dissolved organic carbon (DOC) to the coastal Beaufort Sea is estimated at 1.04-1.76 Tg C per year (Raymond et al., 2007). Seasonal discharge increases after break up, occurring around May, and then decreases throughout the summer (Carmack and Macdonald, 2002; Emmerton et al., 2008). A fraction of DOM is colored (CDOM) and absorbs light over a broad range of ultraviolet (UV) and visible wavelengths. During spring freshet and ice break up, the increase of terrestrial CDOM inputs from rivers to the coastal area will have numerous biological, chemical and physical effects. This could lead to a decrease of the euphotic depth. Then, allochthonous organic matter direct remineralization (i.e. CO and CO_2 production) and labile organic substrates photoproduction rates could increase (Osburn et al, 2009). A combination of low sunlight intensity due to high solar zenith angle, reduction of sunlight penetration in surface waters induced by sea ice cover and Mackenzie plume spreading and changing in CDOM reactivity in relation with the season (Emmerton et al., 2008) make the overall photodegradation effect highly variable over the Canadian shelf (Johannessen and Miller, 2001; Osburn et al., 2009). This is why in environments greatly effected by climate change determining the source, composition and surface distribution of CDOM according to in-air and in-water sunlight optical characteristics,

are crucial to better understanding carbon cycle processes at the sea surface and at the land/sea interface.

Here, we report in-air and in-water sunlight optical characteristics and the spatial distribution of the optical properties of CDOM evolving in surface coastal waters of the Canadian shelf of the Beaufort Sea during summer 2009 (after the break up). Surface CDOM absorption and fluorescence properties, including the combination of three-dimensional excitation/emission matrices (EEMs) with Parallel Factor Analysis (PARAFAC), were investigated in order to (i) determine the absorbant DOM features, (ii) identify and characterize the main DOM fluorescent components and (iii) map their corresponding spatial distributions in surface waters of the Canadian shelf.

2. Materials and methods

2. 1. Study site and sample collection

Hydrological samples were collected in surface waters at 27 stations over the Canadian shelf of the Beaufort Sea onboard the research ice-breaker CCGS Amundsen during the Mackenzie Light and Carbon (MALINA) cruise held from 31 July to 23 August 2009 (Figure IV-1). During this open water study period, the Mackenzie discharge was around 12,000 m^3 s^{-1} (http://www.ec.gc.ca/rhc-wsc/) and the area investigated was characterized by an unusual ice cover extent (appendix 1) and overcast weather.

Samples were collected using Niskin bottles equipped with Teflon-O-ring and silicon tubes to avoid chemical contamination. For DOC determination, samples were directly transferred from the Niskin bottle *via* a Polycap As 75 cartridge (0.2 µm) into precombusted (6 h at 450 °C) ampoules, immediately acidified with 85% of H_3PO_4 (final pH ~2) and flame sealed. CDOM samples were transferred from Niskin bottles into 10% HCl washed and precombusted (6 h at 450 °C) glass bottles and directly filtered in dim light through precombusted 0.7 µm GF/F filters, which had been pre-rinsed with Milli-Q water and sample water, and then through 0.2 µm Nuclepore polycarbonate filters, presoaked in 10% HCl solution and rinsed with Milli-Q water and with the sample according to the SeaWiFS protocol (Mueller and Austin, 1995). During the sampling, *in situ* hydrological context, (temperature and salinity) was determined by using a SeaBird Electronics 911 conductivity temperature depth (CTD) profiler (Table IV-1). Surface irradiance in the UV (305, 325, 340 and 380 nm) and visible (412, 443, 490 and 565 nm) spectral domains were recorded

continuously on the ship roof during the cruise and two profiles of downward irradiance ($E_d(Z,\lambda)$) were also performed at the same channels at 16 of the 27 sampling stations investigated (Figure IV-1).

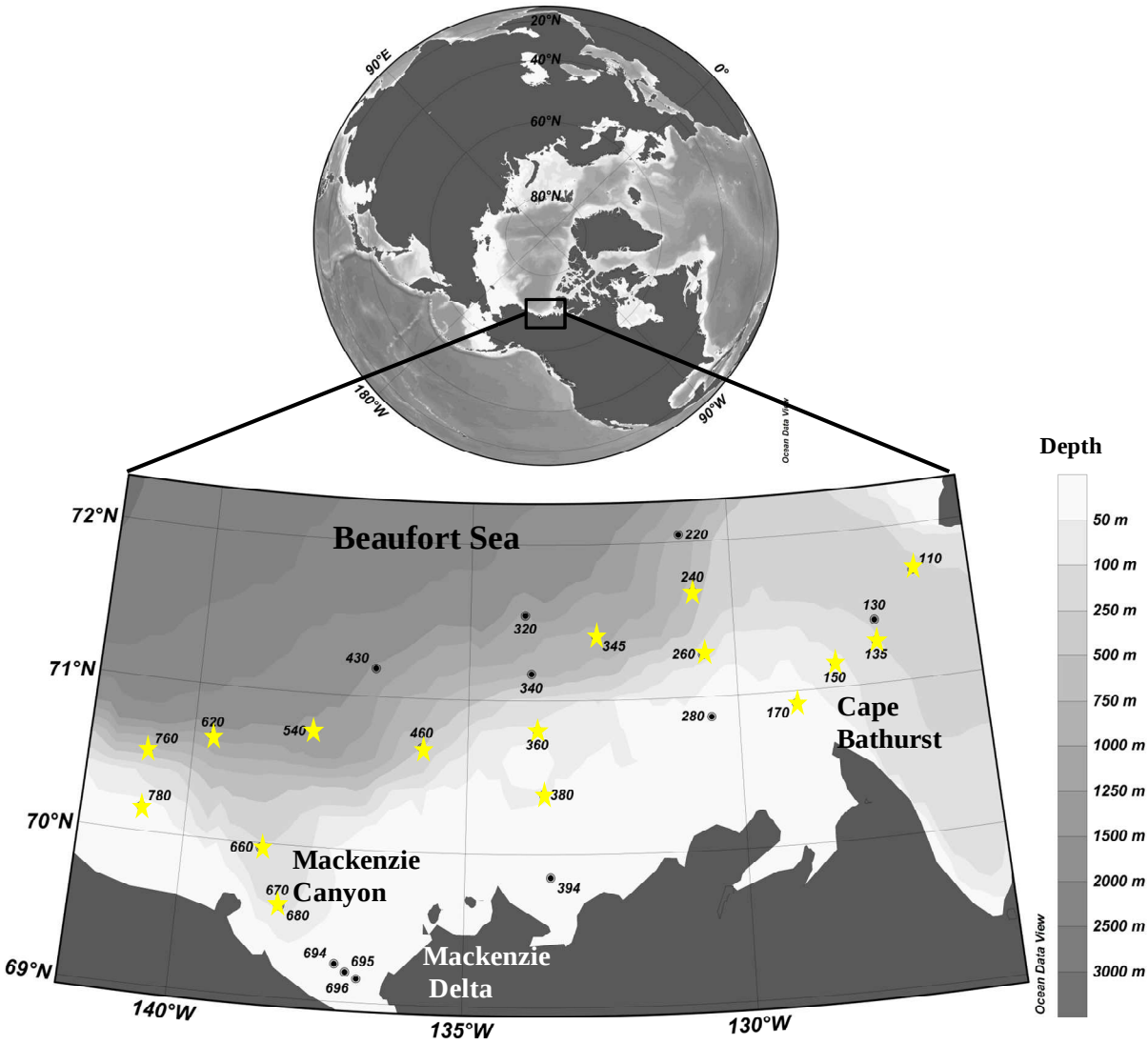

***Figure IV-1**. Location and station number investigated during the MALINA cruise in the Canadian Shelf of the Beaufort Sea. Yellow stars represent the stations where profiles of downward irradiance were performed.*

Table VI-1. *Bottom depth, temperature, salinity, DOC and absorbance properties, including CDOM absorption coefficient, spectral slope and the DOC-specific values for CDOM absorption: $a_{CDOM}(350)$* (i.e. $a_{CDOM}(350)/DOC$) determined in surface waters of each sampling stations and among the different surface salinity sectors investigated (i.e. North East, North West and Mackenzie Delta Sectors) observed (Figure 2) .*

Station	Bottom depth [m]	Temperature [°C]	Salinity	DOC [µM-C]	$a_{CDOM}(350)$ [m^{-1}]	a_{CDOM}*(350) [m^2 mol]	S_{CDOM} [nm^{-1}]
North East Sector (salinity > 25)							
150	65	3,55	29,41	83,6	0,29	3,51	0,020
170	37	3,19	29,37	114,7	0,56	4,89	0,018
260	59	4,61	29,26	79,9	0,19	2,32	0,019
110	407	4,36	28,93	75,2	0,14	1,89	0,019
240	475	3,23	28,90	61,9	_	_	_
130	310	4,63	28,22	67,5	0,17	2,53	0,019
135	227	2,24	28,05	67,0	0,15	2,19	0,020
380	62	4,41	27,67	74,2	0,21	2,88	0,019
280	41	4,71	27,63	89,3	0,38	4,21	0,019
220	940	-0,07	27,54	65,7	0,15	2,31	0,019
345	586	1,96	27,49	62,00	0,12	1,95	0,020
340	559	0,13	26,87	61,1	0,13	2,09	0,020
320	1134	-0,78	26,52	58,4	0,13	2,28	0,019
360	76	-0,17	26,47	61,9	0,12	2,01	0,021
540	1511	-0,41	25,73	61,4	_	_	_
430	1282	-0,78	25,96	59,2	0,14	2,37	0,022
Mean	486	2,18	27,75	71	0,21	2,67	0,020
SD	*486*	*2,18*	*1,21*	*15*	*0,13*	*0,91*	*0,001*
North West Sector (15 < salinity < 25)							
460	357	-0,09	24,78	58,1	0,19	3,26	0,021
760	543	0,54	22,52	73,4	0,43	5,80	0,019
620	1541	2,07	22,06	93,7	0,77	8,20	0,019
660	259	4,25	21,90	104,3	0,77	7,38	0,019
670	124	5,39	21,86	105,2	_	_	_
394	11	8,81	21,45	199,7	2,28	11,42	0,017
780	49	4,10	21,08	110,3	0,77	6,97	0,019
Mean	412	3,58	22,24	106	0,87	7,17	0,019
SD	*531*	*3,06*	*1,21*	*45*	*0,73*	*2,70*	*0,001*
Mackenzie Delta Sector (salinity < 15)							
680	121	8,05	14,76	188,50	2,35	12,49	0,018
694	11	9,28	9,43	316,3	5,05	15,96	0,019
695	4	9,26	7,56	341,7	5,60	16,39	0,019
696	3	10,08	0,23	394,2	6,36	16,13	0,020
Mean	35	9,17	7,99	310	4,84	15,24	0,019
SD	*58*	*0,84*	*6,01*	*87*	*1,74*	*1,84*	*0,001*

2. 2. CDOM optical properties

2. 2. 1. Absorbance measurements

Right after collection and filtration of the samples, absorbance of CDOM was measured onboard (within 24 hours), throughout the UV and visible spectral domains (280-700 nm) using the multiple pathlength, liquid core waveguide system Ultrapath (MPLCW, WPI Inc.). Samples were analysed with reference to a filtered salt solution prepared with HPLC quality water and precombusted salt reproducing the refractive index of samples to minimize baseline offsets in absorption spectra induced by the effect of salinity changes between sample and the corresponding reference (D'Sa et al., 1999). Reference salt solution and samples were brought to room temperature before analysis. Between samples, the sample cell was flushed with successively diluted detergent (Cleaning solution concentrate, WPI Inc.), high reagent grade MeOH, 2 M HCl and Milli-Q water. Cleanliness of the sample cell was verified by comparing with a reference value for the transmittance of the reference salt solution. Trapped microbubbles were minimized by using a peristaltic pump to draw the sample into the sample cell. The spectral absorption coefficients, $a_{CDOM}(\lambda)$ (m^{-1}) were obtained using the following relationship, $a_{CDOM}(\lambda) = 2.303A(\lambda)/L$, where $A(\lambda)$ is the absorbance at wavelength λ (dimensionless) and L is the pathlength in meters. Value of spectral slope of CDOM (S_{CDOM}) was determined after applying a non-linear exponential regression to original $a_{CDOM}(\lambda)$ data measured on the range 350-500 nm, according to the recommendations of Twardowski et al (2004).

2. 2. 2. Fluorescence measurements

For fluorescence measurements, performed at the LMGEM laboratory, samples were transferred into a 1 cm pathlength far UV silica quartz cuvette (170-2600 nm; LEADER LAB), thermostated at 4°C, and analyzed with a Hitachi (Japan) Model F-7000 spectrofluorometer. Instrument settings, measurement procedures and spectral correction procedures are fully described in Tedetti et al. (2010). Briefly, the correction of spectra for instrumental response was conducted according to the procedure recommended by Hitachi (Hitachi F-7000 Instruction Manual). First, the Ex instrumental response was obtained by using Rhodamine B as standard and a single-side frosted red filter in Ex scan mode. Then, the Em side calibration was done with a diffuser in synchronous scan mode. The Ex and Em

spectra obtained over the range 240-550 nm were applied internally by the instrument to correct subsequent spectra.

EEMs were generated over Ex wavelengths between 240 and 550 nm in 5 nm intervals and Em wavelengths between 300 and 550 nm in 2 nm intervals, with 5 nm bandwidths (Full-Width Half-Maximum; FWHMs) on both Ex and Em sides and a scan speed of 2400 nm min^{-1}. Milli-Q water as well as solutions of quinine sulphate (Fluka) in 0.05 M H_2SO_4 (1-10 ppb) were run during fluorescence measurements. Before being processed, all the data (blanks, standards, samples) were normalized to the intensity of the Raman scatter peak at Ex/Em: 275/303 nm (5 nm bandwidths) of pure water (Coble et al., 1993; Coble, 1996; Belzile et al., 2006). Samples were then corrected for the corresponding blanks and converted into quinine sulphate units (QSU).

PARAFAC is a statistical tool used to decompose EEMs data into different components. It is based on an alternating least square (ALS) algorithm. Thus, PARAFAC can statistically decompose the complex mixtures of CDOM into its main fluorescent components (Stedmon et al., 2003). The analysis was carried out in MATLAB 7.1 with the DOMFluor toolbox (Stedmon and Bro, 2008), freely downloadable from the Chemometrics site at the University of Copenhagen (www.models.life.ku.dk).

2. 3. DOC analysis

The Shimadzu instrument used in this study is the commercially available model TOC-5000 Total Carbon Analyzer with a quartz combustion column filled with 1.2% Pt on silica pillows. Several aspects of our modified unit have been previously described (Sohrin and Sempéré, 2005). The accuracy and the system blank of our instrument were determined by the analysis of the reference material (D. Hansell, Rosenstiel School of Marine and Atmospheric Science, Miami, USA) including Deep Atlantic Water (DAW) and Low Carbon Water (LCW) reference standards. The average DOC concentrations in the DAW and in the LCW reference standards were 45 ± 2 µM C, n = 24 and 1 ± 0.3 µM C, n = 24, respectively. Carbon levels in the LCW ampoules were similar to and often higher than the Milli-Q water produced in our laboratory. The nominal analytical precision of the analysis procedure was within 2%.

2. 4. Radiometric measurements

Two profiles of downward irradiance ($E_d(Z,\lambda)$ in µW cm^{-2} nm^{-1}) were performed, under overcast weather, at 16 sampling stations (Figure IV-1) using a Satlantic MicroPro free-fall profiler equipped with OCR-504 downward irradiance sensors in the UVR-B (305 nm), UVR-A (325, 340 and 380 nm) and PAR (412, 443, 490 and 565 nm) spectral domains. Surface irradiance ($E_s(\lambda)$ in µW cm^{-2} nm^{-1}) was simultaneously measured at the same channels on the ship roof using other OCR-504 sensors to account for the variations of the cloudy conditions during the cast as well as to monitor UVR and PAR irradiances during the day time. For in-water sensors, the Full-Width Half-Maximum (FWHM) of the channels was 2 nm for 305, 325 and 340 nm, and 10 nm for PAR. For in-air sensors the FWHM of the channels was 2 nm for 305, 325 and 340 nm and 10 nm for PAR. The MicroPro free-fall profiler, equipped with pressure, temperature and tilt sensors was operated from the front of the ship and deployed 50 m away to minimize the shadowing effects and disturbances of the ship.

Each cast was accompanied by a measurement of the dark current (instrument on deck) and a pressure tare (instrument at sea surface). To get many valid measurements as possible (i.e. tilt < 5°), the profiler was nose ballasted. This resulted in a descent rate of 70 cm s^{-1} and a sampling rate of 7 Hz (i.e. sampling resolution of 10 cm). Measurements were logged using Satlantic's Satview 2.6 software. This allowed for initial data processing, such as PAR data calculation, the application of radiometric calibration, dark correction, pressure tare and the removal of data with tilt > 5°. The interpolation data option of the software was not used in order to work with the raw radiometric data. Profiles of downwelling irradiance in the total PAR range were estimated from the four PAR channels. $E_d(Z,\lambda)$ was first interpolated onto an 1 nm interval from 400 to 700 nm and then integrated using the formula:

$$E_d(PAR, Z) = \int_{400nm}^{700nm} \lambda / hc \, E_d(Z, \lambda) \, d\lambda$$

where $E_d(PAR, Z)$ is the downwelling irradiance in the PAR range at depth Z (µE cm^{-2} s^{-1}), λ is the wavelength (nm), h is Planck's constant ($6.63.10^{-34}$ J s), c is the speed of light in a vacuum (3.10^8 m s^{-1}) and $E_d(Z, \lambda)$ is the downwelling irradiance at depth Z (µW cm^{-2}).

Diffuse attenuation coefficient for downwelling UVR and PAR irradiances ($K_d(\lambda)$ m^{-1}) were calculated in an homogeneous surface water mass from the slope of the linear regression of the log-transformed downwelling irradiance *versus* depth in accordance with the relationship:

$$E_d(Z, \lambda) = E_d(0^-, \lambda) \exp^{(-Kd(\lambda)\ Z)}$$

where $E_d(0^-, \lambda)$, the downwelling irradiance beneath the sea surface, was theoretically computed from deck measurements using the formula (Smith and Baker, 1984):

$$E_d(0^-, \lambda) = E_d(0^+, \lambda) / (1 + \alpha)$$

where α is the ocean surface albedo (OSA) determined using a 'look up table' available online at http://snowdog.larc.nasa.gov/jin/getocnlut.html (Jin et al., 2004). This 'look up table', based on the validated Coupled Ocean-Atmosphere Radiative Transfer (COART) model, requires 4 inputs (SZA, cloud optical depth, Chlorophyll *a* concentration and wind speed) reported in Table IV-2 (except chlorophyll *a* concentration), to retrieve α at any band of the solar spectrum. Chlorophyll *a* data were assessed at 0.1 µg. l^{-1} for all stations (personal communication Simon Bélanger). Therefore, mean α values at 305, 325, 340, 380 nm and PAR were 0.062 ± 0.005, 0.062 ± 0.005, 0.065 ± 0.006, 0.069 ± 0.008 and 0.055 ± 0.001, respectively. Since attenuation decreases with increasing wavelength in the UV range, any $K_d(\lambda)$ value that were lower than those at longer wavelengths were deleted. Values of $K_d(\lambda)$ at 305 nm were particularly prone to error. The mean variability (CV %) of K_d(UVR) and K_d(PAR) determined between the two profiles done was within 3%.

3. Results and discussion

3. 1. Optical sunlight characteristics

3. 1. 1. At the sea surface

During the MALINA cruise, the mean daily doses (kJ m^{-2}) of UVR-B (305 nm), UVR-A (380 nm) and PAR (490 nm) received at the sea surface were 0.12 ± 0.03, 8.46 ± 1.64 and 18.09 ± 4.20 kJ m^{-2}, respectively. These mean daily doses were low and relatively constant throughout the study period due to the presence of persistent clouds that absorbed the overall incident solar radiation and particularly the UVR-B. Van Wambeke et al. (2009) estimated, with the same sensors (OCR-504) that daily doses of UVR-B (305 nm), UVR-A (380) and PAR (490 nm) received at the sea surface of the south pacific gyre during (austral) summer cloudy days were 10, 2 and 1.5 times higher, respectively than those determined during this study. This underlines the fact that solar radiation intensity reaching surface waters during the investigated period was weak, especially concerning UVR-B which are strongly involved in the photodegradation process of DOM.

3. 1. 2. Diffusive attenuation coefficient of light in surface waters

Since the overall E_s(UVR-B) was very weak, the determination of K_d(UVR-B) for more than half of the sampling stations was impossible, particularly for the 'rich-stations' located mostly in the vicinity of the Mackenzie Delta (salinity < 25; Table IV-2). This is why in this section we do not deal with this parameter although some K_d(UVR-B)values were presented in the Table IV-2.

Surface $K_d(\lambda)$ values determined in both UVR-A and PAR (Table IV-2) spectral domains varied a lot among the 16 sampling stations investigated which are located in the two saltiest (salinity > 15; North West and North East Sectors) of the three surface salinity sectors observed during the study (Figure IV-2). Indeed, in the North West Sector (15 < salinity < 25) mean K_d(UVR-A) at 325, 340 and 380 nm and K_d(PAR) values were 1.081 ± 0.532, 0.924 ± 0.430, 0.448 ± 0.204 and 0.125 ± 0.035 m^{-1}, respectively while the corresponding ones in the saltiest sector (North East Sector; salinity > 25) were around 2.5 and 1.5 times lower for UVR-A and PAR, respectively (Figure IV-3; Table IV-2). Since solar radiation depth penetration is inversely proportional to $K_d(\lambda)$, high $K_d(\lambda)$ values illustrate weak light

penetration on the order of a few centimeters for UVR, as it was previously reported for low salinity environments (salinity < 20) surrounding the Mackenzie Delta (Retamal et al., 2008; Gareis et al., 2010). Therefore, the relatively high K_d(UVR-A) values observed in the North West Sector (20 < salinity < 25) coupled to the weak UVR intensity received at the sea surface probably highlight a strong limitation of the photodegradation process of the CDOM during the study period. If this process is occurring, the relatively high UVR-A attenuation along with the relatively low vertical mixing depth (represented here by the depth range from which $K_d(\lambda)$ values were derived, Table IV-2) observed in the North West Sector, and the relatively low UVR-A attenuation along with the relatively high vertical mixing depth for the North East Sector (Table IV-2) will allow both areas to have a comparable potential rate of CDOM photobleaching (Del Vecchio and Blough, 2002). However, previous studies also showed the limitation of UV-photodegradation in the Beaufort Sea region which supports our observations (Bélanger et al., 2006; Osburn et al., 2009). Maximum K_d(UVR-A) and K_d(PAR) values observed in the North West and North East sectors were determined at stations 670 (closest station of the Mackenzie Delta investigated) and 170 (Cape Bathurst area; Figure IV-1), respectively. Minimum K_d(UVR-A) and K_d(PAR) values observed in the North West and North East sectors were determined at stations 345-360 and 460, respectively (Table IV-2).

***Table IV-2**. Values of diffusive attenuation coefficient of light in the UVR-B (305 nm), UVR-A (325, 340 and 380 nm) and PAR spectral domains determined in surface waters of each sampling stations and among the different surface salinity sectors. Environmental conditions, including SZA, wind speed, cloud optical depth estimation are also reported as well as the maximal depth range from which surface $K_d(\lambda)$ values were derived.*

Station	SZA [Deg.]	Wind speed [m. s^{-1}]	Cloud optical depth	Depth range [m]	K_d(305 nm) [m^{-1}]	K_d(325 nm) [m^{-1}]	K_d(345 nm) [m^{-1}]	K_d(380 nm) [m^{-1}]	K_d(PAR) [m^{-1}]
North East Sector (salinity > 25)									
150	71	13	20	0-10	_	0,477	0,367	0,199	0,101
170	56	5	20	0-7	_	1,135	0,959	0,582	0,235
260	58	2	5	0-30	0,461	0,403	0,304	0,159	0,088
110	56	13	15	0-30	0,448	0,346	0,260	0,129	0,076
240	68	9	15	0-30	_	0,342	0,257	0,129	0,071
135	59	9	10	0-30	0,359	0,352	0,264	0,135	0,070
380	66	3	10	0-6	_	0,635	0,495	0,241	0,093
345	58	3	15	0-30	0,366	0,296	0,224	0,111	0,072
360	57	4	10	0-30	0,306	0,283	0,229	0,117	0,063
540	58	3	10	0-30	0,361	0,316	0,241	0,112	0,064
Mean					0,384	0,459	0,360	0,191	0,093
SD					*0,059*	*0,260*	*0,226*	*0,144*	*0,051*
North West Sector (15 < salinity < 25)									
460	66	5	5	0-30	0,360	0,337	0,266	0,127	0,070
760	62	2	10	0-8	_	0,790	0,620	0,298	0,100
620	66	3	5	0-5	_	1,135	0,927	0,423	0,122
660	79	4	5	0-8	_	_	0,999	0,609	0,146
670	55	7	5	0-5	_	1,641	1,414	0,615	0,163
780	80	2	10	0-6	_	1,504	1,316	0,616	0,150
Mean					_	1,081	0,924	0,448	0,125
SD					_	*0,532*	*0,430*	*0,204*	*0,035*

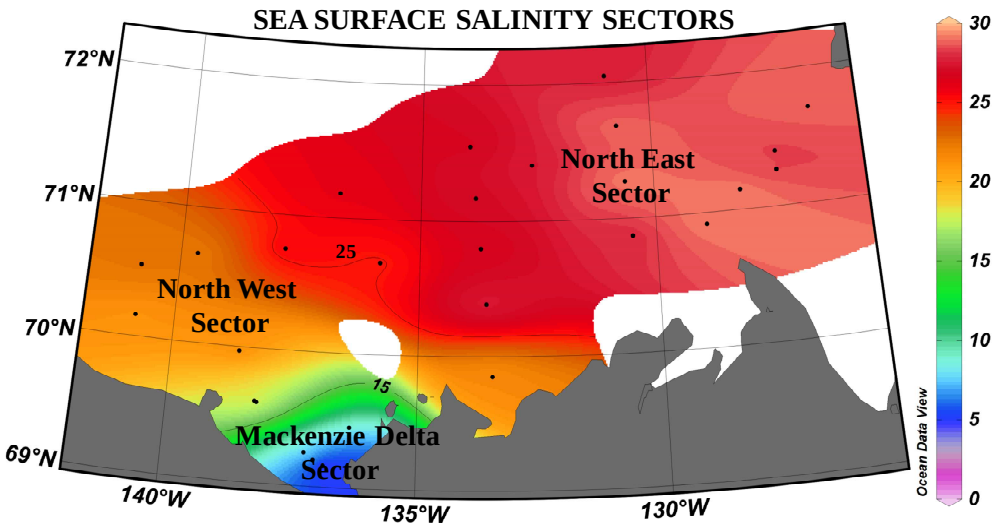

***Figure IV-2.** Map of the sea surface salinity illustrating the different surface salinity sectors observed during the study: Mackenzie Delta Sector (salinity < 15), North West Sector (15 < salinity < 25) and North East Sector (salinity > 25). Isohalines 15 and 25 mark the boundaries of these sectors.*

During the study period characterized by typical but relatively high Mackenzie discharge (12000 m^3 s^{-1}; Carmack and Macdonald, 2002), the overall spatial distribution of both K_d(UVR-A) and K_d(PAR) values in surface waters of the Canadian shelf should theoretically depend on the surface salinity gradient induced by freshwater inputs from the Mackenzie and by its subsequent plume spreading. Indeed, in the North West Sector both K_d(UVR-A) and K_d(PAR) decreased when salinity decreased whereas, in the North East Sector (salinity > 25), we observed interestingly the opposite pattern. In addition, K_d(UVR-A) and K_d(PAR) values in the North East Sector are in the same range as and sometimes higher than those determined in the North West Sector (Figure IV-3; Table IV-2). Therefore, the attenuation of both UVR-A and PAR in the North West Sector appeared mainly controlled and strongly impacted by the Mackenzie plume spreading while in the saltiest surface waters (North East Sector) other processes that have the ability to attenuate both UVR-A and PAR prevailed.

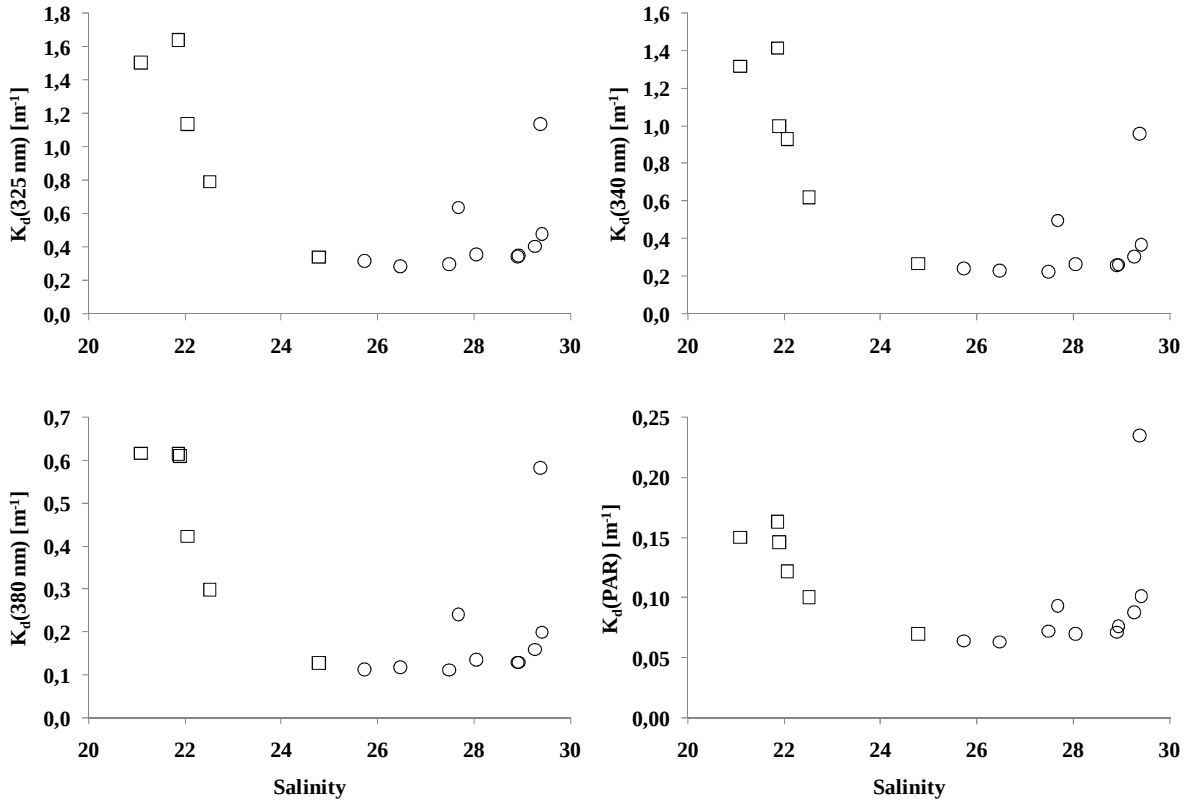

Figure IV-3. *Diffusive attenuation coefficient of light (K_d) at 325, 340, 380 nm and PAR as a function of surface salinity in the North East (circle) and North West (square) sectors.*

3. 2. DOM characteristics

3. 2. 1. Absorbant DOM

The overall DOM characteristics varied in each of the three salinity sectors observed in surface coastal waters of the Canadian shelf during the summer of 2009 (Figure IV-4; Table IV-1). Indeed, surface mean DOC concentration increased from 71 ± 15 µM C in the North East sector (salinity > 25) to 106 ± 45 and 310 ± 87 µM C in the North West (15 < salinity < 25) and Mackenzie Delta (salinity < 15) sectors, respectively. Surface mean DOC and $a_{CDOM}(350)$ values in the Mackenzie Delta Sector were up to 4 and 20 times higher than in the saltiest surface waters (North East sector), respectively (Table IV-1). In the Mackenzie Delta and North West Sectors (salinity < 25), both $a_{CDOM}(350)$ and DOC values decreased linearly (Guéguen et al., 2005) while by contrast, in the North East Sector (salinity > 25) they both increased (Figure IV-4 A and B). This coupled to the two distinct significant and positive relationships linking them along the surface salinity gradient (Figure IV-5 A and B) highlight the fact that in surface waters during the study period $a_{CDOM}(350)$ was a good proxy of DOC in the Mackenzie dilution plume area (Figure IV-5 A) due to their conservative behavior. Interestingly, in the saltiest waters (Figure IV-5 B) we also observed a linear relationship since *in situ* DOM production processes apparently prevailed over *in situ* DOM sinks (photodegradation).

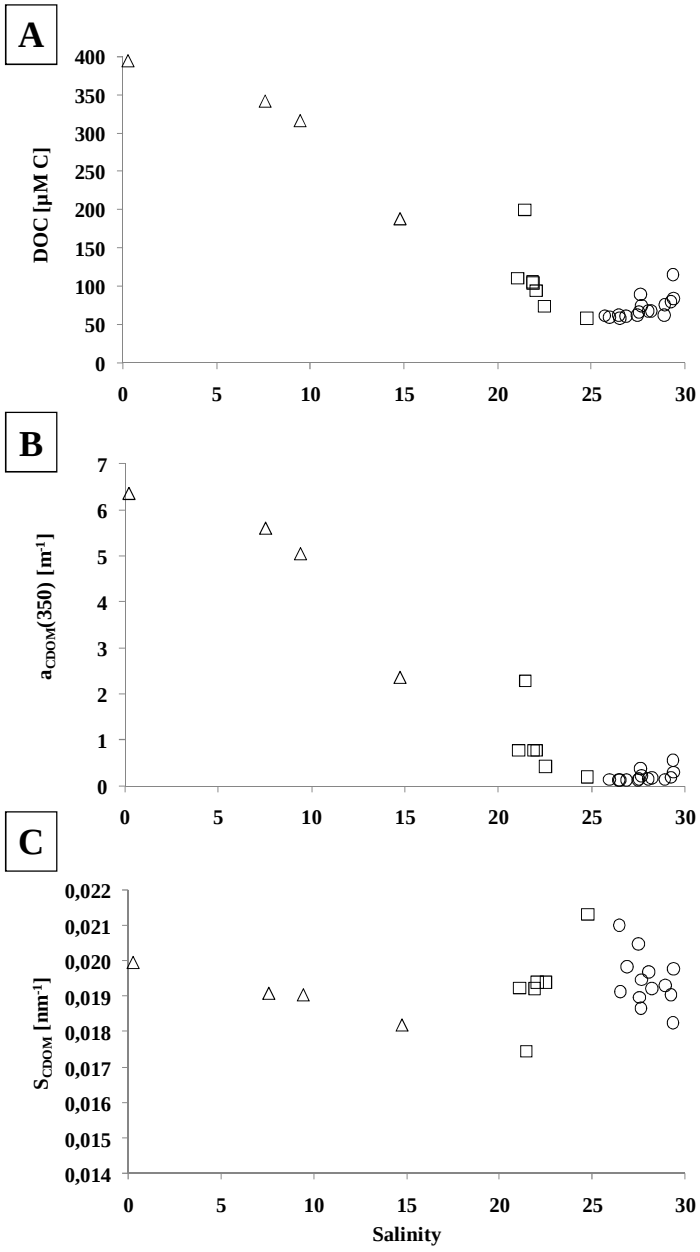

Figure IV-4. *Dissolved organic carbon (DOC) (A), absorption coefficient at 350 nm ($a_{CDOM}(350)$) (B) and spectral slope (S_{CDOM}) (C) as a function of surface salinity in the North East (circle), North West (square) and Mackenzie Delta (triangle) sectors.*

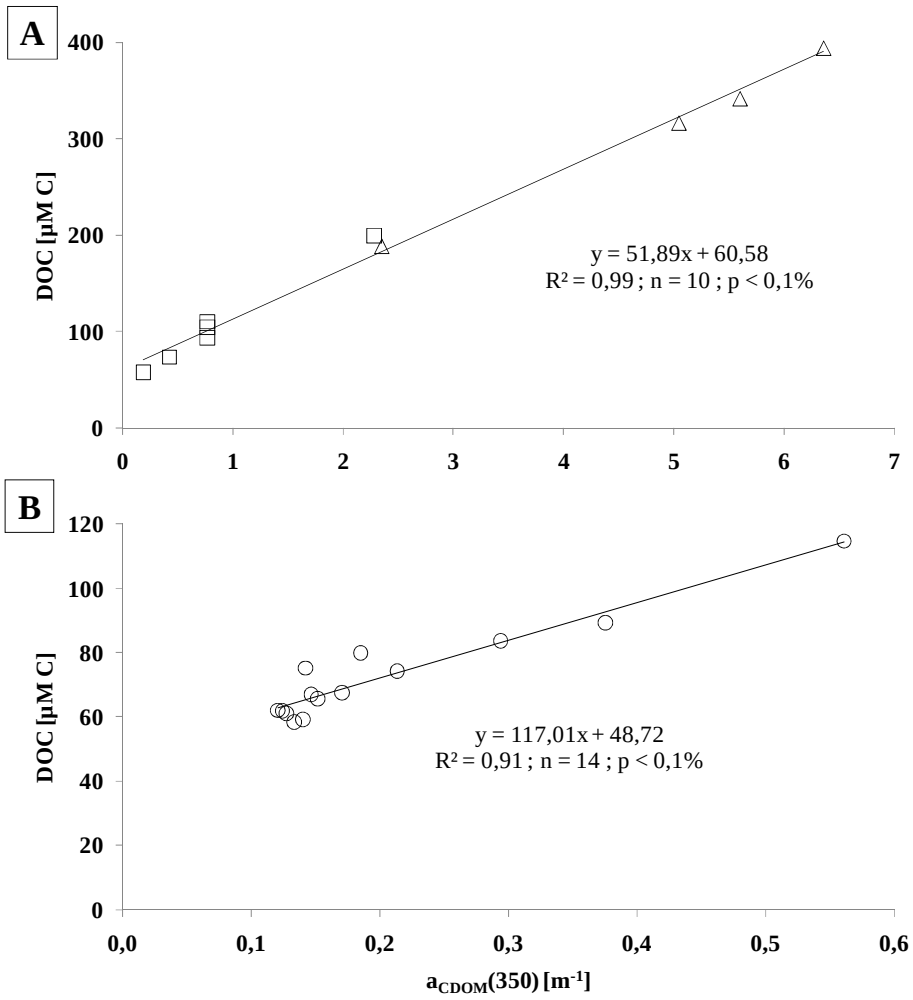

Figure IV-5. *Relationships observed between dissolved organic carbon (DOC) concentration and absorption coefficient of CDOM at 350 nm ($a_{CDOM}(350)$) determined in the Mackenzie Delta and North West sectors (salinity < 25; A) and in the North East Sector (salinity > 25; B).*

Therefore, the origin of the DOM content is different across the system. In the Mackenzie Delta and North West sectors (salinity < 25) the origin of the DOM appeared mostly allochthonous due to the mixing process of the Mackenzie inputs while, in the saltiest surface waters (North East Sector) other processes that have the ability to bring autochthonous DOM or/and enhance its production prevailed. Sea ice formation/brine injection and upwelling processes which are common physical features of this salty area have the capacity to deposit DOM and enhance surface *in situ* production of DOM, respectively (Carmack and Macdonald, 2002; Barber and Hanesiak, 2004; Guéguen et al., 2007; Walker et al., 2009; Mucci et al, 2010). In addition, the relatively recent DOM induced by such processes has the capacity to attenuate efficiently both UVR-A and PAR as shown in Figure IV-3. An upwelling event close to the Cape Bathurst area (Figure IV-1) was clearly identified

during our sampling and was previously observed by Mucci et al (2010). It enhanced primary production in the surface waters surrounding Cape Bathurst as shown by the highest surface chlorophyll *a* concentration ≈ 7 µg l^{-1} determined at station 170 (personal communication Simon Bélanger) and subsequent by-products which could explain the highest values of DOC, $a_{CDOM}(350)$ and K_d(UVR-A and PAR) observed at this station (Tables IV-1 and IV-2).

In a general manner, these results illustrate two distinct origins of the DOM content evolving in surface waters of the Canadian Shelf during the study period. The DOM content of the Mackenzie Delta and North West sectors (salinity < 25) presents a strong allochthonous signature. By contrast, the DOM content of the North East Sector (salinity > 25) appeared more autochthonous. In addition, the estimation of the optically inactive fraction of the averaged DOC pool in the Mackenzie Delta-North West sectors and in the North East Sector (i.e. $a_{CDOM}(350) = 0\ m^{-1}$; Figure IV-5 A and B) is 34 % and 69 %, respectively. This underlines a stronger potential reactivity of the allochthonous DOM pool in the Mackenzie Delta and North West sectors than the autochthonous one in the saltiest waters (North East Sector). However, since K_d(UVR-A) and K_d(PAR) were significantly correlated to $a_{CDOM}(350)$ values (Figure IV-6), the impact of allochthonous and autochthonous CDOM on the underwater UVR-A and PAR light field distribution could be considered similar in the North West and North East sectors (i.e. at salinity > 20; where radiometric measurements were performed) except for the K_d(PAR) value observed at station 170 (Figure IV-6). This allows us to suppose a spatial dominance of the highly reactive allochthonous DOM restricted to the Mackenzie Delta Sector and a relatively important amount of autochthonous DOM in the North West Sector as well. Interestingly, the low residual attenuation values (y-intercept values) of these relationships (Figure IV-6) were close to the corresponding range of attenuation coefficient values of water molecules ($K_w(\lambda)$) determined by Baker and Smith (1982). Therefore, CDOM appears to be the dominant attenuator of UVR-A and PAR through the two saltiest surface sectors (North West and North East Sectors), except at station 170 (Figure IV-6), where additional attenuator(s) of PAR especially, such as phytoplankton, also interfered.

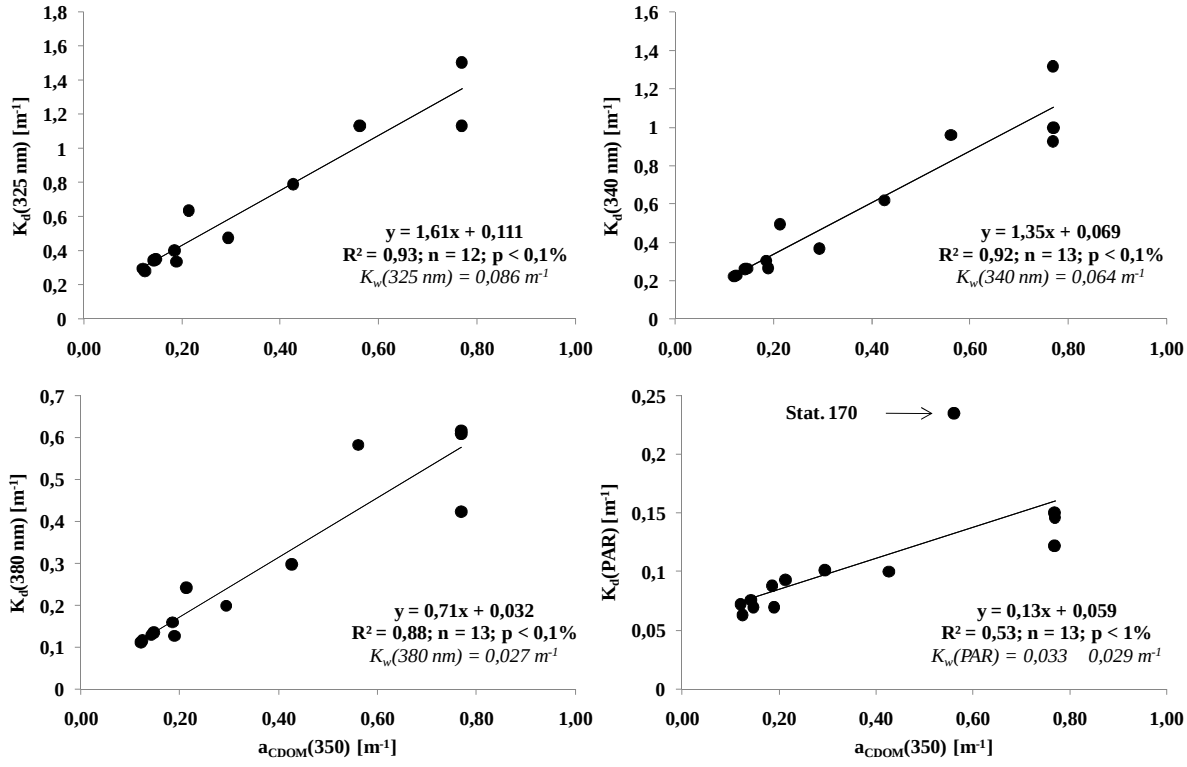

Figure IV-6. *Relationships between surface diffusive attenuation coefficient of light (K_d) determined in the UVR-A (325, 340 and 380 nm) and PAR spectral domains with absorption coefficient of CDOM at 350 nm ($a_{CDOM}(350)$) observed in the two saltiest surface salinity sectors (North West and North East sectors).*

In the following section we investigated the spatial evolution of the S_{CDOM} values and the DOC-specific values for CDOM absorption: $a_{CDOM}(350)^*$ (i.e. $a_{CDOM}(350)$/DOC) which are both subject to change according to the DOM origin, chemical structure, in order to reinforce the hypothesis concerning the restricted spatial dominance of the allochthonous DOM in the Mackenzie Delta Sector (salinity < 15). Unfortunately, during the study period no significant differences between mean S_{CDOM} values determined for each salinity sector could be observed (Table IV-1) despite the scattered S_{CDOM} values observed at salinity > 25 (Figure IV-4 C).This could be attributed to the surprisingly high S_{CDOM} values determine for the allochthonous CDOM of the Mackenzie Delta Sector (S_{CDOM} = 0.019 ± 0.001 nm^{-1}) that may have prevented the establishment of clear spatial contrast in S_{CDOM} values through the system. These S_{CDOM} values seem unusually high for river DOM, however similar values were previously reported for the CDOM of the Mackenzie itself during summer period (Retamal et al., 2007; Osburn et al., 2009; Stedmon et al., 2011). Stedmon et al. (2011) and Osburn et al.(2009) attributed these high S_{CDOM} values to a prefrential sorption of the high molecular

hydrophobic DOM components to the abundant suspended sediments and to a more extensive photodegradation of the high molecular weight fraction in the Mackenzie watershed, respectively. Interestingly, clear spatial differences emerged from the $a_{CDOM}(350)^*$ values which could be used, in such rich-terrestrial environment, as an index of the proportion of terrestrial, aromatic CDOM in the DOC pool (Belzile et al., 2002; Gareis et al., 2010). Indeed, the mean $a_{CDOM}(350)^*$ values determined for each salinity sector were significantly different (Table IV-1), with the highest value (15.24 ± 1.84 m^2 mol) found in the Mackenzie Delta Sector and the lowest value (2.67 ± 0.91 m^2 mol) in the saltiest surface waters (North East Sector) while the North West Sector was characterized by an intermediate value (7.17 ± 2.70 m^2 mol). Therefore, the proportion of allochthonous CDOM or the relative capacity of DOM to absorb light is around 5-6 times higher than in the DOM pool evolving in the Mackenzie Delta Sector than in the DOM pool observed in the saltiest surface waters (North East Sector). This underlines the two distinct origins of the DOM content evolving in this system during the study period and reinforces the predominant highly absorbant allochthonous amount of DOM in the Mackenzie Delta Sector and the autochthonous one in the North East Sector while the North West Sector contains a mixture of DOM from both sources.

3. 2. 2. Fluorescent DOM

Fluorescent components characteristics. Three fluorescent components were identified by PARAFAC analysis using a total of 54 EEMs collected at the surface and at the deep chlorophyll maximum (DCM) of the 27 stations investigated during the MALINA cruise (Figure IV-1). PARAFAC components' spectral characteristics and contour plots identified in this study are shown in Figure IV-7. The three-component PARAFAC model was validated using split-half analysis (Stedmon et al., 2003) and provided low residual EEMs. This shows that a three-component PARAFAC model extracts the majority of EEMs features and is thus able to characterize the surface CDOM composition for this area.

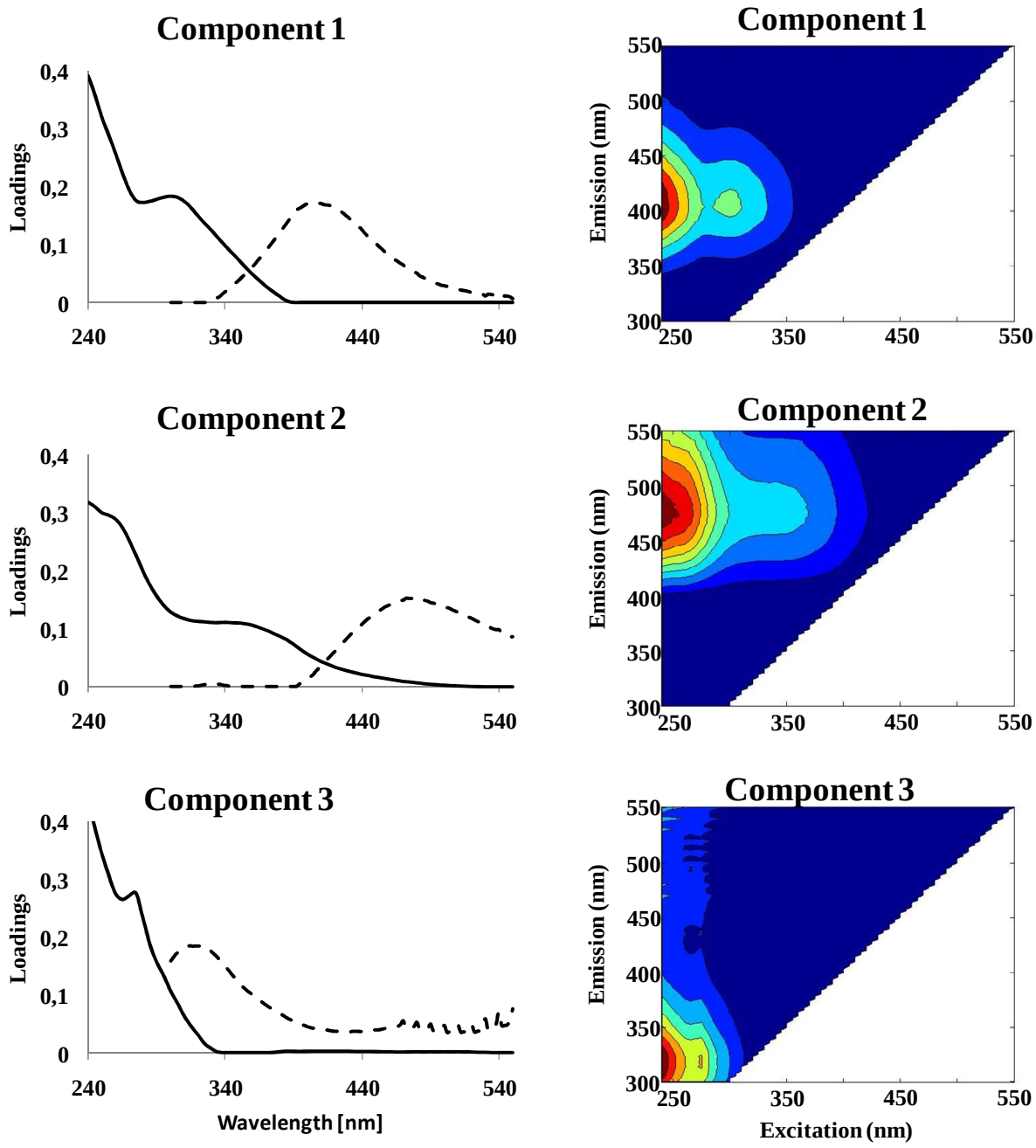

Figure IV-7. *Emission (dashed line) and Excitation (solid line) spectra (left panels) and contour plots (right panels) of the three main fluorescent components identified in the dataset (n = 54). Ex/Em Component 1: 240 (300)/404; Ex/Em Component 2: 240 (340)/472 and Ex/Em Component 3: 240 (275)/314.*

Table IV-3. *Spectral characteristics of the three components identified by PARAFAC analysis compared to previously identified components including Arctic and sub-Arctic studies (Stedmon et al., 2007; Walker et al., 2009; Fellman et al., 2010). Position of Ex/Em maxima of C1, C2 and C3 are deduced from their corresponding spectra reported in Figure IV-7.*

	Components		
	C1	C2	C3
Ex. Maxima (nm)	< 240 (300)	< 240 (340)	< 240 (275)
Em. Maxima (nm)	404	472	314
Coble et al., 1998	M	A and (C)	B and T
Stedmon et al., 2007	C3	C1	C4 and C5
Walker et al., 2009	BERC6	BERC3	BERC5
Fellman et al., 2010	C5	C1 and (C2)	C8 and C7
Source	Marine and Terrestrial	Terrestrial (allochthonous)	Amino acids (autochthonous)

Excitation/Emission (Ex/Em) maxima wavelengths of the three components are recapitulated in Table IV-3 and compared to previously identified fluorescent components, including recent Arctic and sub-Arctic studies (Stedmon et al., 2007; Walker et al., 2009; Fellman et al., 2010). The Ex/Em maxima of the component 1 (C1) are close to the marine humic-like (M peak) as defined by Coble (1996). However, C1 is an ubiquitous component since it could be derived from phytoplankton microbial degradation (Nagata et al., 2000; Stedmon and Markager, 2005; Zhang et al., 2009) and from specific Arctic terrestrial sources at low salinity (Walker et al., 2009). Component 2 (C2) presents the longest Ex/Em maxima wavelengths found in this study and is similar to a mixture containing both humic-like components, A and C peaks determined by Coble et al. (1998). Given that both A and C peaks have previously been associated with high molecular weight and aromatic terrestrial organic matter (Stedmon et al., 2003), the origin of C2 in such environments could be essentially terrestrial. In addition, C2 has similar spectral characteristics of the humic-like component (Table IV-2) observed by Walker et al. (2009) in the same study area (Canadian Arctic Ocean) and which was attributed to a terrestrial origin. The low Ex/Em maxima of C3 are comparable to protein-like components previously observed in surface waters of fresh and marine systems which were attributed to a biological origin (Coble, 1996; Yamashita et al., 2003; Para et al., 2010).

The ratios of fluorescent components identified are used in order to examine potential fluorescence composition variation within the fluorescent DOM pool in the salinity gradient observed in surface waters. Since the origin of the humic-like component C2 appeared to be

exclusively terrestrial, deviations in the ratios of other components to C2 could point out potential autochthonous sources/sinks of CDOM (Figure IV-8). C1/C2 and C3/C2 ratios were relatively constant at salinity < 15, while they both increased at salinity > 15, particularly at station 540. This suggests a non-terrestrial dominant source of the components C1 and C3 except in the vicinity of the Mackenzie Delta Sector and particularly for component 1 where the ratio C1/C2 was surprisingly greater than 1. Station 540, largely influenced by Sea Ice Meltwater (SIM > 20 %; personal communication Bruno Lansard; appendix 1), presents the highest C1/C2 and C3/C2 ratios. This is probably due to brine injection containing a large amount of both humic-like (C1) and protein-like components (C3; Walker et al., 2009).

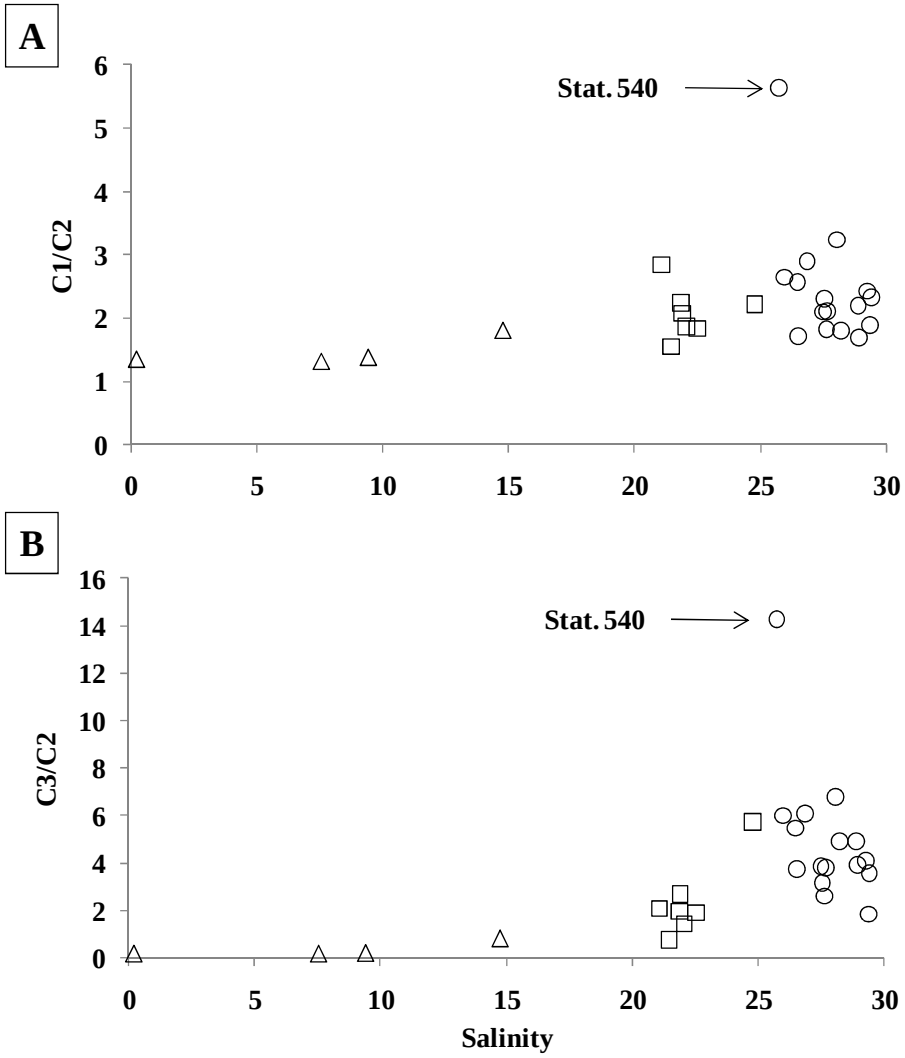

Figure IV-8. *Fluorescence ratios of C1/C2 (A) and C3/C2 (B) as a function of salinity in surface waters of the Mackenzie Delta (salinity < 15; triangles), North West (15 < salinity < 25; squares) and North East (salinity > 25) Sectors.*

Fluorescent components surface distribution. The spatial distribution of the fluorescence intensity of each fluorescent component is illustrated in Figure IV-9 and the mean percentages of their relative contributions for each salinity sector and for the entire system (Total Sector) are shown in Figure IV-10. In the surface waters of the Canadian shelf (Total Sector; Figure IV-10 A) no single fluorescent component dominated. However, the relative contribution of the humic-like component C1 (36 ± 10%) and of the protein-like component C3 (46 ± 18%), which are both biologically-derived, seemed slightly higher than the relative contribution of the terrestrial component C2 (18 ± 9%). Maximum and minimum fluorescence intensity values of both components C1 and C2 were observed at stations located in the vicinity of the Mackenzie Delta and at stations located offshore, respectively. Interestingly, the protein-like component C3 exhibited a relatively homogeneous fluorescent signal except at specific stations (stations 170, 540, 696, 695, 694 and 780) where its corresponding fluorescence intensity increased. This could be attributed to several individual forcings occurring close to these stations such as (i) upwelling event observed at station 170; (ii) brine injection observed at station 540; (iii) freshwater inputs observed for stations located in the vicinity of the Mackenzie Delta (stations 696, 695 and 694) and at their synergy as it was supposed at station 780. Investigating the surface distribution of fluorescent components in the different salinity sectors allows us to put forth insightful trends (Figure IV-10 B).

Indeed, in the North East Sector (salinity > 25), the relative contribution of each fluorescent component was clearly dominated by the protein-like component C3 (57 ± 7%) followed by the humic-like component C1 (30 ± 4%) and the terrestrial component C2 (13 ± 4%) with corresponding mean fluorescence intensities of 9 ± 2, 5 ± 2 and 2 ± 1 QSU, respectively. Concerning the surface waters of the North West Sector (15 < salinity < 25) we observed a co-dominance of both biological components C1 (40 ± 8%) and C3 (40 ± 13%) while the relative contribution of the terrestrial component C2 was around two times less (20 ± 6%). For this surface area, the mean fluorescence intensity of the protein-like component C3 (10 ± 3 QSU) remained unchanged while those of both humic-like components C1 (12 ± 6 QSU) and C2 (6 ± 3 QSU) increased, compared to those determined in the saltiest surface waters (North East Sector). In the Mackenzie Delta Sector (salinity < 15), the relative contribution of the biological component C1 (52 ± 2%) and terrestrial component C2 (36 ± 6 %) reached their highest contribution, while the one of C3 (12 ±7 %), around 5 times less compared to those determined in the saltiest surface waters, was the lowest.

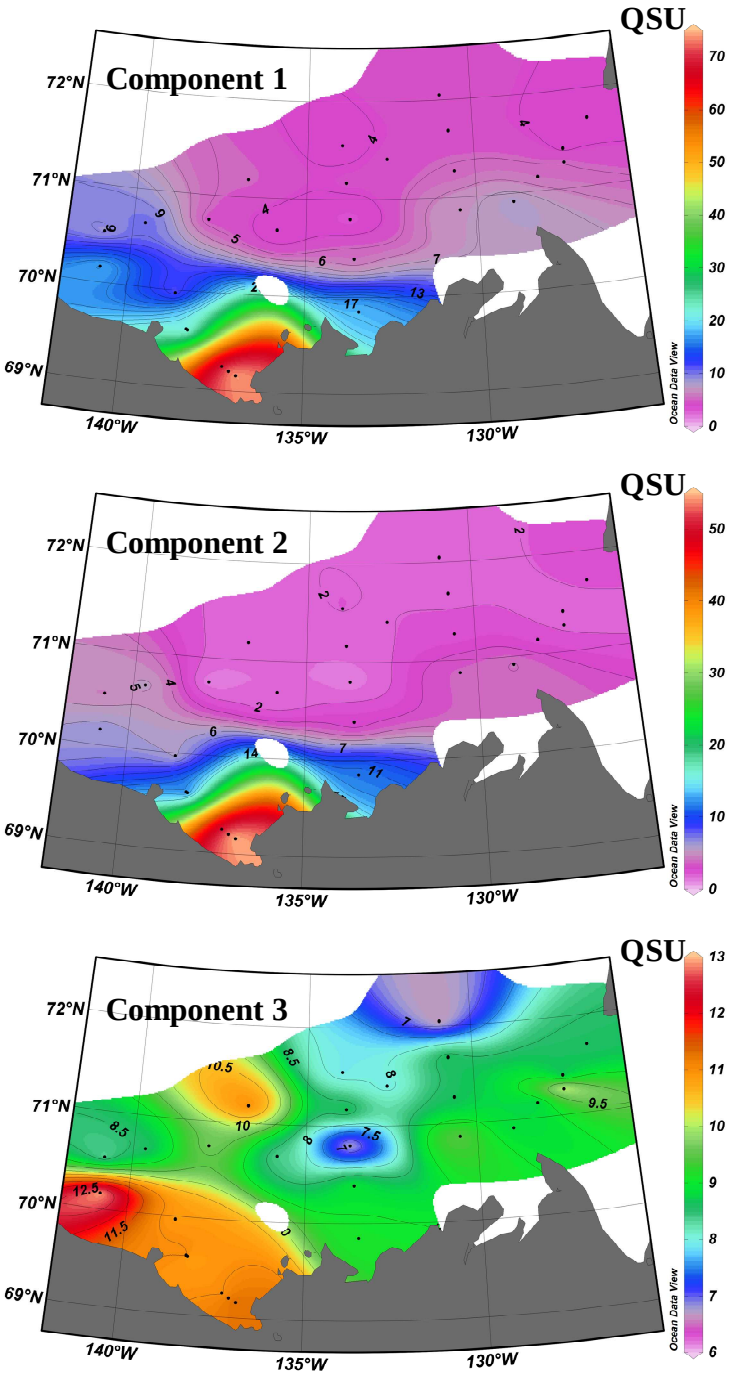

Figure IV-9. *Spatial distribution of fluorescence intensity (QSU) of the component 1, 2 and 3 identified in surface waters of the Canadian shelf in the Beaufort Sea.*

Corresponding mean fluorescence intensity of the biological component C1 and of the terrestrial humic-like component C2 were the highest and similar, with 61 ± 29 and 44 ± 23 QSU, respectively, while that the protein-like component C3 remained significantly unchanged (10 ± 1 QSU) compared to those calculated for the two other salinity sectors.

Therefore, during the study period the fluorescent DOM content evolving in surface waters of the Canadian shelf was strongly influenced by allochthonous DOM originating from the Mackenzie, except in the saltiest waters where autochthonous biological fluorescent DOM prevailed. Surprisingly, the allochthonous fluorescent DOM carried by the Mackenzie into the Beaufort Sea presents a strong biological content in addition to the usual terrestrial content. Indeed, the fluorescence intensity of the biological component C1 co-dominated with the terrestrial humic-like component C2 in the overall allochthonous fluorescent DOM pool of the Mackenzie Delta Sector. Interestingly, the overall distribution of the terrestrial component C2 appeared restricted to the Mackenzie Delta Sector and paralleled well with the highly absorbant allochthonous DOM observed, while the surface distribution of the biological component C1 appeared more ubiquitous.

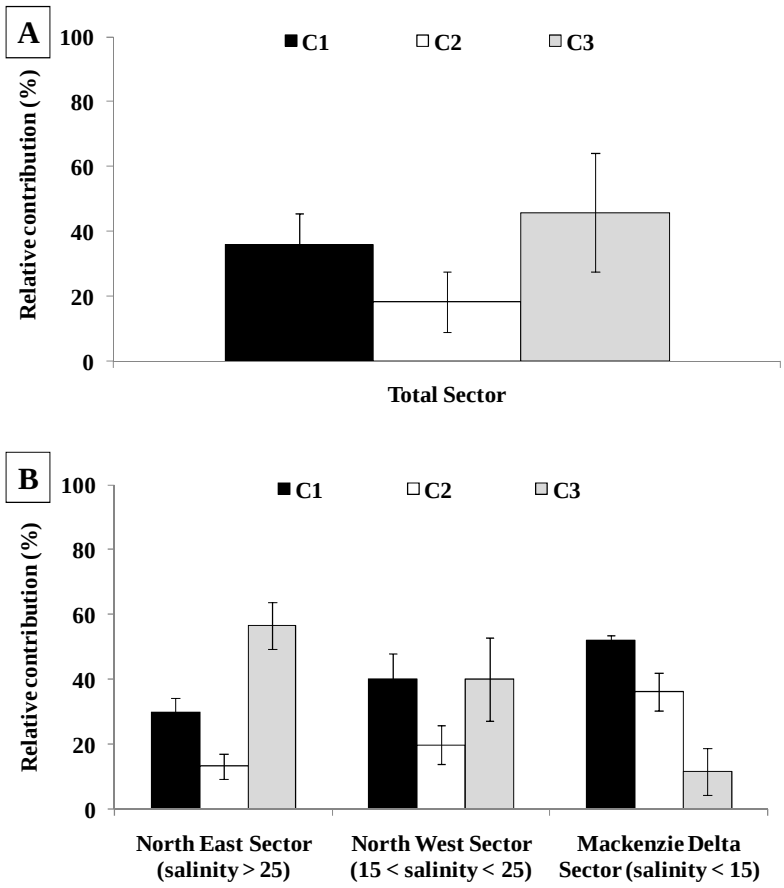

Figure IV-10. *Relative contribution of the fluorescent components C1, C2 and C3 for the Total Sector (A) and per sector (B).*

During summertime the Mackenzie Delta is composed of numerous (around 45000) shallow (1.6 m depth on average) macrophyte-rich lakes (Emmerton et al., 2007; Squires et al., 2009) that significantly influence the Mackenzie DOM content prior to its marine discharge (Emmerton et al., 2008; Gareis et al., 2010). In addition, macrophyte and phytoplankton degradation/exsudation processes in fresh shallow (Zhang et al., 2009) and marine systems lead to the production of the marine humic-like fluorescent component (M peak; Coble, 1996) comparable to our component 1. Therefore, the strong biological fluorescent DOM fraction observed in the Mackenzie Delta Sector quite probably originated from the important biological activity (Squires et al., 2009) occurring in these catchments. This finding completes and provides another valuable explanation concerning the Mackenzie organic matter quality depleted in humic materials previously shown during summer time and attributed to (i) a high freshwater residence time in Mackenzie catchments (Retamal et al., 2007), (ii) a preferential sorption of the high molecular hydrophobic DOM components to the abundant suspended sediments (Stedmon et al., 2011) and (iii) a more extensive photodegradation of the high molecular weight fraction occurring in the important Mackenzie watershed during summer period (Osburn et al., 2009).

4. Conclusion

The investigation of absorption parameters coupled to the application of three-dimensional excitation/emission matrices with Parallel Factor Analysis on a CDOM dataset encompassing a surface salinity gradient from both fresh and marine systems gives for the first time the opportunity to assess quantitatively and qualitatively the changes in surface CDOM of the Canadian shelf which receives the allochthonous load of the fourth largest river in the Arctic: the Mackenzie. In this study, the absorbant capacity ($a_{CDOM}(350)$*) and the amount of (C)DOM in the Mackenzie Delta Sector (salinity < 15) were significantly higher than those observed in saltiest waters (salinity > 25) while the variables ones of the intermediate salinity sector (15 < salinity < 25) characterized a DOM transition zone. Surface CDOM which could be considered as the dominant attenuator of UVR-A and PAR through the salinity system > 20 was a good proxy of DOC in the Mackenzie dilution plume area (salinity < 25; conservative behavior) but also apparently in the saltiest waters (salinity > 25; *in situ* DOM production coupled to a limited DOM photodegradation process). Although, S_{CDOM} values were not significantly different across the different surface salinity sectors, two

distinct origins of the absorbant DOM content were observed. The reactive allochthonous DOM which dominated only in the Mackenzie Delta Sector (salinity < 15) and the autochthonous DOM which prevailed in the North East Sector (salinity > 25).

EEMs along with PARAFAC analysis allowed the spectral decomposition of two biological components: the humic-like component C1 traditionally identified as the marine humic-like component (M peak; Coble, 1996) and the protein-like component C3. One terrestrial component: the humic-like component C2, was also identified. The EEMs composition was surprisingly dominated by both biological components throughout the system. The spatial distribution of the protein-like component was relatively homogeneous throughout the system except at specific offshore stations where processes leading to *in situ* production occurred. By contrast, the terrestrial component C2 was interestingly restricted to the Mackenzie Delta Sector and paralleled exactly the distribution of highly absorbant allochthonous DOM. The surface distribution of the biological component C1 appeared more spread out than the terrestrial component C2 probably due to its ubiquitous nature, however it is clear and surprising that its strongest signature was observed in the Mackenzie Delta Sector. This biological component originated quite probably from the important phytoplankton and macrophytes activity (Squires et al., 2009) occurring in the open waters Mackenzie catchment prior to its marine discharge.

This finding completes and provides another valuable explanation concerning the Mackenzie organic matter quality depleted in humic terrestrial materials previously shown during summer time and attributed to (i) a high freshwater residence time in Mackenzie catchments (Retamal et al., 2007), (ii) a preferential sorption of the high molecular hydrophobic DOM components to the abundant suspended sediments (Stedmon et al., 2011) and (iii) a more extensive photodegradation of the high molecular weight fraction occurring in the important Mackenzie watershed during summer period (Osburn et al., 2009). Moreover, these conclusions taken as whole may explain in part the high proportion of autochthonous CDOM recently shown (Stedmon et al., 2011) in the surface waters of the Canadian Basin compared to the more riverine CDOM of the Eurasian Basin.

APPENDIX 1: *MODIS satellite image (Canadian shelf) showing the extent of sea ice on 23 August 2009 (end of MALINA cruise)*

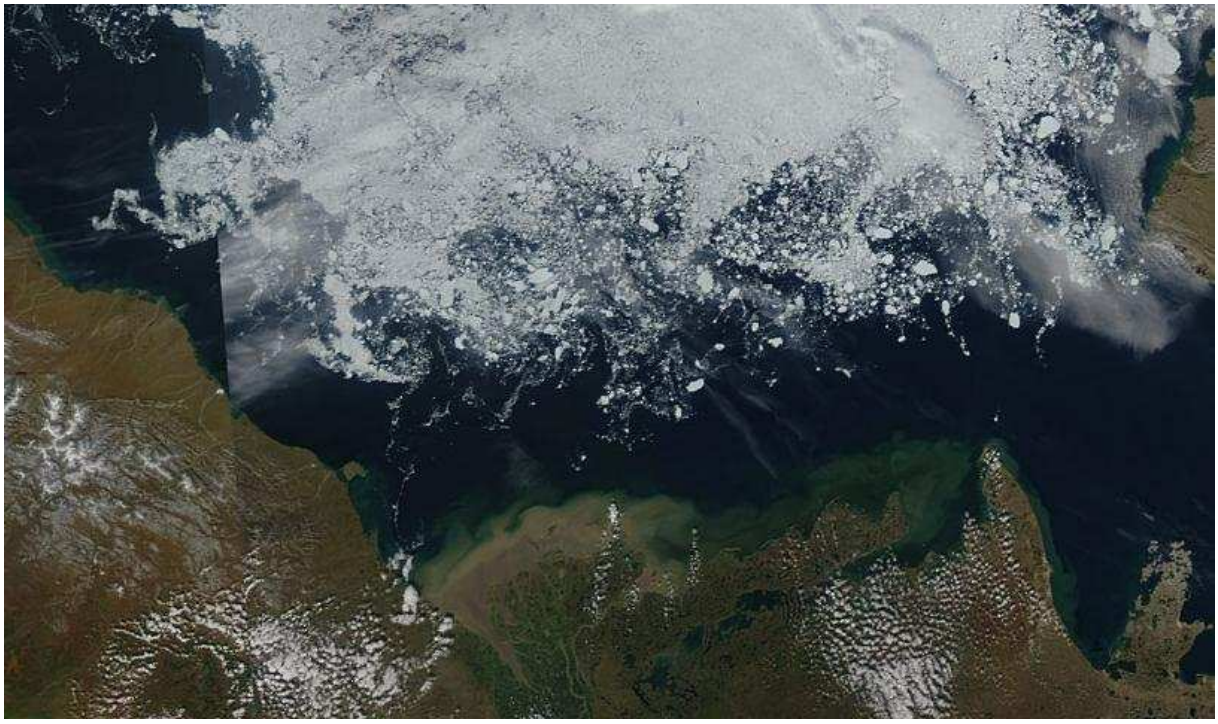

CHAPITRE V

CONCLUSION ET PERSPECTIVES

1. Conclusion

Ce travail de thèse s'est concentré sur l'étude de la dynamique de la CDOM, et de son impact sur l'atténuation de l'éclairement UV-visible dans les eaux de surface côtières de deux systèmes très contrastés et d'intérêts pour l'étude des changements climatiques. D'une manière générale, la Baie de Marseille est un écosystème oligotrophe soumis à un fort ensoleillement qui présente un persistent signal de fond de CDOM de nature complexe sur lequel se superposent des pulses épisodiques de CDOM récente issue de l'activité biologique *in situ* et induite par les intrusions du panache du Rhône. Au niveau du plateau Canadien en Mer de Beaufort, la nature de la CDOM est fortement influencée par les apports allochtones du fleuve Mackenzie qui comportent une importante fraction de CDOM biologique issue de l'intense activité biologique se déroulant dans les nombreux lacs formant le delta. Dans les deux systèmes océaniques étudiés, les mesures radiométriques ont mis en évidence le rôle prépondérant de la CDOM dans le contrôle de l'atténuation de la lumière UV et visible dans les eaux de surface.

Dans le chapitre II nous avons présenté les propriétés optiques de la CDOM des eaux de surface de la Baie de Marseille (Novembre 2007-Décembre 2008). Les valeurs annuelles du coefficient d'absorption de la CDOM à 350 nm sont faibles et relativement constantes [$a_{CDOM}(350) = 0{,}10 \pm 0{,}02$ m^{-1}]. L'augmentation de la pente spectrale de la CDOM (S_{CDOM}) en été ($S_{CDOM} = 0{,}023 \pm 0{,}003$ nm^{-1}) souligne soit un photo-blanchiment estival [si $a_{CDOM}(350)$ faible] ou une production [si $a_{CDOM}(350)$ élevé] de CDOM en surface. La fraction fluorescente de la CDOM caractérisée par la dominance des fluorophores de types protéiques (pic T) et humiques marins (pic M) comparé à la faible représentativité des fluorophores terrestres (pics A et C) atteste d'une origine essentiellement biologique de la CDOM fluorescente. Cette étude a mis en avant la forte production de CDOM fluorescente autochtone (pics M et T) issue de la forte activité biologique lors d'événements d'intrusions du panache du Rhône en Baie de Marseille riche en nutriments et en substrats labiles (photo-dégradation de la CDOM terrestre lors de son transit). Le brassage de la colonne d'eau est également une source importante de CDOM dans les eaux de surface, mais cette CDOM est plus humifiée (pics C et M) alors que la photo-dégradation apparait comme un puits majeur de CDOM, notamment à la fin de l'été (Figure V-1).

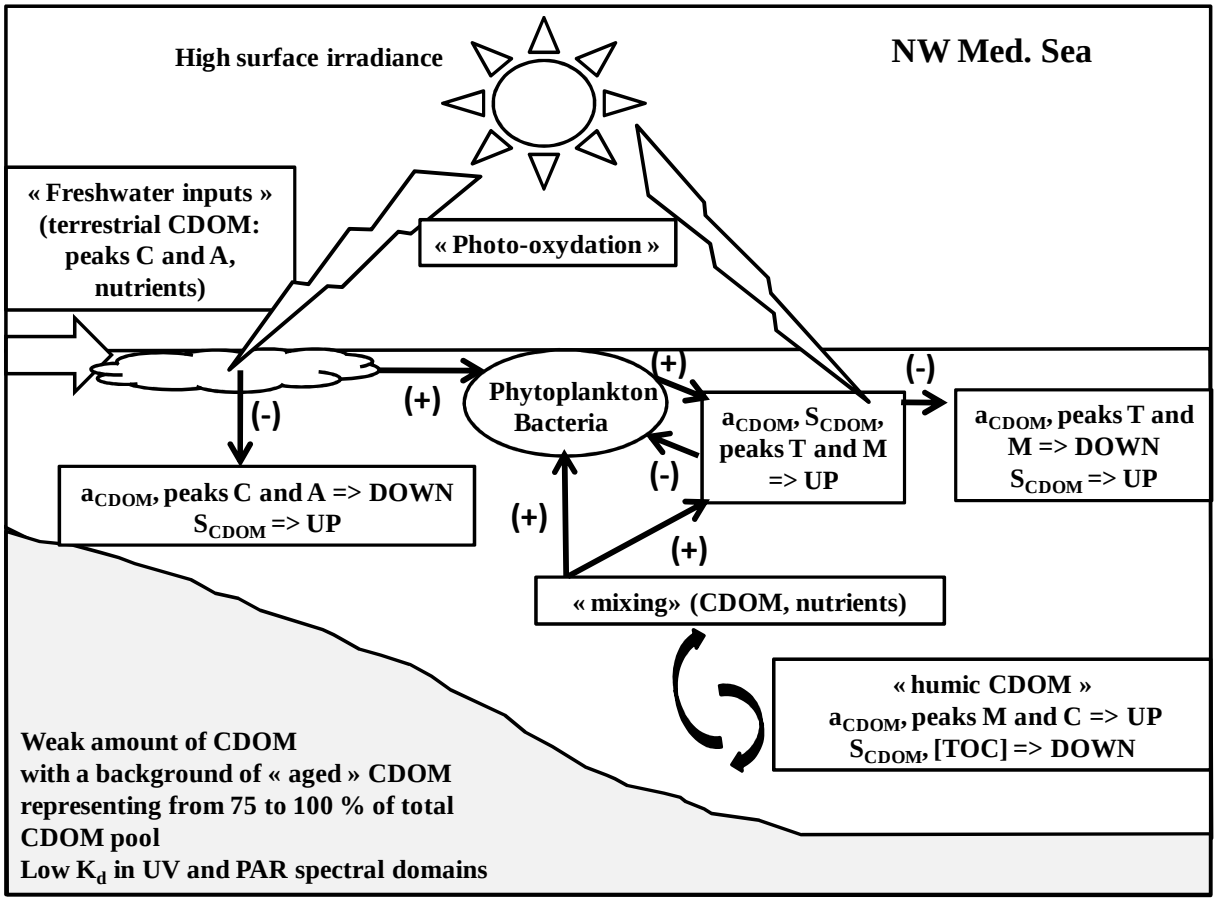

Figure V-1. *Facteurs biotiques et abiotiques contrôlant la dynamique de la CDOM en Baie de Marseille.*

Nous avons également exploré (chapitre III) les propriétés optiques des eaux de surface en Baie de Marseille en fonction des principaux facteurs bio-optiques contrôlant la distribution du champ lumineux solaire sous marin dans cet environnement oligotrophe (CDOM et Chl*a*). Nous avons observé que l'éclairement solaire (UV et visible) reçu en surface ($E_s(\lambda)$) au midi solaire en Baie de Marseille varie saisonnièrement tant quantitativement que spectralement. Ainsi, les $E_s(\lambda)$ comportent une composante en UVR-B 7-8 fois plus importante en période estivale que les UVR-A et PAR. Les valeurs maximales des $E_s(\lambda)$ à 305 nm (UVR-B), 340 nm (UVR-A) et pour le PAR étaient respectivement de 4,64 ; 58,88 µW cm^{-2} et 0,2 µE cm^{-2} s^{-1} et sont représentatives des $E_s(\lambda)$ mesurés dans le bassin Méditerranéen (Obernosterer et al., 1999). Ces $E_s(\lambda)$ sont du même ordre de grandeur que ceux mesurés aux mêmes longueurs d'ondes (9,26 ; 61,29 µW cm^{-2} s^{-1} et 0,22 µE cm^{-2} s^{-1}) au niveau du Tropique du Capricorne (Pacifique SE ; Tedetti, 2006) excepté pour E_s(UVR-B), deux fois plus importants au niveau du Pacifique. Dans les eaux de surface de la Baie de Marseille, les valeurs des coefficients d'atténuation diffus de la lumière UV et visible ($K_d(\lambda)$)

sont faibles et relativement constantes durant l'année d'étude ce qui illustre une importante pénétration de la lumière pour cette zone côtière (Figure V-2). Ces faibles valeurs de $K_d(\lambda)$ associées aux forts $E_s(\lambda)$ soulignent l'importance de la photochimie dans ces eaux de surface.

Bien que les tendances saisonnières des $K_d(\lambda)$ ne soient pas très marquées, nous avons mis en évidence que pour de valeurs de [Chl*a*] > 0,4 µg l^{-1}, la production primaire génère de la CDOM fraiche qui absorbe les courtes longueurs d'ondes (325 et 340 nm). Pour une productivité faible, c'est-à-dire pour des valeurs de [Chl*a*] < 0,4 µg l^{-1}, l'environnement marin contient une CDOM présentant une dépendance spectrale d'absorption significative envers les longueurs d'ondes élevées (340, 380 nm et PAR). Ainsi, dans les eaux de surface de la Baie de Marseille coexistent deux « pools » de CDOM présentant des propriétés optiques différentes. Un pool de CDOM qui présente une dépendance spectrale bathochromique (vers les grandes λ) et qui est certainement constitué de matériel bio-réfractaire qui s'accumule (signal de fond) ; et en période de productivité marine relativement importante on observe un deuxième pool de CDOM qui présente une dépendance spectrale hypsochromique (vers les courtes λ) et qui se compose de matériel frais et bio-disponible.

Cette étude montre que les propriétés optiques des eaux de surface de la Baie de Marseille sont gouvernées essentiellement par le phytoplancton et ses sous produits. La classification de ces eaux côtières, selon les critères biogéochimiques susmentionnés serait donc des eaux du cas 1 (Morel et al., 2007).

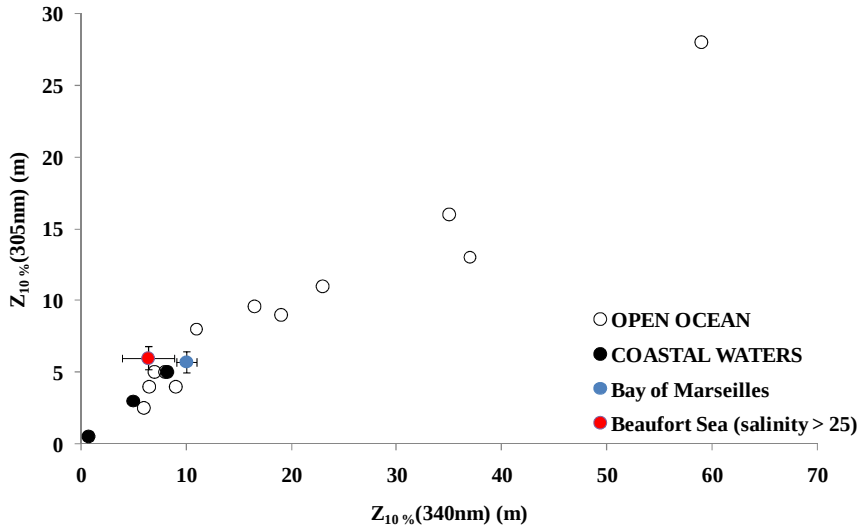

Figure V-2. *Valeurs des $Z_{10\%}$ à 305 et 340 nm mesurées en Baie de Marseille (Nov. 2007- Dec. 2008) et en Mer de Beaufort (salinité > 25, été 2009) comparés à celles reportées pour des systèmes océaniques côtiers et ouverts (Tedetti et al., 2006)*

Le chapitre IV présente la distribution spatiale des propriétés d'absorbance et de fluorescence de la DOM au niveau des eaux de surface du plateau Canadien de la Mer de Beaufort durant l'été 2009. Cette zone d'étude se caractérise par des teneurs fortement variables en CDOM avec des valeurs de $a_{CDOM}(350)$ comprises entre 0,12 m^{-1} au large (salinité > 25) et 6,36 m^{-1} au niveau du Delta du Mackenzie (salinité = 0). Le long du gradient de salinité de surface 0-25, la CDOM présente un comportement conservatif et apparait donc comme un bon estimateur du DOC. Au niveau du delta du Mackenzie (salinité < 15), l'absorptivité de la CDOM est 5-6 fois plus importante que celle de la CDOM évoluant dans le système marin (salinité > 25). Ces résultats attestent d'une origine allochtone de la CDOM évoluant dans le système deltaïque du Mackenzie (salinité < 15). Au-delà (salinité > 15), la CDOM d'origine terrestre est diluée et se mélange avec de la CDOM autochtone et qui domine au large (salinité > 25). Les valeurs élevées de S_{CDOM} sur l'ensemble du système (S_{CDOM} = 0,019 ± 0,001 nm^{-1}) confortent l'origine autochtone de la CDOM au large et soulignent un surprenant appauvrissement en matières humiques de la CDOM du Mackenzie durant l'été. De récentes études rapportent des valeurs similaires de S_{CDOM} pour le Mackenzie à cette période et les expliquent par une adsorption préférentielle des composés humiques hydrophobes sur le sédiment en suspension (Stedmon et al., 2011) et/ou à leur photodégradation durant leur long transit à travers les méandres du delta avant leur arrivée en mer (Osburn et al., 2009). Ces deux processus expliqueraient donc les valeurs élevées de S_{CDOM} observées au niveau du Delta du Mackenzie.

L'analyse des EEMs par la méthode statistique PARAFAC a permis d'extraire 2 composés d'origine biologique (composés 1 et 3) et 1 composé d'origine terrestre (composé 2). Selon la classification de Coble (1996) et Coble et al. (1998), les composés 1, 2 et 3 correspondent respectivement au pic M « marine humic-like », au pic C « humic-like » et au pic T-B « protein-like ». L'intensité de fluorescence des pics M et C diminue fortement depuis la côte vers le large tandis que celle du pic T-B présente une distribution relativement homogène sur la zone d'étude. Cela illustre une source allochtone du pic C mais également pour le pic 1, bien que ce dernier soit censé appartenir à la matière fluorescente marine, et une source autochtone (glace de mer, upwellings) du pic T-B. Les travaux de Zhang et al. (2009) ont récemment mis en évidence la forte production du pic M et une augmentation de S_{CDOM} lors de la dégradation de macrophytes en milieu lacustre peu profond. Or le delta du Mackenzie en été est formé de nombreux lacs de faibles profondeurs drainés par le fleuve et dans lesquels siège une forte activité biologique riche en macrophytes (Tank et al., 2009 ; Squires et al., 2009). Ainsi le pic M observé à proximité de l'estuaire provient très

probablement de l'intense activité biologique de ces lacs. Cette hypothèse complète celles émises par Osburn et al. (2009) et Stedmon et al. (2011) et permet d'expliquer également les fortes valeurs de S_{CDOM} mesurées. De plus, ce fort apport de matière organique biologique allochtone par le Mackenzie peut être une piste d'étude pour expliquer la récente observation de Stedmon et al. (2011) concernant la plus grande proportion de CDOM biologique observée au niveau du Bassin Canadien comparé à celle du Bassin Eurasien. La figure V-3 synthétise les sources et puits majeurs de la CDOM du plateau Canadien.

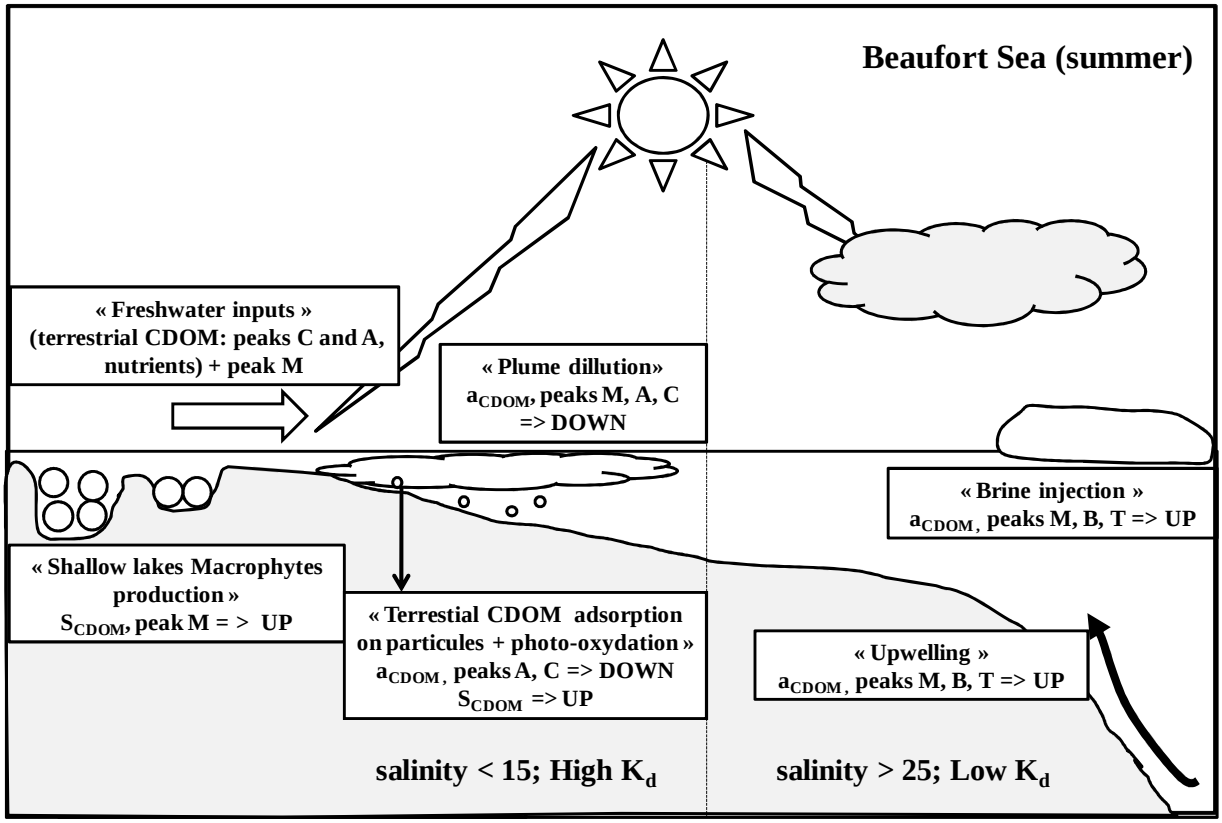

Figure V-3. *Facteurs biotiques et abiotiques contrôlant la dynamique de la CDOM en Mer de Beaufort.*

2. Perspectives

L'étude en Baie de Marseille a permis d'identifier les principaux processus pilotant la dynamique de la CDOM. Cependant, du fait de la disponibilité des moyens à la mer et des conditions météorologiques, notre étude s'est basée sur un nombre réduit d'observations qui ont sans doute sous-estimé l'impact de certains processus dans la dynamique de la CDOM, comme le brassage de la colonne d'eau, en faveur d'autres, comme les intrusions du panache du Rhône. Les études futures devront se baser sur un échantillonnage plus important afin d'élucider l'importance relative de chacun de ces processus et de déterminer leurs implications biogéochimiques respectives. De plus, un suivi à haute fréquence de l'éclairement de surface et dans l'eau ainsi que des paramètres bio-optiques (CDOM, chlorophylle, particules) et physiques (température salinité) permettrait d'avoir des observations sur la dynamique de la CDOM et des autres facteurs bio-optiques à plusieurs échelles : i) à l'échelle journalière, particulièrement intéressante lors des périodes de production biologique et de mélange (couplage production/photodégradation de la CDOM) ; ii) à l'échelle saisonnière, pertinente notamment pour estimer l'importance des processus de mélange et la fréquence des intrusions du panache du Rhône. L'acquisition de données radiométriques à haute fréquence, couplée à des mesures complémentaire d'IOP permettraient quand à elles de valider le rôle prépondérant de la CDOM sur l'atténuation de la lumière et d'établir un budget d'absorption spectral complet selon les saisons. De plus, la connaissance de la variabilité de l'éclairement au cours de la journée sur de longues périodes, couplée à la détermination de K_d, seraient utiles pour connaître les doses cumulées et intégrées dans la couche de mélange et ainsi estimer l'intensité des processus photochimiques et photobiologiques en Baie de Marseille.

Dans ce but, une ligne bio-optique a été déployée en Baie de Marseille par le LMGEM (Ligne SUNMED) dont les mesures ont débuté en avril 2011. Cette ligne permet l'acquisition de paramètres radiométriques (éclairement atmosphérique, éclairements descendant et ascendant), biogéochimiques (CDOM, chlorophylle, rétrodiffusion des particules) et physique (température et salinité). La fréquence d'acquisition, toutes les 20 minutes tout au long de l'année, permettra de mieux caractériser l'importance et l'impact de chaque processus intervenant dans la dynamique de la CDOM et mieux appréhender les relations IOP *versus* AOP en milieu côtier oligotrophe et influencé par la présence de CDOM bio-réfractaire en surface.

Nous avons mis en évidence, en mer de Beaufort, un fort impact des apports de CDOM issu de l'activité biologique en milieu lacustre (pic M provenant probablement des efflorescences de macrophytes). Une étude saisonnière serait nécessaire pour estimer l'importance de ces apports de matière dissoute issu de l'activité biologique au sein du pool total de CDOM atteignant la mer de Beaufort. Cela permettrait aussi de mieux appréhender l'impact possible de cette source de CDOM sur la signature autochtone de la DOM des eaux de surface en mer de Beaufort, et d'expliquer, pour partie, la forte signature biologique observée dans le Bassin canadien par rapport à la signature terrestre beaucoup plus marquée du bassin arctique Eurasien (Amon et Meon, 2004).

D'autre part, le Mackenzie est également un contributeur majeur en matière particulaire, il sera donc essentiel d'étudier les processus biotiques/abiotiques qui affectent la MOP lors de son intrusion dans les eaux marines. Des travaux préliminaires menés sur l'analyse de marqueurs lipidiques par Jean-François Rontani (LMGEM) sur des échantillons de matière en suspension rapportés de la mission MALINA ont été initiés et soulignent déjà l'importance des processus radicalaires (auto-oxydation lors de l'intrusion dans les eaux marines) et bactérien par rapport aux processus photo-oxydatifs dans la dégradation de la POM. Cependant des résultats sur les mêmes marqueurs dans les sédiments mettent en exergue des processus photo-oxydatifs intenses. Une étude temporelle couplée avec des expérimentations sous simulateur solaire permettront de comprendre l'importance relative des ces trois processus sur la dynamique de la POM en zone arctique.

CHAPITRE VI - REFERENCES

Amiotte-Suchet, P., Probst, J. L., Ludwig, W.: Worldwide distribution of continental rock lithology: implications for the atmospheric/soil CO_2 uptake by continental weathering and alkalinity river transport to the ocean, Global Biogeochem. Cy., 17, 1038, doi10.1029/2002GB001891, 2003.

Amon, R. M. W. and Benner, R.: Photochemical and microbial consumption of dissolved organic carbon and dissolved oxygen in the Amazon River system, Geochim. Cosmochim. Acta., 60, 1783-1792, 1996.

Amon, R. M. W. and Meon, B.: The biogeochemistry of dissolved organic matter and nutrients in two large Arctic estuaries and potential implications for our understanding of the Arctic Ocean system, Mar. Chem., 92, 311-330, doi:10.1016/j.marchem., 2004.

Arctic Climate Impact Assessment (ACIA): Arctic Climate Impact Assessment, 1042, Cambridge Univ. Press, Cambridge, U. K, 2005.

Arnoux-Chiavassa, S., Rey, V., Fraunié, P.: Modeling 3D Rhône river plume using a higher order advection scheme, Oceanol. Acta, 26, 299-309, 2003.

Arrigo, K. R. and Brown, C. W.: Impact of chromophoric dissolved organic matter on UV inhibition of primary productivity in the sea, Mar. Ecol. Prog. Ser., 140, 207-216, 1996.

Austin, R. W. and Petzold, T. J.: The determination of the diffuse attenuation coefficient of sea water using the coastal zone color scanner, Oceanography from Space, Plenum Press, 239-256, 1981.

Azam, F., Fenchel, T., Field, F. G., Gray J. S., MeyerReil, L-A and Thingstad F.: The ecological role of water column microbes in the sea, Mar. Ecol. Prog. Ser., 10, 257-263, 1983.

Babin, M., Stramski, D., Ferrari, G. M., Claustre, H., Bricaud, A., Obolensky, G., Hoepffner, N.: Variations in the light absorption coefficients of phytoplankton, non-algal particles, and dissolved organic matter in coastal waters around Europe, J. Geophys. Res., 108(C7), 3211, 2003.

Baker, K. S. and Smith, R. C.: Bio-optical classification and model of natural waters, Limnol. Oceanogr., 27, 500-509, 1982.

Barber, D. G., Hanesiak, J.: Meteorological forcing of sea ice concentrations in the Southern Beaufort Sea over the period 1978 to 2001, J. Geophys. Res., 109, C06014, doi: 10.1029/2003JC00202, 2004.

Bélanger, S., Xie, H., Krotkov, N., Larouche, P., Vincent, W. F., Babin, M.: Photomineralization of terrigenous dissolved organic matter in Arctic coastal waters from 1979 to 2003: Interannual variability and implications of climate change, Global Biogeochem. Cycles, 20, GB4005, doi: 10.1029/2006GB002708, 2006.

Belzile, C., Vincent, W. F., Kumagai, M.: Contribution of absorption and scattering to the attenuation of UV and photosynthetically available radiation in Lake Biwa, Limnol. Oceanogr., 47, 95-107, doi:10.4319/lo.2002.47.1.0095, 2002.

Belzile, C., Roesler, C. S., Christensen, J. P., Shakhova, N., Semiletov, I.: Fluorescence measured using the WETStar DOM fluorometer as a proxy for dissolved matter absorption, Estuar. Coast. Shelf Sci., 67, 441-449, 2006.

Benner, R., Pakulski, J. D., McCarthy, M., Hedges, J. L., Hatcher, R. G.: Bulk chemical characteristics of dissolved organic matter in the ocean, Science, 255, 1561-1564, 1992.

Bertilsson, S. and Tranvik, L. J.: Photochemically produced carboxylic acids as substrates for freshwater bactérioplancton, Limnol. Oceanogr., 43, 885-895, 1998.

Bishop, J. K. B. and Rossow, W. B.: Spatial and temporal variability of global surface solar irradiance, J. Geophys. Res., 96, 16839-16858, 1991.

Blough, N. V. and Zepp, R. G. (Eds.): Effects of solar ultraviolet radiation on biogeochemical dynamics in aquatic environments, Woods Hole Oceanographic Institution technical report WHOI-90-09, 1990.

Blough, N. V., Zafiriou, O. C., Bonilla, J.: Optical absorption spectra of water from the Orinoco River outflow: Terrestrial input of colored organic matter to the Caribbean, J. Geophys. Res., 98(C2), 2271-2278, 1993.

Blough, N. V. and Del Vecchio, R.: Chromophoric DOM in the Coastal Environment, in: Biogeochemistry of Marine Dissolved Organic Matter, Hansell, D. A., Carlson, C. A., Academic Press, San Diego, 509-540, 2002.

Boehme, J., Coble, P., Conmy, R. N., Stovall-Leonard, A.: Examining CDOM fluorescence variability using principal component analysis: seasonal and regional modeling of three-dimensional fluorescence in the Gulf of Mexico, Mar. Chem., 89, 3-14, 2004.

Bouillon, R.-C. and Miller, W. L.: Photodegradation of dimethyl sulfide (DMS) in natural waters: laboratory assessment of the nitrate-photolysis-induced DMS oxidation, Environ. Sci. Technol., 39, 9471-9477, 2005.

Brasseur, P., Beckers, J. M., Brankart, J. M., Schoenauen, R.: Seasonal temperature and salinity fields in the Mediterranean Sea: climatological analyses of a historical data set, Deep-Sea Res. I, 43, 159-192, 1996.

Bricaud, A., Morel, A., Prieur, L.: Absorption by dissolved organic matter in the sea (yellow substance) in the UV and visible domains, Limnol. Oceanogr., 26, 43-53, 1981.

Bricaud, A., Babin, M., Claustre, H., Ras, J., Tieche, F.: Light absorption properties and absorption budget of South East Pacific waters, Journal of Geophysical Research, Vol. 115, C08009, doi:10.1029/2009JC005517, 2010.

Broche, P., Devenon, J. L., Forget, P., De Maistre, J. C., Naudin, J. J., Cauwet, G.: Experimental study of the Rhone plume. Part I: physics and dynamics, Oceanol. Acta, 21, 725-738, 1998.

Brugger, A., Slezak, D., Obemosterer, I., Herndl, G. J.: Photolysis of dimethylsulfide in the northern Adriatic Sea: dependence on substrate concentration, irradiance and DOC concentration, Mar. Chem., 59, 321-331, 1998.

Bushaw, K. L., Zepp, R. G., Tarr, M. A., Schultz-Jander, D., Bourbonniere, R. A., Hodson R. E., Miller, W. L., Bronk, D. A., Moran, M. A.: Photochemical release of biologically available nitrogen from aquatic dissolved organic matter, Nature, 381, 404-407, 1996.

Cachorro, V. E., Toledano, C., Prats N., Sorribas, M., Mogo, S., Berjon, A., Torres, B., Rodrigo, R., de la Rosa, J., De Frutos, A. M.: The strongest desert dust intrusion mixed with smoke over the Iberian Peninsula registered with Sun photometry, J. Geophys. Res., 113, D14S04, doi:10.1029/2007JD009582, 2008.

Carder, K. L., Hawes, S. K., Baker, K. A., Smith, R. C, Steward, R. G., Mitchell, B. G.: Reflectance model for quantifying chlorophyll a in the presence of productivity degradation products, J. Geophys. Res., 96, 20599-20611, 1991.

Carder, K. L., Chen, F. R., Lee, Z. P., Hawes, S. K., Kamykowski, D.: Semi-analytic Moderate-Resolution Imaging Spectrometer algorithms for chlorophyll a and absorption with bio-optical domains based on nitrate-depletion temperatures, J. Geophys. Res., 104, 5403-5421, 1999.

Carmack, E. C. and Macdonald, R. W.: Oceanography of the Canadian shelf of the Beaufort Sea: a setting for marine life, Arctic 55 (Suppl. 1), 29-45, 2002.

Cho, B. C. and Azam, F.: Biogeochemical significance of bacterial biomass in the ocean's euphotic zone, Mar. Ecol. Prog. Ser., 63, 253-259, 1990.

Clark, C. D., O'Connor, A. P., Foley, D. M., de Bruyn, W. J.: A study of fecal coliform sources at a coastal site using colored dissolved organic matter (CDOM) as a water source tracer, Mar. Pollut. Bull., 54, 1507-1513, 2007.

Claustre, H. and Maritorena, S.: The many shades of ocean blue, Science, 302, 1514-1515, 2003.

Claustre, H., Morel, A., Hooker, S. B., Babin, M., Antoine, D., Oubelkheir, K., Bricaud, A., Leblanc, K., Quéguiner, B., Maritorena, S.: Is desert dust making oligotrophic waters greener? Geophys. Res. Lett., 29, 1469, 10.1029/2001GL014056, 2002.

Coble, P. G., Green, S. A., Blough, N. V., Gagosian, R. B.: Characterisation of dissolved organic matter in the Black Sea by fluorescence spectroscopy, Nature, 348, 432-435, 1990.

Coble, P. G., Schultz, C. A., Mopper, K.: Fluorescence contouring analysis of DOC intercalibration experiments samples: a comparison of techniques, Mar. Chem., 41, 173-178, 1993.

Coble, P. G.: Characterization of marine and terrestrial DOM in seawater using excitation emission matrix spectroscopy, Mar. Chem., 51, 325-346, 1996.

Coble, P. G., Del Castillo, C. E., Avril, B.: Distribution and optical properties of CDOM in the Arabian Sea during the 1995 southwest monsoon, Deep-Sea Res. Pt. II, 45, 2195-2223, 1998.

Coble, P. G.: Marine Optical Biogeochemistry - The Chemistry of Ocean Color, Chem. Rev., 107: 402-418, 2007.

Conde, D., Aubriot, L., Sonmiaruga, R.: Changes in UV penetration associated with marine intrusions and freshwater discharge in a shallow coastal lagoon of the Southern Atlantic Ocean, Mar. Ecol. Prog. Ser., 207, 19-31, 2000.

Cristofanelli P. and Bonasoni P.: Background ozone in the southern Europe and Mediterranean area: influence of the transport processes, Environ. Pollut., 157, 1399-1406, 2009.

Cruzado, A. and Velasquez Z. R.: Nutrients and phytoplankton in the Gulf of Lions, Cont. Shelf. Res., 10, 931-942, 1990.

D'Sa, E. J., Steward, R. G., Vodacek, A., Blough N. V., Phinney, D.: Determining optical absorption of colored dissolved organic matter in seawater with a liquid capillary waveguide, Limnol. Oceanogr., 44, 1142-1148, 1999.

Dafner, E. V., Sempéré, R., Bryden, H. L.: Total organic carbon distribution and budget through the Strait of Gibraltar in April 1998, Mar. Chem., 73, 233-252, 2001.

de Mora S., Demers, S., Vernet, M. (Eds.): The Effects of UV Radiation in the Marine Environment, Cambridge University Press, Cambridge, 2000.

De Souza-Sierra, M. M., Donard, O. F. X., Lamotte, M., Belin, C., Ewald, M.: Fluorescence spectroscopy of coastal and marine waters, Mar. Chem., 47, 127-144, 1994.

DeGrandpre, M. D., Vodacek, A., Nelson, R. K., Bruce, E. J., Blough, N. V.: Seasonal seawater optical properties of the U.S. Middle Atlantic Bight, J. Geophys. Res., 101, 22,722-22,736, 1996.

Del Castillo, C. E., Coble, P. G., Morell, J. M., Lopez, J. M., Corredor, J. E.: Analysis of the optical properties of the Orinoco River plume by absorption and fluorescence spectroscopy, Mar. Chem., 66, 35-51, 1999.

Del Castillo, C. E., Coble, P. G., Müller-Karger, F. E.: On the dispersal of riverine colored dissolved organic matter over the West Florida Shelf, Limnol. Oceanogr., 45, 1452-1432, 2000.

Del Vecchio, R. and Blough, N. V.: Photobleaching of chromophoric dissolved organic matter in natural waters: kinetics and modeling, Mar. Chem. 78, 231-253, 2002.

Dera, J. and Olszewski, J.: Experimental study of short-period irradiance fluctuations under an undulated sea surface, Oceanologia, 10, 27-49, 1978.

Dera, J. and Stramski, D.: Maximum effects of sunlight focusing under a wind-disturbed sea surface, Oceanologia, 23, 15-42, 1986.

Determann, S., Reuter, R., Wagner, P., Willkomm, R.: Fluorescence matter in the eastern Atlantic Ocean: part 1. Method of measurement and near-surface distribution, Deep-Sea Res., 41, 659-675, 1994.

Determann, S., Reuter, R., Willkomm, R.: Fluorescent matter in the eastern Atlantic Ocean: part 2. Vertical profiles and relation to water masses, Deep-Sea Res., 43, 345-360, 1996.

Determann, S., Lobbes, J. M., Reuter, R., Rullkötter, J.: Ultraviolet fluorescence excitation and emission spectroscopy of marine algae and bacteria, Mar. Chem., 62, 137-156, 1998.

Devenon, J. L., Broche, P., De Maistre, J. C., Forget, P., Gagelli, J., Rougier, G.: VHF radar measurements in the Rhone river plume, Water Pol. R., 28, 75-87, 1992.

Diaz, S. B., Morrow, J. H., Booth, C. R.: UV physics and optics, in: The effects of UV radiation in the marine environment, edited by S. de Mora, S. Demers and M. Vernet, Cambridge University Press, Cambridge, 35-71, 2000.

Diffey, B.: Climate change, ozone depletion and the impact on ultraviolet exposure of human skin, Phys. Med. Biol., 49, 1-11, 2004.

Doval, M. D., Pérez, F. F., Berdalet, E.: Dissolved and particulate organic carbon and nitrogen in the northwestern Mediterranean, Deep-Sea Res. Pt. I, 46, 511-527, 1999.

Duarte, C. M., Agustí, S., Kennedy, H., Vaqué, D.: The Mediterranean climate as a template for Mediterranean marine ecosystems: the example of the northeast littoral, Prog. Oceanogr., 44, 245-270, 1999.

Durrieu de Madron, X., Denis, L., Diaz, F., Garcia, N., Guieu, C., Grenz, C., Loyë-Pilot, M. D., Ludwig, W., Moutin, T., Raimbault, P., Ridame, C.: Nutrients and carbon budgets for the Gulf of Lion during the Moogli cruises, Oceanol. Acta, 26, 421-433, 2003.

Eichinger, M., Poggiale, J.C., Sempéré, R.: Toward a mechanistic approach to modeling bacterial DOC pathways: a review, Science, In Press.

Emmerton, C. A., Lesack, L. F. W., Marsh, P.: Lake abundance, potential water storage, and habitat distribution in the Mackenzie River Delta, western Canadian Arctic, Water Resour. Res., 43, W05419,doi:10.1029/2006WR005139, 2007.

Emmerton, C. A., Lesack, L. F. W., Vincent, W. F.: Mackenzie River nutrient delivery to the Arctic Ocean and effects of the Mackenzie Delta during open water conditions, Glob. Biogeochem. Cy. 22, GB1024. doi:10.1029/2006GB002856, 2008.

Estournel, C., Broche, P., Marsaleix, P., Devenon, J. L., Auclair, F., Vehil, R.: The Rhone River plume in unsteady conditions: numerical and experimental results, Estuar. Coast. Shelf Sci., 53, 25-38, 2001.

Faust, B. C.: A review of the photochemical redox reactions of iron (III) species in atmospheric, oceanic, and surface waters: influences on geochemical cycles and oxidant formation, in Aquatic and Surface Photochemistry, ACS Symposium Series, 1994.

Fellman, J. B., Spencer, R. G. M., Hernes, P. J., Edwards, R. T., D'Amore, D. V., Hood, E.: The impacts of glacier runoff on the biodegradability and biochemical composition of terrigenous dissolved organic matter in near-shore marine ecosystems, Mar. Chem. 121, 112-122, 2010.

Ferrari, G. M.: The relationship between chromophoric dissolved organic matter and dissolved organic carbon in the European Atlantic coastal area and in the West Mediterranean Sea (Gulf of Lions), Mar. Chem., 70, 339-357, 2000.

Figueroa F. L., Jiménez, C., Viñegla, B., Pérez-Rodríguez, E., Aguilera, J., Flores-Moya, A., Altamirano, M., Lebert, M., Häder, D-P.: Effects of solar UV radiation on photosynthesis of the marine angiosperm *Posidonia oceanica* from southern Spain, Mar. Ecol. Prog. Ser., 230, 59-70, 2002.

Foley, J. A.: Tipping points in the tundra. Science, 310, 627-628, 2005.

Fontana, C., Grenz, C., Pinazo, C., Marsaleix, P., Diaz, F.: Assimilation of SeaWiFS chlorophyll data into a 3D-coupled physical-biogeochemical model applied to a freshwater-influenced coastal zone, Cont. Shelf Res., 29, 1397-1409, 2009.

Fontana, C., Grenz, C., Pinazo, C., Marsaleix, P., Diaz, F.: Sequential assimilation of a year-long time-series of SeaWiFS chlorophyll data into a 3D biogeochemical model on the French Mediterranean coast, Cont. Shelf Res., 30, 1761-1771, 2010.

Forget, P., Devenon, J. L., De Maistre, J. C., Broche, P., Leveau, M.: VHF remote sensing for mapping river plume circulation, Geophys. Res. Lett., 17, 1097-1100, 1990.

Francko, D. A. and Heath, R. T.: UV-sensitive complex phosphorus: Association with dissolved humic material and iron in a bog lake, Limnol. Oceanogr., 27, 564-569, 1982.

Garcia-Pichel, F.: A model for internal self-shading in planktonic microorganisms and its implications for the usefulness of sunscreens, Limnol. Oceanogr., 39, 1704-1717, 1994.

Gareis, J. A. L., Lesack, L. F. W., Bothwell, M. L.: Attenuation of in situ UV radiation in Mackenzie Delta lakes with varying dissolved organic matter compositions, Water Resour. Res., 46, W09516, doi:10.1029/2009WR008747, 2010.

Garver, S. A. and Siegel, D. A.: Inherent optical property inversion of ocean color spectra and its biogeochemical interpretation. 1. Times series from the Sargasso Sea, J. Geophys. Res., 102, 18,607-18,625, 1997.

Gatti, J., Petrenko, A., Devenon, J. L., Leredde, Y, Ulses, C.: The Rhone river dilution zone present in the northeastern shelf of the Gulf of Lion in December 2003, Cont. Shelf Res., 26, 1794-1805, 2006.

Gohin, F., Druon, J. N., Lampert, L.: A five channel chlorophyll concentration algorithm applied to SeaWiFS data processed by SeaDAS in coastal waters, Int. J. Remote Sens., 23, 1639-1661, 2002.

Gohin, F., Loyer, S., Lunven, M., Labry, C., Froidefond, J. M., Delmas, D., Huret M., Herbland, A.: Satellite-derived parameters for biological modelling in coastal waters: Illustration over the eastern continental shelf of the Bay of Biscay, Remote Sens. Environ., 95, 29-46, 2005.

Gordeev, V. V.: Fluvial sediment flux to the Arctic Ocean, Geomorphology, 80, 94-104, doi:10.1016/j.geomorph.2005.09.008, 2006.

Gordon, H. R. and Morel, A.: Remote sensing of ocean color for interpretation of satellite visible imagery; A review, Springer verlag, 114 pp., 1983

Gordon, H. R., Brown, O. B., Ewans, R. H., Brown, J. W., Smith, R. C., Baker, K. S., and Clark, D. K.: A semi-analytical radiance model of ocean color, J. Geophys. Res., 93, 10 909-10 924, 1988.

Green, S. A. and Blough, N. V.: Optical absorption and fluorescence properties of chromophoric dissolved organic matter in natural waters, Limnol. Oceanogr., 39, 1903-1916, 1994.

Grzybowski, W.: Effect of short-term irradiation on the absorbance spectra of the chromophoric organic matter dissolved in the coastal and riverine waters, Chemosphere, 40, 1313-1318, 2000.

Guéguen, C., Guo, L., Tanaka, N.: Distribution and characteristics of colored dissolved organic matter in the western Arctic Ocean, Cont. Shelf Res. 25, 1195-1207, 2005.

Guéguen, C., Guo, L., Yamamoto-Kawai, M., Tanaka, N.: Colored dissolved organic matter dynamics across the shelf-basin interface in the western Arctic Ocean, J. Geophys. Res. 112, C05038 doi: 10.1029/2006JC003584, 2007.

Guo, L., Ping, C. L., Macdonald, R. W.: Mobilization pathways of organic carbon from permafrost to arctic rivers in a changing climate, Geophys. Res. Lett., 34, L13603, doi: 10.1029/2007GL030689, 2007.

Häder, D. P, Kumar, H. D., Smith, R. C, Worrest, R. C.: Effects on aquatic ecosystems, in Environmental effects of ozone depletion: 1998 assessment, J. Photochem. Photobiol., B: Biology, 46, 53-68, 1998.

Häder, D. P., Kumar, H. D., Smith, R. C., Worrest, R. C.: Aquatic ecosystems, effects of solar ultraviolet radiation and interactions with other climatic change factors, Photochem. Photobiol. Sci., 2, 39-50, 2003.

Häder, D. P., Kumar, H. D., Smith, R. C., Worrest, R. C.: Effects of solar UV radiation on aquatic ecosystems and interactions with climate change, Photochem. Photobiol., 6, 267-285, 2007.

Hargreaves, B. R.: Water column optics and penetration of UVR, in: UV Effects in aquatic organisms and ecosystems, edited by Helbling, E. W. and Zagarese, H., The Royal Society of Chemistry, Cambridge UK, 1, 59-108, 2003.

Hedges, J. I.: Global biogeochemical cycles: Progress and problems, Mar. Chem., 39, 67-93, 1992.

Hedges, J. I.: Why Dissolved Organics Matter? in: Biogeochemistry of Marine Dissolved Organic Matter, Hansell, D. A., Carlson, C. A., Academic Press, San Diego, 1-27, 2002.

Hedges, J.: Sedimentary organic matter preservation and atmospheric O_2 regulation, in: Chemistry of marine water and sediments, edited by A. Gianguzza, E. Pelizzeti, S. Sammartano, Springer, Berlin, 105-123, 2002.

Heisler, G. M., Grant, R. H., Gao, W.: Individual and scattered-tree influences on ultraviolet irradiance, Agric. Forest Meteorol., 120, 113-126, 2003.

Helbling, E. W., Buma, A. G. J., Karin De Boer, M., Villafañe, V. E.: In situ impact of solar ultraviolet radiation on photosynthesis and DNA in temperate marine phytoplankton, Mar. Ecol. Prog. Ser., 211, 43-49, 2001.

Helms, J. R., Stubbins, A., Ritchie, J. D., Minor, E. C., Kieber, D. J., Mopper, K.: Absorption spectral slopes and slope ratios as indicators of molecular weight, source, and photobleaching of chromophoric dissolved organic matter, Limnol. Oceanogr., 53, 955-969, 2008.

Herndl, G. J., Anieta, J. M., Obernosterer, I. and Reitner, B.: Role of ultraviolet radiation in the Mediterranean Sea: interaction between mixing processes, photochemistry and microbial activity, Rapp. Comm. tnt. Mer Midit., 35, 24-27, 1998.

Hofmann, D. J. and Deshler, T.: Stratospheric cloud observations during formation of the Antarctic ozone hole in 1989, J. Geophys. Res., 96, 2897-2912, 1991.

Hoge, F. E., Wright, C. W., Lyon, R. E., Swift, R. N., Yungel, J. K.: Satellite retrieval of inherent optical properties by inversion of an oceanic radiance model: A preliminary algorithm, Appl. Opt., 38, 495-504, 1999.

Hoge, F. E. and Lyon, P. E.: New tools for the study of oceanic eddies: Satellite derived inherent optical properties, Remote Sens. Environ., 95, 444-452, 2005.

Højerslev, N. K., Holt, N., Aarup, T.: Optical measurements in the North Sea-Baltic Sea transition zone. I. On the origin of the deep water in the Kattegat, Cont. Shelf Res., 16, 1329-1342, 1996.

Horvath, H., Alados Arboledas, L., Olmo, F. J., Jovanovic, O., Gangl, M., Kaller, W., Sanchez, C., Sauerzopf, H., Seidl, S.: Optical characteristics of the aerosol in Spain and Austria and its effect on radiative forcing, J. Geophys. Res., 107, 10.1029/2001JD001472, 2002.

Hudson N., Baker, A., Reynolds, D.: Fluorescence analysis of dissolved organic matter in natural, waste and polluted waters: a review, River Res. Appl., 23, 631-649, 2007.

Huguet, A., Vacher, L., Relexans, S., Saubusse, S., Froidefond, J. M., Parlanti, E.: Properties of fluorescent dissolved organic matter in the Gironde Estuary, Org. Geochem., 40, 706-719, 2009.

IPCC Climate Change: The Physical Science Basis, Contribution of Working Group I to the Fourth Assessment Report of the IPCC (Cambridge University Press, Cambridge), 7, 514-515, 2007.

Jeffrey, W. H., Kase, J. P., Wilhelm, S. W.: UV radiation effects on heterotrophic bacterioplankton and viruses in marine ecosystems, in: The Effects of UV Radiation on Marine Ecosystems, edited by S. J. De Mora, Demers S., Vernet, M., Cambridge, 206-236, 2000.

Jerlov, N. G.: Optical Oceanography, American Elsevier Publ. Co., Inc., New York, 1968.

Jiao, N., Herndl, G. J., et al.: Microbial production of recalcitrant dissolved organic matter: long-term carbon storage in the global ocean, Nat. Rev. Micro., 8, 593-599, 2010.

Jin, Z., Charlock, T., Smith Jr., W., Rutledge, K.: A parameterization of ocean surface albedo, Geophys. Res. Lett., 31, L22301, doi: 10.1029/2004GL021180, 2004.

Johannessen, S., Ziolkowski, L., Miller, W.: Comparison of photochemical production rates of carbon monoxide and dissolved inorganic carbon in the ocean, abstracts of Pacifichem 1, ENVR-332, 2000.

Johannessen, S. C. and Miller, W. L.: Quantum yield for the photochemical production of dissolved inorganic carbon in seawater, Mar. Chem., 76, 271-283, 2001.

Joux, F., Jeffrey, W. H., Abboudi, M., Neveux, J., Pujo-Pay, M., Oriol, L., Naudin, J. J.: Ultraviolet radiation in the Rhône river lenses of low-salinity and in marine waters of the Northwestern Mediterranean Sea: attenuation and effects on bacterial activities and net community production, Photochem. Photobiol., 85, 783-793, 2009.

Jumars, P. A., Penry, D. L., Baross, J. A., Perry. M. J., Frost, B. W.: Closing the microbial loop: dissolved carbon pathway to heterotrophic bacteria from incomplete ingestion, digestion and absorption in animals, Deep-sea Res., 36, 483-495, 1989.

Kahru, M. and Mitchell, B. G.: Seasonal and non seasonal variability of satellite-derived chlorophyll and dissolved organic matter concentration in the California Current, J. Geophys. Res., 106, 2517-2529, 2001.

Kalle, K.: Meereskundliche chemische Untersuchungen mit Hilfe des Zeisschen Pulfrich Photometers: Ann. Hydrogr. Berlin, 65, 276-282, 1937.

Kalle, K.: Fluoreszenz und Gelbstoff im Bottnischen und Finnischem Meerbusen: Dt. Hydrogr. Z., V., 2, 117-124, 1949.

Kerr, J. B. and McElroy, C. T.: Evidence for large upward trends of ultraviolet-B radiation linked to ozone depletion, Science, 262, 1032-1034, 1993.

Kerr, J., Seckmeyer, G., Bais, A. F., Bernhard, G., Blumthaler, M., Diaz, S. B., Krotkov, N. A., Lubin, D., McKenzie, R. L., Sabziparvar, A. A., Verdebout, J.: Surface Ultraviolet Radiation: Past and Future, Chap. 5, in WMO Report No. 47, Scientific Assessment of Ozone Depletion: 2002 Global Ozone Research and Monitoring Project, 2003.

Kieber, R. J., Zhou, X., Mopper, K.: Formation of carbonyl compounds from UV-induced photodegradation of humic substances in natural waters: Fate of riverine carbon in the sea, Limnol. Oceanogr., 35, 1503-1515, 1990.

Kieber, D. J., Jiao, J., Kiene, R. P., Bates, T. S.: Impact of dimethylsulfide photochemistry on methyl sulfur cycling in the equatorial Pacific Ocean, J. Geophys. Res., 101, 3715-3722, 1996.

Kieber, R. J., Hydro, L. H., Seaton, P. J.: Photooxydation of triglycerides and fatty acids in seawater: implication toward the formation of marine humic substances, Limnol. Oceanogr., 42, 1454-1462, 1997.

Kieber, R. J., Whitehead, R. F., Willey, J. D., Reid, S., Seaton, P. J.: Chromophoric dissolved organic matter (CDOM) in rainwater collected in southeastern North Carolina, USA, J. Atmos. Chem., 54, 21-41, 2006.

Kirk, J. T. O.: Light and Photosynthesis in Aquatic Ecosystems, Second ed. Cambridge University Press, Cambridge, 1994.

Kirk, J. T. O.: Optics of UV-B radiation in natural waters, Arch. Hydrobiol., 43, 1-16, 1994a.

Komada, T., Shofield, O. M. E., Reimers, C. E.: Fluorescence characteristics of organic matter released from coastal sediments during resuspension, Mar. Chem., 79, 81-97, 2002.

Kovac, N., Faganeli, J., Sket, B., Bajt, O.: Characterization of macro-aggregates and photodegradation of their water soluble fraction, Org. Geochem., 29, 1623-1634, 1998.

Kowalczuk, P., Cooper, W. J., Whithead, R. F., Durako, M. J., Sheldon, W.: Characterization of CDOM in an organic rich river and surrounding coastal ocean in the South Atlantic Bight, Aquat. Sci. 65, 381-398, 2003.

Kowalczuk, P., Ston-Egiert, J., Cooper, W. J., Whitehead, R. F. and Durako, M. J.: Characterization of chromophoric dissolved organic matter (CDOM) in the Baltic Sea by excitation emission matrix fluorescence spectroscopy, Mar. Chem., 96, 273-292, 2005.

Kuhn, P., Browman, H., McArthur, B., St. Pierre, J.-F.: Penetration of ultraviolet radiation in the waters of the estuary and Gulf of St. Lawrence, Limnol. Oceanogr., 44,710-716, 1999.

Kuwahara, V. S., Ogawa, H., Toda, T., Kikuchi, T., Taguchi, S.: Variability of bio-optical factors influencing the seasonal attenuation of ultraviolet radiation in temperate coastal waters of Japan, Photochem. Photobiol., 72, 193-199, 2000.

Lakowicz, J. R.: Principles of fluorescence spectroscopy. 3rd edition Springer Science; New York, 158-204, 2006.

Lawrence, D. M., Slater, A. G.: A projection of severe nearsurface permafrost degradation during the 21st century, Geophys. Res. Lett., 32, L24401, doi: 10.1029/2005GL025080, 2005.

Lee, Z. P. and Hu, C.: Global distribution of Case-1 waters: An analysis from SeaWiFS measurements, Remote Sens. Environ., 101, 270-276, 2006.

Lemée, R., Rochelle-Newall, E., Van Wambeke, F., Pizay, M. D., Rinaldi, P., Gatusso, J. P.: Seasonal variation of bacterial production, respiration and growth efficiency in the open NW Mediterranean Sea, Aquat. Microb. Ecol., 29, 227-237, 2002.

Lindell, M. J., Granéli, W., Tranvik, L. J.: Enhanced bacterial growth in response to photochemical transformation of dissolved organic matter, Limnol. Oceanogr., 40, 195-199, 1995.

Llabrés, M., Agustí, S., Alonso-Laita, P., Herndl, G. J.: *Synechococcus* and *Prochlorococcus* cell death induced by UV radiation and the penetration of lethal UVR in the Mediterranean Sea, Mar. Ecol. Prog. Ser., 399, 27-37, 2010.

Ludwig, W., Dumont, E., Meybeck, M., Heussner, S.: River discharges of water and nutrients to the Mediterranean and Black Sea: Major drivers for ecosystem changes during past and future decades?, Progr. Oceanogr., 80, 199-217, 2009.

Mague, T. H., Friberg, E., Hughes, D. J., Morris, I.: Extracellular release of carbon by marine phytoplankton: A physiological approach., Limnol. Oceanogr., 25, 262-279, 1980.

Mallet, M., Tulet, P., Serça, D., Solmon, F., Dubovik, O., Pelon, J., Pont, V., Thouron, O.: Impact of dust aerosols on the radiative budget, surface heat fluxes, heating rate profiles and convective activity over West Africa during March 2006, Atmos. Chem. Phys. Discuss., 9, 2967-3006, 2009.

Margat, J. (Ed.) : L'eau dans le basin de la méditerranéen, situation et prospective, in : les fascicules du Plan Bleu, vol. 6, Economica, Paris, 1992.

Markowicz, K. M., Flatau, P. J., Ramana, M. V., Crutzen, P. J., Ramanathan, V.: Absorbing Mediterranean aerosols lead to a large reduction in the solar radiation at the surface, Geophys. Res. Lett., 29, 1968, doi:10.1029/2002GL015767, 2002.

Mayer, L. M., Schick, L. L., Loder, T. C.: Dissolved protein fluorescence in two Maine estuaries, Mar. Chem., 64, 171-179, 1999.

McCallister, S. L., Bauer, J. E., Kelly, J., Ducklow, H. W.: Effects of sunlight on decomposition of estuarine dissolved organic C, N and P and bacterial metabolism, Aquat. Microb. Ecol., 40, 25-35, 2005.

McKenzie, R. L., Connor, B., Bodeker, G.: Increased summertime UV radiation in New Zealand in response to ozone loss, Science, 285, 1709-1711, 1999.

McKenzie, R. L., Björn, L. O., Bais, A., Ilyasd, M.: Changes in biologically active ultraviolet radiation reaching the Earth's surface, Photochem. Photobiol. Sci., 2, 5-15, 2003.

Miller, W. L. and Zepp, R. G.: Photochemical production of dissolved inorganic carbon from terrestrial organic matter: significance to the oceanic organic carbon cycle, Geophys. Res. Lett., 22, 417-420, 1995.

Miller, W. L. and Moran, M. A.: Interaction of photochemical and microbial processes in the degradation of refractory dissolved organic matter from a coastal environment, Limnol. Oceanogr., 42,1317-1324, 1997.

Milliman, J. D., Rutkowski, C., Meybeck, M.: River discharge to the sea: a global river index (GLORI). LOICZ Reports and Studies, LOICZ Core Project Office, Texel, Netherland Institute for Sea Research (NIOZ), 125, 1995.

Molina, M. J. and Rowland, F. S.: Stratospheric sink for chlorofluoromethanes: chlorine atom-catalyzed destruction of ozone, Nature, 249, 810, 1974.

Mopper, K. and Stahovec, W. L.: Photochemical production of low molecular weight carbonyl compounds in seawater, Mar. Chem, 19, 305-321, 1986.

Mopper, K., Zhou, X., Kieber, R. J., Kieber, D. J., Sikorski, R. J., Jones, R. D.: Photochemical degradation of dissolved organic carbon and its impact on the oceanic carbon cycle, Nature, 353, 60-62, 1991.

Mopper, K. and Schultz, C. A.: Fluorescence as a possible tool for studying the nature and water column distribution of DOC components, Mar. Chem., 41, 229-238, 1993.

Mopper, K. and Kieber, D. J.: Marine photochemistry and its impact on carbon cycling, in: The effects of UV radiation in the marine environment, edited by de Mora, S., Demers, S., Vernet, M., Cambridge University Press, Cambridge, 101-129, 2000.

Mopper, K. and Kieber, D. J.: Photochemistry and the cycling of carbon, sulphur, nitrogen and phosphorus, in: Biogeochemistry of marine dissolved organic matter, edited by Hansell D. A. and Carlson, C.A., Academic Press, San Diego, 455-507, 2002.

Moran, M. A., Sheldon Jr., W. M, Zepp, R. G.: Carbon loss and optical property change during long term photochemical and biological degradation of estuarine dissolved organic matter, Limnol. Oceanogr., 45, 1254-1264, 2000.

Morán, X. A. G. and Estrada, M.: Short-term variability of photosynthetic parameters and particulate and dissolved primary production in the Alboran Sea (SW Mediterranean), Mar. Ecol. Prog. Ser., 212, 53-67, 2001.

Moran, M. A. and Covert, J. S.: Photochemically mediated linkages between dissolved organic matter and bactérioplancton, in aquatic ecosystems: interactivity of dissolved organic matter, edited by Findlay, S. E. G. and Sinsabaugh, R. L., Academic Press, San Diego, 243-262, 2003.

Morel, A.: Optical modeling of the upper ocean in relation to its biogenous matter content, J. Geophys. Res., 93, 10749-10768, 1988.

Morel, A., Claustre, H., Antoine, D., Gentili, B.: Natural variability of bio-optical properties in Case 1 waters: Attenuation and reflectance within the visible and near-UV spectral domains as observed in South Pacific and Mediterranean waters, Biogeosciences, 4, 2147-2178, 2007a.

Morel, A., Gentili, B., Claustre, H., Babin, M., Bricaud, A., Ras, J., Tieche, F.: Optical properties of the "clearest" natural waters, Limnol. Oceanogr., 52, 217-229, 2007.

Morel, A. and Gentili, B.: The dissolved yellow substance and the shades of blue in the Mediterranean Sea, Biogeosciences, 6, 2625-2636, 2009.

Morris, D. P. and Hargreaves, B. R.: The role of photochemical degradation of dissolved organic carbon in regulation the UV transparency of three lakes on Pocono Plateau, Limnol. Oceanogr., 42, 239-249, 1997.

Moutin, T. and Raimbault, P.: Primary production, carbon export and nutrients availability in western and eastern Mediterranean Sea in early summer 1996, MATER Special Issue. J. Mar. Syst., 33-34, 273-288, 2002.

Mucci, A., Lansard, B., Miller, L. A., Papakyriakou, T. N.: CO_2 fluxes across the air-sea interface in the southeastern Beaufort Sea: Ice-free period, J. Geophys. Res., 115, C04003, doi: 10.1029/2009JC005330, 2010.

Mueller, J. L. and Austin, R. W.: Ocean Optics Protocols for SeaWiFS Validation, Revision 1. NASA Tech. Memo. 104566, Vol. 25, Hooker, S. B., Firestone, E. R. and Acker, J. G., Eds., NASA GSFC, Greenbelt, Maryland, 67, 1995.

Muller-Karger F. E., Varela, R., Thunell, R., Luerssen, R., Hu, C., Walsh, J. J.: The importance of continental margins in the global carbon cycle, Geophys. Res. Lett, 32, L01602. doi:10.1029/2004GL02134, 2005.

Myklestad, S. M.: Dissolved organic carbon from phytoplankton, in: The Handbook of Environmental Chemistry, Vol. 5, Part D, Mar. Chem., edited by: Wangersky, P., Springer-Verlag Berlin/Heidelberg, Heidelberg, 111-148, 2000.

Nagata, T.: Production mechanisms of Dissolved Organic Matter, in Microbial Ecology of the Oceans, edited by D. L. Kirchman, 5, 121-152, 2000.

Neale, P. J. and Kieber, D. J.: Assessing biological and chemical effects of UV in the marine environment: Spectral weighting functions, in: Causes and environmental implications of increased chromophoric DOM in the coastal environment UV-B radiation, edited by Hester, R. E. and Harrison, R. M., Issues in Environmental Science and Technology, The Royal Society of Chemistry, Cambridge, UK., 14, 61-83, 2000.

Nelson, J. R. and Guarda, S.: Particulate and dissolved spectral absorption on the continental shelf of the southeastern United States, J. Geophys. Res., 100, 8715-8732, 1995.

Nelson, N. B., Siegel, D. A., Michaels, A. R.: Seasonal dynamics of colored dissolved material in the Sargasso Sea, Deep-Sea Res., 145, 931-957, 1998.

Nelson, N. B. and Siegel, D. A.: Chromophoric DOM in the open ocean, in: Biogeochemistry of Marine Dissolved Organic Matter, edited by Hansell, D. A. and Carlson, C. A., Academic Press, San Diego, 547-578, 2002.

Nelson, N. B., Carlson, C. A., Steinberg, D. K.: Production of chromophoric dissolved organic matter by Sargasso Sea microbes, Mar. Chem., 89, 273-287, 2004.

Nelson, N. B., Siegel, D. A., Carlson, C. A., Swan, C., Smethie Jr, W. M., Khatiwala, S.: Hydrography of chromophoric dissolved organic matter in the North Atlantic, Deep-Sea Res. I, 54, 710-731, 2007.

Nieke, B., Reuter, R., Heuermann, R., Wang, H., Babin, M., and Therriault, J. C.: Light absorption and fluorescence properties of chromophoric dissolved organic matter (CDOM) in the St. Lawrence Estuary (Case 2 waters), Cont. Shelf Res., 17, 235-252, 1997.

Nieto-Cid, M., Alvarez-Salgado, X. A., Perez, F.: Microbial and photochemical reactivity of fluorecent dissolved organic matter in a coastal upwelling system, Limnol. Oceanogr., 51, 1391-1400, 2006.

Niewiadomska, K., Claustre, H., Prieur, L., D'Ortenzio, F.: Meso and submesoscale physical-biogeochemical coupling across the Ligurian current (NW Mediterranean) using a bio-optical glider, Limnol. Oceanogr., 53, 2210-2225, 2008.

Obernosterer, I., Reitner, B., Herndl, G. J.: Contrasting effects of solar radiation on dissolved organic matter and its bioavailability to marine bactérioplancton, Limnol. Oceanogr., 44, 1645-1654, 1999a.

Obernosterer, I., Kraay, G., de Ranitz E., and Hemdl, G. J.: Concentrations of low molecular weight carboxylic acids and carbonyl compounds in the Aegean Sea (Eastem Mediterranean) and the turn-over of pyruvate, Aquat. Microb. Ecol., 20, 147-156, 1999b.

Obernosterer, I., Sempéré, R., Herndl, G. J.: Ultraviolet radiation induces reversal of the bioavailability of DOM to marine bactérioplancton, Aquat. Microb. Ecol., 24, 61-68, 2001b.

Obernosterer, I. and Benner, R.: Competition between biological and photochemical processes in the mineralization of dissolved organic carbon, Limnol. Oceanogr, 49, 117-124, 2004.

Ohno, T.: Fluorescence Inner-Filtering Correction for Determining the Humification Index of Dissolved Organic matter, Environ. Sci. Technol, 36, 742-746, 2002.

Opsahl, S. and Benner, R.: Distribution and cycling of terrigenous dissolved organic matter in the ocean, Nature, 386, 480-482, 1997.

Opsahl, S., Benner, R., Amon, R.: Major flux of terrigenous dissolved organic matter through the Arctic Ocean, Limnol. Oceanogr., 44, 2017-2023, 1999.

O'Reilly, J. E., Maritorena, S., Mitchell. B. G., Siegel, D. A., Carder, K. L., Garver, S. A., Kahru, M., and McClain, C.: Ocean color chlorophyll algorithms for SeaWIFS, J. Geophys. Res., 103, 24937-24953, 1998.

Osburn, C. L., O'Sullivan, D. W., Boyd, T. J.: Increases in the longwave photobleaching of chromophoric dissolved organic matter in coastal waters, Limnol. Oceanogr., 54, 145- 159, 2009.

Para, J., Coble, P. G., Charrière, B., Tedetti, M., Fontana, C., Sempéré, R.: Fluorescence and absorption properties of chromophoric dissolved organic matter (CDOM) in coastal surface waters of the northwestern Mediterranean Sea, influence of the Rhone River, Biogeosciences, 7, 4083-4103, 2010.

Parlanti, E., Wörz, K., Geoffroy, L. Lamotte, M.: Dissolved organic matter fluorescence spectroscopy as a tool to estimate biological activity in a coastal zone submitted to anthropogenic inputs, Org. Geochem., 31, 1765-1781, 2000.

Peterson, B. J., Holmes, R. M., McClelland, J. W., Vorosmarty, C. J., Lammers, R. B., Shiklomanov, A. I., Rahmstorf, S.: Increasing River Discharge to the Arctic Ocean, Science, 298, 2171-2173, 2002.

Pujo-Pay, M., Conan, P., Joux, F., Oriol, L., Naudin, J. J., Cauwet, G.: Impact of phytoplankton and bacterial production on nutrient and DOM uptake in the Rhône River plume (NW Mediterranean), Mar. Ecol-Prog. Ser., 315, 43-54, 2006.

Rachold, V., Eicken, H., Gordeev, V. V., Grigoriev, M. N., Hubberten, H. W., Lisitzin, A. P., Shevchenko, V. P., Schirrmeister, L.: Modern terrigenous organic carbon input to the Arctic Ocean, in: The Organic Carbon Cycle in the Arctic Ocean, edited by Stein, R. and Macdonald, R. W., Springer-Verlag, Berlin, 33-56, 2004.

Raymond, P. A., McClelland, J. W., Holmes, R. M., Zhulidov, A. V.: Flux and age of dissolved organic carbon exported to the Arctic Ocean: A carbon isotopic study of the five largest Arctic rivers, Global Biogeochem. Cy., 21, GB4011, doi: 10.1029/2007GB002934, 2007.

Reche, I., Pace, M. L., Cole, J. J.: Modeled effects of dissolved organic carbon and solar spectra on photobleaching in lake ecosystems, Ecosystems 3, 419-432, doi: 10.1007/s100210000038, 2000.

Reffray, G., Fraunié , P., Marsaleix, P.: Secondary flows induced by wind forcing in the Rhône region of freshwater influence, Ocean Dynam., 54, 179-196, 2004.

Retamal, L., Vincent, W. F., Martineau, C., Osburn, C. L.: Comparison of the optical properties of dissolved organic matter in two river influenced coastal regions of the Canadian Arctic, Estuar. Coast. Shelf Sci., 72, 261-272, 2007.

Retamal, L., Bonilla, S., Vincent, W. F.: Optical gradients and phytoplankton production in the Mackenzie River and the coastal Beaufort Sea, Polar Biol., 31, 363-379, 2008.

Rich, J. H., Ducklow, H. W., Kirchman, D. L.: Concentration and uptake of neutral monosaccharides along 140°W in the equatorial Pacific: contribution of glucose to heterotrophic bacterial activity and the DOM flux, Limnol. Oceanogr., 41, 595-604, 1996.

Rochelle-Newall, E. J., Fisher, T. R.: Production of chromophoric dissolved organic matter in marine and estuarine environments: role of phytoplankton, Mar. Chem., 77, 7-21, 2002.

Romera-Castillo, C., Sarmento, H., Alvarez-Salgado, X. A., Gasol, J. M., Marrasé, C.: Production of chromophoric dissolved organic matter by marine phytoplankton, Limnol. Oceanogr., 55, 446-454, 2010.

Ruiz, S., Gomis, D., Sotillo, M. G., Josey, S. A.: Characterization of surface heat fuxes in the Mediterranean Sea from a 44-year high-resolution atmospheric data set, Global Planet Change, 63, 258-274, 2008.

Saha, A., Mallet, M., Roger, J. C., Dubuisson, P., Piazzola, J., Despiau, S.: One year measurements of aerosol optical properties over an urban coastal site: Effect on local direct radiative forcing, Atmos. Res., 90, 195-202, doi:10.1016/j.atmosres.2008.02.003, 2008.

Santinelli, C., Gasparini, G. P., Nannicini, L., Seritti, A.: Vertical distribution of dissolved organic carbon (DOC) in the Western Mediterranean Sea, Deep-Sea Res. I, 49, 2203-2219, 2002.

Schenck, H.: On the focusing of sunlight by ocean waves, J. Opt. Soc. Am., 47, 653-657, 1957.

Seckmeyer, G., Pissulla, D., Glandorf, M., Henriques, D., Johnsen, B., Webb, A., Siani, A. M., Bais, A., Kjeldstad, B., Brogniez, C., Lenoble, J., Gardiner, B., Kirsch, P., Koskela, T., Kaurola, J., Uhlmann, B., Slaper, H., den Outer, P., Janouch, M., Werle, P., Gröbner, J., Mayer, B., de la Casiniere, A., Simic, S., Carvalho, F.: Variability of UV Irradiance in Europe, Photochem. Photobiol, 84, 172-179, 2008.

Sempéré, R., Charrière, B., Cauwet, G., Van-Wambeke, F.: Carbon inputs of the Rhône River to the Mediterranean Sea: Biogeochemical implications, Global Biogeochem. Cy., 14, 669-681, 2000.

Sempéré, R., Yoro, S. C., Van wambeke, F., Charrière, B.: Microbial decomposition of large organic particles in northwestern Mediterranean sea, Mar. Ecol. Progr. Ser., 5, 198, 61-72, 2000.

Sempéré, R., Panagiotopoulos, C., Lafont, R., Marroni, B., Van Wambeke, F.: Total organic carbon dynamics in the Aegean Sea, J. Marine Syst., 33-34, 355-364, 2002.

Seritti, A., Manca, B. B., Santinelli, C., Murru, E., Boldrin, A., Nannicini, L.: Relationships between hydrological properties and dissolved organic carbon (DOC) in the Ionian Sea (winter 1999), J. Geophys. Res. Oceans, 108, 8112, doi: 10.1029/2002JC001345, 2003.

Seritti, A., Russo, D., Nannicini, L., Del Vecchio, R.: DOC, absorption and fluorescence properties of estuarine and coastal waters of the northern Tyrrhenian Sea, Chem. Spec. Bioavailab., 10, 95-105, 1998.

Shifrin, K. S.: Physical Optics of Ocean Water, American Institute of Physics, New York, 1988.

Siegel, D. A., Michaels, A. R, Sorensen, J., O'Brien, M. C, Hanmier, M. A.: Seasonal variability of light availability and its utilization in the Sargasso Sea, J. Geophys. Res., 100, 8695-8713, 1995.

Siegel, D. A. and Michaels, A. F.: Quantification of non-algal light attenuation in the Sargasso Sea: Implications for biogeochemistry and remote sensing, Deep-Sea Res. II, 43, 321-345, 1996.

Siegel, D. A., Maritorena, S., Nelson, N. B., Hansell, D. A., Lorenzi-Kayser, M.: Global distribution and dynamics of colored dissolved and detrital organic materials, J. Geophys. Res., 107 (C12), 3228, 2002.

Siegel, D. A., Maritorena, S., Nelson, N. B., Behrenfeld, M. J.: Independence and interdependencies of global ocean color properties; Reassessing the bio-optical assumption, J. Geophys. Res., 110, C07011, doi:10.1029/2004JC002527, 2005.

Sierra, M. M. D., Donard, O. F. X., Lamotte, M.: Behaviour of dissolved fluorescent organic matter during estuarine mixing, Mar. Chem., 58, 51-58, 1997.

Sierra M. M. D., Giovanela M., Parlanti E., Soriano-Sierra E. J.: Fluorescence fingerprint of fulvic and humic acids from varied origins as viewed by single-scan and excitation/emission matrix techniques, Chemosphere, 58, 715-733, 2005.

Sinha, R. P. and Häder, D. P.: UV-induced DNA damage and repair: a review, Photochem. Photobiol. Sci, 1, 225-236, 2002.

Smith, R. C., Baker, K. S.: Optical classification of natural waters, Limnol. Oceanogr., 23, 260-267, 1978.

Smith, R. C., Baker, K. S.: Penetration of UV-B and biologically effective dose-rates in natural waters, J. Photochem. Photobiol., 29, 311-323, 1979.

Smith, R. C. and Baker, K. S.: The analysis of ocean optical data. Proceedings of the society of photo-optical instrumentation engineers, Ocean Optics VII, 489, 119-126, 1984.

Smith, R. C., Prezelin, B. B., Baker, K. S., Bidigare, R. R., Boucher, N. P., Coley, T., Karentz, D., MacIntyre, S., Matlick, H. A., Menzies, D., Ondrusek, M., Wan, Z., Waters, K. J.: Ozone

depletion: ultraviolet radiation and phytoplankton biology in Antarctic waters, Science, 255, 952-959, 1992.

Smith, S. V. and Hollibaugh, J. T.: Coastal metabolism and the oceanic organic carbon balance, *Rev. Geophys.*, 31, 75-89, 1993.

Sohrin, R. and Sempéré, R.: Seasonal variation in total organic carbon in the Northeast Atlantic in 2000–2001, J. Geophys. Res., 110, C10S90, doi: 10.1029/2004JC002731, 2005.

Sommaruga, R., Obemosterer, I., Herndl, G. J., Psenner, R.: Inhibitory effect of solar radiation on thymidine and leucine incorporation by freshwater and marine bactérioplancton, Appl. Environ. Microbiol., 63, 4178-4184, 1997.

Squires, M. M., Lesack, L. F. W., Hecky, R. E., Guildford, S. J., Ramlal, P., Higgins, S. N.: Primary production and carbon dioxide metabolic balance of a lake-rich arctic river floodplain: partitioning of phytoplankton, epipelon, macrophyte, and epiphyton production among lakes of the Mackenzie delta, Ecosystems, doi: 10.1007/s10021-009-9263-3, 2009.

Stedmon, C. A., Markager, S., Kaas, H.: Optical properties and signatures of chromophoric dissolved organic matter (CDOM) in Danish coastal waters, Estuar. Coast. Shelf Sci., 51, 267-278, 2000.

Stedmon, C. A., Markager, S., Bro, R.: Tracing dissolved organic matter in aquatic environments using a new approach to fluorescence spectroscopy, Mar. Chem., 82, 239-254, doi: 10.1016/S0304-4203(03)00072-0, 2003.

Stedmon, C. A. and Markager, S.: Tracing the production and degradation of autochthonous fractions of dissolved organic matter using fluorescence analysis, Limnol. Oceanogr., 50, 1415-1426, 2005.

Stedmon, C. A., Thomas, D. N., Granskog, M., Kaartokallio, H., Papadimitriou, S., Kuosa, H.: Characteristics of dissolved organic matter in Baltic coastal sea ice: allochthonous or autochthonous origins?, Environ. Sci. Technol., 41, 7273-7279, 2007.

Stedmon, C. A. and Bro, R.: Characterizing dissolved organic matter fluorescence with parallel factor analysis: A tutorial, Limnol. Oceanogr. Methods, 6, 572-579, 2008.

Stedmon, C. A., Amon, R. M. W., Rinehart, A. J., Walker, S. A.: The supply and characteristics of colored dissolved organic matter (CDOM) in the Arctic Ocean: Pan Arctic trends and differences, Mar. Chem., 124, 108-118, 2011.

Steinberg, D. K., Nelson, N. B., Carlson, C. A., Prusak, A. C.: Production of chromophoric dissolved organic matter (CDOM) in the open ocean by zooplankton and the colonial cyanobacterium *Trichodesmium* spp., Mar. Ecol. Prog. Ser., 267, 45-56, 2004.

Stramska, M. and Dickey, T. D.: Short-term variability of the under-water light field in the oligotrophic ocean in response to surface waves and clouds, Deep Sea Res. I, 45, 1393-1410, 1998.

Tarnocai, C., Canadell, J. G., Schuur, E. A. G., Kuhry, P., Mazhitova, G., Zimov, S.: Soil organic carbon pools in the northern circumpolar permafrost region, Glob. Biogeochem. Cy., 23, GB2023, doi: 10.1029/2008GB003327, 2009.

Tedetti, M.: Impact du rayonnement UV sur la phototransformation de la matière organique dissoute en milieu marin, PhD, 2006.

Tedetti, M. and Sempéré, R.: Penetration of UV radiation in the marine environment: A review, Photochem. Photobiol., 82, 389-397, 2006.

Tedetti, M., Sempéré, R., Vasilkov, A., Charrière, B., Nérini, D., Miller, W. L., Kawamura, K., Raimbault, P.: High penetration of ultraviolet radiation in the southeast Pacific waters, Geophys. Res. Lett., 34, L12610, doi:10.1029/2007GL029823, 2007.

Tedetti, M., Joux, F., Charrière, B., Mopper, K., Sempéré, R.: Contrasting effects of solar radiation and nitrates on the bioavailability of DOM to marine bacteria, J. Photochem. Photobiol., A: Chemistry (201), 243-247, 2009.

Tedetti, M., Guigue, C., Goutx, M.: Utilization of a submersible UV fluorometer for monitoring anthropogenic inputs in the Mediterranean coastal waters, Mar. Pollut. Bull., 60, 350-362, 2010.

The MERMEX group, Marine Ecosystems Responses to climatic and anthropogenic forcings in the Mediterranean, Progr. Oceanogr., in press.

Tranvik, L. J.: Microbial transformation of labile dissolved organic matter into humic-like matter in seawater, FEMS Microbiol. Ecol., 12, 177-183, 1993.

Tranvik, L. J., Bertilsson, S.: Contrasting effects of solar UV radiation on dissolved organic sources for bacterial growth, Ecol. Lett., 4, 458-463, 2001.

Twardowski, M. S., Boss, E., Sullivan, J. M., Donaghay, P. L.: Modeling the spectral shape of absorption by chromophoric dissolved organic matter, Mar. Chem., 89, 69-88, doi: 10.1016/j.marchem. 2004.02.008, 2004.

Uher, G. and Andreae, M. O.: Photochemical production of carbonyl sulfide in North Sea water: a process study, Limnol. Oceanogr., 42, 432-442, 1997.

Vähätalo, A. V. and Wetzel, R. G.: Photochemical and microbial decomposition of chromophoric dissolved organic matter during long (months-years) exposures, Mar. Chem., 89, 313-326, 2004.

Van Wambeke, F., Tedetti, M., Duhamel, S., Sempéré, R.: Diel variability of heterotrophic bacterial production and underwater UV doses in the eastern South Pacific, Mar. Ecol. Progr. Ser., 387, 97-108, 2009.

Vantrepotte, V. and Mélin, F.: UV penetration in the water column, Rep. EUR 22217 EN, 67 pp., Dir. Gen. Joint Res. Cent., Inst. for Environ. and Sustainability, Luxembourg, 2006.

Vasilkov, A., Krotkov, N., Herman, J., Mc Clain, C., Arrigo, K., Robinson, W.: Global mapping of underwater UV irradiances and DNA-weighted exposures using Total Ozone Mapping Spectrometer and Sea-viewing Wide Field-of-view Sensor data products, J. Geophys. Res., 106, 27205-27219, 2001.

Vasseur, C., Mostajir, B., Nozais, C., Denis, M., Fouilland, E., Klein, B., Demers, S.: Effects of bio-optical factors on the attenuation of ultraviolet and photosynthetically available radiation in the North Water Polynya, northern Baffin Bay: ecological implications, *Marine Ecology Progress Series*, 252: 1-13, 2003.

Vignudelli, S., Santinelli, C., Murru, E., Nannicini, L., Seritti, A.: Distributions of dissolved organic carbon (DOC) and chromophoric dissolved organic matter (CDOM) in coastal waters of the northern Tyrrhenian Sea (Italy), Estuar. Coast. Shelf Sci., 60, 133-149, 2004.

Villafane, V. E., Janknegt, P. J., de Graaff, M., Visser, J. W., van de Poll, W. H., Buma, A. G. J., Helbling, E. W.: UVR-induced photoinhibition of summer marine phytoplankton communities from Patagonia, Mar. Biol., 154, 1021-1029, 2008.

Vincent, W. F. and Roy, S.: Solar ultraviolet-B radiation and aquatic primary production: damage, protection and recovery, Environmental Review, 1, 1-12, 1993.

Vincent, W. F. and Neale, P. J.: Mechanisms of UV damage to aquatic organisms, in: The effects of UV radiation in the marine environment, edited by de Mora, S., Demers, S., Vernet, M., Cambridge University Press, New York, 149-176, 2000.

Vodacek, A., Hoge, R, Swift, R. N., Yungel, J. K., Peltzer, E. T., Blough, N. V.: The use of in situ and airborne fluorescence measurements to determine UV absorption coefficients and DOC concentrations in surface waters, Limnol. Oceanogr., 40, 411-415, 1995.

Vodacek, A., Blough, N. V., DeGrandpre, M. D., Peltzer, E. T., Nelson, R. K.: Seasonal variation of CDOM and DOC in the Middle Atlantic Bight: Terrestrial inputs and photooxidation, Limnol. Oceanogr., 42, 674-686, 1997.

Walker, S. A., Amon, R. M. W., Stedmon, C., Duan, S., Louchouarn, P.: The use of PARAFAC modeling to trace terrestrial dissolved organic matter and fingerprint water masses in coastal Canadian Arctic surface waters, J. Geophys. Res., 114, G00F06, doi: 10.1029/2009JG000990, 2009.

Walvoord, M. A. and Striegl, R. G.: Increased groundwater to stream discharge from permafrost thawing in the Yukon River basin: potential impacts on lateral export of carbon and nitrogen, Geophys. Res. Lett., 34, L12402. doi: 10.1029/2007GL030216, 2007.

Wetzel, R. G., Hatcher, P. G. Bianchi, T. S.: Natural photolysis by ultraviolet irradiance of recalcitrant dissolved organic matter to simple substrates for rapid bacterial metabolism, Limnol. Oceanogr., 40, 1369-1380, 1995.

Whitehead, R. F., de Mora, S. J., Demers, S.: Enhanced UV radiation - a new problem for the marine environment, in: The effects of UV radiation in the marine environment, edited by S. de Mora, S. Demers and M. Vernet, Cambridge University Press, Cambridge, 1-34, 2000.

Williamson, C. E., Stemberger, R. S., Morris, D. P, Frost, T. M., Paulsen, S. G.: Ultra-violet radiation in North American lakes: Attenuation estimates from DOC measurements and implications for plankton communities, Limnol. Oceanogr., 41, 1024-1034, 1996.

WMO, 2003: World Meteorological Organization, Scientific Assessment of Ozone Depletion: 2002, Global Ozone Research and Monitoring Project, Report No47, Geneva, Switzerland.

WMO, 2006: World Meteorological Organization, Antartic Ozone Bulletin 2005, No.8, Winter/sping summary.

Wollast R.: Evaluation and comparison of the global carbon cycle in the coastal zone and in the open ocean Brink K.H, Robinson A.R, in The sea, vol. 10 New York*:* Wiley, 213-252, 1998.

Yamashita, Y. and Tanoue, E.: Chemical characterization of protein-like fluorophores in DOM in relation to aromatic amino acids, Mar. Chem., 82, 255-271, 2003.

Yamashita, Y. and Tanoue, E.: In situ production of chromophoric dissolved organic matter in coastal environments, Geophys. Res. Lett., 31, L14302/1-L14302/4, 2004.

Yocis, B. H., Kieber, D. J., Mopper, K.: Photochemical production of hydrogen peroxide in Antarctic Waters, Deep-Sea Res. I., 47, 1077-1099, 2000.

Zaneveld, R. J. V., Boss, E., Barnard, A.: Influence of surface waves on measured and modeled irradiance profiles, Appl. Opt., 40, 1442-1449, 2001.

Zepp, R. G.: Environmental photoprocesses involving natural organic matter, in: Humic Substances and their Role in the Environment, edited by Frimmel F. H. and Christman R. F., John Wiley & Sons, New York, 193-214, 1988.

Zepp, R. G., Callaghan, T. V., Erickson, D. J.: Effects of enhanced solar ultraviolet radiation on biogeochemical cycles, Photochem. Photobiol., B 46, 69-82, 1998.

Zepp, R. G., Shank, G. C., Stabenau, E., Patterson, K. W., Cyterski, M., Fisher, W., Bartels, E., Anderson, S. L.: Spatial and temporal variability of solar ultraviolet exposure of coral assemblages in the Florida Keys: importance of colored dissolved organic matter, Limnol Oceanogr., 53, 1909-1922, 2008.

Zhang, Y., van Dijk, M. A., Liu, M., Zhu, G., Qin, B.: The contribution of phytoplankton degradation to chromophoric dissolved organic matter (CDOM) in eutrophic shallow lakes: field and experimental evidence, Water. Res., 43, 4685-4697, 2009.

Zsolnay, A., Baigar, E., Jimenez, M., Steinweg, B., Saccomandi, F.: Differentiating with fluorescence spectroscopy the sources of dissolved organic matter in soils subjected to drying, Chemosphere, 38, 45-50, 1999.

CHAPITRE VII - ANNEXES

ANNEXE 1

Principe de fonctionnement du spectrophotomètre multi-trajets optiques « Ultrapath UV-visible (WPI Inc.) »

Le système Ultrapath présente 4 trajets optiques sélectionnables (2, 10, 50 et 200 cm) contenus dans une cellule de mesure unique (Teflon AF-2400 Type I cell, DuPont Fluoroproducts, DE, USA). La source lumineuse provient d'une lampe deutérium/halogène (D2H, WPI) et est acheminée par une fibre optique jusque dans la cellule de mesure. La lumière sortante est collectée par une fibre optique reliée à une barrette de photodiodes (PDA) au niveau du spectromètre. L'échantillon est introduit dans la cellule au moyen d'une pompe péristaltique (voir figure ci-dessous, Miller et al., 2002).

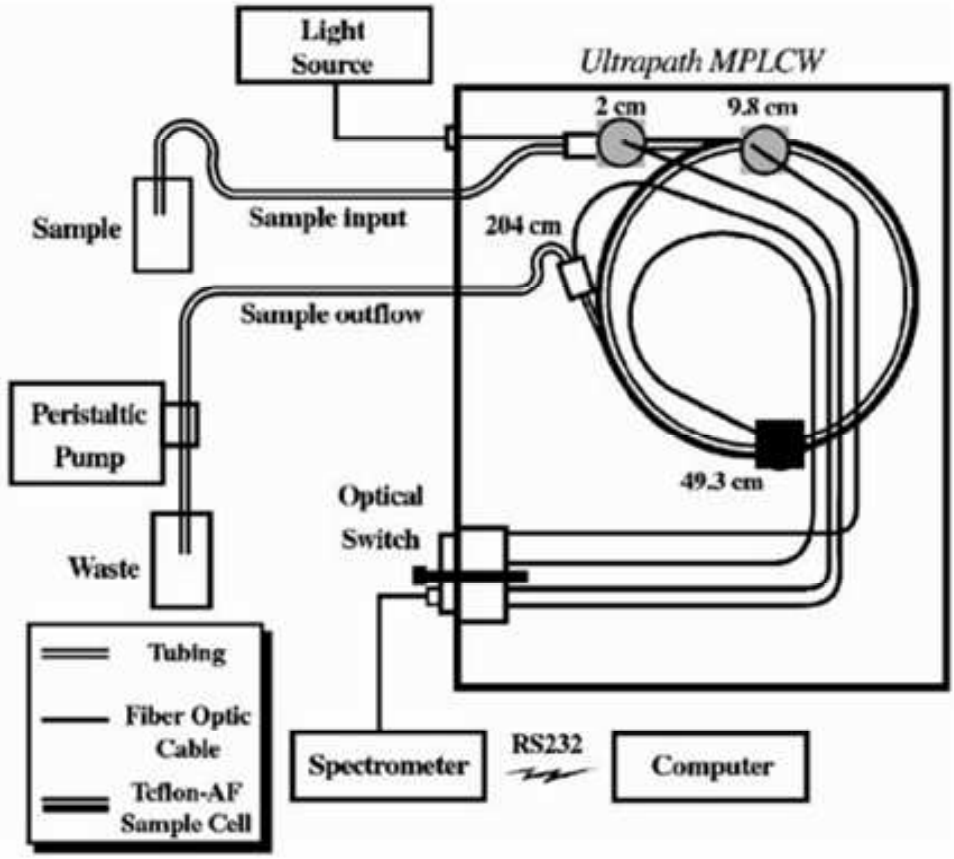

Source: Richard L. Miller, Mathias Belz, Carlos Del Castillo, Rick Trzaska, *"Determining CDOM Absorption Spectra in Diverse Coastal Environments Using a Multiple Pathlength, Liquid Core Waveguide System", Continental Shelf Research, July 2002, 22:9, p 1301-1310.*

ANNEXE 2

Principe de fonctionnement du spectrofluorimètre « HITACHI F-7000 »

La lumière émise par la lampe à xénon est condensée sur la fente d'entrée (S1) du monochromateur d'excitation par des lentilles (L1 et L2). La lumière d'excitation (λ_{Ex}) ressort par la fente (S2) et est réfléchie par le miroir concave M1 en direction du splitter (BS). Au niveau de ce dernier la lumière se divise en deux faisceaux dont une part va vers un détecteur qui en mesure l'intensité et l'autre part est condensée au niveau de la cuve de mesure par la lentille L3. La fluorescence émise par l'échantillon entre dans le monochromateur d'émission par la fente S3. La direction d'observation de la fluorescence est perpendiculaire au faisceau d'excitation car dans cette direction la diffusion moléculaire de la matrice est minimale. La lumière d'émission (λ_{Em}) ressort par la fente S4 et est réfléchie par le miroir concave M2 en direction du tube photomultiplicateur (PMT) qui va amplifier et mesurer le signal d'émission.

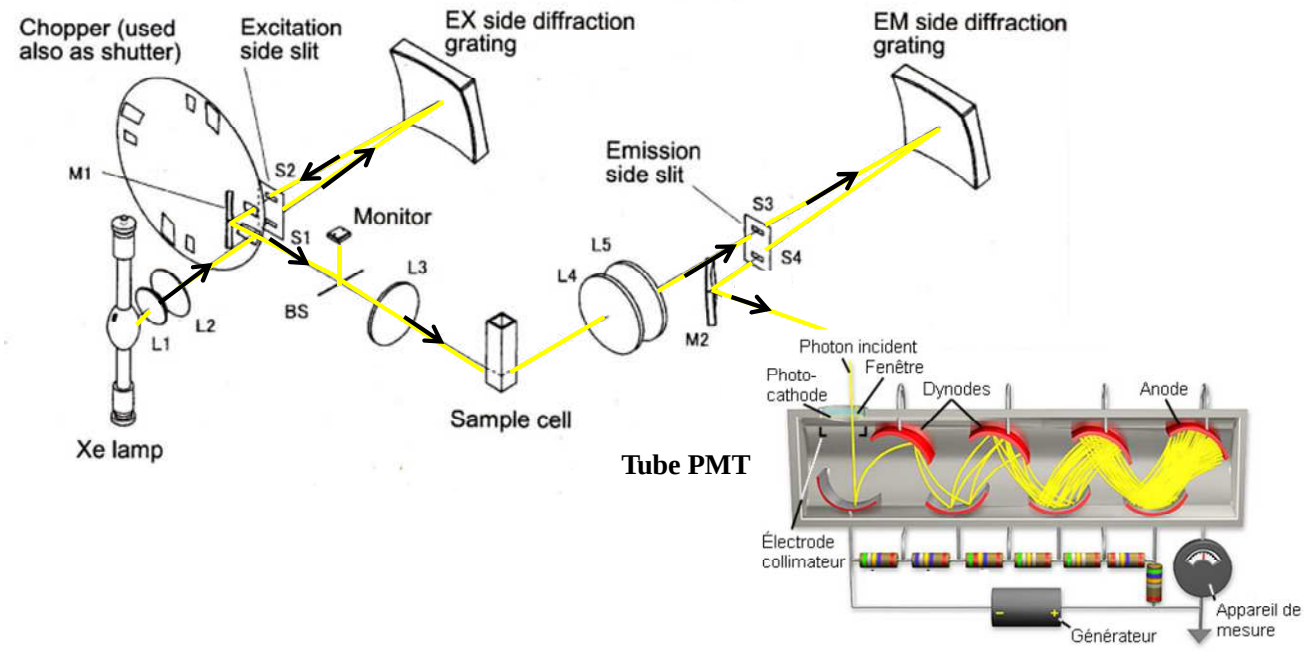

Sources : Manuel d'utilisation de l'Hitachi F-7000 et Gillet Steve (PMT)

ANNEXE 3

Principe du traitement statistique PARAFAC appliqué à un jeu de données de matrices d'excitation-emission (EEMs)

Le PARAFAC compile un jeu de données contenant n EEMs en un cube $X_{(i,j,k)}$

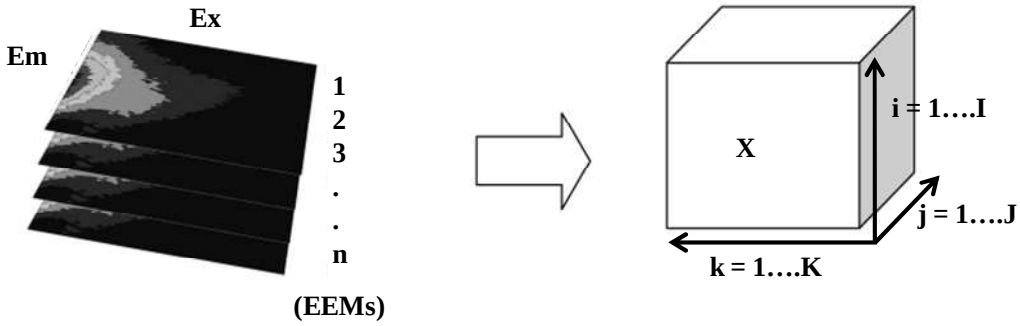

Ensuite, le PARAFAC va décomposer mathématiquement le cube en composants trilinéaires selon l'équation suivante :

$$X_{i,j,k} = \sum_{f=1}^{F} a_{i,f} b_{j,f} c_{k,f} + \varepsilon_{i,j,k}$$

Ou $X_{i,j,k}$ est l'intensité de fluorescence de la matrice i à la $j^{ième}$ longueur d'onde d'Em et à la $k^{ième}$ longueur d'onde d'Ex, F est le nombre de fluorophores présents dans chaque matrice, $a_{i,f}$ est un facteur proportionnel à la concentration du fluorophore f dans la matrice i, $b_{j,f}$ est l'estimation du spectre d'Em du fluorophore f à la longueur d'onde j, $c_{k,f}$ est l'estimation du spectre d'Ex du fluorophore f à la longueur k et $\varepsilon_{i,j,k}$ représente la somme des résidus des matrices. Les sorties du modèle PARAFAC sont donc des matrices a, b et c représentant respectivement, la concentration de chaque fluorophore dans chaque matrice, l'estimation du profile d'Em et d'Ex de chaque fluorophore.

Pour résoudre l'équation présentée ci-dessus, le PARAFAC utilise une méthode itérative des moindres carrés (ALS) qui va permettre d'estimer la structure des principaux fluorophores F contenus dans les matrices en minimisant les résidus.

ANNEXE 4 : Contribution scientifique

Biogeosciences, 7, 4083–4103, 2010
www.biogeosciences.net/7/4083/2010/
doi:10.5194/bg-7-4083-2010

Biogeosciences

Fluorescence and absorption properties of chromophoric dissolved organic matter (CDOM) in coastal surface waters of the northwestern Mediterranean Sea, influence of the Rhône River

J. Para[1,2], P. G. Coble[3], B. Charrière[1,2], M. Tedetti[1,2], C. Fontana[4,5], and R. Sempéré[1]

JOURNAL OF GEOPHYSICAL RESEARCH, VOL. 115, C02010, doi:10.1029/2009JC005289, 2010

Click Here for Full Article

Distribution of normalized water-leaving radiances at UV and visible wave bands in relation with chlorophyll *a* and colored detrital matter content in the southeast Pacific

Marc Tedetti,[1] Bruno Charrière,[1] Annick Bricaud,[2] Julien Para,[1] Patrick Raimbault,[1] and Richard Sempéré[1]

PROOCE 1079
2 March 2011
ARTICLE IN PRESS
No. of Pages 72, Model 5G

Progress in Oceanography xxx (2011) xxx–xxx

Contents lists available at ScienceDirect

Progress in Oceanography

journal homepage: www.elsevier.com/locate/pocean

Review

Marine ecosystems' responses to climatic and anthropogenic forcings in the Mediterranean

X. Durrieu de Madron[a,ag], C. Guieu[b,ag], R. Sempéré[f,ag,*], P. Conan[g,ag], D. Cossa[o,ag], F. D'Ortenzio[b,ag], C. Estournel[i,ag], F. Gazeau[b,ag], C. Rabouille[m,ag], L. Stemmann[b,ag], S. Bonnet[d,ag], F. Diaz[d,ag], P. Koubbi[b,ag], O. Radakovitch[p,ag], M. Babin[b,ag], M. Baklouti[d,ag], C. Bancon-Montigny[ac,ag], S. Belviso[y,ag], N. Bensoussan[y,ag], B. Bonsang[m,ag], I. Bouloubassi[c,ag], C. Brunet[l,ag], J.-F. Cadiou[o,ag], F. Carlotti[d,ag], M. Chami[b,ag], S. Charmasson[q,ag], B. Charrière[f,ag], J. Dachs[aa,ag], D. Doxaran[b,ag], J.-C. Dutay[l,m,p,y,ag], F. Elbaz-Poulichet[ac,ag], M. Eléaume[ae,ag], F. Eyrolles[s,ag], C. Fernandez[g,ag], S. Fowler[ab,ag], P. Francour[ad,ag], J.C. Gaertner[f,ag], R. Galzin[v,ag], S. Gasparini[b,ag], J.-F. Ghiglione[g,ag], J.-L. Gonzalez[o,ag], C. Goyet[n,ag], L. Guidi[b,ag], K. Guizien[g,ag], L.-E. Heimbürger[b,o,ag], S.H.M. Jacquet[d,ag], W.H. Jeffrey[h,ag], F. Joux[g,ag], P. Le Hir[w,ag], K. Leblanc[d,ag], D. Lefèvre[f,ag], R. Lemé[b,ag], M.-D. Loye-Pilot[c,ag], M. Mallet[i,ag], L. Méjanelle[g,ag], F. Melin[j,ag], C. Mellon[t,ag], B. Mérigot[f,ag], P.-L. Merle[x,ag], C. Migon[b,ag], W.L. Miller[k,ag], L. Mortier[c,ag], B. Mostajir[ag], L. Mousseau[b,ag], T. Moutin[d,ag], J. Para[f,ag], T. Perez[u,ag], A. Petrenko[d,ag], J.-C. Poggiale[f,ag], L. Prieur[b,ag], M. Pujo-Pay[g,ag], Pulido-Villena[b,f,ag], P. Raimbault[f,ag], A.P. Rees[z,ag], C. Ridame[c,ag], J.-F. Rontani[f,ag], D. Ruiz Pino[c,ag], M.A. Sicre[m,ag], V. Taillandier[b,ag], C. Tamburini[f,ag], T. Tanaka[b,ag], I. Taupier-Letage[e,ag], M. Tedetti[f,ag], P. Testor[c,ag], H. Thébault[o,ag], B. Thouvenin[w,ag], F. Touratier[n,ag], J. Tronczyński[r,ag], C. Ulses[i,ag], F. Van Wambeke[f,ag], V. Vantrepotte[j,ag], S. Vaz[af,ag], R. Verney[w,ag], 'The MERMEX Group'

Résumé :

Afin de comprendre, caractériser et prédire l'évolution des cycles biogéochimiques océaniques face au changement climatique global, il est nécessaire d'appréhender au mieux la dynamique de la matière organique (MO) au niveau des interfaces « terre/océan ». Dans ce contexte, l'objectif général de cette thèse était d'améliorer les connaissances sur la dynamique de la fraction dissoute chromophorique de la MO (CDOM) des eaux de surface côtières méditerranéennes et arctiques, et d'en déterminer l'impact sur l'atténuation du rayonnement UV (UVR) et visible (PAR) sous-marin. Pour cela, l'étude des propriétés optiques d'absorbance et de fluorescence de la CDOM, couplée à des mesures radiométriques atmosphériques et sous-marines, ont été réalisées lors d'un cycle saisonnier en Baie de Marseille (station SOFCOM), et lors d'une mission océanographique en Mer de Beaufort durant l'été 2009.

La Baie de Marseille est caractérisée par des quantités de CDOM faibles ($a_{CDOM}(350)$ = 0,10 ± 0,02 m^{-1}), particulièrement à la fin de la période estivale de stratification, à cause de l'intensité de l'éclairement solaire, enrichi en UVR-B, qui dégrade et blanchie cette CDOM (S_{CDOM} = 0,023 ± 0,003 nm^{-1}). Dans cette zone côtière fortement urbanisée, la dynamique de la CDOM est pilotée par des processus biotiques (production biologique *in situ* et induite par les intrusions épisodiques du panache du Rhône) et abiotiques (photo-blanchiment et brassage). La CDOM est essentiellement d'origine autochtone, même lors d'événements d'intrusion du panache du Rhône (photo-dégradation de la CDOM terrestre durant son transit). Lors des périodes d'efflorescences algales, la CDOM se compose principalement de matériel récent, de type protéique (pic T), qui absorbe préférentiellement les courts UVR. Ces pulses de CDOM récente se superposent à un persistent signal de fond de CDOM composé majoritairement de matériel âgé, de type humique (pics M et C), qui absorbe les UVR et également le PAR.

Au niveau du plateau Canadien de la Mer de Beaufort, la CDOM est très abondante ($a_{CDOM}max(350)$ = 6,36 m^{-1}), fortement influencée par les apports allochtones du Mackenzie (pics A-C et M) et décroit de manière conservatrice avec la salinité. Dans les eaux marines (salinité >25), la CDOM, qui présente de plus faibles concentrations ($a_{CDOM}(350)$ = 0,21 ± 0,13 m^{-1}), provient d'une production biologique *in situ* récente favorisée par des upwellings ainsi que d'injections de CDOM (pics B-T et M) lors de la formation/fonte de la glace de mer. Etonnamment, la source principale du composé « humique marin » (pic M) n'est pas autochtone. Elle est issue d'apports allochtones provenant du Mackenzie. Celui-ci draine en effet de nombreux lacs qui sont le siège d'une intense activité biologique, et il est proposé dans cette thèse que les macrophytes qui s'y développent seraient à l'origine du pic M. Cette source de CDOM biologique allochtone, couplée aux processus de photo-blanchiment et d'absorption sur les particules de la CDOM terrestre, pourraient expliquer les valeurs élevées de S_{CDOM} (≈ 0,020 nm^{-1}) du Mackenzie en été.

Abstract:

To understand, characterize, and predict the evolution of oceanic biogeochemical cycles in relation to the global climate change, it is necessary to better understand the dynamics of organic matter (OM). In this context, the overall objective of this thesis was to get more insights chromophoric dissolved fraction of OM (CDOM) dynamics in surface Mediterranean and Arctic coastal waters and to determine the impact on attenuation of ultraviolet (UVR) and visible (PAR) underwater radiation. For this, the study of optical properties of absorbance and fluorescence of CDOM, coupled with atmospheric and underwater radiometric measurements, were made during a seasonal cycle in the Bay of Marseille (SOFCOM station), and in the Beaufort Sea during summer 2009.

The Bay of Marseilles is characterized by low amounts of CDOM ($a_{CDOM}(350)$ = 0.10 ± 0.02 m^{-1}), particularly in end summer stratification period due to the intensity of the solar irradiance, enriched in UVR-B, which degrades and bleaches CDOM (S_{CDOM} = 0.023 ± 0.003 nm^{-1}). In this highly urbanized coastal area, the dynamics of CDOM are driven by biotic processes (in situ biological production and within the Rhône River plume) and abiotic (photo-bleaching and mixing). Our results showed that CDOM is mostly of autochthonous origin, even during Rhône plume intrusion events (photo-degradation of terrestrial CDOM during the transit). During bloom periods, the CDOM consists mainly of a recent type protein (peak T), which preferentially absorbs in the short UVR. These pulses of recent CDOM are superimposed on a persistent background of CDOM mainly composed of aged material, humic-type (peaks M and C), which absorbs UVR and PAR.

Over the Canadian shelf of the Beaufort Sea, CDOM is highly abundant (a_{CDOM}max (350) = 6.36 m^{-1}) and strongly influenced by allochthonous inputs from the Mackenzie (peaks A-C and M) decreasing conservatively with salinity. In marine waters (salinity> 25), CDOM had lower concentrations ($a_{CDOM}(350)$ = 0.21 ± 0.13 m^{-1}) and originated from a recent in situ biological production favored by upwelling and brine injections (peaks B-T and M). Surprisingly, the main source of the marine humic-like component (peak M) was not autochthonous. This material originates from allochthonous inputs from the Mackenzie River, which traverses numerous lakes where intense biological activity occurs. We suggest that this activity is mainly due to the macrophytes development, which may in part explain the origin of the peak M. This source of organic allochthonous CDOM coupled to other processes such as photobleaching and absorption on the particles of terrestrial CDOM, could explain the high values of S_{CDOM} (≈ 0.020 nm^{-1}) recorded in the Mackenzie during summertime.